Coordination Chemistry Reviews 451 (2022) 214273

Contents lists available at ScienceDirect

Coordination Chemistry Reviews

journal homepage: www.elsevier.com/locate/ccr

Mixed component metal-organic frameworks: Heterogeneity and complexity at the service of application performances

Marta Viciano-Chumillas [a], Xiangyu Liu [b], Antonio Leyva-Pérez [c], Donatella Armentano [d], Jesús Ferrando-Soria [a,*], Emilio Pardo [a,*]

[a] Instituto de Ciencia Molecular (ICMol), Universitat de València, 46980 Paterna, València, Spain
[b] State Key Laboratory of High-efficiency Coal Utilization and Green Chemical Engineering, College of Chemistry and Chemical Engineering, Ningxia University, Yinchuan 750021, China
[c] Instituto de Tecnología Química (UPV–CSIC), Universitat Politècnica de València–Consejo Superior de Investigaciones Científicas, Avda. de los Naranjos s/n, 46022 Valencia, Spain
[d] Dipartimento di Chimica e Tecnologie Chimiche, Università della Calabria, 87030 Cosenza, Italy

ARTICLE INFO

Article history:
Received 18 June 2021
Accepted 10 October 2021
Available online 28 October 2021

Keywords:
Mixed-component metal-organic frameworks
Multivariate MOFs
Multicomponent MOFs
Mixed-metals MOFs
Mixed-ligands and metals MOFs

ABSTRACT

The synthesis of mixed-component metal-organic frameworks (MOFs) –including multivariate MOFs (MTV-MOFs), multicomponent MOFs, mixed-metals MOFs and mixed-ligands and metals MOFs– is becoming a very active research field. This is mainly based on the unique possibilities these materials offer to incorporate multiple functionalities and in how this heterogenity and complexity is translated in unexpected properties, which are not just the sum of each component. This review critically encompasses the progress made in this field, covering the synthetic approaches, and specially focusing on the current reported applications –such as gas storage and separation, catalysis, luminescence, conductivity, biological ones and water remediation. It also raises, as a perspective, some of the challenges the field has to overcome to reach their full-potential, and through two applications –(bio)enzymatic catalysis and synthesis of heterometallic subnanometric clusters and nanoparticles–, as exemplary cases, present some promising ways to take advantage of the intrinsic properties of mixed-components MOFs to make a breakthrough on the respective fields of application.

Contents

* Corresponding authors.
E-mail addresses: jesus.ferrando@uv.es (J. Ferrando-Soria), emilio.pardo@uv.es (E. Pardo).

https://doi.org/10.1016/j.ccr.2021.214273
0010-8545/

Nomenclature

Abbreviations

H_2ABDC	2-aminoterephthalic acid
5-Aa-IPA	5-acetamide-isophthalate
AL	alendronate
ALD	atomic layer deposition
APT	atom probe tomography
H_2ATC	5-aminoisophthalic acid
ATR	attenuated total reflectance
AZDC	azobenzene-4,4′-dicarboxylate
BDC	benzenedicarboxylate
Im-BDC	2-(imidazole-1-yl)terephthalate
BET	Brunauer-Emmett-Teller
BIH	1,3-dimethyl-2-phenyl-2,3-dihydro-1*H*-benzo[*d*]imidazole
B_2pin_2	bis(pinacolato)diboron
BPDC	biphenyl-4,4′dicarboxylate
H_3BPT	biphenyl-3,4′,5-tricarboxylic acid
H_3BTB	4,4′,4″-benzene-1,3,5-tryl-tribenzoic acid
BTC	1,3,5-benzenetricarboxylate
BTDD	bis(1H-1,2,3-triazolo[4,5-b;4′,5′-i])dibenzo[1,4]dioxin
BTE	4,4′,4″-(benzene-1,3,5-tryl-tris(ethyne-2,1-diyl))tribenzoate
H_2IZA	4-imidazoleacrylic acid
H_2BZZ	5-benzimidazolecarboxylic acid
CAU	Christian-Albrechts-University
CBAB	4-carboxybenzylidene-4-aminobenzoate
H_2CDC	cubane-*p*-dicarboxylic acid
CCT	correlated color temperature
α-CHHC	α-cyano-4-hydroxycinnamic acid
CO_2RR	CO_2 reduction reaction
COD	1,5-cyclooctadiene
COMOC	Center for ordered materials, organometallics and catalysis, Ghent University
CP/MAS NMR	cross-polarization/magic angle spinning nuclear magnetic resonance
CRI	color-rendering index
CUB	cubane-1,4-dicarboxylate
CWA	chemical warfare agent
DCA	dichloroacetate
DCBPY	2,2′-bipyridine-5,5′dicarboxylate
H_2PDAC	1,4-benzenediacrylic acid
H_2DCDPS	4,4′-dicarboxydiphenyl sulfone
DFT	density functional theory
DMNP	dimethyl 4-nitrophenylphosphate
DOBDC	2,5-dioxido-1,4-benzenedicarboxylate
DPPE	1,2-bis(diphenyl-phosphino)ethane
DUT	Dresden University of Technology
DRIFTS	diffuse reflectance infrared fourier transform spectroscopy
EDT	electron diffraction tomography
EXAFS	X-ray absorption fine structure
FDM	Fudan material
HER	hydrogen evolution reaction
IAST	ideal solution adsorbed theory
ICP-AES	inductively coupled plasma-atomic emission spectroscopy
IPA	isophthalate
IPr	[1,3-bis(2,6-diisopropylphenyl)imidazole-2-ylidene
IRMOF	isoreticular metal–organic framework
HKUST	Hong Kong University of Science and Technology
LIFM	Lehn Institute of Functional Materials
LOHC	liquid organic hydrogen carriers
MCF	Michigan Cancer Foundation
MCP	methylcyclopentane
MDR	multidrug-resistant
MFU	metal–organic framework Ulm University
MIL	Materials Institute Lavoisier
MIP	Materials of the Institute of porous materials from Paris
MMM	mixed-matrix membrane
MOF	metal–organic framework
MOP	metal–organic polymer
MTV-MOF	multivariate metal–organic framework
MUV	Materials of University of Valencia
H_2NDC	2,6-naphthalenedicarboxylic acid
NPF	Nebraska Porous Framework
N_3-BPDC	2-azido-1,1′-biphenyl-4,4′dicarboxylate
NF	tetramethylquaterphenyldicarboxylate
NMI	*N*-methylimidazole
NMR	nuclear magnetic resonance
NP	nanoparticle
NU	Northwestern University
PCN	porous coordination network
PEMFC	proton exchange membrane fuel cell
PET	photoinduced electron transfer
PLGA	poly(lactic-co-glycolic acid)
PLQY	photoluminescence quantum yield
PMOF	Porphyrin-based metal–organic framework
PPY	2-phenylpyridine
PT	phenanthroline dibenzoate
PDT	photodynamic therapy
PTIR	photothermal induced resonance
PSMs	postsynthetic methodologies
PVDF	poly(vinylidene fluoride)
PVP	poly(vinylpyrrolidone)
PVSI	post-synthetic variable spacer installation
PXRD	powder X-ray diffraction
H_2PyC	4-pyrazolecarboxylic acid
HPZDC	1H-pyrazole-3,5-dicarboxylate
QY	quantum yield
RAM	redox active mediators
RE	rare-earth
REDOR	rotational-echo double resonance
RH	relative humidity
ROS	reactive oxygen species
SALE	solvent assisted linker exchange
SALEN	*N*,*N*′-ethylenebis(salicylimine)
SALI	solvent assisted linker incorporation
SBU	secondary building unit
SCXRD	single-crystal X-Ray diffraction
SERS	surface-enhanced raman spectroscopy

SLI	sequential linker installation
ST	ShangaiTech University
SUBNMC	subnanometric metal cluster
TATAB	4,4′,4″-*s*-triazine-1,3,5-triyltri-*p*-aminobenzoate
H_4TCBPE	1,1,2,2-tetrakis(4-(4-carboxyphenyl)phenyl)ethene
H_6TCPP	tetrakis(4-carboxyphenyl)porphyrin
TCSR	temperature-concentration swing recycling
TEM	transmission electron microscopy
TEMPO	2,2,6,6-tetramethylpiperidin-1-oxyl
H_2TFBDC	tetrafluoroterephthalic acid
TGA-MS	thermogravimetric analysis–mass spectrometry
TPHN	4,4′-bis(carboxylatephenyl)-2-nitro-1,1′-biphenyl/2″-nitro-[1,1′:4′,1″:4″,1‴-quaterphenyl]-4,4‴-dicarboxylate
TON	turnover number
TOF	turnover frequency
UiO	University of Oslo
UMCM	University of Michigan Crystalline Material
UV Led	ultraviolet light emitting diode
VOC	volatile organic compound
XANES	X-ray absorption near edge structure
XPS	X-ray photoelectron spectroscopy
WHO	World Health Organization
ZIF	zeolitic imidazolate framework

1. Introduction

Since the advent of metal–organic frameworks (MOFs) [1–5] –porous crystalline materials made up of metal ions or secondary building units (SBUs) [6] linked to organic ligands– a large number of diverse framework topologies with different surface area and pore size distributions have been unveiled [3,4,7–9]. Synthetic strategies for the preparation of MOFs have been related, traditionally, to direct self-assembly methods –mainly solvothermal reactions [10,11]. However, other synthetic approaches have been also largely exploited, especially the so-called postsynthetic methodologies (PSMs) [12–17] –where a preformed MOF can experiment precise modifications of their constituents, in a solid-state manner, to render a new material with improved features respect to the pristine MOF, while retaining the crystallinity. Thus, the almost limitless number of possible combinations of MOFs constituents, together with the unique possibilities of PSMs have enabled MOFs with thrilling properties in a wide range of applications, such as gas storage and separation [18,19], catalysis [20–26], chemical sensing [27], light-harvesting/solar-energy conversion [28], drug delivery [29], and environmental remediation [30,31,31–33] or water harvesting [34–36].

Nevertheless, despite the great advances performed in MOF chemistry, the heterogeneity and complexity of the majority of reported MOFs is still quite limited, chiefly, to only one type of SBUs and organic ligand [3,4,7–9]. In this respect, somehow mimicking the way that nature builds up complex architectures, it was envisioned to construct complex MOFs networks from simple different building units, with the aim to translate the higher degree of complexity into more sophisticated and efficient functionalities [37–39]. Indeed, a growing body of work have been devoted to increase our knowledge on the controlled synthesis and precise characterization of MOFs build up from distinct constituents. Mixed-component MOFs can be constructed by the use of distinct organic ligands and/or different metal ions/SBUs. Several terms have been assigned to these new MOFs depending on the followed approach, and sometimes, researcher's wish to coin a new term. So, for example, these types of MOFs have been named as MIXMOFs [40], coordination co-polymers [41], mixed-component MOFs [39], mixed-metals MOFs [42], multivariate MOF (MTV-MOFs) [43,44] and multicomponent MOFs [45]. Among them, the most used terminologies –that focus on the nature of the organic linkers– are MTV-MOFs and multicomponent MOFs. MTV-MOFs possess linkers of identical backbones but different functionalities decorating the ligand, whereas in multicomponent MOFs, organic ligands are structurally and compositionally different (Fig. 1).

MTV-MOFs have been proven as the perfect platforms to provide highly heterogenous pores, with a wide diversity of organic ligands, possesing diverse linkers distribution, which makes quite difficult to ascertain the precise position of each functionality, due to disorder factors. Conversely, in multicomponent MOFs, since the linkers are well differentiated and ocuppy distinct crystallographic positions, they can be more easily characterized by single-crystal X-ray crystallography. However, the main drawback of this approach is that multiple phases can also compete in MOF formation, affording other thermodynamically favored MOFs as the main product instead of the multicomponent MOF, which makes extremely challenging to increase, to more than a few, the number of different organic building units. As we have mentioned, in most of these cases, MOFs are obtained in one-pot reactions. Nevertheless, different PSMs, such as Sequential Linker Installation (SLI) [46–49] and Solvent Assisted Linker Exchange (SALE) [50], have been succesfully developed, which have led to increase heterogeneity within order (Fig. 2) [16]. Dealing with the metal ions/SBUs, there are three main synthetic possibilities to build up heterogeneous systems, different metal ions in the SBUs, distinct SBUs –with the same or different metal ion–, as well as the combination of the two previous options. As in the case of MTV-MOFs, it is still quite difficult to determine with precision

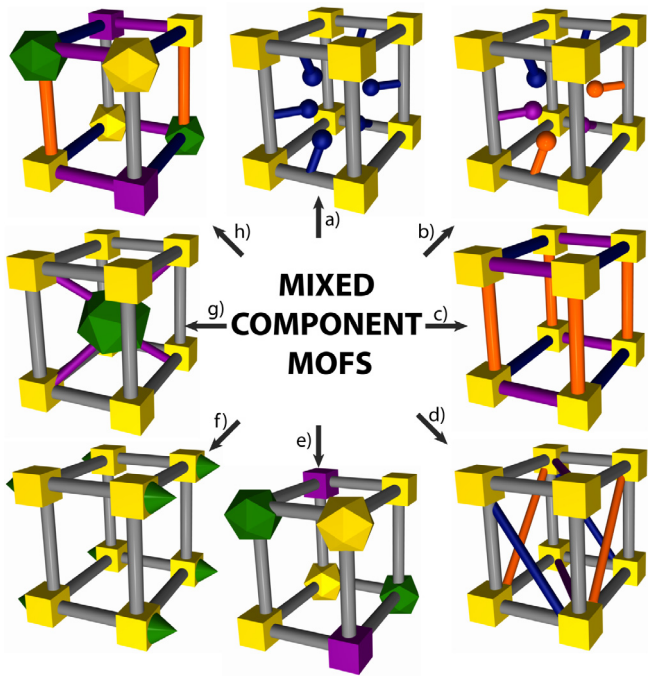

Fig. 1. Schematic representation of the different types of mixed-component MOFs: a) and b) MTV-MOFs; c) and d) multicomponent MOFs; e) and f) mixed-metals MOFs and g) and h) mixed-ligands and metals MOFs.

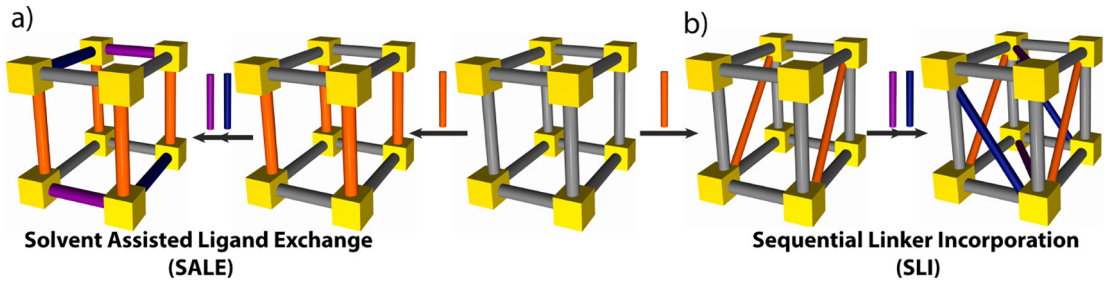

Fig. 2. Schematic representation depicting the two main postsynthetic strategies, such as Sequential Linker Installation (SLI) and Solvent Assisted Linker Exchange (SALE), to obtain MTV-MOFs and mainly multicomponent MOFs.

the position of each metal ion in these complex SBUs. However, considerable endeavours have been pursuit to try to shed light on it. Finally, it is important to consider the combination of simultaneous heterogeneity at the inorganic and organic sites in both types of MOFs. This represents the ultimate level of sophistication and, given that it also requires a high level of synthetic control, at the same time constitutes a challenge. Obviously, this level of complexity makes the number of reported examples reduced to a few. But, their mere existance is the evidence that MOFs chemistry have the possibility to engender really sophisticated systems, which are hardly accessible with other type of materials.

Despite the remarkable advances, important challenges remain to be overcome and further work is required to get a deep understanding of this new generation of mixed component metal–organic frameworks. In particular, the characterization of these heterogeneous systems, in most of cases, is still poorly developed, and commonly rely on a multi-technique approach [51–60]. This result as consequence of the complexity of mixed component MOFs, and contrast with the common situation in conventional MOFs, where X-ray crystallography is the basic characterisation tool [61–65]. With the aim to solve this issue, several physical techniques, such as microscopic attenuated total reflectance (ATR) infrared spectroscopy [66], photothermal induced resonance (PTIR) [67], surface-enhanced Raman Spectroscopy (SERS) [53], Raman microscopy/spectroscopy [68], fluoresccence confocal microscopy [69], multi-wavelength anomalous X-ray dispersion [51], rutherford backscattering spectrometry [57], atom probe tomography [70], fluorescence lifetime imaging [58], diffraction techniques –neutron and X-ray– and DFT calculations [56], solid-state nuclear magnetic resonance (NMR) [52,55] and theoretical calculations [71], have been proved quite efficient to elucidate specific cases of mixed component MOFs. However, their complexity, high degree of sophisitication and/or unaccesability in conventional synthetic laboratories makes still highly desirable the development of new characterization techniques that could afford synthetic chemist with the necessary tools to understand such complex MOFs. Introducing heterogeneity in these systems –in a completely controlled manner– constitutes another major challenge, which would allow to maintain a uniform and ordered distribution of the different groups as well as to characterize them.

In this review, we describe an overview of mixed components MOFs. After presenting some of the more relevant/recent examples of each different subfamily, we will be especially focusing on highlighting, with a critical vision, the current reported applications of these materials; where in most of the cases the behavior is enhanced compared to single-ligand parent compounds as consequence of the synergetic effects between different components. In particular, we will describe mixed components MOFs with exciting applications in such diverse fields as gas storage and separation, heterogeneous catalysis, luminescence, conductivity, biological and environmental applications (Fig. 3). Then, we will expose, under our humble opinion, which are some of the potential applications of such complex materials, and will finish with some perspectives and a critical conclusion of the state-of-the-art in the field.

It is important to note here some particularities of the systems that will be considered in this review. In this sense, we will not consider as mixed component MOFs, the systems where bipyridine

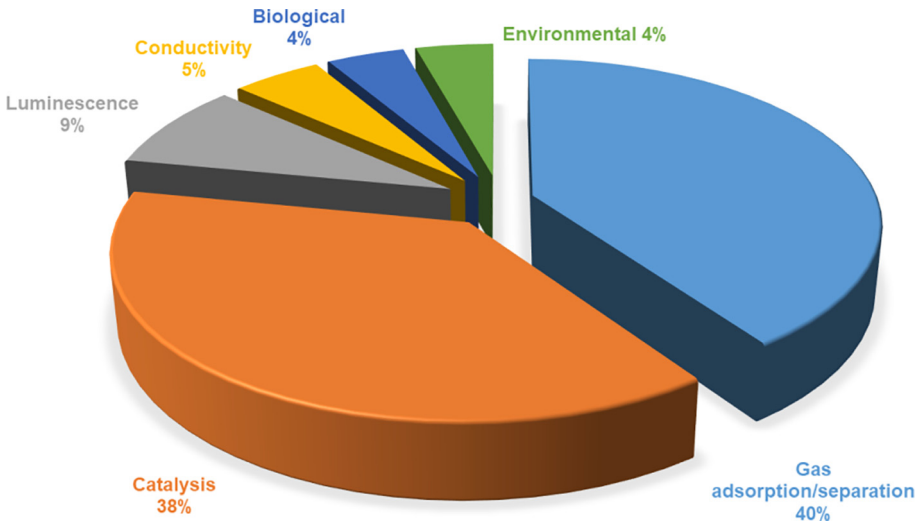

Fig. 3. Pie chart showing the fields of application of mixed components MOFs (%) obtained from the reported publications (see references below).

derivatives are used as struts to pillar two-dimensional carboxylate bridged architectures [72–81]. Despite the exceptional features some of these materials exhibited, we will mainly circumscribe to systems where the linkers present coordinating groups able to form bonds of somehow similar binding energies. In the same way, core–shell structures, defects or hierarchical systems will not be treated, and we refer the eager reader to some of the recents works published [38,59,68,69,82–84]. This reasoned decision was taken with the intention to not overexpose the potential reader with too many different examples of mixed-components MOFs, which ultimately could dilute the core part of this review devoted to their applications. Finally, dealing with mixed-metals networks we will not include heterometallic MOFs with strictly defined stoichiometries, which have been really appealing systems in a wide range of differents applications and led to some interesting multifunctional materials. However, we consider, they do not contain the essence of the materials considered in the review, where the degree of mixing can be synthetically tailored *à la carte*.

2. Illustrative examples of mixed-component MOFs: Synthesis and characterization

2.1. Multivariate metal–organic frameworks (MTV-MOFs)

The most straightforward strategy to introduce heterogeneity and complexity within a given MOF is using organic linkers with identical backbones –meaning same length, geometry and connectivity– but different substituents, and thus functionalities. While it is true that some examples, that could be considered as MTV-MOFs, had been previously reported [40,85–89], these types of materials were coined as multivariate metal–organic frameworks (MTV-MOFs) in a seminal work by Omar Yaghi et al. [43], where up to 18 different MTV-MOFs of the archetypical MOF-5 were reported. In this work, Deng *et al.* nicely demonstrated how it is possible to construct a MOF with multiple functional groups decorating the channels in different ratios in a controlled manner. In particular, they showed different MOF-5 materials that combine sets of two to eight distinct 1,4-benzenedicarboxylate(BDC)

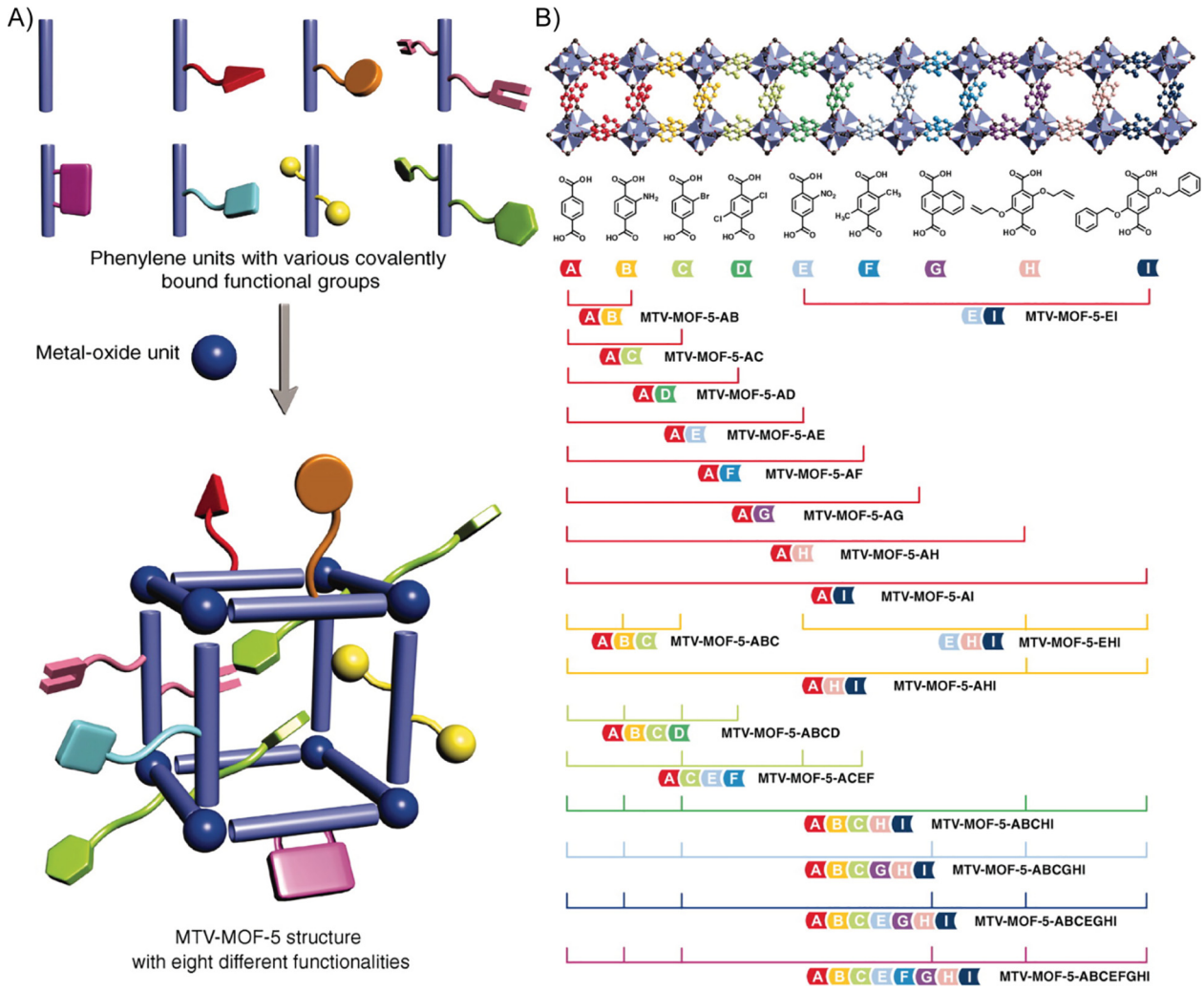

Fig. 4. A) Schematic representation of the MTV-MOF-5 structure showing the multivaried arrangements of the different functional groups that are covalently bound to the links. B) Different combinations of the functional groups to yield the 18 different MTV-MOFs. Adapted from ref. [43] with permission from the American Association for the Advancement of Science (AAAS), Copyright 2010.

derivatives (–NH_2, -Br, -Cl_2, –NO_2, -$(CH_3)_2$, -C_2H_4, -$(OC_3H_5)_2$ and -$(OC_7H_7)_2$) (Fig. 4). The compounds were synthesized, in one-pot reactions, from equimolar amounts of the linkers. Moreover, in the specific case of MTV-MOF-5-ABCD, they proved it is possible to control the linker ratio by modifying the reaction stoichiometry. ^{13}C cross-polarization/magic angle spinning nuclear magnetic resonance (^{13}C CP/MAS NMR) and ^{1}H NMR spectra of a DCl-digested solution afforded the precise linker composition and their ratio, respectively. Attempts to characterize the samples by means of single crystal X-ray crystallography showed an ordered network with a variable distribution of functional groups, which lead to pore heterogeneity. In our opinion, the most remarkable conclusion, that can be extracted from this work, is the concept that the properties of MTV-MOFs are not a simple linear combination of those of pure MOFs but, in turn, novel and/or improved properties can originate in these novel MOFs. Later on, some of the same authors, beautifully illustrated the distribution of the functionalities of some of the reported MTV-MOFs by the combined use of solid-state rotational-echo double resonance (REDOR) NMR and molecular dynamics simulations. In this sense, they found different scenarios, varying between random, alternating and clustered distribution, depending on the chemical nature of the combined functionalities [71]. Obviously, this work did not solve the problem of the precise atomic characterization of MTV-MOFs. But, remarkably, it represented the first solid evidence of the heterogeneity and complexity of MTV-MOFs, and even more interestingly, it helped to predict and explain some of the exciting physical properties of synthesized MTV-MOFs.

After this discovery, this type of chemistry was extended to other different linkers/platforms [90–104]. For example, Burrows *et al.* [97] studied the selective incorporation of functional dicarboxylates into $[Zn_4O(BDC)_{3-x}(BDC\text{-}X)_x]$ (X = Br or I, BDC = benzene dicarboxylate) MOF. They performed a detailed study on how the different proportions of ligands would influence the final composition of the MTV-MOF. It was observed a preferential incorporation of less sterically crowded ligand, as in a previous study [43], and that this process is related to crystal growth rates. Also, they realized proportion of BDC-X incorporation rises with increasing reaction time [97]. In another work, it was reported an interesting family of 14 MTV-MOFs of MOF-177(Zn) [99] using two or three different types of 1,3,5-benzenetribenzoic acid (H_3BTB) linkers, with varied ratios and functionalities (Fig. 5) [98]. Interestingly, they found that all the reported MTV-MOFs-177 exhibited the ***qom*** net, instead of the default ***pyr*** or ***rtl*** ones, and that some functional groups –*i.e.* NO_2– could be easily incorporated, while it was extremely difficult to use them to build the respective single-ligand MOF-177.

Materials Institute Lavoisier (MILs) are one subclass of MOFs that have been more extensively studied for different applications [105–107]. This is largely due to the exciting breathing behaviours, physical/chemical robustness and/or large cavities of some of their members. Indeed, and somehow related to these features, they have been also evaluated as platforms for the development of MTV-MOFs. Particularly interesting is the study of Dong *et al.* [100] with robust MIL-101(Fe) [89]. They reported three distinct MTV-MOFs, with up to three distinct functionalities decorating their mesoporous cavities –*i.e.* -H, –NH_2 and -C_4H_4. Interestingly, the systematic variation of these functionalities was exploited to gain insight on the energetic magnitude of host–guest interactions, which was also useful to develop a simple model, capable to predict the adsorption/release properties of any specific linker ratio combination. At this point, despite the authors considered the frameworks as multivariate, we consider that this material would be, more appropriately classified as a multicomponent MOF given that three differents linkers –two of them having the same organic backbone– were used to construct the MOF.

The interesting breathing behaviour of MIL-53 have also attracted the attention of researchers to construct MTV-MOFs based on this MOF [101]. For example, Marx *et al.* [102] reported the random distribution BDC and 2-aminoterephtalic acid (ABDC) in MTV-MIL-53(Al), $Al(OH)(BDC)_{1-x}(ABDC)_x$ –with × = 0.1, 0.5 and 0.9 [102]. This was a basic work, but it was useful to expand the MTV concept to such an important family of MOFs as MIL-53, and also to understanding the relationship between the linkers ratio and the chemical/physical features of the obtained MTV-MOF.

Rare-Earth (RE)-based MOFs [103,104] represent an extense family of porous materials with a great diversity of network dimensionalities and topologies, as a direct consequence of the rich and diverse coordination environment/numbers lanthanoids ions can adopt. Indeed, these features lead to novel and intricate topolo-

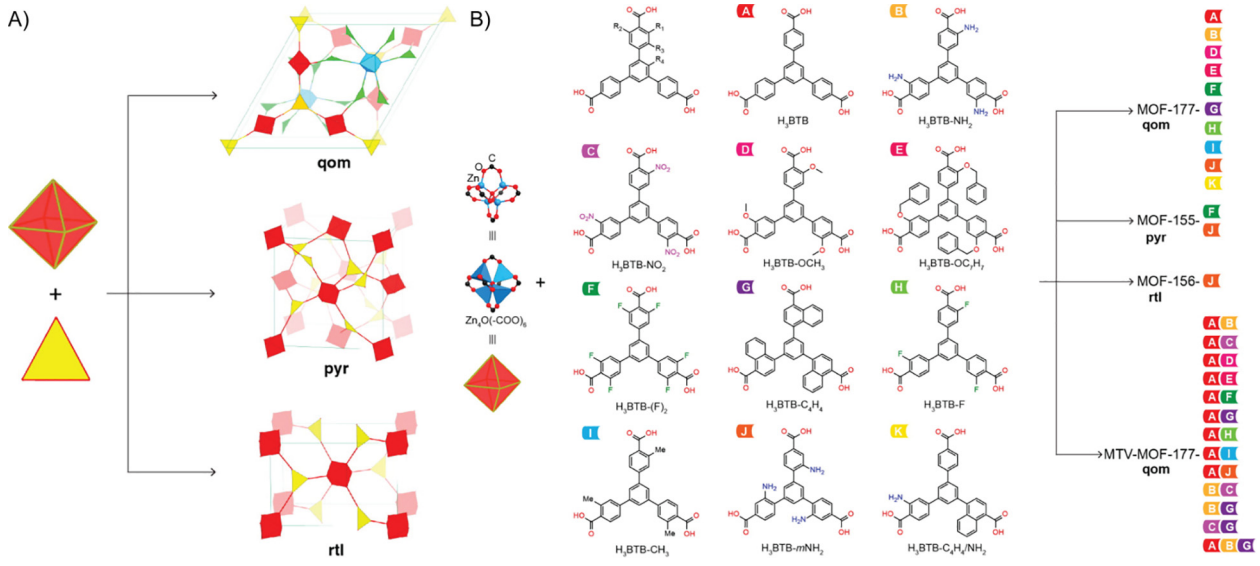

Fig. 5. A) Schematic representation of the three possible (6,3)-coordinated nets formed from octahedron and triangle building units with alternative arrangements. B) Different H_3BTB linkers with different functional groups at selected positions and the corresponding MOFs formed from either pure linker or mixing of various linkers. Adapted from ref. [98] with permission from the American Chemical Society, Copyright 2015.

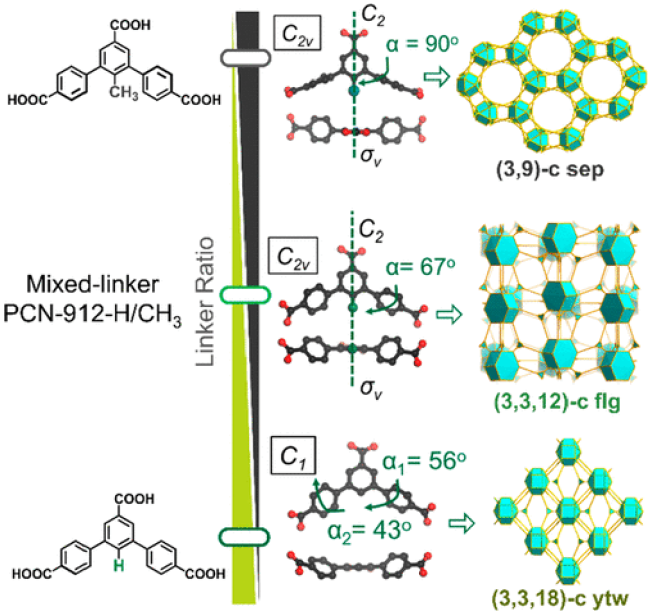

Fig. 6. Continuous tuning of linker steric hindrance through multivariate (MTV) strategy that leads to the formation of MTV-PCN-912. Reproduced from ref. [104] with permission from the American Chemical Society, Copyright 2019.

gies. In particular, a work reported by Wang *et al.*, [104] results especially relevant to our topic. They make use of the steric control approach –previously reported for Zr-MOFs [104,108,109]– to build up a series of 12-connected RE_9 clusters MTV-MOFs, $[RE_9(\mu_3\text{-}OH)_{12}(\mu_3\text{-}O)_2(O_2C-)_{12}]$ (PCN-912, PCN = Porous Coordination Network), with **flg** topology [8] and tunable distinct proportions of two linkers with different degree of steric hindrance. Interestingly, molecular simulations support that the judicious combination of these substituents –through a continuous steric hindrances tuning– dictates the final MOF architecture (Fig. 6), which undoubtely would help for the discovery of unprecedented topologies and thrilling applications.

University of Oslo (UiO) type materials are one of the most studied systems, as consequence of their great chemical, thermal and physical robustness [110,111]. Indeed, UiO frameworks paved the way for the subsequent development of Zr-based MOFs, which nowadays represent one of the most precious assets in MOFs chemistry [112–114]. Different MTV-UiO materials have been synthesised [92–95]. For example, Kalaj *et al.* [96] reported a library of 26 MTV-UiO-66 derivatives using various combinations –*i.e.* two, three, four and five– of five distinctly functionalized BDC linkers with electron donating –NH_2-BDC and OH-BDC– and electron withdrawing –NO_2-BDC and Br-BDC– groups. In this work, they showed that the performances, in warfare agents degradation, of the MTV-MOFs are superior to the pristine MOF, single-linker MOFs or physical mixtures of them (see section 3.6). The authors suggested a synergetic effect of the mixed functionalities in the same pore. But, further work is still necessary to elucidate the connection between structure and property, which it would unveil the origin of this synergetic behaviour.

Titanium-based MOFs have attracted a big deal of attention due to their great structural stability and potential applications, especially in photocatalytic processes [60,115–119]. Although, they are really highly challenging systems to crystallize, and few structures are known, some noteworthy advances have been devoted in this topic. For example, Wang *et al.* [120] reported recently a multivariable 3D network with double-walled 1D channels along the *c* axis, based on the MOF Ti(μ_2-O)(5-Aa-IPA) –where 5-Aa-IPA is the *in-situ* generated 5-acetamide-isophtalate– build up of one dimensional helical chains of *cis*-connected corner-sharing TiO_6 polyhedra and two different isophthalic acid derivatives –5-Aa-IPA and one of the following IPA, 5-Me-IPA, 5-Br-IPA and 5-^{t}Bu-IPA. The authors also reported a multicomponent system using as the second linker the 3,5-pyrazole-dicarboxylic acid. The mixed linker strategy applied in this work not only offers the possibility to finely tune the chemical functionalities of the pore in Ti-based MOFs. But, more interestingly, offer the possibility to incorporate especific functionalities in a targeted network, even when their isoreticular material with a single linker is hardly accessible. Previously isophthalic acid derivatives were used to obtain MTV-MOFs with CAU-10(Al) structure –CAU stands for Christian-Albrechts-University [121].

All the previous examples were obtained by direct synthesis in one-pot reaction by mixing differently functionalized linkers. Nevertheless, post-synthetic methodologies have been also succesfully applied to afford MTV-MOFs, and to increase the complexity and heterogenity within them. In fact, any intermediary moment during the total postsynthetic modification or a partial modification of a given MOF led to materials with distinct ratio of their functionalities [87,88,122,123]. In this context, Karagiaridi *et al.* [124] reported the application of the solvent-assisted linker exchange (SALE) methodology on ZIF-8 (ZIF stands for zeolitic imidazolate framework) to replace up to 85% of 2-methylimidazole by imidazole. This allowed the obtention for the first time of a network with SOD topology, where the majority component was an unfunctionalized imidazolate ligand. This partially-modified material retained the stability of ZIF-8 and provided larger windows for the uptake of guests [124]. Interestingly, it was observed by Jayachandrababu *et al.* [69] that the linker distribution and properties of a MTV-ZIF build up with 2-methylimidazole and imidazole-2-carboxyaldehyde (ZIF-8–90) [125,126], were different depending on the synthetic route. *De Novo* synthesis led to well-mixed structures, meanwhile SALE process to core–shell structures [69]. PSMs have been also exploited by Gotthardt *et al.* to obtain accesible MTV-MOF-supported single-site catalyst [127]. They synthesized NH_2-MIL-53(Al) with different and defined amounts of terephtalic and aminoterephtalic acids, and took advantage of its hetereogenity to tune the amount and distribution of catalyst –precluding pore blocking–, by controlling the number of amine groups incorporated, which were the ones in the MTV-MOF able –after two-consecutive PSM– to anchor a palladium complex (Fig. 7). The first step was a reaction of the aromatic amine with maleic anhydride, and then, a complexation with palladium(II) acetate. Relevant to this point, is the fact that the first post-synthetic modification did not occur in a quantitative manner, which intrinsically increased the heterogeneity and complexity of the MTV-MOF. However, it is equally true that this approach lacked of control on the distribution of amine groups, as well as on the ones that experiment functionalization. Some of these authors also reported the same concept in an isoreticular expansion of MIL-53(Al): DUT-5 (DUT = Dresden University of Technology), with functionalized and non–functionalized 4,4′-biphenyldicarboxylic acid ligands with amine, alkyne, azide or nitro groups, which evidences the versatility of this approach, despite its limitations [128].

PSMs have been also performed in a sequential manner to exchange some of the constituting linkers by different functionalized derivatives. Liu *et al.* applied this approach on a multicomponent zinc-adeninate MOF with 2-azido-1,1′-biphenyl-4,4′dicarboxylate (N_3-BPDC) ligands, the so-called N_3-bMOF-100 [129]. They were able to perform two sequential post-synthetic modifications with 2-amino-1,1′-biphenyl-4,4′dicarboxylate (NH_2-BPDC) and 2-formyl-1,1′-biphenyl-4,4′dicarboxylate (F-BPDC). In addition, they also reported different binary MTV-MOFs starting from bMOF-100 [130] –constructed with 4,4′-biphenyldi

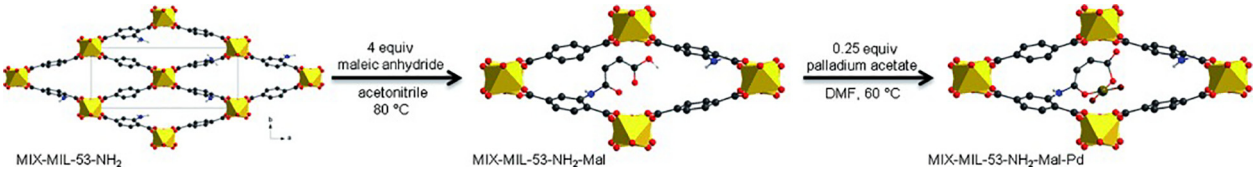

Fig. 7. Two-step postsynthetic preparation of MIX-MIL-53-NH_2-Mal-Pd. Reproduced from ref. [127] with permission from John Wiley & Sons, Copyright 2015.

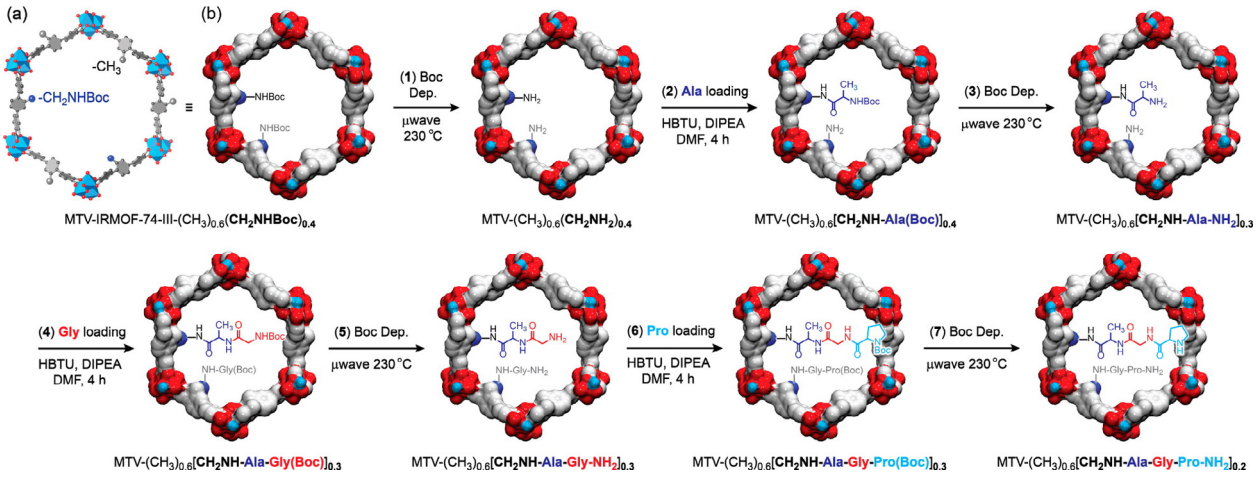

Fig. 8. a) Crystal Structure of MTV-IRMOF-74-III-$(CH_3)_{0.6}(CH_2NHBoc)_{0.4}$ and b) the seven consecutive post-synthetic reactions within its channels. Reproduced from ref. [132] with permission from the American Chemical Society, Copyright 2016.

carboxylic acid– and N_3-bMOF-100. Noteworthy, the ortogonality nature of the incorporated functional groups, allowed that large organic dyes and quencher molecules could be post-synthetically added, which after spectrophotometric analysis, suggested a random distribution of functional groups in binary functionalized 1:1 N_3-F-bMOF-100 [131]. Later on, Fracalori *et al.* [132] reported a beautiful example that contains several of the strengths of the direct synthetic methods and PSMs to get highly complex MTV-MOFs. On one side, they reported different MTV-IRMOF74-III –constructed from magnesium oxide rods and two distinctly functionalised 3,3′′-dihidroxy-(1,1′:4′,1′′-terphenyl)-4,4′′-dicarboxylic acid derivatives with $–CH_3$ and $-CH_2NHBoc$ in diferents ratios, MTV-$(CH_3)_{(1-x)}(CH_2NHBoc)_x$, x = 0.2–0.8– which precluded pore-blocking and consequently lack of functionality (Fig. 8a). Then, they selected one of them, and performed up to seven post-synthetic reactions in tandem on the primary amines ($-CH_2NHBoc$) decorating the large pores. This allowed to *in-situ* generate two covalently-attached different tripeptides $–H_2N$-Pro-Gly-AlaCONHL and H_2N-Cys-His-Asp-CONHL; with Pro = proline, Gly = glicine, Ala = alanine, Cys = cysteine, His = histidine, Asp = aspartic acid and L = organic backbone. Interestingly, the pores of these MTV-MOFs do not only contain the target tripeptides, but also a complex mixture of products generated in the consecutive post-synthtetic steps (Fig. 8b). Despite the materials presented on this work are far from being close to the active center of enzymes in terms of regularity and order, they open the gate to get complex pores functionalized with different amino acid residues, as it occurs in the active site of enzymes.

Alternatively to previous PSMs described to generate heterogeneity, rationally, in MTV-MOFs, Zhou *et al.* [133] reported a novel approach to gain control on the apportionment of functional groups in MTV-ZIF-8. In a first step, they took advantage of interlocked imine-based linkers of different lengths with cleavable links (Fig. 9a), which were incorporated inside the ZIF-8 under mild post-synthetic conditions (Fig. 9c) [133]. Then, the interlocked imine-based linkers were removed by hydrolysis (Fig. 9b-d), leading to a network with a more controlled heterogeneity. Interestingly, the interlocked chain length of these linkers tuned the distribution of functional groups, as studied by DFT methods.

Li et al. also studied the differences between the synthesis of a MTV-MOF with BDC and BDC-NH_2 via direct synthesis with a linker mixture, and PSM in MOF-5 and IRMOF-3 by linker exchange [134]. Optical microscope images showed different linker distribution depending on the synthesis method. In addition, their thermal and chemical stabilities were also studied [134].

2.2. Multicomponent metal–organic frameworks

Previously to the development of MTV-MOFs, the first approach that rendered heterogeneity and complexity within MOFs channels was the mixing of organic linkers with different chemical nature. This class of materials has received diverse names, but here we have gathered them under the group of multicomponent MOFs [135–137]. Initial efforts were made with the aim to explore new MOFs compositions and expand the plethora of novel structures, which eventually allowed to obtain higher porosities, circumventing interpenetration issues when using very large linkers. In direct synthesis, the obvious first step was the use of two distinct organic linkers. Koh *et al.* [41,138,139] reported a family of materials, known as University of Michigan Crystalline Material (UMCM), where Zn_4O SBUs were connected with both, a tritopic and a linear ligand (Fig. 10). This strategy led to novel porous solids with large pore volumes. For example, those constructed with 1,3,5-tris(4-carboxyphenyl)benzene presented mesoporosity [139]. Later on, the authors extended their approach to two linear linkers of distinct lenghts [140]. Furukawa *et al.*, with the aim to increase the surface area reached with MOF-177 [99] –constructed with Zn_4O SBUs and the triangular linker 4,4′,4″-benzene-1,3,5-tryl-tribenzoate (BTB)– took advantage of elongated ligands and/or mixed linkers approach [43]. In particular, connecting Zn_4O clusters with an elongated ver-

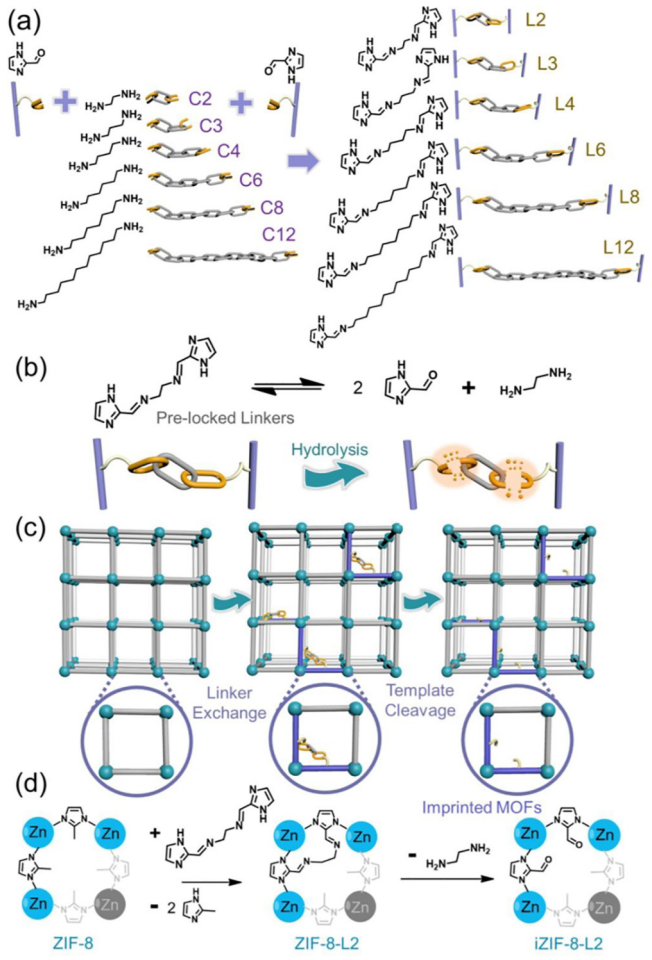

Fig. 9. Controlled heterogeneity in MTV-MOFs: a) Synthesis of organic linkers. (b) Schematic representation of the dissociation and association of imine bonds in prelocked linker. (c, d) Sequential linker exchange and dissociation processes. Reproduced from ref. [133] with permission from the American Chemical Society, Copyright 2019.

sion of BTB –4,4′,4″-(benzene-1,3,5-tryl-tris(ethyne-2,1-diyl))tri benzoate (BTE)– and biphenyl-4,4′dicarboxylate (BPDC) constructed a highly porous framework, MOF-210, which at that moment exhibited the highest Brunauer-Emmett-Teller (BET) and Langmuir surface area and pore volume reported. In an analogous way, there are some relevant examples of Dresden University of Technology (DUT) MOFs [141–143]. Particularly interesting results DUT-60, constructed with tritopic 1,3,5-tris(4′-carboxy[1,1′-biphenyl]-4-yl)benzene and ditopic 1,4-bis-p-carboxyphenylbuta-1,3-diene ligands and Zn_4O clusters [143]. In this study, it was evaluated the mechanical stability limits of a network with ultrahigh porosity. Indeed, DUT-60 presents the highest recorded accessible pore volume (5.02 cm^3 g^{-1}), and represents an strong step towards reaching the upper limits of porosity in MOFs, which is of fundamental relevance in clean energy applications [144].

The next step using direct synthesis for obtaining more complex multicomponent MOFs was represented by Massey University Framework (MUF) materials [145–148]. Liu *et al.* [145] developed the strategy of programmed pore architectures, which consist on the use of three topologically different organic linkers. This led to build up the first highly porous quaternary MOF –MUF-7a, [$Zn_4O(BTB)_{4/3}(BDC)_{1/2}(BPDC)_{1/2}$] [145]. Despite many different MOFs can be constructed with these three linkers, phase-pure MUF-7a was obtained by optimising the ratio of precursors and the reaction conditions. The strength of this strategy resides on the use of topologically distinct linkers, which consequently occupied defined and predetermined positions in the crystalline lattice. This allowed to generate complexity without sacrificing homogeneity, and, even more importantly, to locate multiple functional groups in predefined positions. Indeed, the authors reported isoreticular variations of this structure –MUF-7b-h–, where different functionalities/ligands that match the space group symmetry of the structure –to mitigate positional and crystallographic disorder– were decorating/replacing each of the constituting ligands. Continuing with this work, the use of different sets of ligands has led to other quaternary Zn_4O-based MOFs [148–153]. Especially relevant resulted the multicomponent MOFs containing tritopic truxene-based ligands –MUF-77 [148,151,154]. The authors showed, in a first study, how its greater conformational rigidity prevented the for-

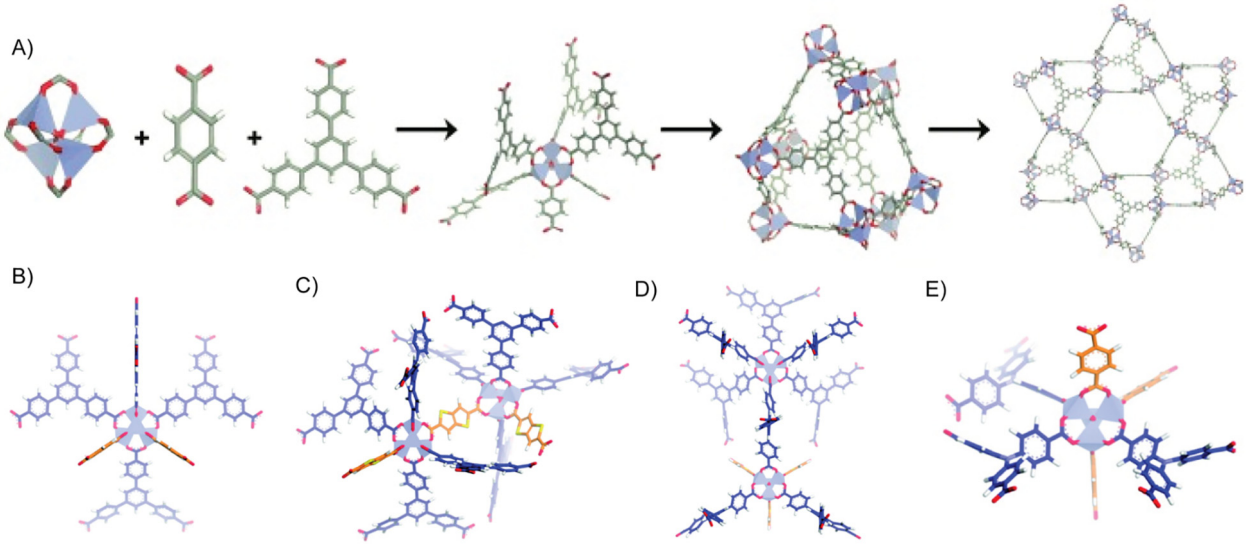

Fig. 10. A) Synthetic route for the formation of UMCM-1. Ditopic linkers and tritopic linkers and Zn_4O clusters forming UMCM-1 (B), UMCM-2 (C) UMCM-3 (D) and UMCM-4 (E). Adapted from refs. [139] and [140] with permission from the John Wiley & Sons and the American Chemical Society, Copyright 2018 and 2010.

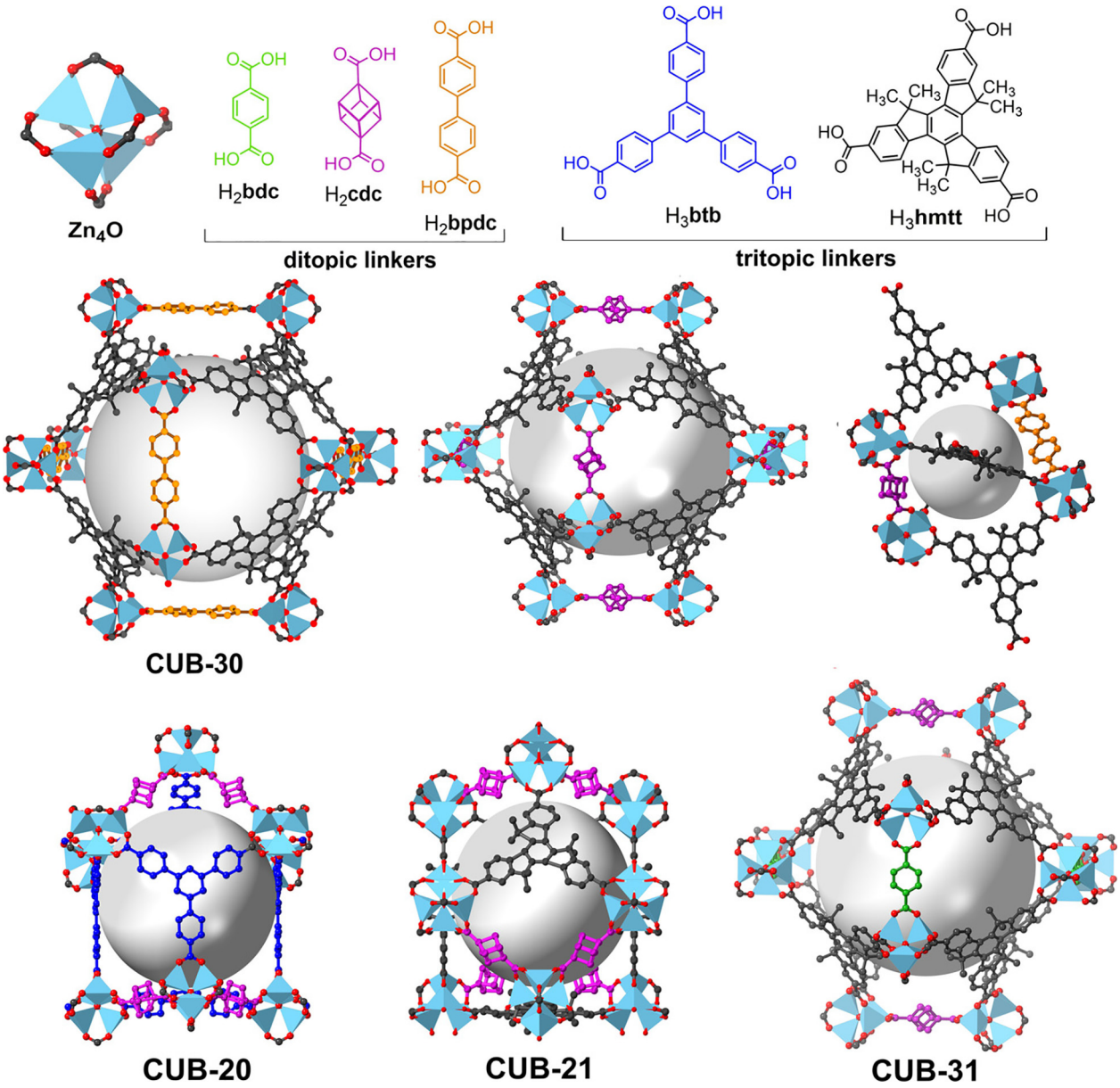

Fig. 11. Zn_4O clusters and organic linkers used for the synthesis of cubane multicomponent MOFs (top). Crystal structures of the cavities of multicomponent CUB MOFs emphasizing the different linkers. Reproduced from ref. [153] with permission from John Wiley & Sons, Copyright 2020.

mation of competing phases, which also enhanced their stability toward humidity. Later on, they demonstrated the versatility of MUF-77 platform to develop materials with a wide range of applications, where the functional groups decorating the ditopic ligands marked the functionality of the multicomponent framework [148,151,154]. More recently, some of the same authors reported novel multicomponent Zn_4O-MOFs, CUB-20 and CUB-30 and 31 –analogous to UMCM-1 and MUF-77, respectively–, but using cubane-1,4-dicarboxylic acid instead of BDC (Fig. 11). Interestingly, this work nicely illustrates how subtle changes in multicomponent MOFs have a major influence on their functionality [153]. Partial PSMs have shown also efficient for the obtention of Zn-based multicomponent MOFs [155,156]. Liu *et al.* studied in detail the same process on bMOF-100 [156]. Interestingly, they observed an incremental stepwise pore expansion, which occurred in a gradual manner from the periphery to the core. This endowed such systems with directional pore gradients, and consequently, greater degree of complexity, which eventually, could be used for applications related to control the flow of matter within ordered 3D networks.

Despite the synthetic and structural interest of the mentioned Zn_4O-based multicomponent MOFs, their known poor hydrolytic stability has evolved on the development of more robust frameworks with different constituting linkers. In this context, zirconium-based multicomponent MOFs have been intensively investigated [95,113,157–159]. Initially, it was based on UiO-type materials with two different linear organic ligands –in an analogous manner to zinc-based systems. A quite common combination was the use of BPDC and a bypiridyl-type ligands, which could be pre- or post-synthetically metallated with a metal ion of interest for a particular application [160,161]. Then, this strategy was extended to other two ligands, which gave rise to novel families of Zr-based multicomponent MOFs. To this end, Yuan *et al.* [162] took advantage of the thermodinamically favored process of achieving highly connected Zr_6 SBUs. For that, they used BTB as

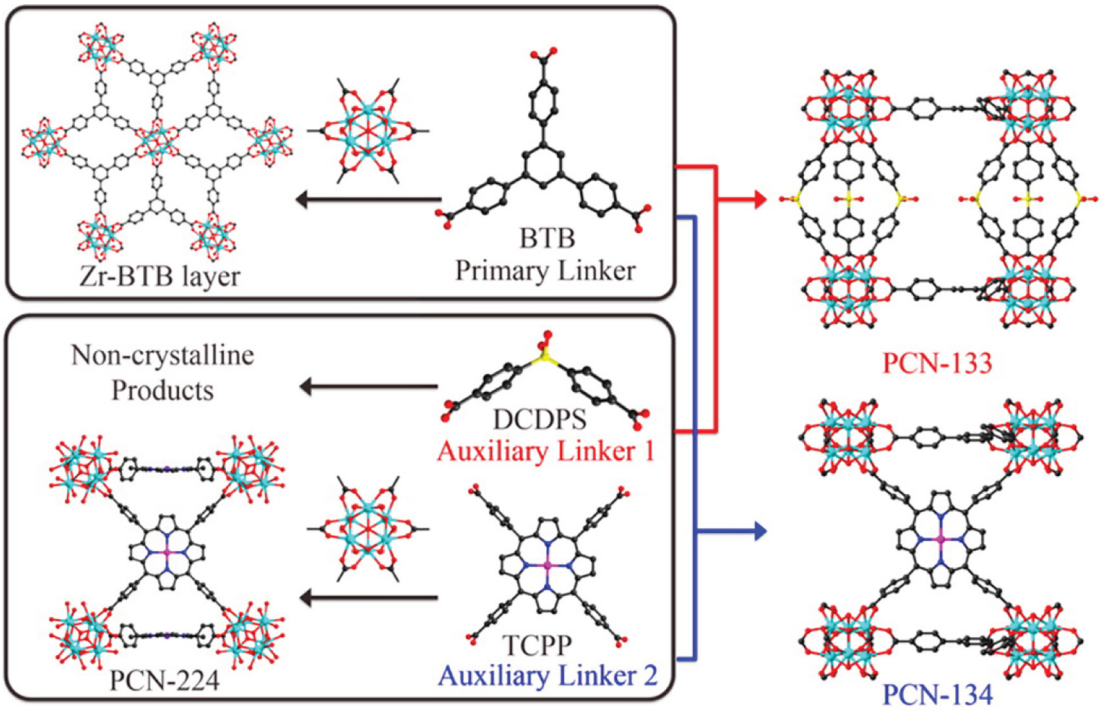

Fig. 12. Thermodinamically-driven construction of mixed-linker Zr-MOFs PCN-133 and PCN134 using BTB as primary linkers and DCDPS and TCPP, respectively, as auxiliary linkers. Adapted from ref. [162] with permission from the American Chemical Society, Copyright 2016.

primary linker that led to the formation of a 2D **kdg** layer [8], which was further connected with an auxiliary ligand, 4,4′-dicarboxydiphenyl sulfone (H_2DCDPS) and tetrakis(4-carboxyphenyl)porphyrin (H_6TCPP), to yield 3D layer-pillared PCN-133 and 134, respectively (Fig. 12). Also, they studied the tolerance to defects in PCN-134, and even more interestingly, how the defect density influence the functionality of the multicomponent material [162]. Another alternative to Zn-based MOFs is represented by MOFs build up with iron-based oxo-centered trimers [163,164]. Despite the difficulties to obtain new examples, due to their tendency to form oxides/hydroxides in common solvothermal conditions, their interesting potential applications in a wide range of fields have made researchers to focus to develop new methodologies to enlarge this family of materials. At this respect, Chevreau *et al.* reported the use of two distinct linkers –BDC and BTB– to built novel Fe-based MOFs [164]. Particularly relevant resulted the mesoporous zeotypic, with a β-cristobalite structure, MOF MIL-143. Although it could not be properly purified, this material represented an interesting avenue to be further followed, and interestingly, it was built up with linkers that can be easily functionalized, which make quite easy to obtain appealing multivariable-multicomponent Fe-based MOFs. In-based MOFs were also prepared from a combination of two distinct ligands [165], which evidenced the general validity of this approach to increase heterogeneity and complexity in MOFs build up with metal ions with very distinct chemical nature.

Although direct synthetic methods have been shown efficient for the obtention of Zr-based multicomponent MOFs, they are quite limited in terms of number of different organic linkers incorporated and with linear linkers tend to form UiO-type frameworks. Conversely, the post-synthetic approach has demonstrated a great versatility to incorporate up to three different linkers into zirconium-based MOFs [48,166–168]. In this context, the so-called sequential linker installation (SLI) [166–168] (Fig. 13A) was firstly validated with PCN-700 –build up with eight-connected $Zr_6O_4(OH)_8(H_2O)_4$ clusters linked with 2,2′-dimethylbiphenyl-4,4′-dicarboxylate (Me_2-BPDC) ligands [166]. This MOF with unsaturated Zr_6 clusters contains two different sizes pockets that enabled the replacement of the terminal OH^-/H_2O ligands in the cluster by distinct (one and two) linear dicarboxylate linkers. This structural feature allowed to obtain a considerable number of multicomponent MOFs (Fig. 13B) –characterized by single-crystal X-ray crystallography– with a precise control of ligands position/functionalities, that otherwise have been found extremely challenging to be synthesized [167]. The limitation of this approach resides on the number of pockets the MOF posses, or in other words the number of accessible unsaturated sites of the SBU. Thus, to extend the complexity of the obtained MOFs, they proposed the use of a linker of low symmetry, which favours the formation of symmetry-reduced MOFs [168]. This led to the obtention of PCN-609, constituted by 8-connected Zr_6 clusters and carbazole tetracarboxylate linkers, which presented three pockets with different lenghts. The post-synthetic insertion of three linkers with the appropiate lenghts and the right order rendered a quinary MOF, where multivariate pore environments could be created. Indeed, the authors proposed a panel of different ligands that could fit in each pocket, which could yield up to 447 distinct MOFs [168].

Previously, Zhang *et al.* [49] reported the first quinary MOF using as initial platform NPF-300 (NPF = Nebraska Porous Framework). In this case, they took advantage of its unique **scu** topology [8], the exchangeable OH^-/H_2O ligands and the relatively large size and flexibility of the primary tetratopic ligand used to build up NPF-300, which offered three singular spaces to enable the linker insertion [49]. Remarkably, they showed that the size-matching of the incorporated linker and the framework strain possesed an important influence on the overall stability of multicomponent MOFs. On the basis of SLI, the approach post-synthetic variable spacer installation (PVSI) [46–49] was developed to been able to install ligands with variable lengths at specific desired positions. PVSI further proved the validity of the post-synthetic approach to obtain multicomponent MOFs, in a controlled manner. An isostructural MOF of PCN-700, LIFM-28 (LIFM = Lehn Institute of Func-

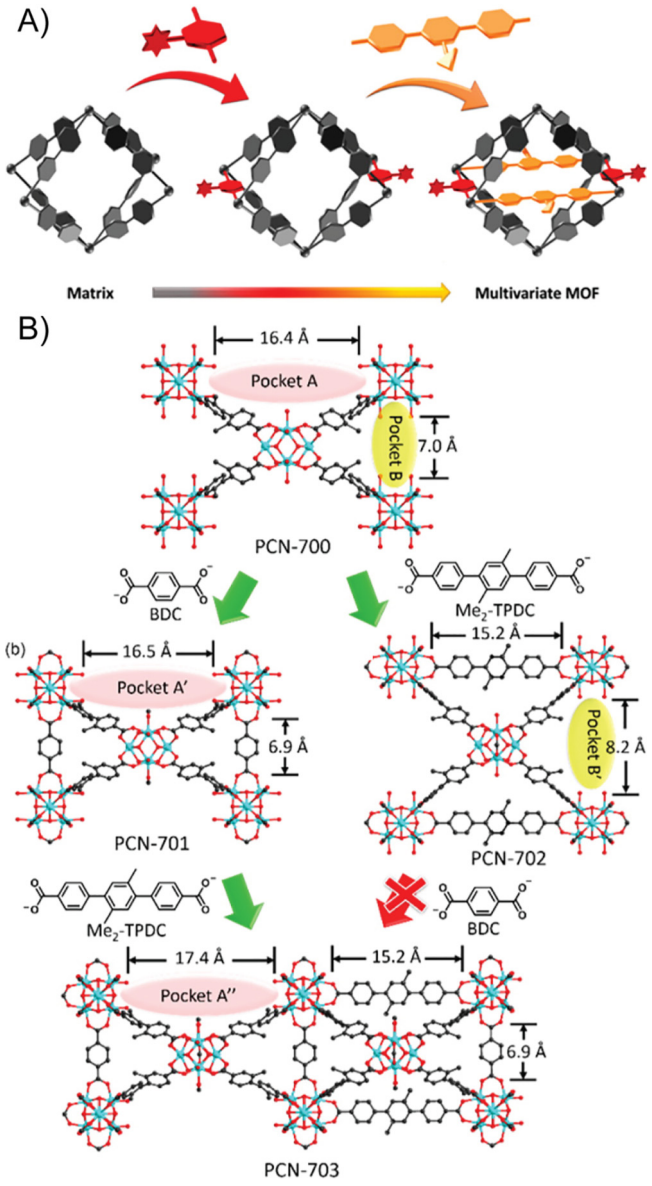

Fig. 13. A) Schematic representation of the sequential linker installation (SLI) strategy consisting on the consecutive "instalation" of BDC and Me_2-TPDC linear dicarboxylate linkers. B) Different multicomponent PCN MOFs obtained by following the SLI strategy. Adapted from ref. [166] with permission from the American Chemical Society, Copyright 2015.

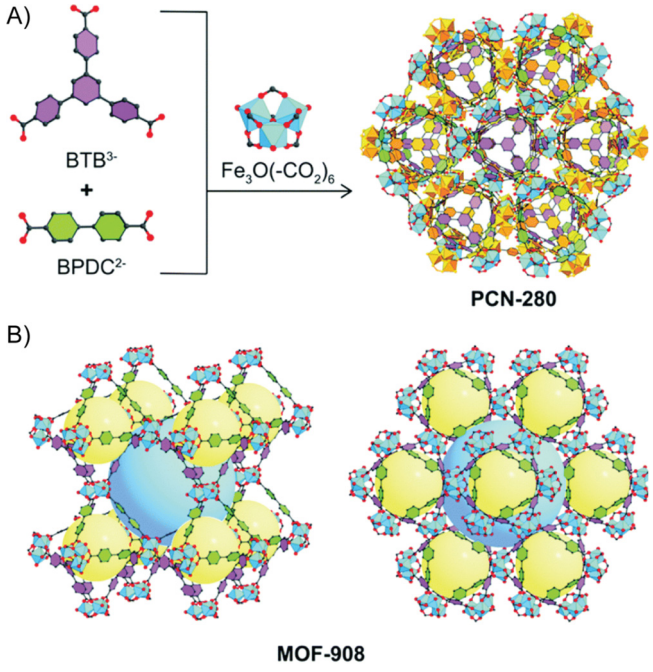

Fig. 14. A) Synthetic route for the preparation of multicomponent MOF PCN-280 by the combination of BTB^{3-}, $BPDC^{2-}$ and $Fe_3O(-CO_2)_6$. B) Structure of MOF-908. Adapted from ref. [175] with permission from the Royal Society of Chemistry, Copyright 2018.

tional Materials) constructed with 2,2′-bis(trifluoromethyl)-4,4′-biphenyldicarboxylate, was selected as initial platform [46]. Interestingly, this MOF presented the particularity that was able to self-adjust to install linkers of variable length –in a reversible way– on one of its pockets, while the other one remained unaltered for functional modification or to host other events [46]. Later on, the authors further studied the reversible installation/uninstallation of linkers of diverse size –shorter for one pocket and longer for the other– on this framework [47]. They exploited these reversible transformations to switch between multicomponent MOFs. This swing-role MOF allowed to develop materials with different applications from a common initial platform [47]. In an analogous manner, by taking advantage of the replacement of the terminal OH ligands at Zr_6 SBUs in NU-1000 by different carboxylate-based molecules, the Solvent-Assisted Ligand Incorporation (SALI) have enabled to obtain different examples of the functionalization of MOFs nodes, and consequently, an increase of MOFs heterogeneity and complexity [50,169–173].

The concept of geometry mismatch has been recently incorporated as a new approach to enlarge the number of known non-default frameworks [174]. Under this frame, different multicomponent Zr_6- and Fe_3-MOFs [175–177] have been prepared using transversal reticular chemistry [178]. For example, Nguyen *et al.* [175] reported two multicomponent MOFs, achieved through a reticular control of the interpenetration in multicomponent MOF PCN-280 (Fig. 14A), where the trigonal prism $Fe_3O(COO)_6$ clusters were connected by BTB and azobenzene-3,3′-dicarboxylic acid (3,3′-azoBDC) in MOF-909 and BTB, BPDC and 3,3′-azoBDC in MOF-908 (Fig. 14B). Both MOFs were isoreticular to MIL-142B [164], but exhibited non-interpenetrated frameworks, which constrasts with the two-fold interpenetrated frameworks, with a **nth** topology [8], of MIL-142B. The authors showed –supported by theoretical calculations– this was due to the presence of the zigzag-shaped 3,3′-azoBDC linker, which generated distortion of the framework preventing the intergrowth of a second **nth** network. These seminals works evidenced the potential of the geometry mismatch concept, which until now have been scarcely exploited. But, for sure it will deliver exciting results in the near future.

ZIFs constitute an especial family of MOFs [179–183], where researchers have also investigated the benefits of building up multicomponent frameworks [85,86,184,185]. Initial efforts on this family were devoted to apply high-throughput methods to discover unprecendeted compositions and structures, which led to multicomponent ZIFs with high thermal and chemical stability, as well as interesting gas adsorption selectivities (Fig. 15) [85,186]. Then, the investigations focused on building up specific targeted topologies [8], such as the **GME** –*e.g.* ZIF-68 to 70 and 78 to 82– or **CHA** –*e.g.* ZIF-300 to 302– with different pore sizes/apertures and functionalities decorating the network, which generates a strong impact on their application performance [86,184]. Then, these investigations have been further extended to develop some design priciples to build up, in a controlled manner, multi-

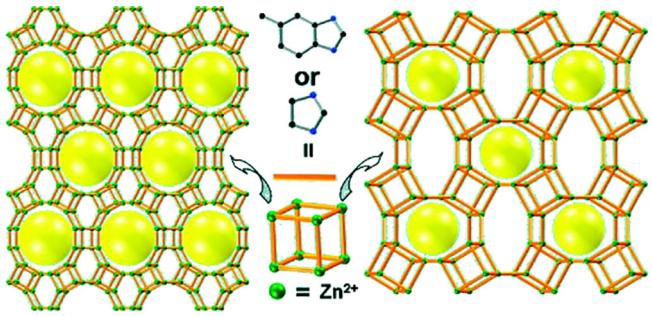

Fig. 15. Schematic representation of the use of complementary ligands strategy for the preparation of novel multicomponent ZIF MOFs. Adapted from ref. [186] with permission from the American Chemical Society, Copyright 2008.

component ZIFs with extra-large pore openings and cages [185]. The authors defined a steric index (δ), and they presented how the combination of different linkers –two and three– with specific range and ratios of δ enabled to obtain novel tetrahedral topologies, some of them unrealized in ZIFs –**afx** and **kfi**– or even in any structure –**ykh**, **gcc**, **ucb** and **bam** [8]. From them, ZIF-412 and 725, which possess the largest cage and aperture size, respectively, are particularly relevant. Besides their structural and synthetic interest, the fascinating large cages of ZIF-412 have shown good performances on the removal of volatile organic compounds (VOCs) from humid air (see section 3.1).

2.3. Mixed-metals metal–organic frameworks

The inorganic part in MOFs represent also an extense area of research to increase the heterogeneity and complexity within them [42,187–193]. Two different subfamilies/scenarios can be considered on the basis of their distinct inorganic constituents: (*i*) metal ions –pre- or post-synthetically incorporated– and (*ii*) SBUs –with one or two distinct metal ions.

Dealing with the first subfamily [194–197], the archetype study was elaborated by Wang *et al.* [198] with five isostructural MOF-74 having 2 (Mg and Co), 4 (Mg, Co, Ni and Zn), 6 (Mg, Sr, Mn, Co, Ni and Zn) 8 (Mg, Ca, Sr, Mn, Fe, Co, Ni and Zn) and 10 (Mg, Ca, Sr, Ba, Mn, Fe, Co, Ni, Zn and Cd) distinct divalent metal ions, respectively [198]. In this investigation, they observed that mixed-metals MOF-74 could be prepared in one-pot reaction of the different metal salts and 2,5-dihydroxyterephtalic acid with good reproducibility (Fig. 16). Also, they reported that this approach enabled the incorporation of metal ions from which the parent (single-metal) MOF structure could not be obtained. Although the precise location of the metal ions could not be elucidated, the high heterogeneity and complexity of the materials obtained in this study were the spark to imagine a more complex metal-composition in MOFs. Indeed, attracted by its potential, different studies have been reported using MOF-74 as platform to build up mixed-metals MOFs with the aim to gain control on metal ions arrangement, and eventually understand their relationship with functionality [199–201]. In this context, Ji *et al.* [70] performed, recently, an intensive study on bimetallic MOF-74 (Co/Cd@85 and 120 °C, Co/Pb@85 °C and Co/Mn@85 °C) systems to elucidate the spatial arrangement of the different metal ions. Indeed, atom probe tomography (APT) (Fig. 17) revealed a different distribution depending on the synthesis temperature and metal ions used. This allowed to obtain unprecedented information of the metal sequences within the metal-oxide rods building heterobimetallic MOF-74. Besides, they proved the validity of the method proposed to map the sequences of neighboring chains.

Mixed-Metals MOFs of other representative networks, such as MOF-5 [202,203], HKUST-1 [204], UiO-66 [205], MIL-53 [206] and 100 [207], have been also synthesized by mixing of metals in one-pot reactions. In particular, different bimetallic combinations of MIL-53(Al/Fe, Cr/Fe, Al/V and V/Cr) [206,208–210], as well as an isoreticular expansion with BPDC ligands [211], have been obtained to investigate the influence on the flexibility and functionality of the resulting materials. Interestingly, it was observed that the breathing was different from either of the single cation analogues and the different composition of metal ions affect to the framework flexibility. Also, it was observed, in some cases, that the synthetic route affect to the arragement of the metal ions on the mixed-metals MIL-53. For instance, Depauw *et al.*, observed microwave procedure led to "egg yolk" mixed-metals MIL-53(Cr/V), meanwhile the solvothermal method renders homogenous mixed-metals MOFs [209]. In a similar manner, Osadchii *et al.* [210] reported that the electrochemical synthesis of MIL-53(Al/Fe) offered improved homogeneous distribution respect post-synthetic methods, which remarkably had a severe impact on its catalytic C–H activation behaviour that ressembled methane monooxygenase enzymes. However, despite the exciting results and remarkable advances –especially in recent examples– on the characterization of the local coordination environment of different metals, it has found still difficult to have a precise control on their spatial arrangement through the network. In this sense, a remarkable work was developed by Liu *et al.* [54] who showed beautiful examples of the different organization through the network of distinct combinations of two metal ions building the triangular oxo-centered SBUs (Fig. 18). From the nine mixed-metals MOFs reported, the authors focused –with the aim to unveil metal ions arrangement– on $(Mn_{1.45}Fe_{1.55}O)_2(TCPP\text{-}Ni)_3$ and $(Ni_{2.07}Fe_{0.93}O)_2(TCPP\text{-}Co)_3$, where TCPP stands for tetrakis(4-carboxylatephenyl)p

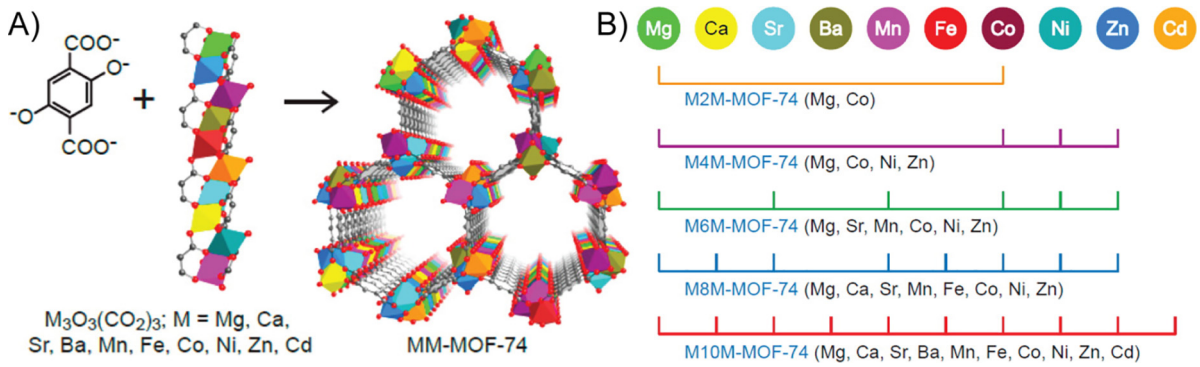

Fig. 16. A) Schematic representation of the synthetic approach for the preparation of MM-MOF-74. B) Different combination of metals used to synthesize MM-MOF-74. Adapted from ref. [198] with permission from the American Chemical Society, Copyright 2014.

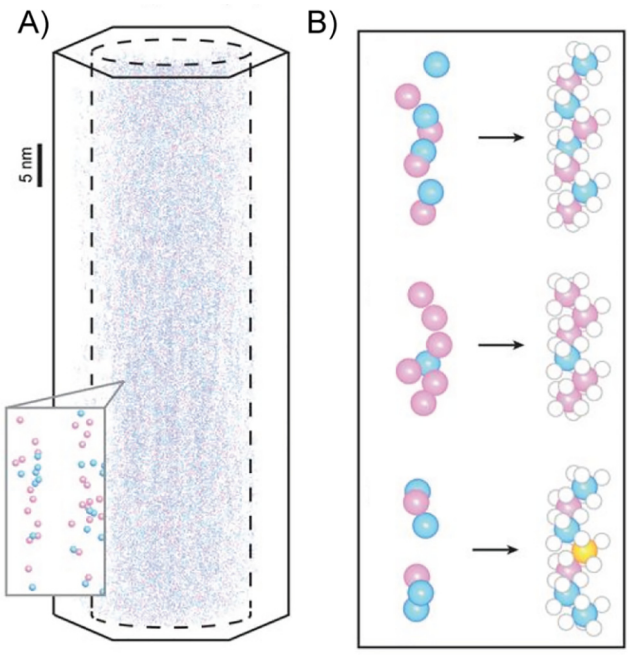

Fig. 17. A) 3D-APT reconstruction of MOF-74 (Co/Cd) showing all the metals detected (Co and Cd are represented by blue and pink spheres respectively). B) Different zoomed-in regions showing, in more detail, the metal chains in MOF-74 (Co/Cd). Adapted from ref. [70] with permission from the American Association for the Advancement of Science (AAAS), Copyright 2020.

orphyrin. From a combination of spectroscopic techniques, the authors observed a domain arrangement of metal ions in $(Mn_{1.45}Fe_{1.55}O)_2$(TCPP-Ni)$_3$ and a well-mixed scenario for $(Ni_{2.07}Fe_{0.93}O)_2$(TCPP-Co)$_3$. Most likely, as it has been suggested by the authors, this was related to the differences/semblances of each pair of metal ions in terms of ionic radius and affinity to coordinate with oxygen. Interestingly, this different arrangement showed a severe impact on the band structure of MOFs, and consequently, on their catalytic performance.

Besides mixing metals in one-pot reactions, PSMs have also shown efficient for the obtention of mixed-metals MOFs. Mainly three different situations have been observed, the partial cation exchange of structural ions, the metalation of SBUs and the coordination to ligands. Post-synthetic ion-exchange have revealed as a very poweful tool to develop a wide range of multifunctional MOFs with improved stability and performances respect to the pristine MOFs [12–17,212]. However, it has been commonly associated to achieve a full metal exchange. So, only the intermediate species and not the final materials could be considered as mixed-metals MOFs [213–220]. In this sense, Brozek *et al.* [216] reported post-synthetic metal exchange of different transition metal ions –Ti^{3+}, $V^{2+/3+}$, $Cr^{2+/3+}$, Mn^{2+} and Fe^{2+}– in MOF-5 (Fig. 19). They observed the degree of exchange was dependant of the nature of the metal ion, and in any case led to a complete transmetallation [216]. Remarkably, this study was a clear example of the potential of PSMs allowing to obtain novel materials, which could not be obtained by typical synthetic pathways.

Song *et al.* [218] observed the influence of the framework flexibility on the degree of post-synthetic metal-exchange. While the rigid Zn-HKUST-1 [221] could be partially transmetallated with copper(II), the flexible Zn-PMOF-2 [222] was possible to achieve a full transmetallation –PMOF stands for MOP-based MOFs. Interestingly, partially transmetallated ZnCu-PMOF-2 presented a core–shell heterostructural framework [218]. This post-synthetic metal ion exchange also have been performed in more robust MOFs. For instance, Kim *et al.* [123] reported the metal exchange between preformed MIL-53(Al) and MIL-53 (Fe). In this work, attempts to incorporate Ti(IV) and Hf(IV) to UiO-66(Zr), were shown unsuccessful, as some of the same authors uncovered latter [223]. Other groups have tried this challenging process using different titanium precursors. However, the reported results respect the position the titanium(IV) ions ocuppied were not in agreement. Santaclara *et al.* [224] demonstrated in detail that in NH_2-UiO-66 Ti^{IV} was appended to a linker vancancy. Meanwhile, Tu *et al.* [225] and Chen *et al.* [226] reported the post-synthetic replacement of zirconium(IV) ions by titanium(IV) following a microwave procedure in UiO-66 (Fig. 20A) and PCN-224 (Fig. 20B), respectively. Thus, further work to develop and precisely characterize novel [227] systems incorporating titanium(IV) will be highly desirable. This not just will allow to deliver very interesting materials from a functionality viewpoint. But also, it will help to unveil with atomic precision the arrangement of titanium ions within the framework and its relationship with their performance, which undoubtedly have been the sharpest striking force in the exponential growth of MOFs.

Another recent relevant example was the work by Padial *et al.*, [60] where the authors studied in detail the metal-induced topological transformations on a previously reported heterobimetallic Ti_2Ca_2 MUV-10 [119] (MUV = Materials of University of Valencia) into MUV-101(Fe,Co,Ni,Zn) and MUV-102(Cu), which are isostructural to MIL-100 and HKUST, respectively (Fig. 21). Indeed, the information extracted from this investigation was useful to envision future real-world applications of these materials, such as the degradation of nerve agents simulants in non-buffered conditions [228].

Post-synthetic metalation of SBUs have been commonly addressed with traditional common solution-phase procedures [229–236] and atomic layer deposition (ALD) [227,237–240]. Here, we would like to note that despite the studies on most of the reported examples are focused in particular metal contents, the approach used to synthesize them make possible to obtain other metal ratios. For this reason, they have been considered in this manuscript. A nice exponent of the first type was reported by Manna *et al.*, [231] where to a Zr-MOF –constructed with 4,4′-bis (carboxylatephenyl)-2-nitro-1,1′-biphenyl (TPHN) linker– with an UiO-69 topology, were incorporated MgMe by treating the MOF with Me_2Mg in THF at room temperature [231]. The thorough characterization of this MOF showed that 4 Mg centers were anchored per Zr_6 node. Unfortunately, in contrast to other reported cases [230], it was not possible to solve by SCXRD the Mg coordination environment. Nevertheless, this study evidences the potential of MOF methodologies to develop novel and highly performant single-site earth-abundant metal catalysts, circunventing traditional synthetic drawbacks. In an alternative manner, ALD has added new possibilities to increase complexity and metal ions diversity within MOFs. Recently, Hackler *et al.* [240] have kept demonstrating the potential of this approach with the metalation of NU-1000 –NU = Northwestern University; this is a zirconium-MOF built up with $[Zr_6(\mu_3\text{-}O)_4(\mu_3\text{-}OH)_4(OH)_4(H_2O)_4]^{8+}$ SBUs and tetratopic 1,3,6,8-tetrakis(*p*-benzoate)pyrene ligands– through the hydroxyl and aquo groups residing at the Zr node within the large (31 Å) hexagonal pores (Fig. 22A). In particular, they incorporated diverse metal ions –Cu, Cd, Co, Fe, Ga, Mn, Mo, Ni, Sm, W, Zn, In and Al–, and even more interestingly, bimetallic combinations of Co-Zn and Zn-Co [240]. Lately, Thiam *et al.* [241] have applied novel techniques for SBU metalation, commonly applied in surface organometallic chemistry. They reported the anchoring of a W $(\equiv C^tBu)(CH_2{}^tBu)_3$ complex on the mesoporous NU-1000 (Fig. 22B). However, instead to be located in the expected large hexagonal channels, first-principles simulation showed that the grafted complexes were found preferentially localized in the small

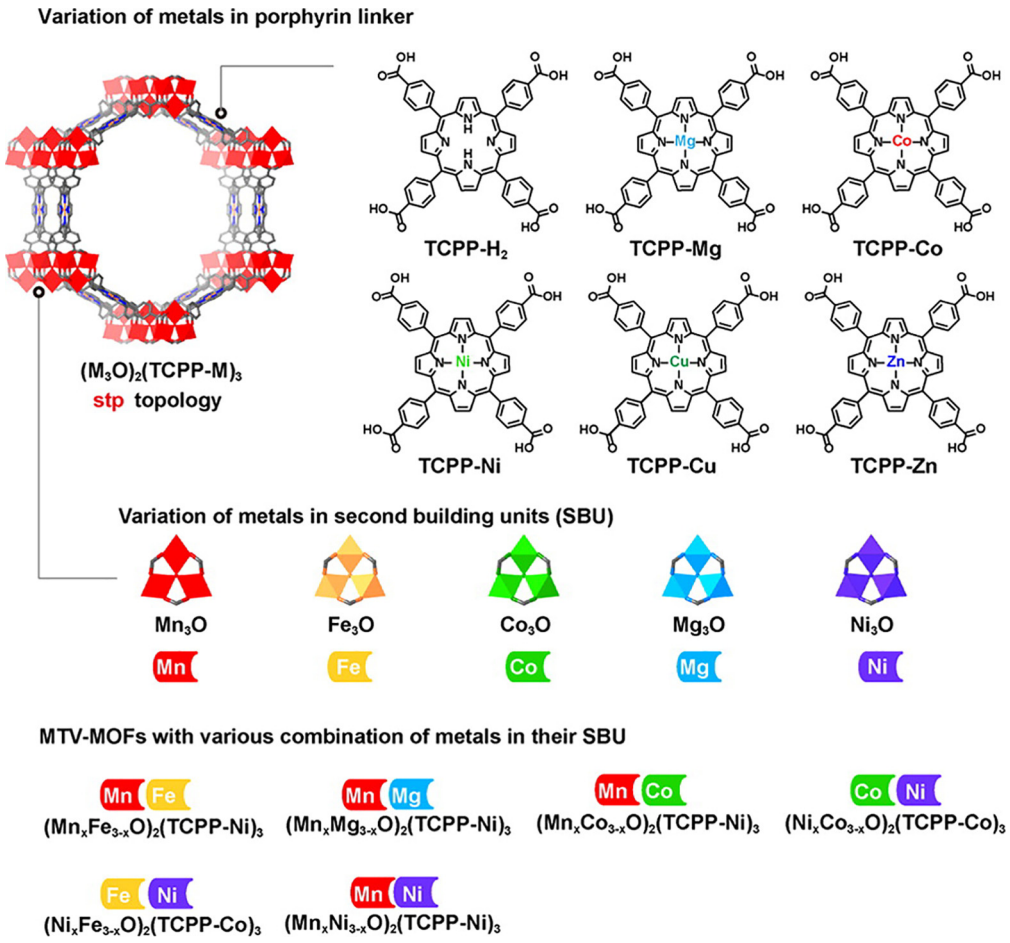

Fig. 18. Different combinations of SBUs and porphyrin ligands that yield MTV-MOFs with mixed-metals SBUs. Reproduced from ref. [54] with permission from the American Chemical Society, Copyright 2016.

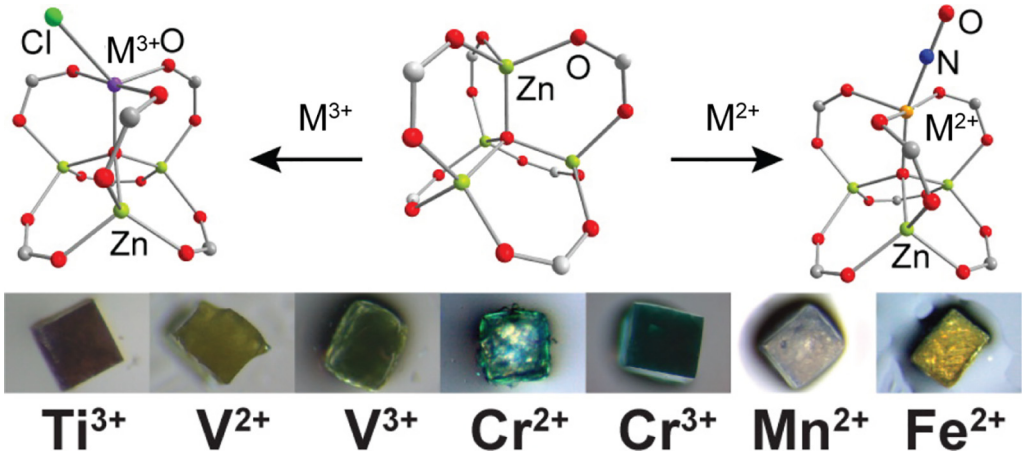

Fig. 19. Partial post-synthetic metal exchange in MOF-5 clusters yielding pseudotetrahedral V^{2+}, Cr^{2+}, Mn^{2+}, Fe^{2+}, Co^{2+}, and Ni^{2+} and pseudotrigonal bipyramidal Ti^{3+}, V^{3+}, and Cr^{3+} with terminal chloride moieties. Single crystals after every PS process can be observed in the bottom. Adapted from ref. [216] with permission from the American Chemical Society, Copyright 2013.

ones. DFT calculations were also used to identify all the steps leading to the final anchored tungsten complex. This work nicely illustrates that the potential MOFs intrinsically posses to benefit of cross-fertilization from other research fields, which undoubtedly strengthten and enlarge the academic and industrial interest of MOFs.

The use of auxiliary chelating groups –commonly with soft-basicity, *e.g.* (by)piridine, pyrazole, thiol/thiolate and phosphine derivatives– in the organic linkers used to build up a targeted MOF and pre-/post-synthethic functionalization of linkers to introduce preformed complexes/coordinating sites have been widely used for embedding metal ions in MOFs. This not only have ren-

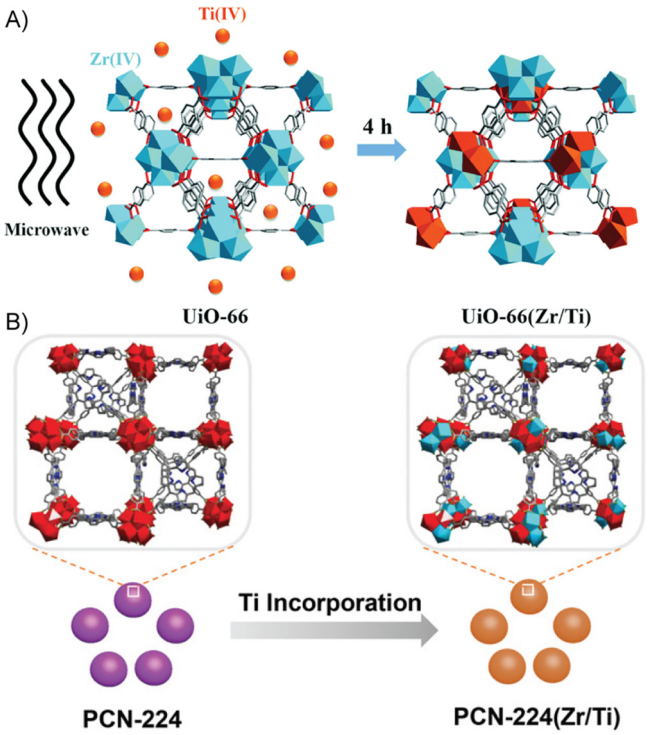

Fig. 20. Partial post-synthetic exchange of Zr(IV) metal cations by Ti(IV) ones in UiO-66 and PCN-224 MOFs, respectively. Adapted from refs. [225] and [226] with permission from the Royal Society of Chemistry and John Wiley & Sons, Copyright 2017 and 2020.

dered frameworks with increased complexity and heterogenity, but more interestingly, with novel functionalities [242–256]. In this context, a fascinating example was reported by Gonzalez *et al.* [249] with the development of a Zr_6-MOF constructed with 2,2′-bipyridine-5,5′dicarboxylate (DCBPY). This enabled to obtain a bipyridine-multidentate coordination environment, which stabilize discrete inorganic clusters constrained within MOFs channels (Fig. 23A). By controlling the metalation conditions, they showed the controlled growth of atomically defined $NiBr_2$ and MCl_2 (M = Ni, Co, and Fe) sheets. Interestingly, as it has been observed in others clusters formation [23,24,257–262], the confinement and functionalities within the MOFs pores defines the composition and structure of these sheets, and interestingly, it helps to unveil in differents steps of the metalation and sheets-growth process –by means of single-crystal X-ray crystallography– their structure. The metalation process has been also recently coupled with other post-synthetic processes to design enzyme-inspired environments within mesoporous MOFs (Fig. 23B) [255]. They prepared a multicomponent MOF of formula $Al(OH(DCBPY)_{0.8}(PDAC)_{0.2}$ (H_2PDAC = 1,4-benzenediacrylic acid) to which after ozonolysis [263] the PDAC linkers were removed to afford $Al(OH(DCBPY)_{0.8}(OH)_{0.4}(H_2O)_{0.4}$. Then, treatment with trimethylsilyl trifluoromethanesulfonate (Me_3Si-OTf) and installation of preformed complex $[Ir(PPY)_2(DCBPY)]^+$ (PPY = 2-phenylpyridine) allowed to generate strongly Lewis Al-OTf and photoredox sites, respectively, within Al-MOF mesopores [255].

Alternatively to previous methodologies to incorporate metal ions in MOFs, Wang *et al.* reported the molecular vise approach (Fig. 24) [253]. This consisted on the construction of a multicomponent MOF, where there has been a partial replacement of the positions occupied by tetratopic linkers by a pair of tritopic and monotopic ones, which were arranged in opposite positions. This allowed to create a metal binding-site that can be modulated through the exchange of the monotopic linker, which provides unique coordination environments to bind with distinct metal ions –Mg^{2+}, Al^{3+}, Cr^{3+}, Mn^{2+}, Fe^{3+}, Co^{2+}, Ni^{2+}, Cu^{2+}, Zn^{2+}, Ag^{+}, Cd^{2+} and Pb^{2+} (Fig. 24C).

Respect the family of distinct SBUs, it has been to say that the degree of control to build up them in a highly controlled manner is still quite limited, and even some of them have been obtained in a serendipitous manner. Nevertheless, different strategies have been followed to succeed on this challenging task [264–267]. For example, the use of non-symmetric linkers somehow guides to the formation of different SBUs using a unique single metal ion. This has been evidenced with the formation of UMCM-150 [264] –constructed with biphenyl-3,4′,5-tricarboxylic acid (H_3BPT) and two types of SBUs, the well-known Cu(II) paddle-wheel and a rare trinuclear Cu(II) cluster (Fig. 25)– and a MOF consisting of truncated cuboctahedra as supermolecular building blocks (SBBs) connected to trigonal Cu(II) trimers, when reacting 5-

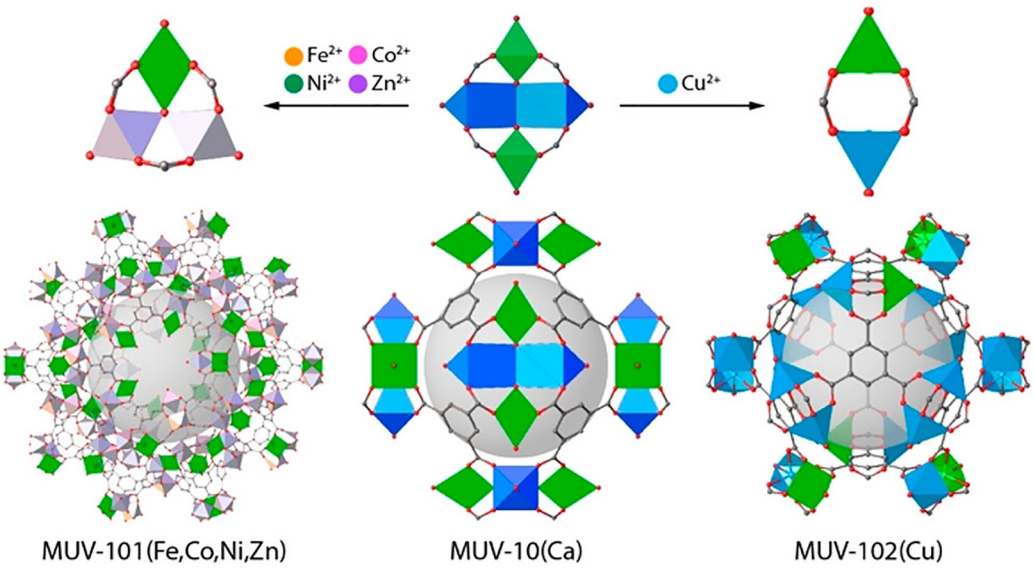

Fig. 21. Partial post-synthetic metal cation exchange in MUV-10(Ca) to give MUV-101(Fe, Co, Ni, Zn) and MUV-102(Cu). Adapted from ref. [60] with permission from the American Chemical Society, Copyright 2020.

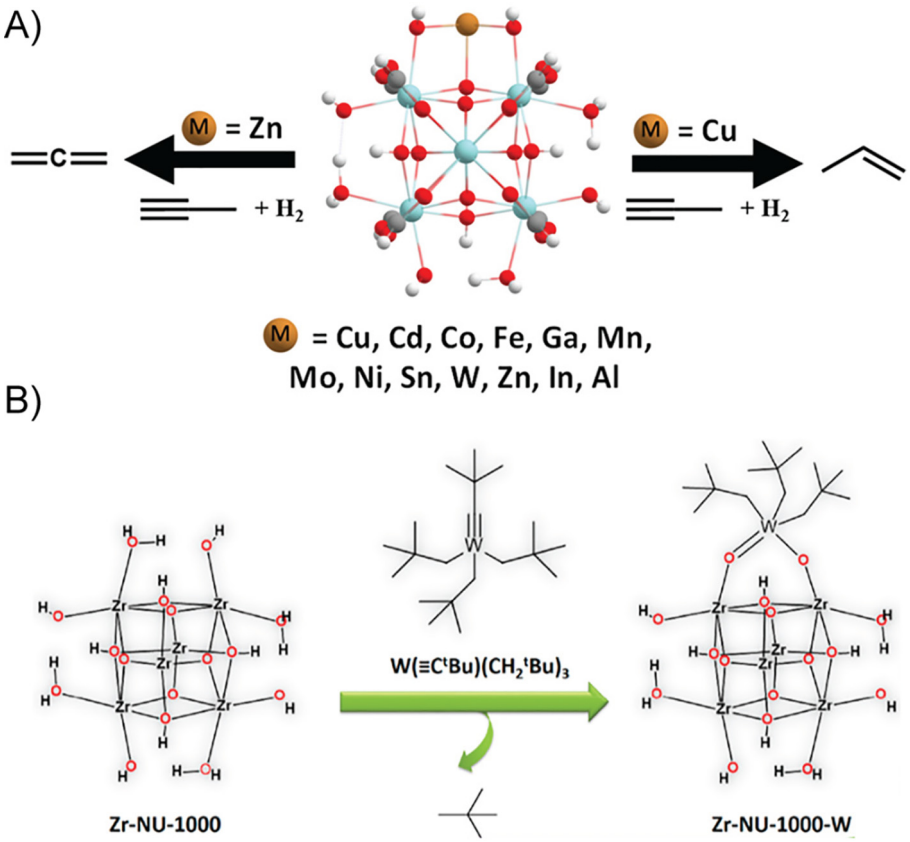

Fig. 22. Schematic representation of the incorporation of metal oxide clusters into the pores of the NU-1000 via atomic layer deposition (ALD) (A) and anchoring of W(≡C^{t}Bu)($CH_2{}^t$Bu)$_3$ complexes on the mesoporous NU-1000 (B). Adapted from refs. [240] and [241] with permission from the American Chemical Society, Copyright 2020.

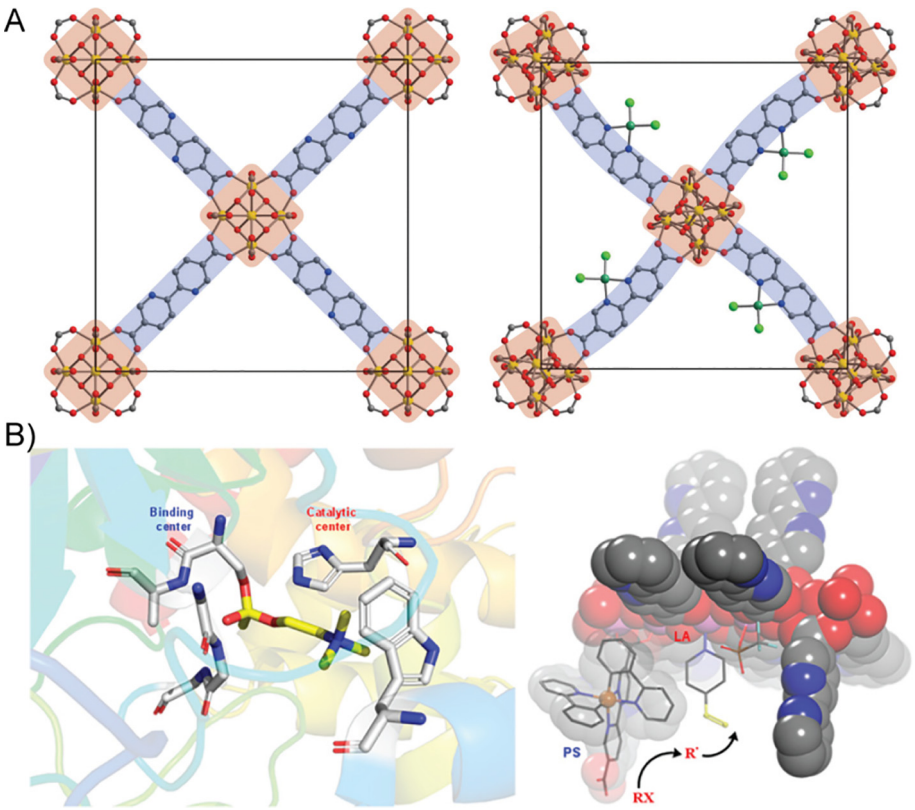

Fig. 23. A) Crystal structures of Zr_6-MOF constructed with DCBPY before (left) and after metalation (right). B) Enzyme active site with binding center (left) and mesopore in **1**-OTf-Ir MOF with the $[Ir(PPY)_2(DCBPY)]^+$ complex (right). Adapted from refs. [249] and [255] with permission from the American Chemical Society, Copyright 2015 and 2020.

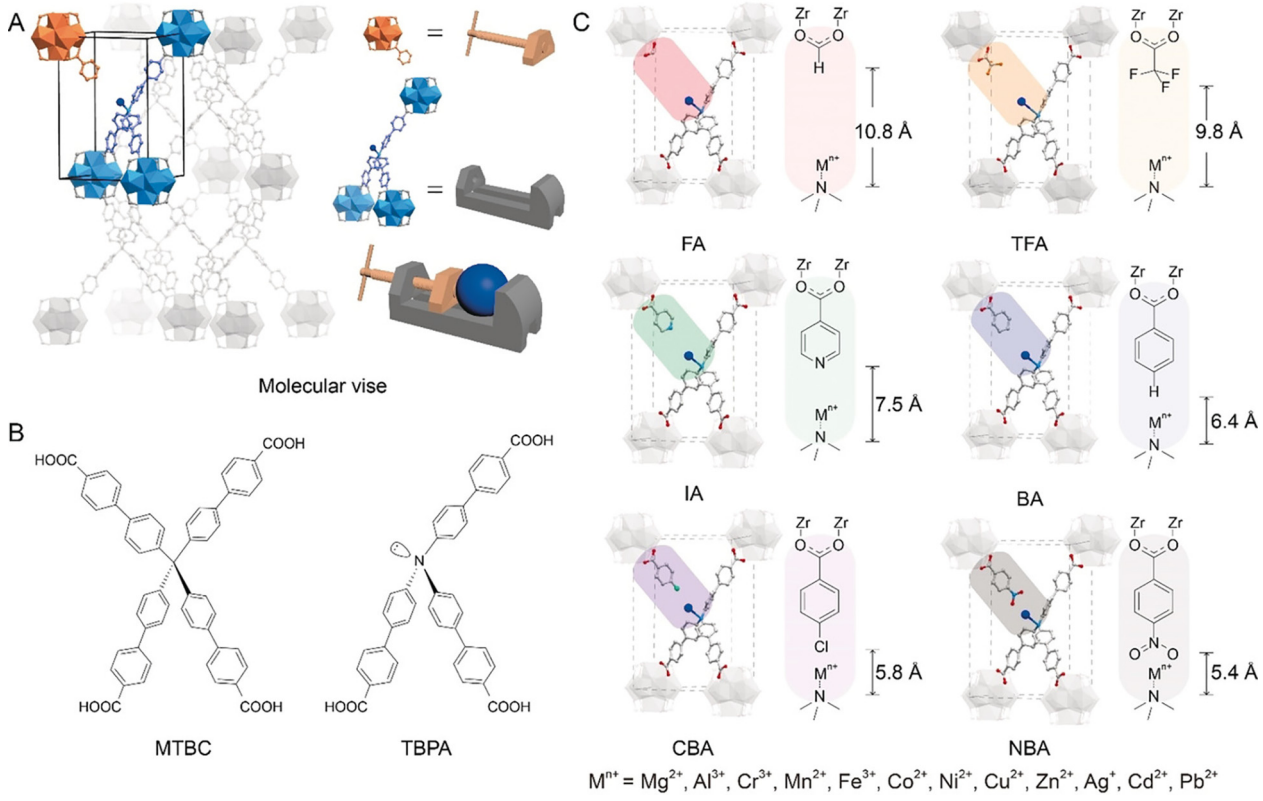

Fig. 24. A) Illustration of the multicomponent PCN-521 MOF created by the molecular vise approach. B) Organic ligands used. C) Different metal-binding sites created by various monotopic linkers. Reproduced from ref. [253] with permission from the American Chemical Society, Copyright 2008.

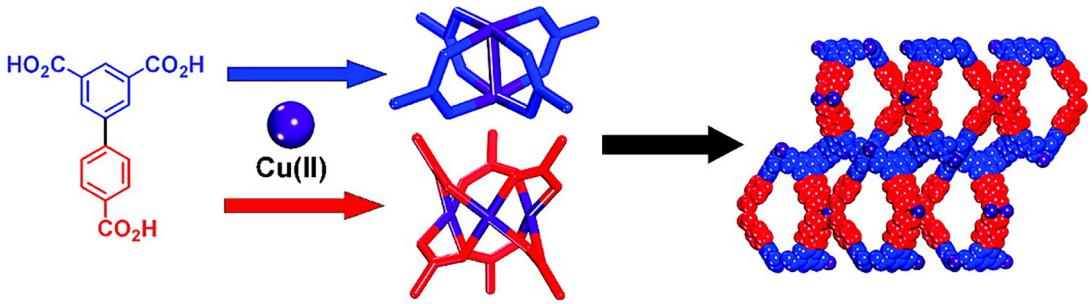

Fig. 25. Schematic representation of the formation of UMCM-150 by combining the non-symmetric linker H_3BPT and two different SBUs. Reproduced from ref. [266] with permission from the American Chemical Society, Copyright 2008.

tetrazolylisophthalic acid and copper(II) nitrate hemihydrate [266].

The use of metal ions with great coordination plasticity have been also proposed to construct MOFs with different SBUs, which have led to very intrincate structures [268–271]. Besides, it has been proposed the use of two distinct metals ions [272–274]. This approach was mainly based on the different coordination environment preferences of each of them. Tu *et al.* [273] reported a mesoporous MOF built up from three geometrically different SBUs. Despite only one organic ligand –4-pyrazolecarboxylic acid (H_2PyC)– was used, the mixing with two metal ions –Cu(II) and Zn(II)– form the triangular Cu_3 and octahedral and square pyramidal Zn_4 SBUs, which led to four types of polyhedral cages in the framework [273]. Other authors have also applied the same approach with PyC as linker, but using different pairs of metal ions [274]. This have led to the formation of MOF-818 and 919 (Fig. 26), which contain three unprecented mesoporous cages **wuh** (MOF-818) and **yys** and **liu** (MOF-919) [8]. In these MOFs, the PyC linker acted as edge in the structure, while the distinct SBUs functioned as vertices. In particular, MOF-818 was built up with $Zr_6(\mu_3\text{-}O)_4(\mu_3\text{-}OH)_4(OH)_6(\mu\text{-}PyC)_6(H_2O)_6$ and $Cu_3(\mu_3\text{-}O)(\mu\text{-}PyC)_3(H_2O)_3$ SBUs, whereas MOF-919 was constructed by $M_3(\mu_3\text{-}O)(OH)_3(\mu\text{-}PyC)_6$ (M = Sc, Fe and Al) and the same triangular Cu_3-SBU of MOF-818. Remarkably, this work unveils precious information of the relevance of the connectivity of vertices to synthesize large molecular cages –which until that moment was either focused on the use of large linkers or increase the number of vertices [152,275,276]. From the systematical analysis performed, they concluded that the size of the cage was directly proportional to the number of vertices –when equal connectivity– and that a reduced connectivity of the vertices in the polyhedral renders larger growth of cage size, when the number of vertices is the same.

The metalloligand design strategy have rendered beautiful examples of mixed-metals frameworks with exciting functionali-

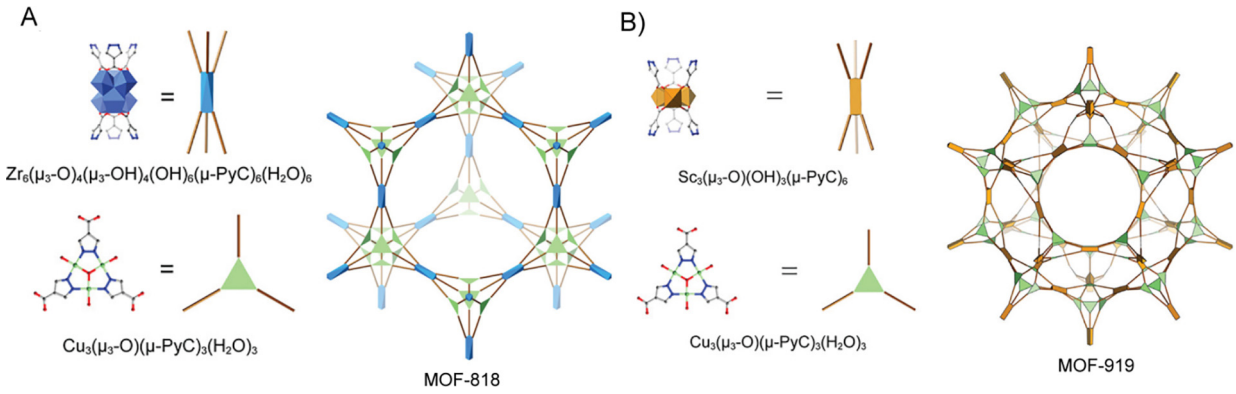

Fig. 26. Schematic representation of MOF-818 (A) and MOF-919 (B) and their respective SBUs. Adapted from ref. [274] with permission from the American Chemical Society, Copyright 2019.

ties [277–279]. However, most of them led to MOFs where the metal ions ratio is difficult to be modified. An elegant approach to obtain mixed-metals MOFs using preformed metalloligands was reported by Tan *et al.*, [280] where they performed one- or two-step post-synthetic ligand exchange on UiO-68 with preformed chiral metallosalen complexes [280]. Using direct synthesis, Xia *et al.* [281] reported the use of up to three distinct chiral metallosalen complexes to build seven chiral, porous and interpenetrated 3D Zn_4-MOFs with ***pcu*** topology –five with combinations of two distinct metalloligands (CuV, CuMn, CuCr, CuFe and CuCo) and two with three of them (CuMnCr and CuMnCo). Interestingly, the interpenetration nature of these materials brings distinct metallosalen subunits adjacent to each other, which endows them with the possibility of cooperative activation of substrates, and then improved functional performance.

2.4. Mixed-ligands and metals metal–organic frameworks

The incorporation of different linkers and metal ions/SBUs, represents the highest level of synthetic complexity. Thus, it results reasonable that the number of examples belonging to this group is still quite scarce, compared to previous sections. Nevertheless, some beautiful systems have already been reported [282–286], which evidence the feasibility of this task. Moreover, these works allow to envision that the rational construction of highly heterogenous MOFs platforms, able to reach the complexity of biological systems from both a structural and functional viewpoint, is also achievable.

Pore partition strategies have shown successful to obtain materials with enhanced functionalities respect the pristine MOFs [78,79,287,288]. Relevant to our topic, this approach has enabled to obtain different systems –constructed in one-pot reactions– with distinct organic and inorganic constituents [282–284]. In this sense, Zhao *et al.* [282] reported the construction of 23 multicomponent MOFs with a partitioned **acs** topology –**pacs**– [8], where they use di- and trinuclear 1,2,4-triazolate (TRZ) based complexes as pore-partition agents [282]. From them, it results especially relevant the high tunability reached with the family coined as TRZ-pacs-D with the general formula $[(M_1)_3O(L_1)_3][(M_2)_3(L_2)_3X_6]$ ($X = H_2O$ or Cl^-). The $[(M_1)_3O(L_1)_3]$ subunit represents the core formula of the **acs** net and the triazolate dimer $[(M_2)_3(L_2)_3X_6]$ –where M_1 = Fe, In and In/Co; L_1 = BDC or its derivatives; M_2 = In, Zn, Ni, Co, Fe, Mn, Mg and In/Co and L_2 = TRZ or its derivatives. Remarkably, compared to the partition approach with 2,4,6-tri(4-pyridyl)-1,3,5-triazine, this approach allows to have a much greater diversity and heterogeneity –due to the countless combinations of azolate ligands and metals ions as partition agents– and introduces in a controlled manner different SBUs, which enable to control the arrangement and orientation of open metal sites and have the potential to endow materials with multifunctionality.

Several examples of quaternary and quinary systems have been prepared using direct syntheses. For example, using PyC ligands and based on the different binding affinities of pyrazolate and carboxylate toward copper and zinc, Tu *et al.* [289] reported two quaternary MOFs with BDC as cooperative second organic linker for the construction of FDM-6 and 2,6-naphthalenedicarboxylic acid (H_2NDC) for FDM-7 –FDM stands for Fudan material (Fig. 27) [289]. In both cases, the trinuclear complex $[Cu^{II}_3(\mu\text{-OH})(HPyC)_3]^{2+}$ acted as tritopic carboxylate-metalloligand during the MOF synthesis. In FDM-6, each octahedral Zn_4O SBUs was coordinated with four triangular Cu_3 units and two BDC linkers, which led to a framework with **umt** topology [8] and isoreticular to (3,6)-coordinated UMCM-2 [41,138,139] with five kinds of microporous cages and two mesoporous ones. On the other hand, FDM-7 contains two types of octahedral Zn_4O SBUs, the trinuclear complex and as linear ditopic linkers NDC and PyC, which led to three different types of cages (Fig. 27). Interestingly, the trinuclear complex $[Cu^{II}_3(\mu\text{-OH})(HPyC)_3]^{2+}$ can be reduced, in a reversible manner, to $[Cu^{I}_3(HPyC)_3]$, without altering the connectivity of the frameworks. This has a significant impact on their catalytic functionality, and more importantly, evidences the potential redox-active MOFs posses in a wide range of fields [290]. They would add a novel vertex of complexity in mixed-component MOFs. But, this has been scarcely investigated. Thus, it represents an area that deserve more attention and further exploring. In addition, in this work the authors also reported two fascinating mixed-metals MOFs (FDM-4 and 5) with six and five distinct SBUs, respectively –due to the chemical plasticity/versatility of Zn in contructing different SBUs and the easiness of copper to form a triangular metalloligand with PyC. Later on, some of the same authors, reported the first quinary MOF synthesised in a one-pot self-assembly process (FDM-8) [291], which was constructed with three linear ditopic linkers –PyC, BDC and NDC– and two metal ions –Zn and Cu, that form octahedral $Zn^{II}_4O(COO)_6$ and triangular $Cu^{I}_3(NN)_3$ SBUs involving all three organic linkers and the PyC ligand, respectively [291]. The authors obtained FDM-8 combining their experience with the previous knowledge on assembly multicomponent MOFs –the diversified node geometry applied to get UMCM-1 and the diversified edge length approach to prepare MUF-7a– together with the proposed deconstruction strategy, based on the use of triangular Cu^{I}_3 SBUs, instead of commonly used tris(carboxylates) to obtain other mixed-component MOFs. Remarkably, they turn of the screw on the complexity point-of-view and took advantage of the distribution of organic linkers on the cages presents in FDM-8 to construct two

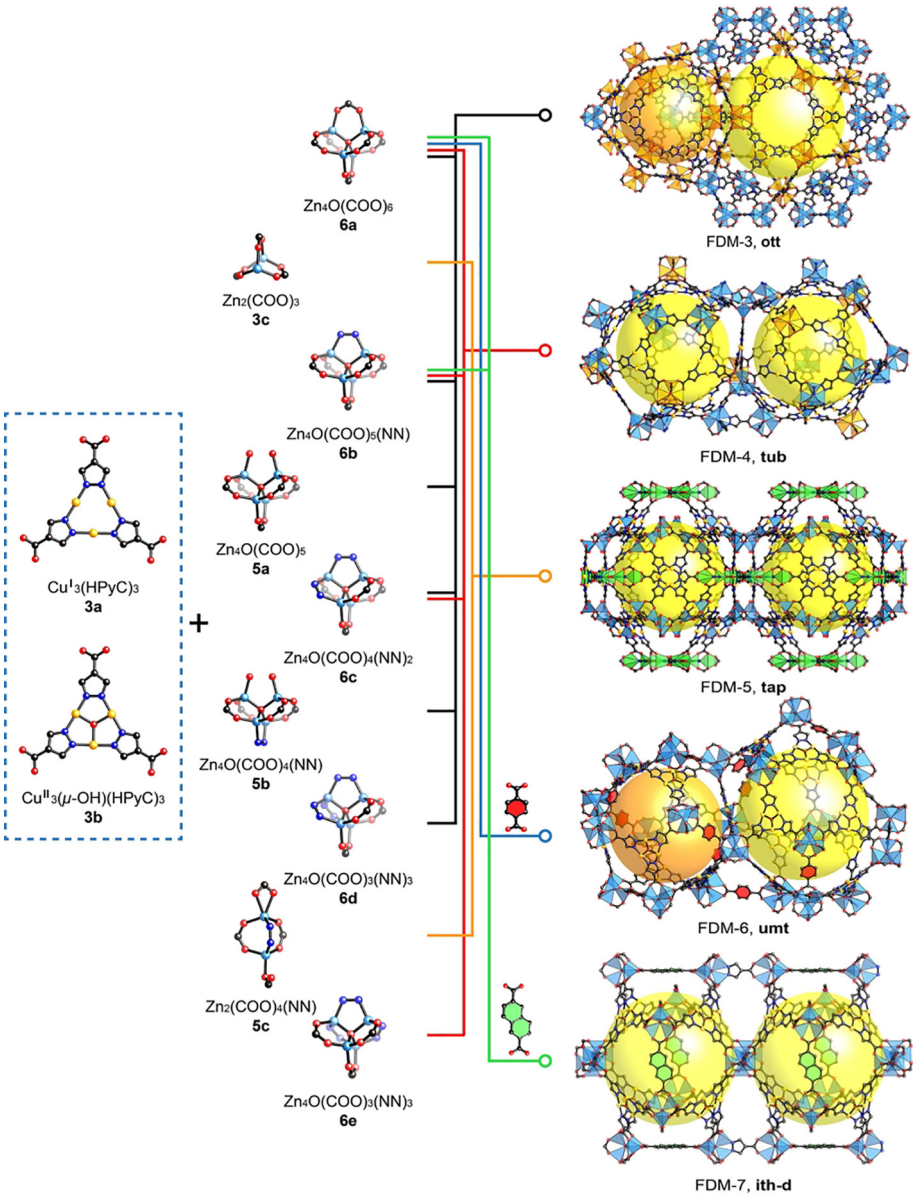

Fig. 27. Construction of multicomponent FDM MOFs and the different present SBUs. Reproduced from ref. [289] with permission from the American Chemical Society, Copyright 2017.

isoreticular MOFs, where it is possible to specifically functionalize one cavity, without modifying the environment of the other.

Alternatively, Fei *et al.* [292] used PSMs to develop mixed-ligands and metals MOFs. They selected ZIF-8 and 71 as initial platforms and applied stepwise tandem post-synthetic exchange of metal ions and linkers (Fig. 28). In particular, they introduced redox-active Mn(II) ions into both Zn(II)-based ZIFs and 4-bromo-imidazole replacing 4,5-dichloro-imidazole. Interestingly, they found the order of the tandem exchange do not have an appreciable influence on the final MOF [292]. In a similar manner, applying PSMs, Tu *et al.* [293] reported the creation of ordered ligand and metal vacancies in a cubic Zn-based MOF with pyrazole carboxylic acid as linker. Then, they used these vacancies to incorporate new metals and organic ligands, which allow them to obtain up to eight novel mixed ligands and metals MOFs with absolute control and order in a single-crystal to single-crystal manner [293].

3. Current reported applications

The interest of mixed-component MOFs results not only in the structural richness, as seen below, also in the properties (Fig. 3) that are not just a mere linear combination of the pure constituents. In the following subsections we will present some of the most recent/relevant advancements in different research areas, trying to highlight the main importance of the intrinsic features of mixed-component MOFs to render superior features than single-component ("traditional") MOFs.

3.1. Gas storage and separation

Since the advent of MOFs, significant research has been made on the gas sorption properties of these materials due to their exceptional porosity. In this sense, the ability to tailor pore size

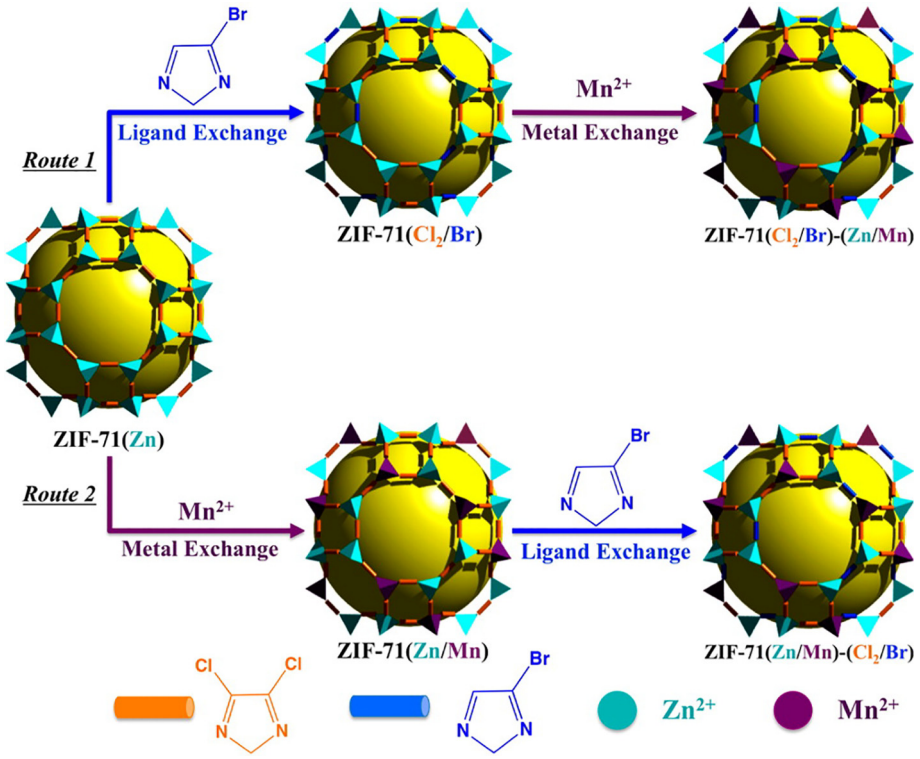

Fig. 28. Stepwise strategy to develop mixed-ligands and metals MOFs from ZIF-8 and MOF-71. Reproduced from ref. [292] with permission from the American Chemical Society, Copyright 2013.

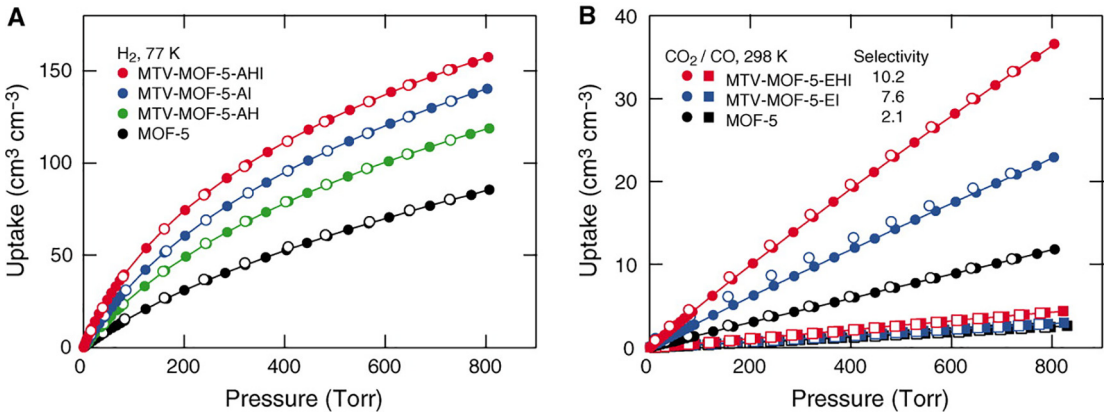

Fig. 29. H_2 (A) and CO_2/CO (B) adsorption isotherms of MTV-MOF-5-EI (blue), -EHI (red), and MOF-5 (black). Reproduced from ref. [43] with permission from the American Association for the Advancement of Science (AAAS), Copyright 2010.

and environment functionalization has revealed as an extremely important tool to gain control on the stablished host–guest interactions, as well as to understand MOFs adsorption capacity of small molecules and ability for their separation. Although, these properties have been extensively studied on simple MOFs, the intrinsic and increased complexity of mixed-component MOFs have opened a myriad of new opportunities. Indeed, initial efforts to obtain multivariate and multicomponent systems were somehow related to improve the gas adsorption and separations properties of MOFs [43,49,78,98,150,153,291,294,295]. This was beautifully illustrated with MTV-MOF-5 (Fig. 4) [43], where the authors reported a 400% improved selectivity for CO_2 over CO, compared with pristine MOF-5 (Fig. 29). This point, together with the improved H_2 storage capacity of another MTV-MOF reported [296], clearly evidenced that the properties on MTV-MOFs are not simple linear combinations of their constituents. Later on, some of the same authors, further proved this with MTV-MOF-177 [98]. In this case, they observed an increase in volumetric hydrogen uptake in all MTV-MOFs respect the parent unfunctionalized structure. Although each mixed-component MOF represents a unique playground on its own, and consequently it would be really hard to extrapolate and generalize the information extracted from one system to others, experimental evidence of adsorbent-adsorbate interation and the primary adsorption sites of guest molecules is crucial to understand the structure-properties correlation and improve the materials performance. In this context, methods based on 1D $^{1}H\{^{13}C\}$J-HMQC-SD NMR were introduced to unravel the primary adsorption sites of light alkanes on MTV-UiO-66-(BDC-CH_3)$_{0.24}$-(BDC-NH_2)$_{0.44}$-(BDC-2OH)$_{0.32}$ at room temperature [294]. From this study, it was observed, and supported by DFT calcula-

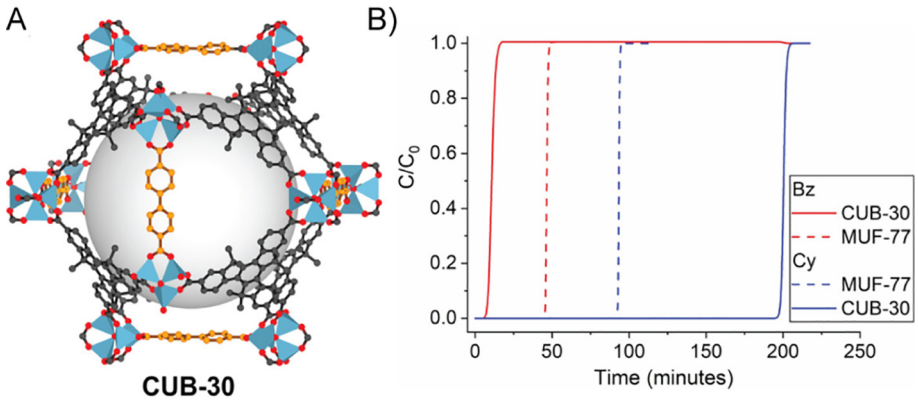

Fig. 30. A) Crystal structure of quaternary CUB-30. B) Simulated breakthrough curves for a mixture of benzene/cyclohexane diluted with excess amount of helium for CUB-30 (solid lines) and MUF-77 (dash lines). Reproduced from ref. [153] with permission from John Wiley & Sons, Copyright 2020.

tions, that methane, ethane and propane were preferentially present near the BDC-2OH sites [43].

Multicomponent materials have also exhibited exciting adsorption and separation properties. The modification of the pore size –with alkyl chains of different size functionalizing the truxene-based ligand– of the quaternary MTV-MUF-77 derivatives revealed a tunable affinity for CO_2 and CH_4 [150]. From them, MUF-77-hexyl exhibited increases of 237 and 172% for CO_2 and CH_4, respectively, with respect the related MUF-7a. This approach contrasted with the more common ones, based on the introduction of open metal sites or polar functional groups. In addition, in this work, the authors unveiled another advantage of multicomponent systems respect traditional MOFs, this consisted on the cooperative effect of all the constituting ligands to maintain structural integrity and open pores, even though one of them suffer significant changes. Besides, in this work, the authors envisage the potential of this platform for the functionalization of all three ligands to render MOFs with targeted and distinct functionalities [148,151,154]. The path of increasing complexity in multicomponent MOFs have also been successfully seized to deliver MOFs with interesting gas adsorption and separation properties [49,291]. A nice example is represented with the quinary framework FDM-8, where the existing hierarchical pores enabled a working capacity of 193 cm^3/cm^3 at 5–80 bar, which is among the best materials known for high-pressure methane storage [291]. Macreadie *et al.* [153] presented a family of two ternary and two quaternary multicomponent MOFs that contain the cubane-*p*-dicarboxylic acid (H_2CDC), which showed exciting selectivity and capacity for liquid organic hydrogen carriers (LOHCs) (Fig. 30). From them, the authors focused on the gas adsorption and separation properties of quaternary CUB-30 (Fig. 30A), a structural analogue of MUF-77, where the BDC had been replaced by CDC. In particular, it was reported that CUB-30 showed higher CO_2 and CH_4 adsorption than MUF-77, which was attributed to the greater number of adsorption sites within CUB-30. Then, they studied the single component vapor adsorption of a range of hydrocarbons, which included cyclic (benzene, cyclohexane, toluene and methylcyclohexane), linear (*n*-hexane and *n*-heptane) and branched (*i*-hexane and 2,3-dimethylpentane) hydrocarbons. Unprecendently, CUB-30 presented a high preference for cyclohexane adsorption over benzene at low partial pressures, which contrasts with the common adsorption preference reported and broadens the range of applications of MOFs in industrially relevant challenging separations (Fig. 30B). The authors attributed this exciting separation to the different pore environment generated by the CDC ligands, leading to a smaller dodecahedral pore with substantially more van der Waals interaction sites for interaction, as well as the higher molecular flexibility of cyclohexane respect benzene. This contrasted with the accepted explanation of the relevance of π-π interactions for hydrocarbons adsorption in MOFs. From the simulated breakthrough curves, it could be observed a time lapse of 3.5 h. Also, CUB-30 outperforms MUF-77 in five times at 0.5 kPa for cyclohexane adsorption and in 2.5 times at 0.7 kPa for benzene adsorption. In addition, CUB-30 markedly outperformed MUF-77 on toluene and methylcyclohexane adsorption, and in minor degree in the adsorption of *i*- and *n*-hexane. This work nicely illustrated how subtle changes can make a big difference in mixed-ligands MOFs, as well as have opened a new direction to follow for selective hydrocarbon adsorption.

Pore space partition design strategies have also revealed as an excellent manner to modulate the size, functionalities and number of open metal sites in multicomponent MOFs. Zhao *et al.* [78] in the family of **TRZ-pacs-D**, with formula $[(M_1)_3O(BDC)_3][(M_2)_2(TRZ)_3\text{-}X_6]$, reported an extensive study of the influence on the gas adsorption properties of the use of different M_1/M_2 or L_1/L_2 compositions. They observed the CO_2 uptake can be controlled in the range 44.5–129.7 cm^3/cm^3 by changing the M_1/M_2 nature of metals in the increasing order of Fe/Fe, Fe/Mg, In/Mn, Fe/Ni, In/In, In/Co and In/Ni. Interestingly, they reported this was also influenced by the M_1/M_2 ratio by varying the In/Co from 1:4 to 4:1 between 53.2 and 146.7 cm^3/cm^3. The functionalization of the constituting ligands with amino and hidroxy groups produced a significant positive impact on the CO_2 adsorption properties, with an increase of 29 and 42% respect the unfunctionalised material, respectively. Also, an analogous trend was observed for the hydrogen adsorption at 77 K in both families. In addition to be exciting exponents of new possibilities to enlarge the reticular chemistry approaches, multivariate [104] and multicomponent [295] rare-earth-based MOFs have been also successfully applied for light hydrocarbons adsorption. In particular, Tb-**sph**-MOF-1 [295] –the framework with the most confined pore system of this family of networks–, showed less adsorption affinity for CO_2 respect C_nH_{2n+2}, in contrast to 13X zeolites. Similarly, PCN-909(Tb)–NH_2 [104] exhibited a much higher heat of adsorption for C_3 light hydrocarbons with respect to CH_4 and C_2. Indeed, ideal solution adsorbed theory (IAST) revealed a nice selectivity for C_3H_8 and C_3H_6 over CH_4 –96.9 and 97.8 at 1 bar and 298 K, respectively– which situate this complex framework as a potential candidate for the efficient removal of C_3 light hydrocarbons from natural gas at room temperature.

In a different synthetic approach, this was also reported by Chen *et al.* [47] with the application of PSMs. They showed in the Zr-MOF LIFM-28 the reversible installation/uninstallation of linkers of different lengths and functionalities with the aim to achieve

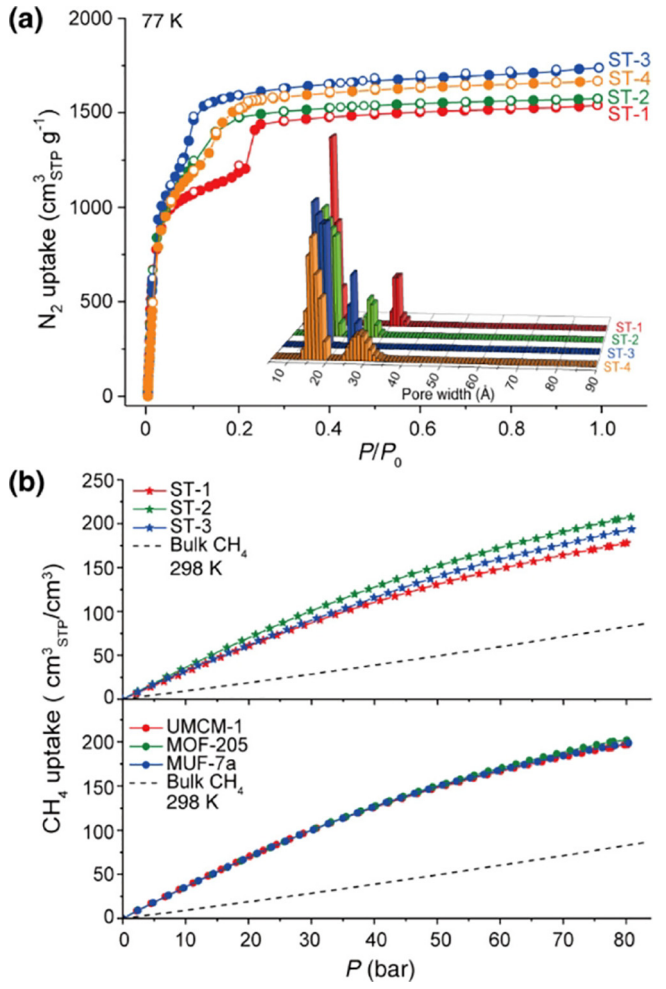

Fig. 31. (A) N_2 adsorption isotherms for ST1-4 and their corresponding pore size distributions. (B) High-pressure CH_4 uptake isotherms for these ST MOFs compared to other analogue MOFs. Reproduced from ref. [152] with permission from the American Chemical Society, Copyright 2017.

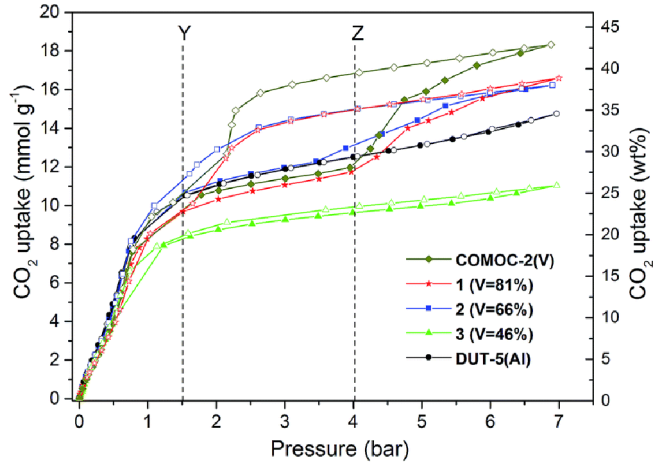

Fig. 32. High Pressure CO_2 adsorption measurements of COMOC-2(V), 1 (V = 81%), 2 (V = 66%), 3 (V = 46%) and DUT-5(Al) from 0 to 7 bar at 228 K. Reproduced from ref. [211] with permission from the Royal Society of Chemistry, Copyright 2017.

a multipurpose material. Relevant to this section, the functionalities decorating the ligands incorporated on the pristine MOF, together with the reduced pore aperture and compartimentalization of cages, led to the obtention of four different multicomponent materials with outstanding CO_2/N_2 and CO_2/CH_4 (LIFM-77), R22/N_2 (LIFM-86) separation properties and ultrahigh methane storage working capacity at 5–80 bar and 298 K (LIFM-82 and 83).[47] In the same line, Liang *et al.*[152] presented different multicomponent MOFs with ultrahigh capacity methane storage (Fig. 31). [152] In particular, ST-2 (ST stands for ShangaiTech University) with formula $(Zn_4O)_3(TATAB)_4(NDC)_3$ (TATAB = 4,4′,4″-*s*-triazine-1,3,5-triyltri-*p*-aminobenzoate) reached the highest deliverable capacity of 289 cm^3/cm^3 at 298 K and 5–200 bar, which surpassed all the reported porous materials at that time, and even more interestingly, evidence the relevance of being able to fine-tune the mesoporosity of MOFs to further improve the deliverable capacities at ultrahigh pressure.

The influence of open metal sites on the adsorption and separation properties has been largely investigated in traditional MOFs. [297–302] To this end, and as a logical extension, it has been also studied the different chemical nature of metal ions and/or SBU topology in mixed-metals MOFs. Kim *et al.* [199] showed that, in bimetallic MZn-MOF-74 (M = Ni and Mg), the CO_2 uptake was superior for the Mg one, reaching 6.7, 5.1 and 3.6 mmol/g at 273, 303 and 323 K, respectively. More importantly, the isosteric heat of adsorption (Q_{st}) values experimented a gradual decrease with increasing CO_2 loading, which contrasted with the behaviour of MOF-74. The Q_{st} values were found to be between those of the single-metal MOFs, and thus can be controlled by the combination of metal ions, which evidenced the synergetic effect of possessing different metal ions [199]. Yang *et al.* [220] reported four bimetallic PCN-6′(M) (M = Mn, Fe, Co and Zn) materials, obtained by a vapor-assisted solid-phase methodology, which showed better adsorption properties than pristine PCN-6′, especially at low pressure region. From them, PCN-6′(Fe) exhibited the highest uptake of CO_2 at 273 K and H_2 at 77 K. Although this manuscript lacks of a more deeply physical characterization, the gas properties rendered by the reported materials were illustrative of the potential mixed-metals MOFs possess [94]. Depauw *et al.* [211] used the incorporation of a second metal ion in COMOC-2(V) to form bimetallic Al/V frameworks –isoreticular to MIL-53– where it has been observed it was possible to tailor the breathing behavior (Fig. 32). From this study, it was also evidenced the presence of two different large and a narrow pore phases, which depend on the aluminium content. With a high aluminium content, it occurs a transtition from narrow to larger pores at low pressures. In turn, at higher pres-

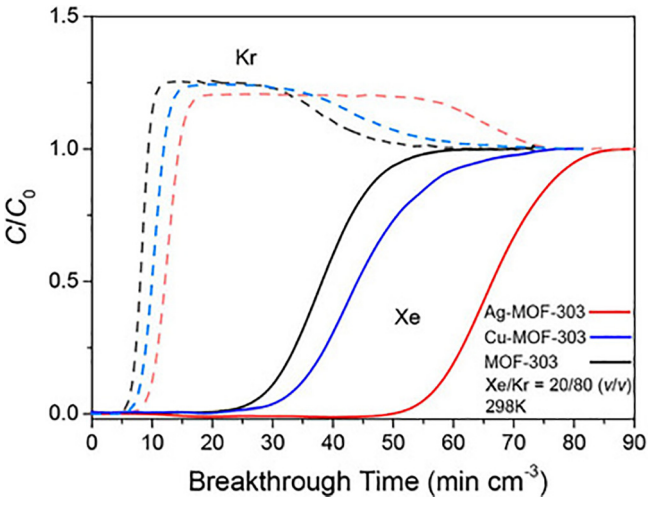

Fig. 33. Experimental breakthrough curves for a binary Xe/Kr mixture [20/80 (v/v)] showing the separation performance of MOF-303, Cu-, and Ag-MOF-303. Adapted from ref. [248] with permission from John Wiley & Sons, Copyright 2021.

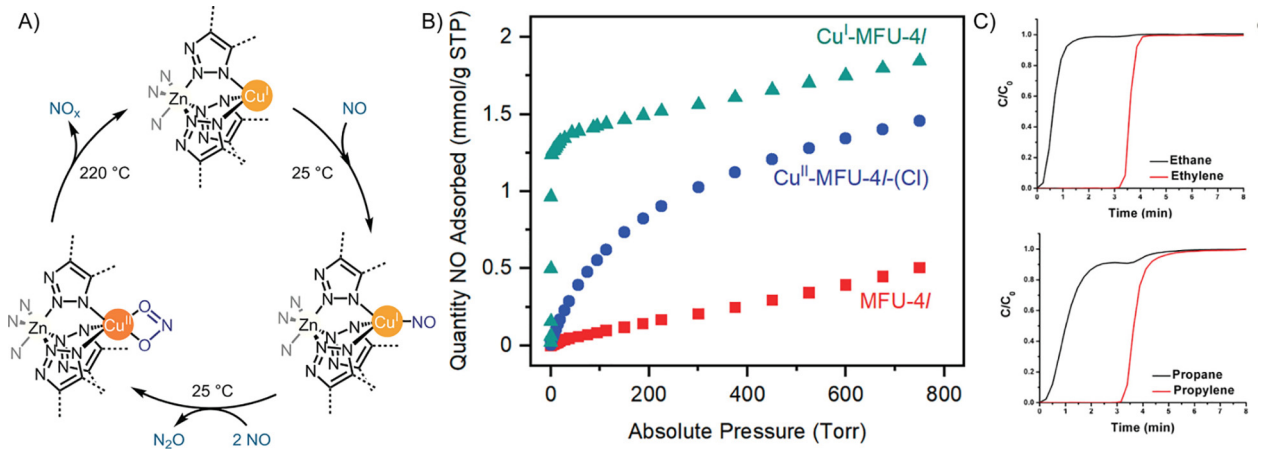

Fig. 34. A) Proposed NO disproportionation cycle with MOF Cu^I-MFU-4*l*. B) NO adsorption isotherms for MFU-4*l* (red squares), Cu^{II}-MFU-4*l*-(Cl) (blue circles), and Cu^I-MFU-4*l* (green triangles) (298 K). C) Experimental breakthrough curves showing the olefin/paraffin separation with Cu^I-MFU-4*l* MOFs. Adapted from refs. [309] and [307] with permission from the American Chemical Society, Copyright 2019 and 2021.

sures, the high of the hysteresis loop decreases, leading to a reduced CO_2 uptake [211]. Adsorption of xenon and Xe/Kr separation has been also pursued using mixed-metals MOFs, with the aim to find novel materials able to perform this separation efficiently and avoid traditional energy-intensive cryogenic distillation. In this context, considering that polar groups and metal sites favour the interactions with Xe, due tho their larger polarizability respect Kr, Wang *et al.* [248] presented the metalation of MOF-303, built up with rod-based Al–O SBUs and 1H-pyrazole-3,5-dicarboxylate (HPZDC) linkers, with Cu^I and Ag^I to yield the metalated Cu- and Ag-MOF-303 materials [248]. From the low-pressure Xe and Kr adsorption isotherms at 273, 283 and 298 K of MOF-303 and metalated Cu- and Ag-MOF-303, it was observed that Ag-MOF-303 presented a remarkable Xe uptake capacity of 59 cm^3/cm^3, which is among the highest reported for MOFs [248,303,304], and remains consistent throught 80 cycles of adsorption–desorption experiments. Interestingly, fixed-bed breakthrough experiments for Xe/Kr mixture (20/80, v/v) at 298 K and 1.1 bar revealed Ag-MOF-303 was able to perform dynamic separations with capacities of 3000 and 600 s/cm^3 for Xe and Kr, respectively, which represented a 100% improved retention time respect the pristine MOF (Fig. 33). The nice performance of this metalated material was attributed to its reduced pore size –underpinned by 3D electron diffraction tomography (EDT) and extended X-ray absorption fine structure (EXAFs)– which nicely matched the size of Xe, and consequently enabled the selective binding of Xe from Xe/Kr mixtures.

The development of robust mixed-metals MOFs for gas adsorption and separation have been also extended to other ligands different from carboxylate, such as the triazolate in MFU-4 [305] type materials (MFU = Metal-Organic Framework Ulm University) [306–309]. At this respect, Wright *et al.* [309] reported the application of Cu^I-MFU-4 *l*, with formula $Zn_3Cu^I_2Cl_2(BTDD)_3$ –BTDD = bis(1H-1,2,3-triazolo[4,5-b;4′,5′-i])dibenzo[1,4]dioxin), for the chemisorption of NO at room temperature and low pressures, forming a Cu^I-nitrosyl complex. Its subsequent catalytic NO disproportion leading to Cu^{II}-nitrite complex and nitrous oxide, and the thermal-induced release of NO_x species –where NO was the main component, as mass spectrometry supported– from the network and regeneration of the pristine mixed-metals MOF (Fig. 34A). Cu^I-MFU-4 *l* was obtained applying post-synthetic metal exchange with $CuCl_2$ on pristine MFU-4 *l*(Zn) of two of the four peripheral zinc ions of each SBU, and posterior reduction of Cu^{II} to Cu^I [308]. The resulting material exhibited a considerable improvement on NO adsorption properties respect the related Cu^{II}-MFU-4 *l* and MFU-4 *l*(Zn), adsorbing 1.24 mmol/g below 1.4 Torr and reaching 1.84 mmol/g at 760 Torr and 298 K, with a remarkable hysteretic desorption, which is consequence of the strong interaction between Cu^I and NO (Fig. 34B). From an application viewpoint, it is noteworthy that Cu^I-MFU-4 *l* captures NO at concentrations below 10 ppm. Yet, further work is required to improve the recyclability of this mixed-metals MOF as, despite it could be reused up to three times, it was observed a slight drop of uptake at low and high pressures after the first cycle. An interesting study on this MOF was reported by Mohamed *et al.*, [307] where it was examined the influence of the different amount of Cu^I open metal sites, in a family of five Cu^I-MFU-4 *l* variants, on olefin/paraffin separation performance. It was observed a linear increase of olefin adsorbed amount with increasing Cu^I loading, without a decrease of the binding energy –as predicted by density functional theory (DFT). Temperature-programmed desorption (TPD) revealed similar ethene desorption energies for all the variants, which indicates the independence of the Cu^I sites to adsorb ethene and that no interactions occurred between neighbour sites. Interestingly, column breakthrough experiments on the variant $Zn_3Cu^I_2Cl_2(BTDD)_3$ showed the great potential to perform industrially relevant olefin/paraffin separations to obtain polymer-grade (>99.999%) olefins ((Fig. 34C)). In particular, they observed, in ethene/ethane and propene/propane gas mixtures, that paraffins were not adsorbed, while olefins were retained in the column *ca.* 190 s, which confirmed its ability for olefin/paraffin separation and to obtain ethene with > 99.999% purity. Indeed, the mixed-metals MOF could be regenerated using temperature-concentration swing recycling (TCSR) and used up to 10 times without depletion of its adsorption capacity (0.73 mol/kg).

The development of ZIFs have been intimately related to the obtention of robust MOFs, analogues to zeolites, as well as the exploration of new ones with unprecedented topologies and controlled cage size. To this end, the development of multivariate and multicomponent ZIFs have been extremely useful, and, in turn it has revealed as an appealing approach to tailor MOFs pores and functionalities, and consequently, to impact gas selectivity [85,86,126,184,185]. Eum *et al.* [125] evidenced this with the preparation of a series of mixed linkers ZIFs, where it was observed a tunable molecular sieving in nonpolar alkanes (*n*-butane and *i*-butane) and highly polar alcohols, whereas a tunable adsorption for water and alcohols at low pressures [125]. Yang *et al.* [185] prepared 15 novel ZIFs by combination of two or three imidazole ligands, where their steric index –related to the size and shape of the imidazole derivatives– together with the linker ratio and com-

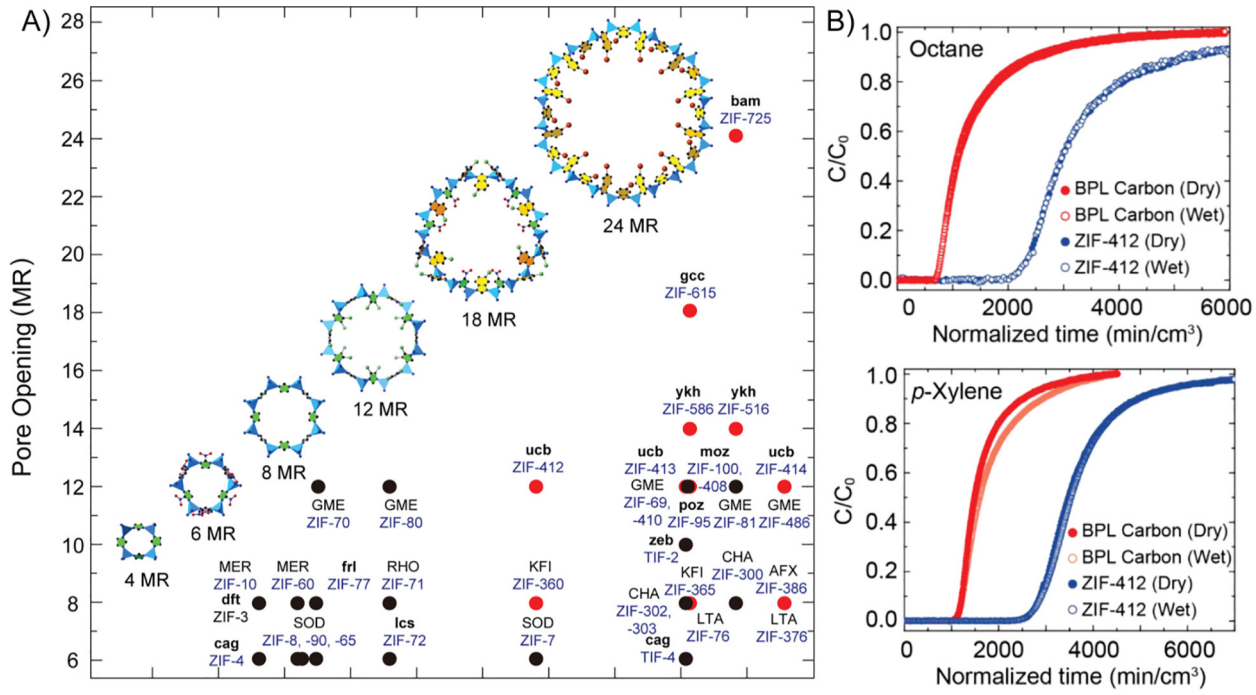

Fig. 35. A) Different ZIF MOFs emphasizing cages size. B) Breakthrough curves under both dry and wet conditions (RH 0% and 65%, respectively) using ZIF-412 and BPL carbon at 298 K for octane (left) and *p*-xylene (right). Adapted from ref. [185] with permission from the American Chemical Society, Copyright 2017.

bination allowed to tune the size of the rings and cages, as well as the final topology. From them, ZIF-412, the one with the largest cage size (Fig. 35A), showed the best selectivity of porous materials tested for octane and *p*-xylene removal from humid air, which was attributed to its permanent porosity and hydrophobicity (Fig. 35B) [185].

The negative environmental implications of CO_2 have made its capture becomes one of the most intense area of research. Traditional MOFs have been extensively investigated for its capture, and in lab-scale some of the reported MOFs have outperform traditional adsorbents used in industry [310–313]. A particularly challenging adsorption process is the capture of CO_2 from wet flue gas, where, despite the difficulties, remarkable advances have been perfomed taking advantage of chemisorption sites or hydrophobic pore environments [314–319]. Mixed-ligands approach has been also exploited for CO_2 capture [320]. Particularly relevant was the work developed by Hu *et al.*, [94] where they reported a triphasic modulated hydrothermal approach to obtain MTV UiO-66(Zr) MOFs, constituted with 2-aminoterephthalate (ABDC) and tetrafluoroterephthalic acid (H_2TFBDC) ligands, for moisture-resistant CO_2 capture [94]. The resultant MTV-MOFs, due to the presence of hydrophobic TFBDC linkers, exhibited enhanced water stability, hydrophobicity and water vapour repellent property. Among them, UiO-66(Zr)–NH_2-F_4-0.53 showed a CO_2 working capacity of 0.76 mmolg^{-1} at 0.15 bar and CO_2/N_2 (15/85) selectivity of 18.9 at 298 K [94]. Despite these values are not comparable to the best-performing materials, and are also lower of what is expected from IAST, the remarkable feature of this MTV-MOF is that it only loses 30% of its CO_2 uptake capacity under wet (70% relative humidity) CO_2/N_2 (15/85) mixture condition, which contrasted with 88% loss of pristine UiO-66(Zr)–NH_2 MOF. UiO-66(Zr)–NH_2-F_4-0.53 also demonstrates enhanced breakthrough dynamics with less cross-column pressure drop ($\Delta P \approx 0$ bar) and 2.7 times larger mass transfer coefficient (k = 0.1235 s^{-1}) than that of UiO-66(Zr)–NH_2 ($\Delta P \approx 0.25$ bar, k = 0.0334 s^{-1}). Nevertheless, this approach still needs further improvement to retain more efficiently CO_2 uptake in moisture conditions, as occurred with ZIF-300 [184] and Mg_2(-DOBDC)$(N_2H_4)_{1.8}$ [321] that showed almost no loss at > 80% relative humidity [94].

3.2. Heterogeneous catalysis

MOFs have become an alternative for heterogenization of homogenous catalysts [20–22,25,26,322–324]. Researchers have exploited the intrinsic catalytic activity of the MOFs by introduction of open metal sites, creation of defects or by using an organic linker as a catalyst. MOFs are also platforms to host catalytic sites such as nanoparticles or enzymes. In the same manner, catalytic applications of MTV MOFs have also been explored. For instance, Kleist *et al.* designed a modified MOF-5 with the formula $[Zn_4O(BDC)_{3-x}(ABDC)_x]_n$ where they study the thermal stability depending on the amino content linker, and the propylene carbonate formation [40] and the immobilization of Pd species for CO oxidation [325]

Multicomponent MOFs arise as suitable systems to modulate the spatial environment around the active sites, which has been an exceedingly challenge in synthetic heterogeneous catalyst [95,137,176]. Liu *et al.* [151] took advantage of the structural regularity of MUF-77 platforms, to obtain 15 quaternary MOFs, where prolinyl groups, catalytically active toward asymmetric aldol reactions, were incorporated in one ligand, and the other two linkers beared functional groups able to modulate –via noncovalent interactions– the reaction rate and the enantiomeric excess of the aldol products, in a reminiscent manner to enzymes [151]. From this study, several exciting conclusions can be extracted: (*i*) the modulator functional groups seem to act in synergy, instead of in a linear way and (*ii*) the location of the catalytic site can induce enantioselectivity reversal respect the homogenous prolinyl-based linker, which can be restored by tuning the active site microenvironmentwith achiral modulators. Despite the catalytic results do not outperform the state-of-the-art catalyst, this work reveals the great potential that multicomponent MOFs can have in heterogeneous catalysis, and even more interestingly, it set the foundations to develop efficient synthetic catalysts for a given target reaction by

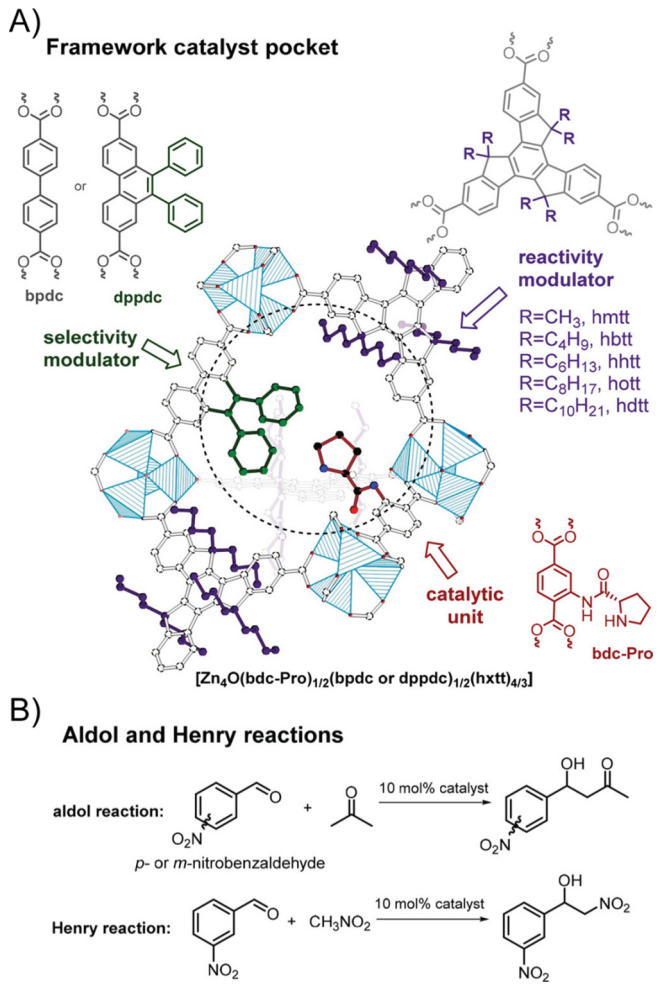

Fig. 36. A) Schematic illustration of the catalytic pocket in MUF-77 series, based on single-crystal X-ray diffraction (SCXRD) structures, where it shows a site for catalysis and modulator groups that are positioned to influence the course of the reaction. B) Aldol and Henry reactions are reported herein. Adapted from ref. [148] with permission from the American Chemical Society, Copyright 2019.

a controlled tuning of the active sites and modulators. This concept was extended later, by the same research group, by investigating the use of different modulators in multicomponent MOFs, capable to exhibit both a high stereochemical selectivity and reactivity in aldol reactions (Fig. 36A) [148]. Interestingly, they found it was even possible to discriminate between different reactions pathways (Henry *vs* aldol), and that such highly complex MOFs were able to catalyze reactions which can not occur in homogenous phase (Fig. 36B) [148]. Nguyen *et al.* reported the synthesis of multicomponent MOF-907 –constructed from trigonal six-connected Fe_3O SBUs and triangular BTB and linear NDC linkers, with **nha** minimal transitivity net topology– and their use as efficient catalyst for the microwave-assisted radical polymerization of methyl methacrylate. Indeed, the high porosity with one-dimensional interconnected channels and accessible pore window of MOF-907, together with the presence of unsaturated strong Lewis acid Fe_3O SBUs, allowed to obtain polymethyl methacrylate in a very short reaction time (30 min.) –conventional methods trigger one day– with remarkable high yield (98%), high molecular weight (Mn = 20.680 g mol^{-1}) and low polydispersity (PID = 1.23). For comparison, it was evaluated the activity of MIL-101(Fe) [89] and PCN-285 [163] –both of them with Fe_3O SBUs– and it was observed MOF-907 showed better PDI and higher yield and Mn. The authors attributed this to the particular structural features of MOF-907, which evidenced the key role novel multicomponent MOFs with high symmetry/minimal transitivity could play in designing very efficient catalyst.

Post-synthetic ligand exchange or installation of one of the components of a multicomponent MOF, could also provide another vertex of complexity and improved functionality to these mixed-component MOFs [167]. Zhang *et al.* [326] presented the post-synthetic ligand exchange and metalation on PCN-900(Eu) –a mixed-component MOF constituted by twelve connected rare-earth hexaclusters linked by TCPP and DCDPS– with 2,2′-bipyridine-5,5′dicarboxylate (DCBPY) and $CoCl_2$, respectively, to led to a mixed-ligands and metals PCN-900(Eu)-CoTCPP-CoDCBPY. This material shows improved catalytic performance for the cycloaddition of CO_2 with epoxides compared to the pristine PCN-900(Eu), its partially metalated derivatives and the physical mixtures of them. Despite it only exhibits a moderate catalitic activity, the proposed methodology opens the way to design mixed-component MOFs with metal ions located at specific positions, which undoubtedly will enlarge the number of heterogeneous MOFs catalysts. As we have mentioned, PSMs have revealed as an outstanding approach to contruct highly complex mixed-component MOFs [124127284327,328]. This was beautifully illustrated by Fracaroli *et al.*, [132] where seven sequential post-synthetic reactions on a MTV-IRMOF-74-III, constructed with magnesium oxide rods linked by two distincly functionalized H_4L organic struts –H_4L-CH_3 and H_4L-CH_2NHBoc, H_4L = 3,3″-dihydroxy-(1,1′:4′,1″-terphenyl)-4,4″-dicarboxylic acid– with formula MTV-$(CH_3)_{0.6}(CH_2NHBoc)_{0.4}$, enabled to load two types of tripeptides (H_2N-Pro-Gly-Ala-CONHL and H_2N-Cys-His-Asp-CONHL) with interesting catalytic activity (Fig. 8). In particular, MTV-IRMOF-74-III-CH_2NH-Asp-His-Cys-NH_2, containing the peptide sequence of the endopeptidase enzyme tobacco etch virus (TEV), was investigated as mimick of this enzyme on the sequence-specific peptide bond cleavage of the pentapeptide H_2N-Ala-Tyr-Ala-Ser-Ala-$CONH_2$. Despite only a 5% conversion to the cleavage product was obtained and further work would be required for their practical application, this work nicely illustrated that is possible to achieve a fine molecular control of MOF pores functionalities with a complexity close to enzymes [132]. The same concept has been lately exploited by Zhang *et al.* [329] in a MTV-UiO-68 with accessible alkyne and azyde groups in a 1:1 ratio, which experienced post-synthetic quantitative tandem click reactions and enabled to incorporate, in a controlled manner, groups of distinct functionality (Fig. 37). In this sense, it was reported that the same product could be obtained in two independent tandem click reaction routes. The development of this synthetic strategy, for example, enabled to obtain an efficient heterogeneous acid-base MTV-MOF organocatalyst for aldol addition reactions. Especifically, the authors compared the catalytic activity of the MTV-MOF with acid and base sites with the MTV-MOFs with only either acidic or basic sites. It was observed that the bifunctional MTV-MOF outperforms other MTV-MOFs and retained its activity after three reuses, which evidenced the cooperation of the active sites of distinct nature. Despite it has not been presented in the manuscript, the authors envisioned that this approach, together with the possibility to tune the ratio of azide and alkyne functionalities, represents a fantastic manner to design bifunctional MOFs for targeted desired applications.

Besides being active parts on the catalytic processes, the unique pore environment of each mixed-component MOF can have a severe influence on the catalytic performance of catalysts residing in their pores [40]. In this context, Choi *et al.* [93] proved the importance of the chemical nature of the functionalities decorating the UiO-66 frameworks on the catalytic activity of embedded Pt nanoparticles (NPs). They incorporated alone or in pairs sulfonic acid (-SO_3H), ammonium (–NH_3^+) and their deprotonated forms as

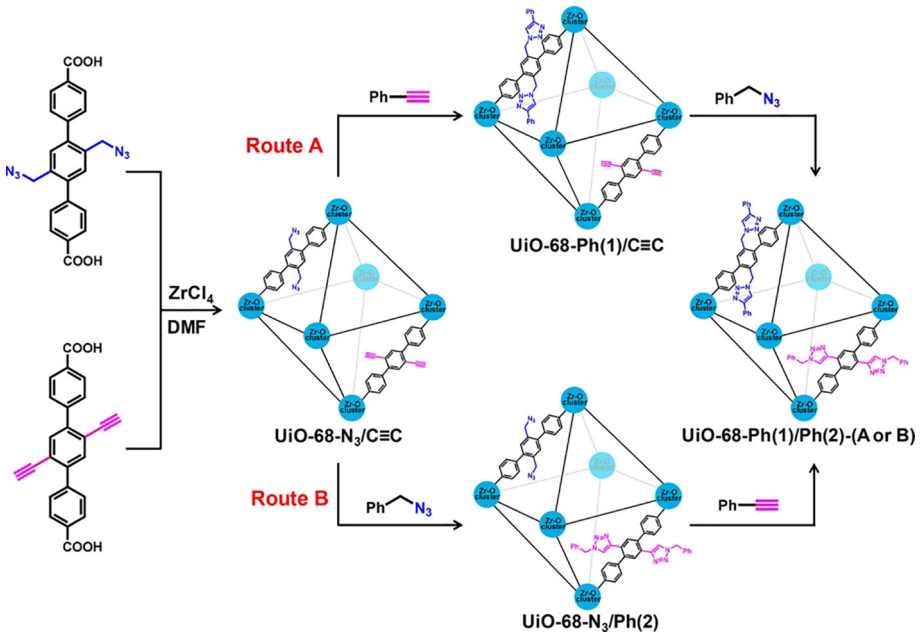

Fig. 37. A) Schematic representation of the PSMs of UiO-68-N_3/C≡C via tandem click reactions from two different routes. Adapted from ref. [329] with permission from the American Chemical Society, Copyright 2018.

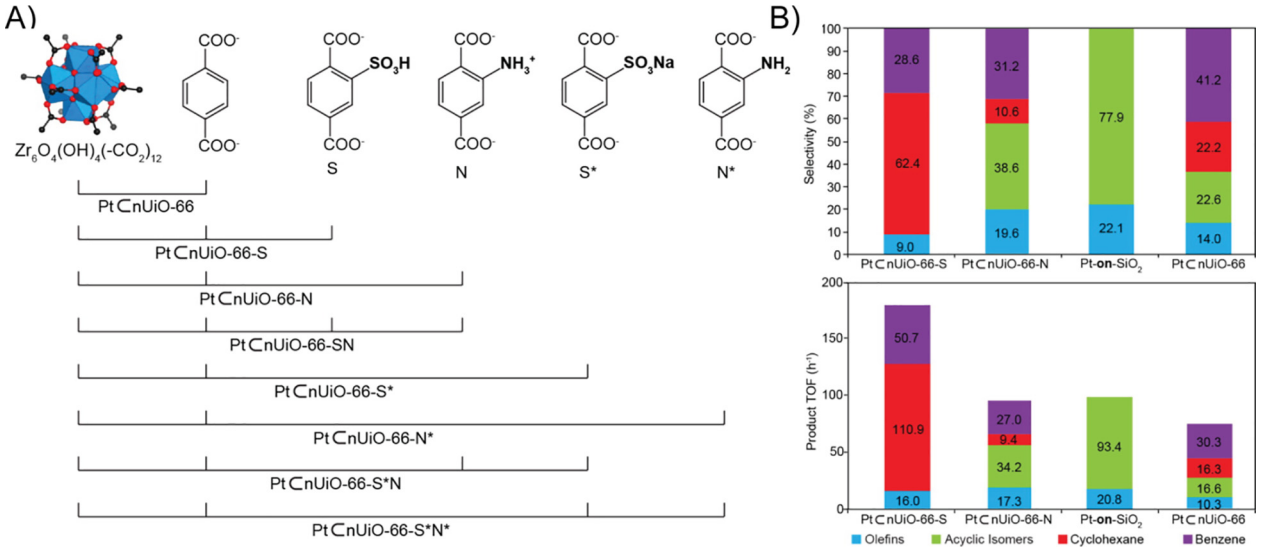

Fig. 38. A) Schematic representation of the combination of functionalized linkers used to make the nMOFs in the Pt ⊂ nUiO-66 constructs. B) Product selectivity (top) and turnover frequency (TOF, h^{-1}) (bottom) obtained at 150 °C over Pt ⊂ nUiO-66-S and N, Pt ⊂ nUiO-66, and Pt-on-SiO_2. Adapted from ref. [93] with permission from the American Chemical Society, Copyright 2015.

functionalities (Fig. 38A), and reported their critical role in product selectivity and activity in the gas-phase conversion of methylcyclopentane (MCP) to acyclic isomer, olefins, cyclohexane and benzene [93]. Relevant to our topic are the results of the MTV-UiO-66 and Pt ⊂ nUiO-66-SN, combining the strong (-SO_3H) and weak (–NH_3^+) acid functionalities, which gave different product selectivity to that of their constituents (Fig. 38B). No cyclohexane was produced, while benzene was the dominant product with olefins and acyclic isomers as minor products [93]. This was a quite unexpected result, because this material maintained the high activity of the MOF, decorated only with sulfonic acid, but the catalytic pathway was changed. This work further evidenced the unique characteristic of mixed-components materials that their behavior is not an intermediary of its constituents, but a novel one.

Solvent assisted linker incorporation (SALI) methodologies have been applied to generate multicomponent MOFs, where the incorporated linkers can be used to tune the activity of SBU-anchored catalyst [172] or as initial platforms to construct within MOFs pores the catalytic species [173]. The latter application was reported by Goswami *et al.* [173] to synthesize gold nanoparticles within triangular and hexagonal channels of NU-1000, with dimensions matching the size of them, and acceptable catalytic activity for the hydrogenation of aqueous 4-nitrophenol to aminophenol. In order to do so, the authors followed a three-step post-synthetic strategy on preformed NU-1000. Firstly, they applied SALI to attach 4-carboxy-phenylacetylene ligands –in monodentate ester-like fashion– to the eight connected Zr_6-aqua/hydroxo/oxo SBUs of NU-1000, as SCXRD supported. Then, they

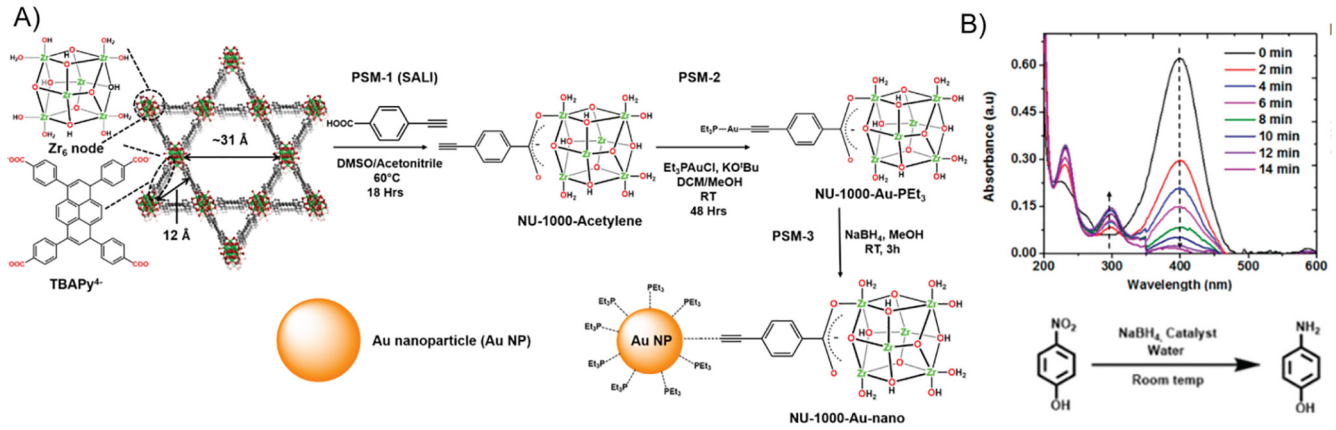

Fig. 39. A) Structure of NU-1000 MOF and the three consecutive post-synthetic modification reactions that yield AuNPs. B) Time dependent evolution of UV–vis absorption spectra for the catalytic hydrogenation of 4-nitrophenol to 4-aminophenol. Adapted from ref. [173] with permission from the American Chemical Society, Copyright 2019.

coordinated the $Au^{I}PEt_3^+$ salt to the acetylene unit of the incorporated linker –with a loading of 1.4 ± 0.2 Au atoms per Zr_6 node– and, finally, chemically reduced the Au^{I} to led to the formation of Au nanoparticles with a bimodal distribution of particle size –*ca.* 1.5 (98%) and 3.7 nm (2%)– and phosphine ligands strongly adsorbed (Fig. 39A). Despite the pristine synthesised Au nanoparticles do not exhibited an outstanding catalytic activity (Fig. 39B), for the thermally treated version –where most of the adsorbed phosphine ligands were removed– the rate of the reaction was considerable higher. Nevertheless, the presented material showed a nice structural stability and retained the gold content after four reuses.

The presence of catalytically active metal ions in mixed-metals MOFs have make them outstanding platforms in heterogenous catalysis [194,197,207,225,330]. A very interesting study was reported by Liu *et al.*, [54] showing the influence on the photocatalytic activity of the metal spatial arrangement in the family of porphyrin-based mixed-metals MOFs with general formula $(M_3O)_2(TCPP\text{-}M)_3$ [54]. The authors reported that the tested mixed-metals MOFs, with a domain spatial distribution, exhibited a catalytic activity falling in between their respective MOFs with one type of SBU metal, meanwhile well-mixed spatial arrangement showed better conversion rates than their corresponding single-metal MOFs or their physical mixtures. For example, $(Mn_{1.77}Ni_{1.23}O)_2(TCPP\text{-}Ni)_3$ and $(Ni_{2.07}Fe_{0.93}O)_2(TCPP\text{-}Co)_3$ presented a 26 and 54% increase, respectively, in their catalytic performance respect their best single-metal MOF component. A careful study of the band structure revealed that in domain distribution the corresponding band structures was very close to the single-metal MOF. However, in well-mixed MOFs their band gaps present a dramatic difference in the band structure. This resulted in a better overlap with that of the singlet oxygen, which led to an improved reaction rate. Electrochemically synthesised mixed-metals MIL-53 (Al/Fe) have been reported [210] as enzyme-mimick catalyst for the C–H activation of methane to produce methanol –using H_2O_2 as oxidant under mild reactions conditions– with TOFs on the order of 90 h^{-1} and selectivitives to oxygenates of *ca.* 80% [210]. From a thorough spectroscopic characterization, the authors demonstrated the presence of the desired antiferromagnetically coupled high-spin Fe^{III}-Fe^{III} dimeric entities, which are reminiscent of the active site in methane monooxygenase enzymes. This was also supported with computational methods, where these atomically dispersed dimeric iron(III) moieties in the network were confirmed as the most likely active species of the mixed-metals MOFs reported. In addition, based on these calculations, the authors proposed a plausible reaction mechanism for the oxidation of methane. This started with the activation of H_2O_2 by a Fe site, with a replacement of one of the carboxylate ligands from the node by H_2O_2. Then, a homolytic dissociation of the O-O bond led to the formation of a terminal OH-Fe site and the concominant abstraction of a H atom from a bridging OH group to form H_2O. Afterwards, it occurs the subsequent homolytic dissociation of the C–H bond from CH_4 by the bridging O site to yield a OH group and a CH_3 radical that recombines with the terminal hydroxyl to form CH_3OH adsorbed on Fe site, which later on migrate to the pore. The oxidation state of one Fe site increase from III to V, without dissociation of the dimeric entities, which evidence the potential of

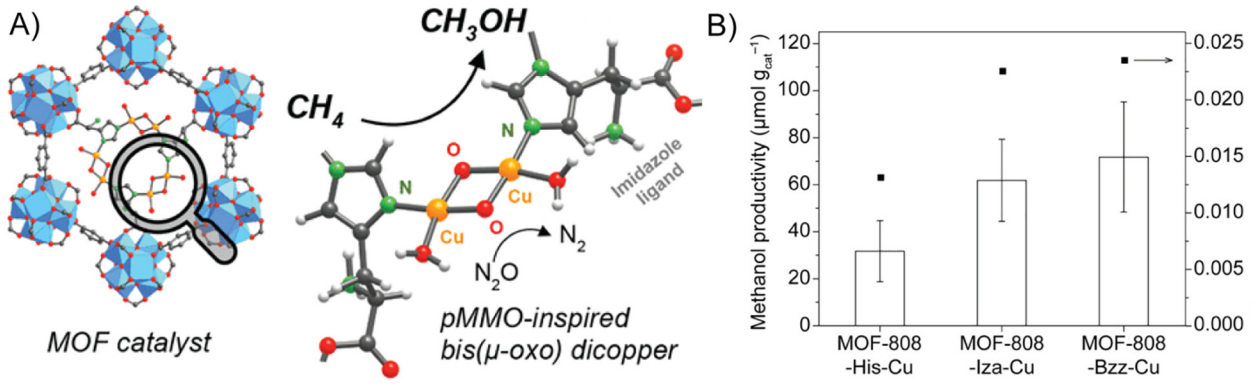

Fig. 40. A) MOF-808 modelled structure bearing copper–oxygen complexes. B) Methanol conversion produced by MOF-808-His-Cu, MOF-808-IZA-Cu, and MOF-808-BZZ-Cu. Adapted from ref. [252] with permission from the American Chemical Society, Copyright 2018.

mixed-metals MOFs to find solution where others materials have failed, as well as to open novel oppurtunities to gain better understand of oxidative activation of CH_4 and as model systems to mimicking bioenzymatic catalytic processes.

Baek *et al.* [252] reported another interesting study on the selective oxidation of methane to methanol within the post-synthetic modified channels of MOF-808 (Fig. 40) [252], where dimeric bis(μ-oxo)copper complexes –reminiscent of particulate methane monooxygenase (pMMO)– were identified as the most likely active site [252]. In this case, the authors selected MOF-808, $Zr_6O_4(OH)_4(BTC)_2(HCOO)_5(H_2O)(OH)$ –BTC = 1,3,5-benzenetri carboxylate– as suitable platform to incorporate, in a first-step, three metal-binding ligands –*L*-histidine (His), 4-imidazoleacrylic acid (H_2IZA) and 5-benzimidazolecarboxylic acid (H_2BZZ)– by replacement of formate units. From ^{1}H NMR it was observed that nearly half of formate ligands were substituted by these ligands, leading to three novel MOFs –MOF-808-His, -IZA and -BZZ– with imidazole units dangling towards the center of the channels. This replacement was also contrasted by SCXRD, despite the disorder did not allow to obtain a full determination with atomic precision, it was possible to observe their location. In a second step, it occurred the metalation of these MOFs with Cu^I in acetonitrile, where inductively coupled plasma-atomic emission spectroscopy (ICP-AES) revealed Cu/Zr_6 ratios of 4.9, 6.0 and 7.1 for MOF-808-His-Cu, MOF-808-IZA-Cu and MOF-808-BZZ-Cu, respectively. Unfortunately, the crystallographic disorder after metalation neither allowed to use SCXRD as basic characterization tool, and to gain insight of active site structure and oxidation state of copper ions it was used a multi-technique spectroscopic approach. Indeed, from the information extracted with all these techniques, especially X-ray absorption near edge structure (XANES) and EXAFS on the different conditions of activation of the catalyst, methane conversion and regeneration of the catalyst, it was possible to use computational methods to construct a model of the active sites. All three mixed-metals MOFs exhibited high selectivity for methane oxidation to methanol under isothermal treatment at 150 °C and very good conversions, being MOF-808-BZZ-Cu the more performant one with 71.8 μmol g^{-1}. Despite the recyclability of the material was not remarkable, with an overall considerable depletion of its activity after the first catalytic cycle –as consequence of the presence of strongly coordinated water molecules to the active sites–, this material represented the most active catalyst under tested conditions.

Metalation of the SBU have rendered to a wide plethora of mixed-metals ions with exciting catalytic activites [229,231–234]. Abdel-Mageed *et al.* [235] reported the attachment of copper atoms to the defect sites of UiO-66 (Fig. 41A), by anchoring them at the oxygen atoms of OH/H_2O terminal groups, being the limiting/-controlling agents of the amount of metal incorporated and leading to single-atom Cu catalyst, as well as its performance –prior activation in 10% H_2/N_2 at 250 °C for 1 h– in the CO oxidation reaction under realistic conditions, which represents a very important reaction from both a fundamental viewpoint and practical applications (Fig. 41B) [235]. In particular, the authors tested this highly stable single atom Cu heterogenous catalyst in the oxidation of CO at temperatures up to 350 °C, which results of interest for application in cars' catalytic converters, and for the selective oxidation of CO in hydrogen-rich feed gases, of main relevance for H_2 purification. This heterogenous catalyst was highly active –at least three times more than the most active copper-based catalyst for CO oxidation and comparable to more expensive platinum ones– and stable even in oxygen-rich atmospheres and for large times (20 h), as PXRD, TEM and DRIFTS measurements revealed after catalysis. Moreover, it showed a great selectivity (100%) for CO oxidation in the presence of large amounts of hydrogen (up to 80%) in the gas feed. Also, taking advantage of different spectroscopic techniques, the authors reported atomically disperse positively charged Cu species were the active species in catalysis and precluded the presence of small clusters or nanoparticles. The relevance of this study was not only the interesting catalytic results presented, but also, the general applicability to other metal ions of the reported synthetic strategy to obtain heterogeneous single atom catalyst. Metalation with distinct titanium salts of Zr_6-SBU in NH_2-UiO-66 has been studied with the aim to improve our understanding in photocatalytic hydrogen evolution [224]. They reported that, when using $TiCl_4$ as precursor, the resulted material exhibited 1.5 greater activity than the pristine NH_2-UiO-66, while using $Ti(O^nBu)_4$ the photocatalytic activity experienced a 14 times enhancement respect the one with $TiCl_4$. From the throrough theoretical and experimental study performed, the authors concluded the defect environment and coordination environment of photoactive metal ions are both relevant for improving the photocatalytic activity for such type of materials.

As we have mentioned before, atomic layer deposition (ALD) has revealed as a formidable technique to incorporate metal oxide clusters of very distinct metal ions at the SBUs and generate in a controlled manner mixed-metals MOFs [50]. Thus, it represents a formidable approach to generate unique heterogeneous catalyst [227,239,240,331]. A beautiful exponent was reported by Hackler *et al.*, [240] where the authors studied a plethora of supported

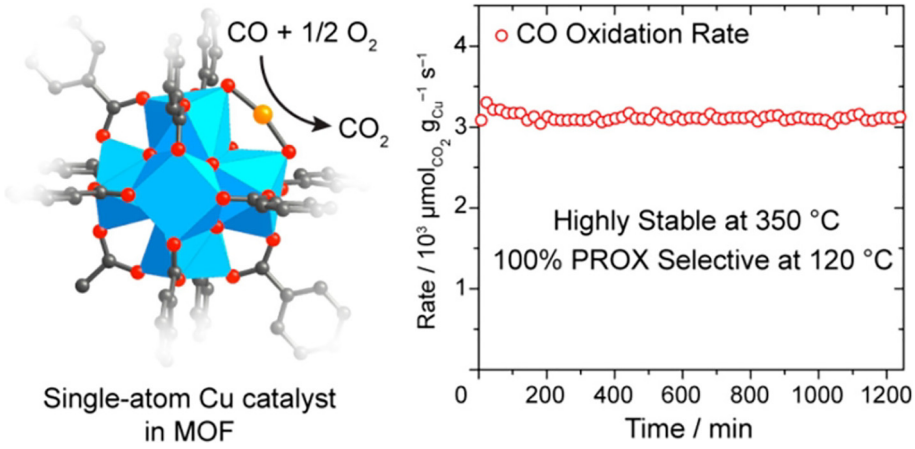

Fig. 41. Simulation of the Cu single atom catalyst anchored in MOF UiO-66 (left) and CO oxidation with time on stream (right). Reproduced from ref. [235] with permission from the American Chemical Society, Copyright 2019.

mono- and bimetallic oxide clusters on NU-1000 MOF for the partial hydrogenation of propyne to propene and the catalytic isomerization of propyne to propadiene [240]. Among them, the highest selectivity and yield for the isomerization of propyne was reported for Zn- and Cd-anchored NU-1000, which was attributed to the basic nature of these metal oxide sites and their capacity to promote 1,3-hydrogen shift for alkynes. Meanwhile, the Cu-supported MOF presented the maxium yield and selectivity for the partial hydrogenation of propyne to propylene, as it was expected based in the literature reports. Complete hydrogenation to propane was predominant in Zn-loaded NU-1000. However, it was observed a decreasing trend for bimetallic systems, while retaining propyne conversions and increasing the propensity to others reactions, such as isomerization and partial hydrogenation. Indeed, to study the synergistic effects between distinct catalytic sites in promixity, the authors perfomed a variable pressure and time study in Co-Zn bimetallic supported cluster on NU-1000. Moreover, they observed, for Co-Zn-NU-1000, higher selectivity and yield toward propadiene than in the Co-supported MOF, while the performance toward the generation of side products –propylene, propane and the production of coking– was lower for the bimetallic system, which suggested their synergistic effect. Interestingly, it was observed a difference in propadiene yield between Co-Zn and Zn-Co supported NU-1000, where the one with more exposed Zn ions exhibited better performance –which agree with the catalytic results of monometallic-modified MOFs. A theoretical study on the different mechanisms for isomerization and hydrogenation for Cu and Zn supported clusters evidenced that the distinct tendency toward either propadiene or propylene rely in their respective preference for homolytic or heteroleptic H_2 cleavage and hydrogen shuttling mechanism between 1,3 and 2,3-hydrogen shift. The great potential of mixed-metals MOFs has been recently further evidenced by Thiam *et al.* [241] (Fig. 22) with the step-by-step incorporation of $W(\equiv C^tBu)(CH_2{}^tBu)_3$ complex on NU-1000 and its use for gas and liquid phase olefin metathesis. A profound spectroscopic and microscopy characterization allowed to determine the coordination environment of the initial anchored precatalyst and its activated carbene form in the presence of an olefin, which validate the proposed synthetic method for the synthesis of W = O alkyl complexes using W carbyne precursors. The resulting mixed-metals MOF was first tested in a batch reactor for propylene methatesis at 80 °C, leading to thermodynamic mixtures of ethylene, propene and 2-butene. In a dynamic flow reactor, it delivered 250 accumulated TON after 16 h, which outperform other reported sytems anchored on NU-1000. Then, the authors investigated the kinetic conversion of 1-octene to 7-tetradecene at 80 °C. They observed that after and induction period (2–3 h), where it took place the formation of the active carbene site, a fast conversion occurred to the target primary metathesis product, with a maximum selectivity at 5 h. After that, there was an increase of selectivity toward isomerization products of 1-octene. Overall, this system showed a moderate activity with good selectivites toward primary metathesis compounds. But, noticeably, the reported system presented a higher catalytic performance than other reported W-based systems, and represent an appealing candidate to have a better model for the industrially relevant WO_3/SiO_2 catalyst.

As an alternative to metalation of discrete SBUs, Feng *et al.* [236] presented the metalation with $CoCl_2$ and $FeCl_2$ of rod-based aluminium hydroxide SBUs in the MIL-53(Al) MOF, and investigated their use in broad-scope important organic transformations. MIL-53(Al)-CoCl after activation with $NaBEt_3H$ led to MIL-53(Al)–CoH, which efficiently catalyzed hydrofunctionalization reactions, such as hydrosilylation of esters and hydroboration of alkynes and nitriles with good functional group tolerance. Meanwhile, MIL-53 (Al)-FeCl nicely catalyzed Wacker-type alkene oxidation and

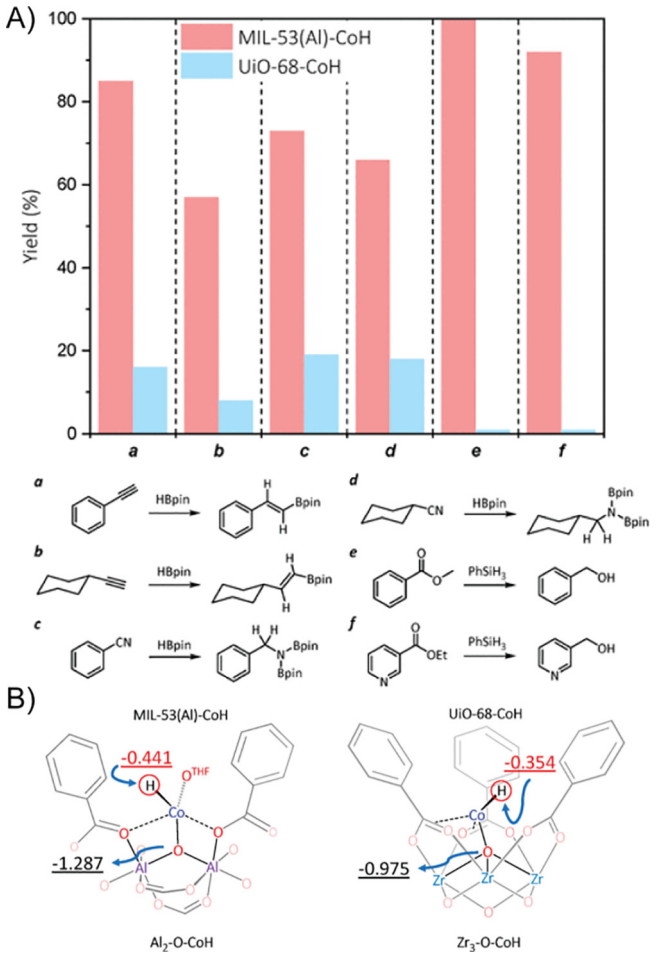

Fig. 42. A) Hydroboration of alkynes and nitriles and hydrosilylation of esters with different MOF SBU-supported Co catalysts. B) Natural Bond Orbital (NBO) charges of Co centers and hydride and bridging oxo groups in MIL-53(Al)–CoH and UiO-68-CoH. Adapted from ref. [236] with permission from the American Chemical Society, Copyright 2018.

oxidative Csp^3-H amination reactions. This work evidenced the unique potential heterogenous mixed-metals MOFs present in outperforming traditional materials with intrinsic heterogeneity, as γ-alumina, to support single-site earth-abundant metal heterogeneous catalyst, where is highly challenging to perform a uniform modification, as well as the characterization of catalytic species and unveil mechanistic details of the catalytic reactions. Indeed, profound spectroscopic studies together with deuterium labelling allowed to propose σ-bond metathesis as a key step for the hydroboration of terminal alkynes with MIL-53(Al)CoH (Fig. 42A). Also, comparative studies with UiO-68-Co and DFT computational calculations enabled to identify the electron-rich oxo sites as responsible for the efficient catalytic behaviour of MIL-53(Al)CoH (Fig. 42B). For the MIL-53(Al)-FeCl, extensive spectroscopic studies revealed the redox process Fe^{II}/Fe^{III} was involved in the oxidative transformations, and even more interestingly, allowed to propose a mechanism reaction for the C–H amination [236].

The use of preformed metalloligands have reveal as an appealing strategy to build up mixed-component MOFs with incorporated catalytically active metal ions.

Lee *et al.* [247] reported the use of IRMOF-10 and bio-MOF-100 for the structural stabilization of a gold(III) catalyst, IPrAu(III)(biphenyl)X –IPr = [1,3-bis(2,6-diisopropylphenyl)imidazole-2-yli dene and X = SbF_6 and PF_6 for IRMOF-10 (Fig. 43A) and bio-MOF-100, respectively– which, in homogenous conditions, or sup-

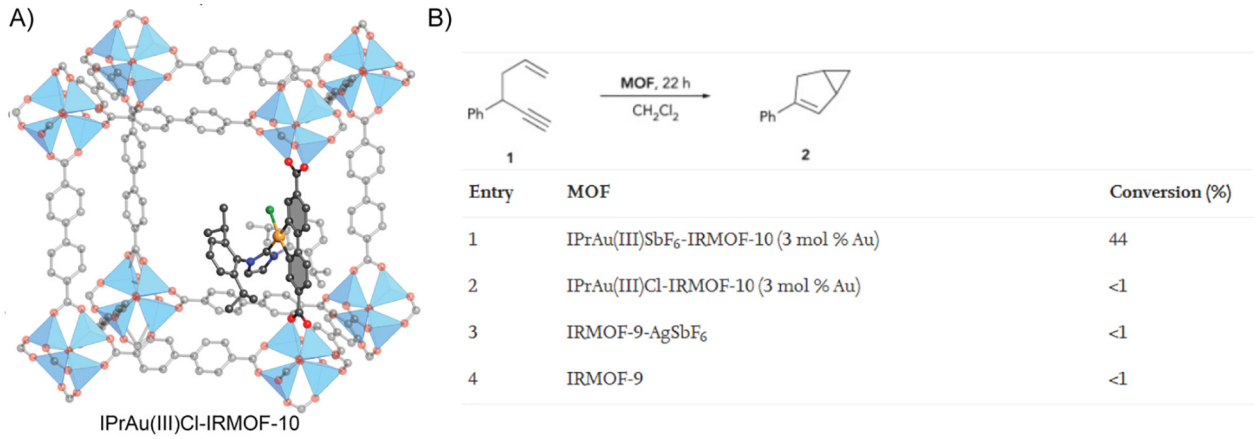

Entry	MOF	Conversion (%)
1	IPrAu(III)SbF_6-IRMOF-10 (3 mol % Au)	44
2	IPrAu(III)Cl-IRMOF-10 (3 mol % Au)	<1
3	IRMOF-9-$AgSbF_6$	<1
4	IRMOF-9	<1

Fig. 43. A) Modelled structure of IPrAu(III)Cl-IRMOF-10. B) Catalytic activity for a cycloisomerization reaction for IPrAu(III)SbF_6-IRMOF-10 compared to IPrAu(III)Cl-IRMOF-10, IRMOF-9-$AgSbF_6$ and IRMOF-9. Adapted from ref. [247] with permission from Elsevier, Copyright 2020.

ported in other type of solids tends to suffer unimolecular decomposition, and their application as catalyst in cycloisomerization reactions (Fig. 43B) [247]. In particular, the gold catalyst was incorporated using a mixed-linker strategy and SALE approach for IRMOF-10 and bio-MOF-100, respectively. The low gold(III) loading in IRMOF-10 precluded the direct observation of the incorporated catalyst by SCXRD. Thus, ^{1}H NMR and ICP-AES were used to determine the successful incorporation of the catalyst. Conversely, the particular linkers distribution in bio-MOF-100, allowed to replace selectively one type of BPDC ligands in the framework and, thus, made it possible to obtain a suitable occupancy to enable the partial determination of gold catalyst structure by SCXRD. This structural stabilization was confirmed on the study of the catalytic performance of the gold-incorporated MOFs. IPrAu(III)SbF_6-IRMOF-10 catalyzed with moderate yield the cycloisomerization of 1,5-enyne to the corresponding bicyclohexene, while IPrAu(III) PF_6-bio-MOF-100 showed a very efficient conversion of alkynyl cycloheptatriene to the corresponding mixture of indene products. The key role of the MOF on the supported catalyst stability was confirmed with the retention of its structure and functionality when it was tested in conditions where the homogenous catalyst experienced decomposition, as well as on their nice reusability and long-term strorage stability. Liu *et al.* [158] presented the synthesis of two multicomponent Zr_6-MOF constructed with different ratio of 2-(imidazole-1-yl)terephthalate (Im-BDC) and *N,N′*-bis(3-carboxyl-salicylidene)-1,2-cyclohexane-diamino cobalt(III) acetate (salen-Co^{III}) and their sequential post-synthetic ionization, by reacting the imidazole-functionalized MOF with bromoethane [158]. Thus, the resulting bifunctional MOFs contained nucleophilic imidazolium entities and salen-Co^{III} Lewis acidic sites, which showed a noticeable activity and selectivity in the cycloaddition reaction of carbon dioxide with a variety of long-chain and aromatic-substituted epoxides. Indeed, this performance was enhaced respect related MOFs with one type of functionality or physical mixtures of them, and it was maintained after five reuses. More importantly, this work also exemplifies the advantage that MOFs present as heterogenous catalysts of organic reactions, avoiding specific drawbacks of homogenous phase catalysts such as a very difficult isolation of products and recovery and reuse of the catalyst. Instead of using one metallosalen complex, Xia *et al.* [281] reported the application of 2-fold interpenetrated mixed-metals MOFs containing two and three distinct chiral metallosalen catalyst –1^{CuM} M = Mn, Fe, Co, Cr and V and $1^{CuMnM'}$ M′ = Cr and Co (Fig. 44A)– as efficient and recyclable heterogeneous catalyst for a wide variety of asymmetric tandem/sequential alkene epoxidation/epoxide ring-opening reactions (Fig. 44B) [281]. Extensive catalytic studies in binary mixed-metals MOFs 1^{CuM} revealed, M (salen) (M = Mn, Fe, Co, Cr and V) moieties were the active sites and the Cu(salen) ones had a crucial structural role for the formation of the 2-fold interpenetration, which, in turn, was the underlying reason behind the outstanding catalytic activity of ternary MOFs $1^{CuMnM'}$. In fact, it enables distinct M(salen) moieties being in close proximity to allow bimetallic cooperative activation, which renders improved activity and enantioselectivity compared with physical mixtures of the MOFs with individual M(salen) entities or binary MOFs. These results further remark the exciting possibilities the confinement effect in mixed-metals MOFs possess and validate a novel way to prepare multifunctional heterogeneous catalyst [281].

Alternatively, another strategy to incorporate mixed-M(salen) linkers is based on SALE postsynthetic methods. Tan *et al.* [280] reported the sequential incorporation of two distinct chiral M (salen) linkers in an achiral and highly-robust UiO-68 type network to led to the formation of UiO-68-Mn-Cr and UiO-68-Mn-V, which combined two catalytic metal centres in a chiral MOF and offered the possibility to promote sequential reactions. Indeed, UiO-68-Mn-Cr showed an excellent performance on the epoxidation of alkene 2,2-dimethyl-2*H*-chromene with 2-(*tert*-butylsulfonyl) iodosylbenzene and subsequent ring-opening with different anilines in chloroform at room temperature to produce the target amino alcohol in high yields (80–85%) and enantiomeric excess (80–99.5%). Also, it exhibited a nice recyclability (10 reuses) without depletion of activity or enantioselectivity. Besides the relevance from a catalytic viewpoint, we would like to remark the relevance of this approach to obtain highly stable chiral MOFs, which somehow have been underexplored due to the difficulties of incorporate enantiopure ligands by direct synthesis, and traditionally, it has been focused on more inestable Zn_4-based MOFs [280].

Metalation of organic auxiliary ligands have been widely used to develop mixed-metals MOFs with remarkabale catalytic aplications [137,161,242,243,246,250,251,254,255,332,333]. Feng *et al.* [251] post-synthetically metalated a Zr-based MOF build up with either 4,′4,″,4‴ ‴-phosphanetriyltris-([1,1′-biphenyl]-4-carboxylic acid) (H_3P_1) or 2,2′-bipyridine-5,5′dicarboxylic acid (DCBPY) with $[Ir(COD)Cl]_2$ to render two mixed-metals MOFs, Zr-P1-Ir and Zr-BPY-Ir, with stable low-coordinate Ir complexes. These hybrid materials catalyze, in an efficient and selective manner, the methane borylation –using bis(pinacolato)diboron (B_2pin_2)– to yield the monoborylated product [251]. Despite the authors did not attempted to use SCXRD for the characterization of the final catalyst, they performed extensive EXAFS and XANES studies to

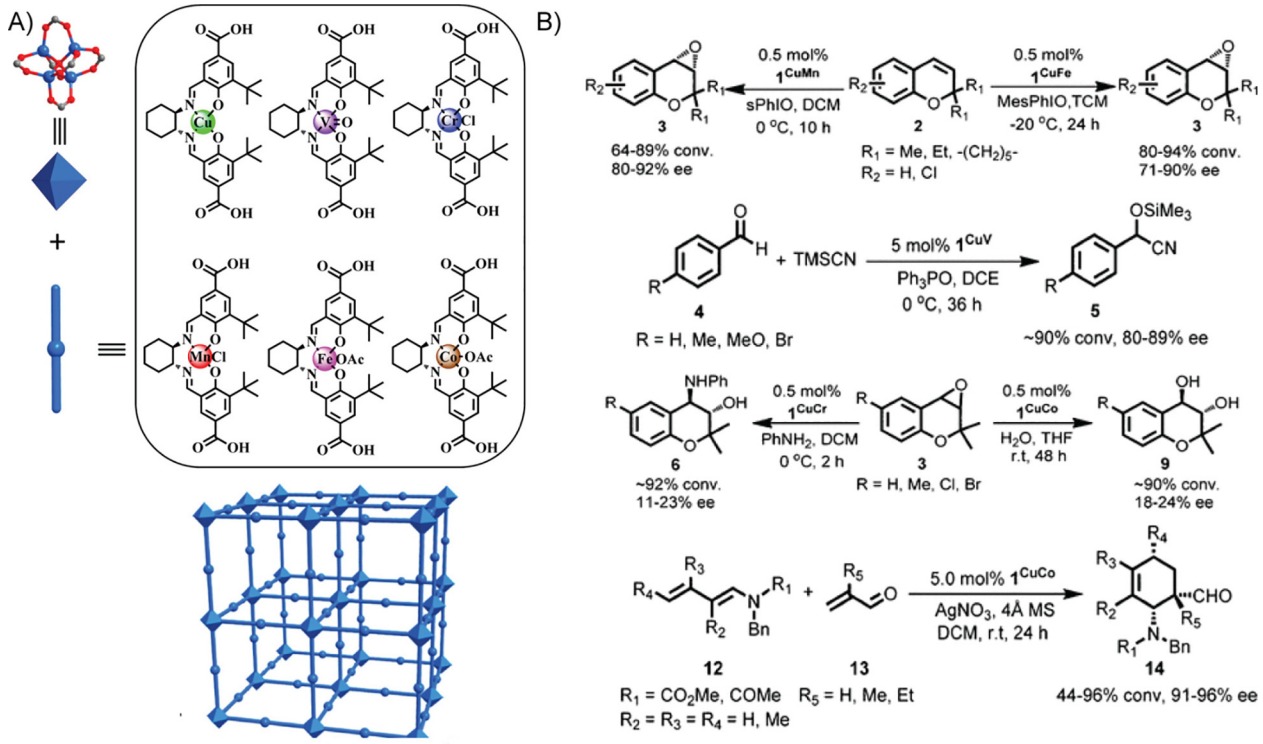

Fig. 44. A) Construction of the MTV-MOFs $\mathbf{1}^{\mathbf{CuM}}$ and $\mathbf{1}^{\mathbf{CuMM'}}$ with different metallosalen linkers. B) Different asymmetric reactions catalyzed by the binary MOFs. Adapted from ref. [281] with permission from the American Chemical Society, Copyright 2017.

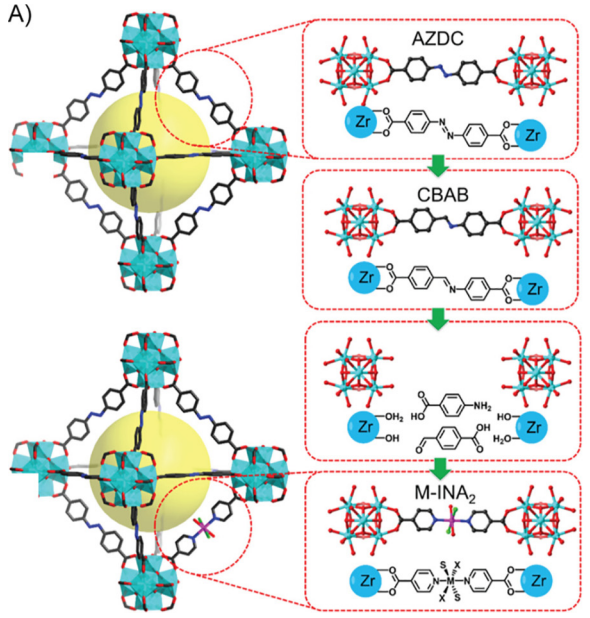

B)

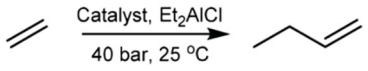

catalyst[b]	C_4 intrinsic activity[c] (h^{-1})	selectivity (%)		
		1-C_4	2-C_4	C_6 + C_8
PCN-160	0	0	0	0
none	0	0	0	0
$NiCl_2$@PCN-160	171 ± 30	81.1	9.9	9.0
Ni-INA_2	304 ± 50	75.9	21.1	3.0
(bpy)$NiCl_2$	288 ± 20	74.1	19.5	6.4
UiO-67-50%Ni	455 ± 40	66.7	29.0	4.3
PCN-160-47% Ni	3360 ± 240	82.4	15.8	1.8

Fig. 45. A) Construction of PCN-160-R%M with *trans*-chelating ligands from PCN-160 via elimination and installation. B) Ethylene dimerization reaction catalyzed by PCN-160-R%M, PCN-160 and other Ni containing materials. Adapted from ref. [333] with permission from the American Chemical Society, Copyright 2018.

elucidate the coordination environment and oxidation state of the iridium complexes. The authors found that the phosphine-Ir MOF showed the best results, outperforming previous reported methane borylation catalyst, with a yield of 38% for CH_3Bpin and a TON of 127 at 110 °C. Based on computational studies, they attributed this outstanding catalytic activity to the lower activation energy barrier for the oxidative addidition of methane to the homogeneously isolated four-coordinated iridium catalyst, (P1)-$Ir^{III}(Bpin)_3$, in Zr-P1-Ir, which led to the formation of a six-coordinate (P1)-$Ir^{V}(Bpin)_3(CH_3)(H)$ intermediate and precluded the formation of more sterically crowded seven-coordinated Ir^{V} intermediates, as occured when using other Ir catalyst based on chelating N- and P-ligands. Also, it was denoted as important the stabilization role the MOF scaffold played on the low-coordinated iridium catalyst, preventing its

redistribution and agregation, and its structural constraint/rigidity, avoiding the formation of sterically impeded overborylated byproducts.

Yuan *et al.* [333] reported a more elaborated protocol to incorporate *trans*-coordinated metal centres in the Zr_6-based MOF, PCN-160, with accesible equatorial positions to substrates. These mixed-metals MOFs were obtained by the sequential partial ligand exchange of azobenzene-4,4′-dicarboxylate (AZDC) by 4-carboxy benzylidene-4-aminobenzoate (CBAB) to led to a mixed-linker MOF, denoted as PCN-160-R% –R% stands for the percentatge of CBAB ligand replaced in the sample– (Fig. 45A), the elimination of CBAB and installation of isonicotinic acid and MCl_2 (M = Mn, Fe, Co, Ni, Cu and Pd), to form *in-situ trans*-pyridyl coordinated octahedral complexes connecting Zr_6-SBUs. Here, it is important to note that direct synthetic protocols did not showed successful for the obtention of such complex MOFs, but the development of sophisticated PSMs enabled their synthesis. SCXRD studies were attempted on Ni and Pd derivatives but, unfortunately, only partial resolution of coordination environement of *trans*-coordinated metal ions could be elucidated from it. Further spectroscopic characterization (EXAFS and XANES) and TGA-MS were used to elucidated the octahedral geometry of nickel and the square-planar of palladium. From the different materials reported, the authors showed PCN-160–47%Ni present better catalytic performance for the ethylene dimerization reaction (Fig. 45B) than homogeneous molecular catalyst and related MOFs with *cis*-chelated Ni centers. This was attributed to the *trans*-coordination of the Ni ion, which facilitates the substrate binding and accelerate the reaction. Remarkably, PCN-160–47%Ni was reused three times, without compromising the structural integrity of this material and with a minimal depletion of its activity. Besides the interest from a catalytic point-of-view, this manuscript represents a beautiful example of the potential of MOFs to construct species, which otherwise are hardly accessible. Mixed-metals and linkers MOFs represents exciting platforms to improve the performance of copper photosensitizers and molecular catalyst in relevant solar energy conversions. In this context, Feng *et al.* [332] reported the stepwise post-synthetic metalation of a mixed-linker UiO-type MOF, denoted as mPT-MOF [161] –constituted of phenanthroline dibenzoate (PT) and 2″-nitro-[1,1′:4′,1″:4″,1‴-quaterphenyl]-4,4‴-dicarboxylate (TPHN) ligands. For the hydrogen evolution reactions (HER), they first metalated mPT-MOF with $Cu(CH_3CN)PF_6$, and coordinated the copper ions with 1,2-bis(diphenyl-phosphino)ethane (DPPE), and then, $CoCl_2$ was incorporated to the remaining PT sites to led to the formation of mPT-Cu/Co. Instead, for CO_2 reduction reactions (CO_2RR), they performed sequential metalation with $Re(CO)_5Cl$ and $Cu(CH_3CN)_4PF_6$, followed by chelation with DPPE of copper sites, to yield mPT-Cu/Re [332]. On one side, the visible-light driven HER activity of mPT-Cu/Co –perfomed in acetonitrile with acetic acid as proton source and 1,3-dimethyl-2-phenyl-2,3-dihydro-1*H*-benzo[*d*]imidazole (BIH) as sacrificial agent– showed an outstanding TON of 18700, which outperforms most of better Cu-, Ir- and Ru-photosensitizers, and was reused at least three runs without an appreciable decrease in catalytic activity. On the other side, the CO_2RR under 350–700 nm irradiation with mPT-Cu/Re –in a mixed solution of water and *N*,*N*-dimethylacetamide and BIH as sacrificial agent– produced CO with a TON of 1328 and CO/H_2 selectivity of 9:1, which outperforms in two orders of magnitude the related homogeneous molecular control. In addition, the authors performed photophysical and electrochemical studies to gain understanding on the mechanism of HER and CO_2RR, which evidenced a reductive quenching pathway. This was initiated by the electronic transfer from BIH to the photoexcited $[Cu\text{-}PS]^*$ to generate $[Cu\text{-}PS]^-$, which transfer electrons to Co/Re catalytic sites for HER/CO_2RR. This mechanism supported the improved performance of the reported MOFs respect their homogenous counterparts on the basis of the close proximity between Cu-PSs and molecular active catalyst, and their stabilization by the MOF network. This stepwise synthetic approach was also successfully followed by some of the same authors to perform bioinspired synergistic catalysis within the pores of a sequentially post-synthetically modified Al-based mesoporous MOF [255]. In particular, after this post-synthetic route, they were able to present, within the same channel, strong Lewis acid sites as binding centers and Ir-based photoredox catalytic active sites for the reductive cross-coupling of aryl bromomethyl ketones or *N*-hydroxyphthalimide esters with alkynyl or vinyl-azaarenes to afford new azaarenes derivatives in a very efficient manner. Among a wide plethora of different products, the authors showed this highly complex MOF was able to synthesize drug molecules –pheniramine and chlorpheniramine– in moderate yields. Remarkably, this material exhibited a high robustness, which allowed it to be reused up to five times with no decrease in its catalytic performance. Based on control and quenching experiments, the authors also suggest a potential mechanism for the reaction, which highlights the relevance of the pore confinement effect, and consequently close proximity of both types of sites, in the efficient catalytic performance.

Pi *et al.* [334] combined the metalation of SBUs and organic auxiliary ligands, in a sequential manner, to report a highly complex mixed-metals MOF for visible-light photocatalytic hydrogen evolution. This is a very challenging reaction and a considerable amount of work has been devoted. However, there is still the need to develop low-cost, earth abundant materials with an appealing number of light-harvesting and proton reduction entities in close proximity for efficient hydrogen generation. In order to achieve these milestones, the authors prepared a robust multicomponent Zr_6-MOF (Fig. 46A) –constructed with nitro-quaterphenyl dicarboxylate (TPHN) and *p*-phenantroline dibenzoate (PT) linkers– to whom, in a first step, Cu^I ions were incorporated to the PT groups and then coordinated by 1,2-diphenylphosphinoethane (DPPE), and subsequently, in a second step, different FeX_2 salts (X = AcO, Cl, Br and BF_4) were anchored to the μ_3-OH sites of the Zr_6-SBUs. This led to mixed-metals MOFs with cuprous photosensitizing (Cu-Ps) ligands and catalytically active Fe^{II} sites supported on the SBUs in pretty close proximity (*ca.* 1 nm). This, together with the stabilization of low-coordinated iron ions by the SBUs, enabled to obtain a highly active catalyst for photocatalytic H_2 evolution (Fig. 46B). Indeed, the authors studied the impact of changing the iron metal ions by cobalt and niquel and observed nearly five and nine times fewer turnover numbers (TONs), respectively. Also, they presented the influence of the coordinated counteranion, where the ones with a more labile character exhibited the hightest performance. In particular, the tetrafluoraborate one, was the best with TONs up to 33,700 at 48 h and turnover frequencies (TOFs) up to 880 h^{-1} at 6 h with an apparent quantum yield of 7.9%. Such outstanding behaviour was explained on the basis of the facility to generate open coordination environments on Fe sites, which facilitates the formation of key Fe-hydride intermediates in the proton reduction event. Interestingly, the extensive and precise characterization of this material allowed them to propose a photocatalytic cycle for the H_2 evolution (Fig. 46C).

Mixed-component MOFs with distinct SBUs and linkers represent an excellent opportunity to perform catalytic reactions where one of the components acts as the active catalytic center, while the others play a structural role or somehow influence the catalytic outcome. In this context, the family of multicomponent compounds FDM-3–7 developed by Tu *et al.* [289] took advantage of the trinuclear complex $[Cu^{II}_3(\mu\text{-}OH)(HPyC)_3]^{2+}$, which can be reduced in a reversible manner to $[Cu^{I}_3(HPyC)_3]$ without altering the connectivity of the framework (Fig. 47A), to efficiently catalyze the oxidation of CO (Fig. 47B) and aromatic alcohols and the

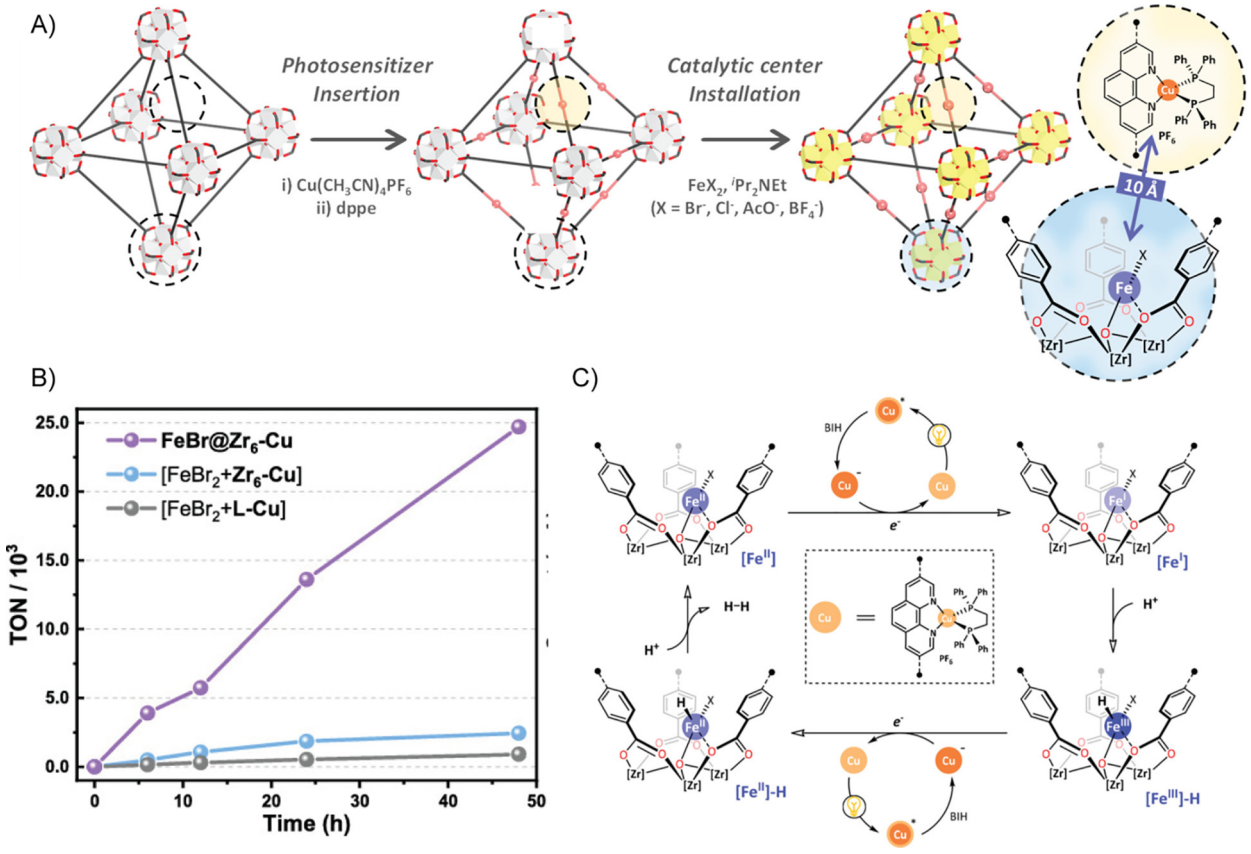

Fig. 46. A) Sequential installation of Cu^{I} photosensitizers and Fe^{II} catalytic centers in **Zr_6-mPT** to afford **FeX@Zr_6-Cu** (X = Br^-, Cl^-, AcO^-, and BF_4^-). B) Time-dependent photocatalytic H_2 evolution TONs of **FeBr@Zr_6-Cu** compared to **Zr_6-Cu** + $FeBr_2$ and **L-Cu** + $FeBr_2$. C) Proposed photocatalytic cycle for H_2 evolution. Adapted from ref. [334] with permission from the American Chemical Society, Copyright 2020.

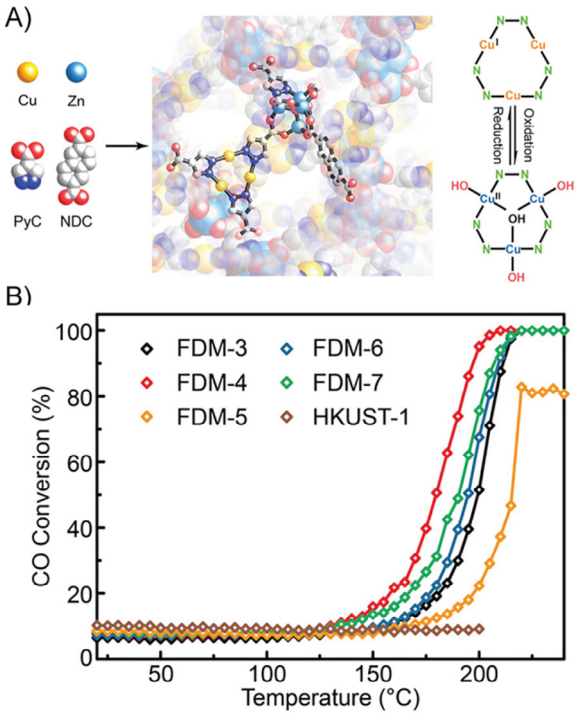

Fig. 47. A) Representation of multicomponent FDM-3–7 and interchangeability of Cu valences in the frameworks of FDM-3–7. B) CO conversion as a function of reaction temperature over activated FDM-3–7 compared to HKUST-1. Adapted from ref. [289] with permission from the American Chemical Society, Copyright 2017.

decomposition of H_2O_2 [289]. In particular, FDM-3–7 could catalyze the full conversion of CO to CO_2 –*ca.* 210 °C for FDM-4 and *ca.* 220 °C for FDM-3, –6 and –7– retaining their structures and without the appereance of peaks attribuible to Cu_2O or CuO, as PXRD patterns supported, which confirmed the triangular Cu^{I} entities as the catalytic active sites. Indeed, from a comparative study with HKUST-1 and a non-redox active Cu^{II} pyrazolatecarboxylate MOF, the authors concluded that the high density of Cu^{I} sites and their ability to change their oxidation state were behind the great performance of the presented multicomponent MOFs. This was further confirmed with the excellent activity of FDM-3, –4, –6 and –7 in the aerobic oxidation of benzyl alcohol with the aid of 2,2,6,6-tetramethylpiperidin-1-oxyl (TEMPO) and *N*-methylimidazole (NMI) as cocatalysts, despite the MOFs loses their crystallinities after their first use. Also, this interchangeability of the copper oxidation states in FDM-3–7 resulted very useful to catalyze the decomposition of H_2O_2. For example, each copper site in FDM-4 was involved at least in 500 cycles of H_2O_2 conversion without depletion of its activity. Although, in this case of study, the multicomponents MOFs also lose their crystallinity after catalysis –most likely due to H_2O coordination to Zn-SBUs– the relevant point of this manuscript resides on the proof-of-concept design of multicomponent redox-active MOFs for catalytic applications, which have set the basis for the future development of such MOFs with more robust SBUs.

3.3. Luminescence (luminescent sensors)

Luminescence in MOFs have been traditionally tailored by selecting particular emissive organic linkers, metal ions or SBUs,

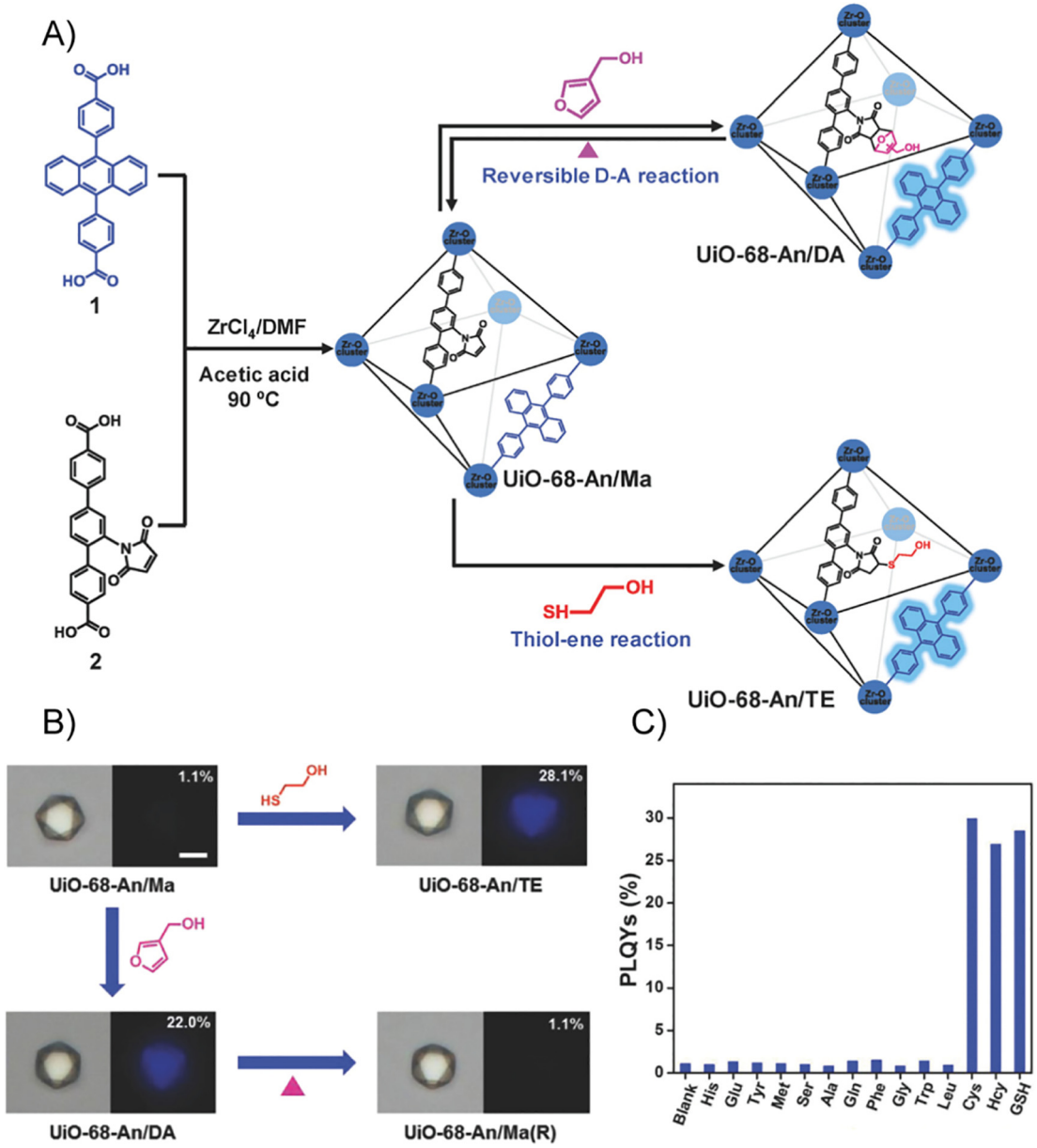

Fig. 48. A) Synthesis of UiO-68-An/Ma and tuning the fluorescent PET in the MOF through reversible D–A reaction or thiol-ene reaction. B) Bright-field and photoluminescence images (excited with mercury lamp) of fresh UiO-68-An/Ma, UiO-68-An/DA, UiO-68-An/Ma(R), and UiO-68-An/TE. C) Absolute PLQYs (±0.5%) of UiO-68-An/Ma immersed into different amino acids ($c = 10^{-3}$ mol L^{-1}). Adapted from ref. [157] with permission from John Wiley & Sons, Copyright 2018.

and/or by encapsulation of emissive guest molecules. Although single-component MOFs have displayed a broad range of applications in sensing, photocatalysis and non-linear optics, as well as more recently in solid-state lighting, data storage or biomedical sensing [335–338]. Heterogeneity in mixed-components MOFs offers novel opportunities, which could not be easily achieved using traditional MOFs [90,91,154,157,190–193,265,339,340]. Yu *et al.* [91] reported a Zn-based MTV-MOF, built up with 5,5′-(pyridine-2,5-diyl)-diisophthalic acid and 2,5-bis(3,5-dicarboxyphenyl)-1-methylpyridinium hydroxide, where the nonlinear optical nature of the latter ligand enabled the MOF to exhibit a significant red-shift change in two-photon excited fluorescence, as consequence of the photochemical reaction this ligand suffers under femtosecond laser [91]. More interestingly, from applications viewpoint, the two-phonon effects with the laser at 710 nm led to a 3D pattern (write) with high spatial resolution ($1 \times 1 \times 5$ μm^3), which could be imaged (read) with a laser at 900 nm using multiphoton fluorescence microscopy. This represents novel opportunities for MOFs in emerging fields such as data storage media or sensor arrays. Luminescence applications have been also investigated by Gui *et al.*, [157] who took advantage in a UiO-68 type mixed-linker MOF of their heterogenous nature to investigate the photoinduced electron transfer (PET) in solids supports [157]. In particular, they constructed a Zr_6-based MOF with carboxylate-based ligands containing either anthracene (An, fluorophore) moieties or maleimide (Ma, acceptor) groups in a 1:1 ratio (UiO-68-An/Ma) (Fig. 48A), where the close arrangement between both separately inmobilized entities favor a pseudo-intramolecular fluorescent PET, leading to a very low absolute photoluminescence quantum yield (PLQY) of 1.1%. Remarkably, they observed the PET could be controlled by tuning the electron-accepting features of maleimide groups by means of Diels-Alder (D-A) and thiol-ene reaction, leading to PLQY of 22 and 28.1%, respectively (Fig. 48B). In addition, the fluorescence-triggered by

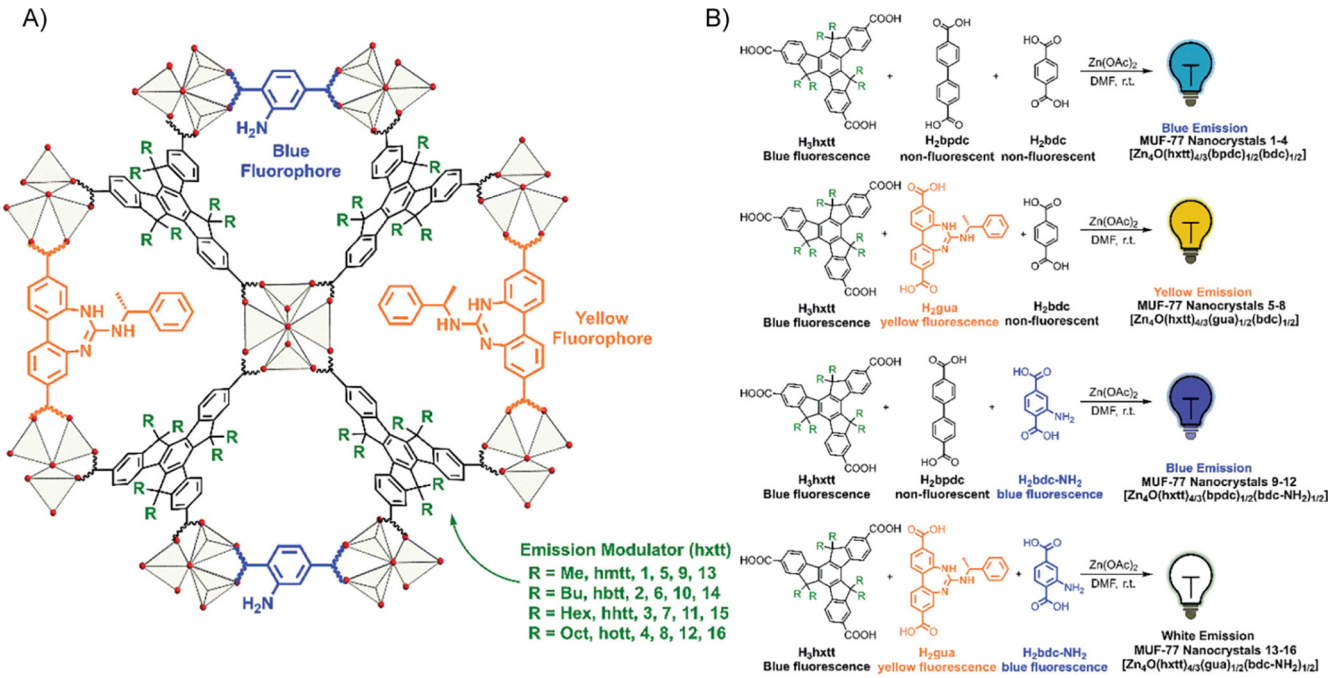

Fig. 49. A) Schematic representation of the structure of MUF-77 showing the relative arrangement of the ligands. B) Preparation of the 16 luminescent MUF-77 nanocrystals and luminescent properties. Adapted from ref. [154] with permission from the American Chemical Society, Copyright 2018.

D-A reaction in UiO-68-An/Ma could be reversibly thermally-modulated –up to three switching cycles– which makes it an efficient solid-state fluorescent molecular switch. Remarkably, the thiol-ene fluorescent-triggered reaction could be used to convert UiO-68-An/Ma (Fig. 48A) in a solid-state fluorescent turn-on sensor for important molecules in living organisms such as biothiols –cysteine, homocysteine and glutathione– at very low concentrations (50 μmol L^{-1}) (Fig. 48C). Overall, this work represents a general and efficient approach to design fluorescent PET switches/sensors in the solid state, and nicely evidences the potential of mixed-linkers MOFs in luminescent properties.

The multicomponent approach has been also applied by Cornelio *et al.* [154] in MUF-77 derivatives (Fig. 49A), where they presented that through the functionalization of the organic linkers it was possible to tune the color-light emission in a family of sixteen isoreticular multicomponent MOFs, which represented an alternative method respect commonly used approaches based on the encapsulation of emissive guests or the use of different luminescent metal ions [154]. In particular, white-light emission with tunable correlated color temperature (CCT) from UV input was achieved by combining blue (NH_2-BDC, λ_{em} = 427 nm) and yellow (guanidine functional group attached to BPDC, λ_{em} = 570 nm) fluorophores in four different MUF-77 derivatives, where the third ligand was a truxene-type linker (with a characteristic very weak blue emission) with different alkyl (methyl, butyl, hexyl and octyl) substituents. From them, the one with hexyl functionalization on truxene linker exhibited Commission Internationale de l'Éclairage (CIE) coordinates of (0.3218, 0.3590) and CCT of 5935 K, which was close to that of pure white light (0.33, 0.33). Also, the authors reported experiments demonstrating that the emission features of these multicomponent MOFs could be tunned by interligand energy transfer and guest binding (Fig. 49B). Finally, the authors presented the viability of white-emitting MUF-77 devices, by coating it with an UV LED.

A similar study, using MTV-MOFs, was reported by Newsome *et al.* [90] The authors prepared a family of Zr_6-based MTV-MOFs –the major component being tetramethylquaterphenyldicarboxylate (NF) linkers and the three types of fluorescent linkers (Fig. 50A), based on quaterphenyl links functionalised with 1,2-diarylphenanthro[9,10-*d*]imidazole fluorophores– where the unsubstituted phenol emits in the blue (B), the phenyl subtituted shifts its emission to green (G) and the naphtol moiety emitting in the red (R) (Fig. 50B) [90]. The work reports the incorporation from one up to three distinct fluorophores, leading to MTV-MOFs that emit multicolor and white-light –depending on the relative content of each fluorophore– with high quantum yields, and allows to transfer the concept of substitutional solid solutions (SSS) of solid-state chemistry to MOFs chemistry. For example, the three-fluorophore MTV-MOF $Zr_6O_4(OH)_4[(R_{0.4}G_{0.2}B_{0.4})_{0.01}NF_{0.99}]_6$ exhibited the combined broadband emission from all three fluorophores with CIE (0.31, 0.33) pretty close to the pure white-light and a CCT of 6480 K, which was nearly identical to that of natural daylight (6500 K). Also, this material presented a remarkable good color-rendering index (CRI) of 95, being 100 the score for an identical standardized daylight, typical fluorescent bulbs being around 50 and white LEDs commonly scoring > 80. In addition to such nice physical features, the authors reported a very long-shelf life (at least up to 10 months), low inner filtering, economically-viability –due to not use expensive lanthanoids– and high hydrolytic stability at ambient conditions, which situate these materials in an excepcional position to think on their application in photonic devices and high-definition displays [90]. Later, some of the same authors, investigated the J-dimer emission in a family of double interwoven Zr_6-based MTV MOFs, built up with different ratios of bis(phenylethynyl)anthracene (An, J-dimer linker) and bis(phenylethynyl)xylene (Xy, structural ligand) ligands [341]. The characteristic feature of J-dimer emission is the fluorescence shift, with respect the monomer, as consequence of changes in the electronic structure of the emitting ligand due to π-π stacking. The authors reported fluorescence shifts from green to red with lifetimes up to 13 ns and good quantum yields (76%), which correlates directly to the equilibrium link-link interactions occurring at crystallization. Solid-state fluorescence studies (λ_{ex} = 415-nm) evidenced a J-dimer emission band, which shifted with

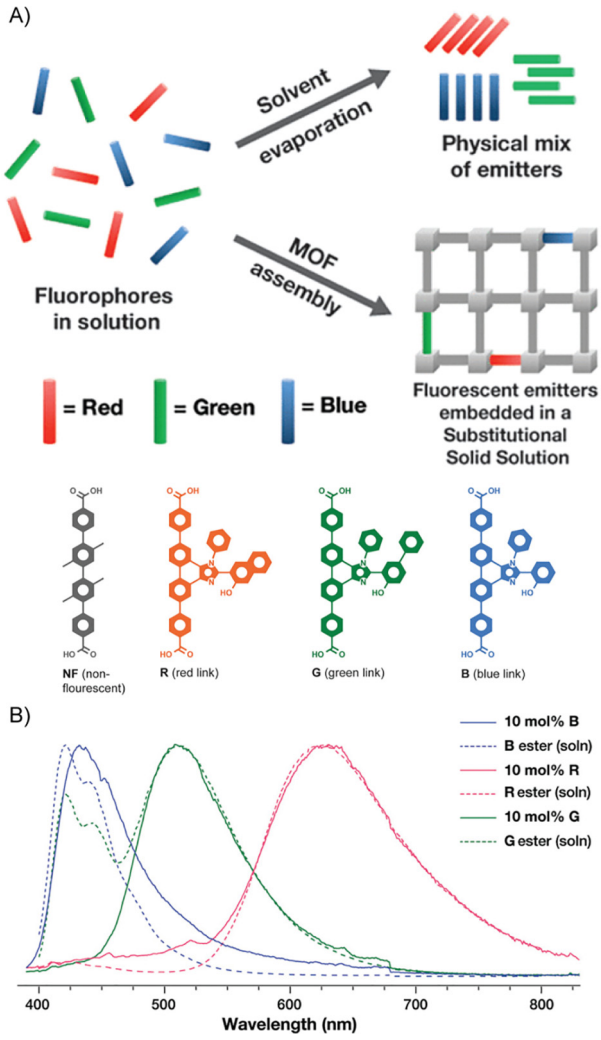

Fig. 50. A) Schematic representation of the organic-based substitutional solid solution formation of MTV-MOFs showing the organic links used in this study. B) Overlay of toluene-solvated fluorophore esters (dashed lines) and single fluorophore MOFs. Adapted from ref. [90] with permission from the American Chemical Society, Copyright 2019.

concentration from 532 to 609 (1–100% An), and contrasted with the monomer emission peak of An (λ = 515 nm). Through an extensive spectroscopic study, they also observed the lifetime and emission quantum yield varied depending on the fluorophore concentration. From it, they were able to obtain the equilibrium constant of dimerization, K_D, which was found to be three orders of magnitude larger than other well-known fluorescent dyes in solution, and the authors attributed this to the special mechanically interlocked structure of such complex MTV-MOF.

Following the same multivariate approach, Lustig *et al.* [342] presented the optimization of the previously reported LMOF-231 (LMOF stands for luminescent metal–organic framework) –constructed with rod-based Zn-carboxylate chains linked with the tetraanion of 1,1,2,2-tetrakis(4-(4-carboxyphenyl)phenyl)ethene (H_4TCBPE)– with an impressive quantum yield (QY) of 76%, based on intensive photoluminescence (PL) spectroscopic studies and guided by DFT calculations. The synthetic strategy relies on the construction of the MTV-MOF LMOF-305 –isoreticular to LMOF-231, and built up with TCBPE and the tetraanion of 1,1,2,2-tetrakis(4-(3-fluoro-4-carboxy-phenyl)phenyl)ethane (H_4TCBPE-F) [342]. They showed this heterogenous MTV-MOF set a new record in rare-earth element free yellow-emiting LMOF based phosphor-converted white LED (PC-WLED) with an internal QY of 88% (λ_{em} = 550 nm) upon excitation with 455 nm blue light. The authors investigated, through polarized and temperature dependent PL studies, the emission mechanism and found that the underlying reason for the improved behaviour was the narrowing of the material's band gap as consequence of the mixed-linker approach pursued. Indeed, the study of the influence of the TCBPE-F content demonstrated that the QY increases with the amount of fluorinated ligand. They also found that the emissive properties would come from both the interligand emission, as consequence of the interactions, between distinct neighboring ligands, and the intraligand emission from the two types of ligands constituting the MTV-MOF. Besides the performance of LMOF-305 is still not comparable to the commercial phosphor YAG:Ce (QY = 96%), its lower cost, due to the lack of expensive rare-earth elements, and their environmentally benign nature, in contrast to hazardous mining operations associated with lanthanoids extraction, make this material a very appealing system to enable the global adoption of WLED, which eventually will result in important energy savings and consequently a more sustainable development.

Zeng *et al.* [343] reported a dual-emissive MOF, where H_2N-$BPDC^{2-}$ and $BPyDC^{2-}$ were integrated into MOF-253 in one-pot synthesis and, afterwards, postsynthetic methods allowed the incorporation of Eu(III) cations to afford 5–5-Eu/BPyDC@MOF-253-NH_2 (Fig. 51A) [343]. As the blue emission derived from the $BPDC^{2-}$ ligand is sensitive to hypochlorite (Fig. 51B), while the red emission derived from Eu(III) cations remains invariable, 5–5-Eu/BPyDC@MOF-253-NH_2 was proposed as "on–off" sensor of hypochlorite (Fig. 51C) with low detection limit (0.094 μM), fast response (within 15 s), relative high specificity and wide linear range (0.1–30 μM). The suppressed blue emission was recovered after the consumption of ClO^- via the redox reaction with ascorbic acid.

3.4. Conductivity

Electronic- or ion-conducting MOFs are potential candidates to substitute membranes, electrolyte or the electrode of fuel cells, Li- and Na-ion batteries. In this context, for example, MOFs have become a promising approach for improving fuel cells by replacing the amorphous polymers, where it is not possible to establish structure–property relationships due to their lack of long-range order [212,344–346]. Despite mixed-components MOFs have been scarcely used for this application, several relevant examples have been reported.

In proton conduction, perfluorosulfonic acid polymers (*e.g.* Nafion) are the benchmark materials as consequence of their great performances. However, their large-scale applicability is somehow hampered by some of their weakness –*e. g.* high costs, complex synthesis, low performance at temperatures above 353 K and poor dimensional stability. Thus, it would be highly desirable to find a material able to maintain/improve performances of Nafion, while circumventing their drawbacks. In this context, pending sulphonic moieties (-SO_3H) [347] in mixed-components MOFs have revealed as very promising proton conductors materials, even some of them surpassing Nafion [348–350]. Nandi *et al.* [351] reported a family of multicomponent Ti_8-MOFs isoreticular to MIP-207 [115], constituted with BTC and 5-SO_3H-isophthalate (SO_3H-IPA) –MIP-207-(SO_3H-IPA)$_x$-(BTC)$_{1-x}$, where × = 0–0.66–, as super-protic conductors. They found the proton conductor behaviour rise from 8.9×10^{-5} to 2.6×10^{-2} S cm^{-1} at 363 K –95% relative humidity (RH)– with increasing amount of sulfonic groups until × = 0.28, while retaining the structural integrity under operating conditions. These reported values situate this multicomponent MOF among the best performing proton-conducting MOFs [347–350], which is particularly relevant considering that other materials possess

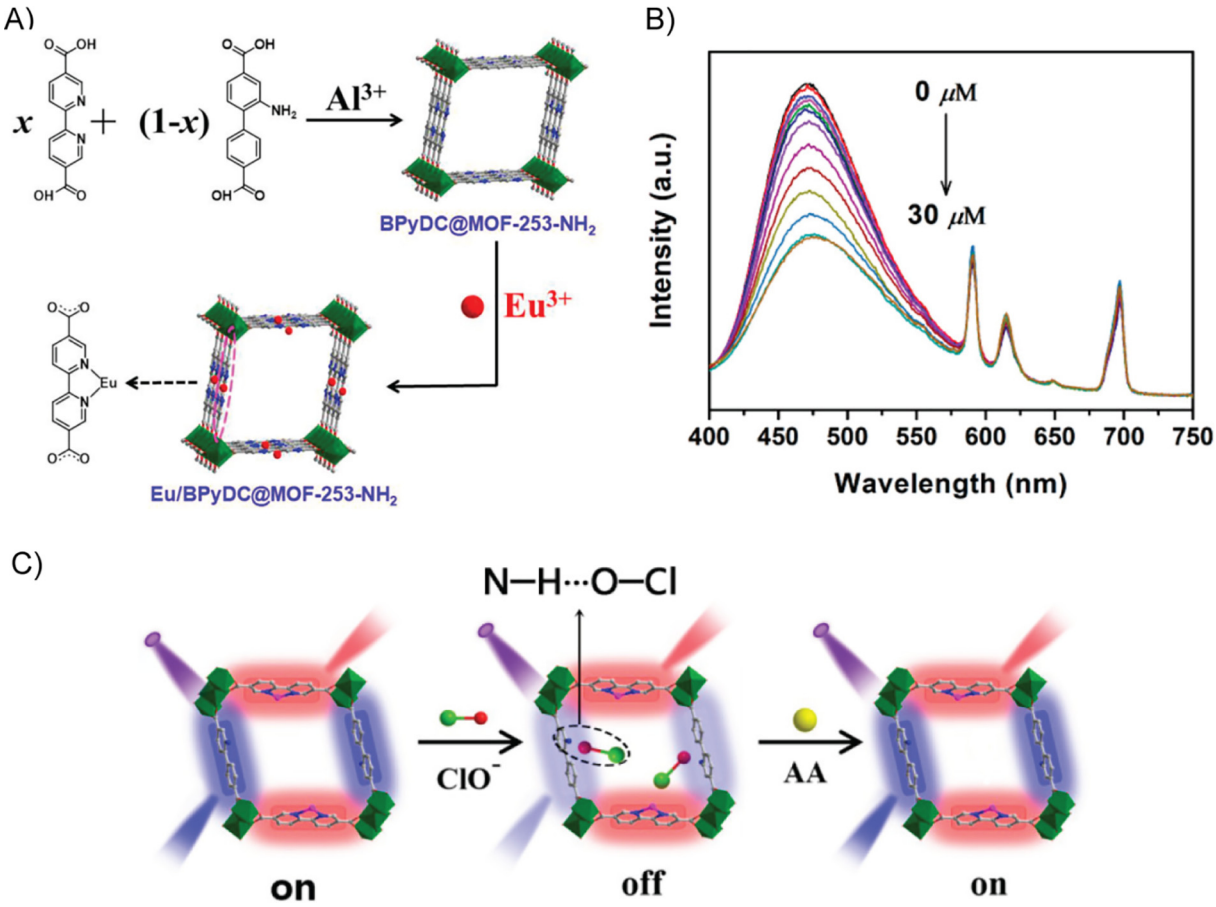

Fig. 51. A) Schematic representation and structure of MTV Eu/BPyDC@MOF-253-NH_2. B) ClO^- dose-dependent fluorescent spectra of 5–5-Eu/BPyDC@MOF-253-NH_2 suspensions. C) Proposed mechanism of the fluorescent "switch". Adapted from ref. [343] with permission from the American Chemical Society, Copyright 2019.

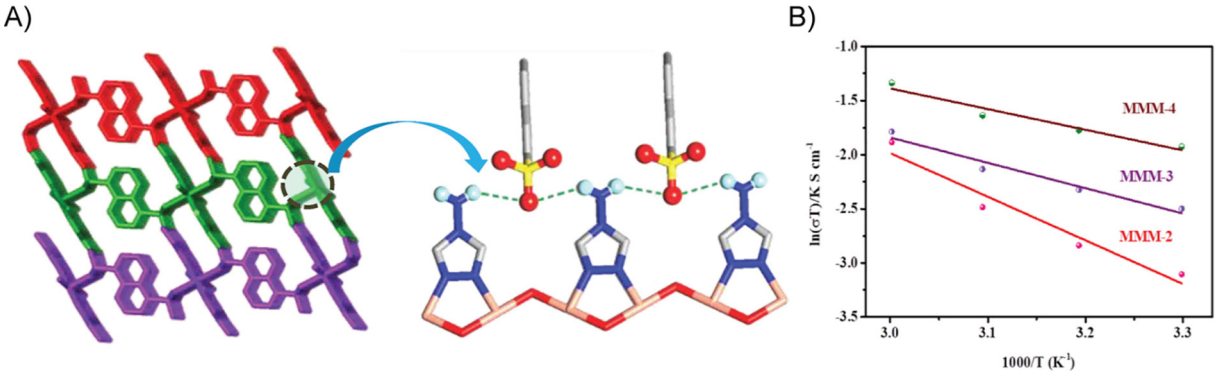

Fig. 52. A) Structure of the MOF and illustration of N–H···O hydrogen bonding between the stacked 2D layers. B) Arrhenius plots for all of the composite membranes in the temperature range of 50–80 °C at 98% RH. Adapted from ref. [353] with permission from the American Chemical Society, Copyright 2020.

higher content of SO_3H groups. The authors found that the activation energy (ΔE) was equal to the pristine MIP-207 (0.25 eV), which evidenced the Grotthus-like proton transfer mechanism nature [352], and further supported both that the enhancement of conductivity was due to the increase amount of the strongest proton donor –SO_3H groups– and the H-bonded network remains unchanged respect MIP-207. From variable-RH impedance measurements it was evidenced that water molecules strongly participate in the proton transfer pathway within the MOF, interconnecting SO_3H donors and acceptors, and securing a continuous H-bonded network. Indeed, theoretical simulations supported the proposed proton transfer mechanism, which evidenced the fast release of the acidic protons of sulfonic moieties to water molecules and the subsequent presence of a percolated H-bonded network within multicomponent MOF.

Moi *et al.* [353] prepared a mixed-component MOF –built up with 1,5-naphthalenedisulfonic acid (NDS) and 1,2,4-triazol-4-amine (T4A), that connect copper(II) ions leading to 1D chains, which are connected together by sulfonates to form a 2D layer and, further joined through N–H···O hydrogen bonding between amine and sulfonate groups to yield a 3D hydrogen-bonding framework (Fig. 52A). This MOF exhibits a remarkable proton con-

ductivity (0.53×10^{-3} S cm^{-1}) at 353 K and 98% of relative humidity (RH). Indeed, from proton conductivities studies, the authors found that the conduction was based in a Grotthuss mechanism, where the inherent hydrogen-bonded framework was the main reason of its nice proton conduction, together with the adsorbed water molecules, which may have a role on assisting the hydrogen-bonded networks across the proton transfer pathways. Aiming at the potential application in proton exchange membrane fuel cells (PEMFCs), the authors also reported the structuration of this MOF in mixed-matrix membranes (MMMs), whose composition was a mixture of the organic polymers poly(vinylidene fluoride) (PVDF) and poly(vinylpyrrolidone) (PVP) and different amounts of this MOF (0, 20, 40 and 60%, MMM-1, 2, 3 and 4, respectively) as filler. They found that the proton conductivity of the MMM increased with the percentage of MOF present, reaching a proton conductivity of 0.80×10^{-3} S cm^{-1} at 353 K and 98% RH (Fig. 52B). Indeed, the MMM-4 exhibited even higher proton conductivity than the pristine MOF. This was explained with the intrinsic features of the membrane, where grain boundaries are filled with the organic polymers, making easier the proton transfer. Remarkably, the performance of such composite was reported to be maintained even after 5 days [353]. Overall, this is a nice example of how the combination of different types of ligands (proton–donor and –aceptor) can lead to enhanced proton conductivity.

Sulfonic groups were also incorporated in MOFs using PSMs, specially in UiO-derivatives as consequence of their great structural robustness and versatility, leading to MTV-MOFs with noticeable proton conducting properties [348–350]. Mukhopadhyay *et al.* presented the modification of preformed UiO-66-NH_2 with two sultones with different size of the alkyl chain length holding the SO_3H moities and studied the influence of this subtle change on the conductivity properties of the resulting post-synthetic modified materials [349]. From thorough characterization of both materials, it was found that only one half of amino groups were modified and that the structural stability and crystallinity was not compromised after PSMs –these MTV-MOFs retain their crystallinity after 1 year in open air and after 7 days in hot water. Also, after PSM both materials exhibited higher water adsorption –10-fold increase–, which clearly indicates their enhanced hydrophylic nature. Noteworthy, the authors observed a significant difference in proton conductivity between both post-synthetic modified MOFs, being the one with the shortest alkyl chain the most performant. It exhibited conductivities of 5.83×10^{-2} and 1.64×10^{-1} S cm^{-1} at 11.5 and 80 °C, respectively, and 95% of RH, which are comparable to Nafion. This performance was retained in the long-term (48 h) and at least up to five heating and cooling cycles, evidencing their stability and reusability. To further understand the underlying reason behind this difference in performance, they carried out different conductivity experiments in different RH and theoretical calculations. They confirmed the key-role of water in the proton conduction, and comparing with related materials with higher content of sulfonic groups, it could be interfered that, more importantly than the number, is the availability of labile protons. Indeed, the exhibited conductivity could be rationalized on the basis of pK_a values, where lower ones imply greater lability of sulfonic protons, and thus higher proton conductivity. Even other factors could not be excluded, the extensive characterization and the theoretical calculations supported this is the most important factor. This also allowed to explain the extremely low activation energy of the shortest alkyl chain modified MOF (0.107 eV). This study nicely evidenced the game-changing role mixed-component MOFs could make in this area of research, on the basis of their tailored nature, which enabled to understand key factors and improve performance of targeted materials in a rational manner.

Dealing with MTV-MOFs, Mohammad-Pour *et al.* [354] reported a Zr_6-based thin film grown onto fluorine-doped tin oxide (FTO) with a controlled amount of redox active mediators (RAMs) (Fig. 53A), based on ω-alkyl-ferrocene groups, which allowed to tune the redox conductivity of the resulting material [354]. Indeed, they found the electron hoping between redox active moieties changes with its concentration, with the maximum electron conductivity being for the MOF with only the ferrocene-functionalised linker (1.10 mS m^{-1}) (Fig. 53B). Also, from electroanalytical studies, they observed that the conductivity is diffusion controlled and dependent on the content of ferrocene RAMs –in line with percolation theory– and, as these groups were covalently attached to the MTV-MOF network, this intrinsically imply the conductivity comes only from the electron exchange between pendant RAMs. Noteworthy, the reported MTV-MOF thin films were very stable, not showing any significative change on their electrochemical features over 1000 cyclic voltammetry cycles. Overall, these features situate this material in an advantage position not only from fundamental understanding of electron charge transport in MOFs, but also for MOF-based devices, where it is mandatory the integration of MOFs as thin-films.

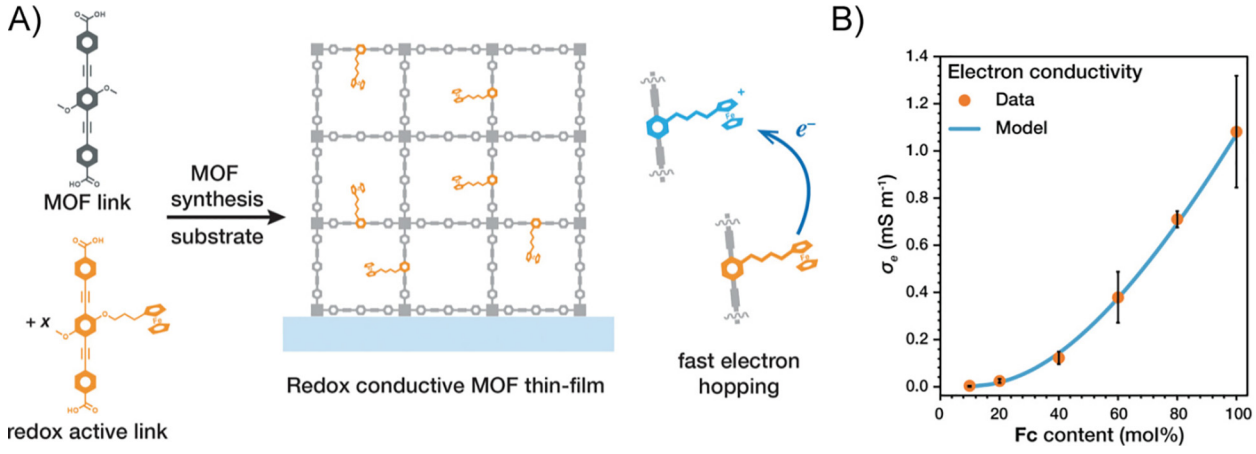

Fig. 53. A) Schematic representation of the synthesis/structure of the MOF containing varied amounts of redox active links that enable fast redox conductivity via redox hopping. B) Diffusion coefficient of electron transfer derived from Anson plots as a function of **Fc** content (orange symbols), compared to modeled D_e (blue line). Adapted from ref. [354] with permission from the American Chemical Society, Copyright 2019.

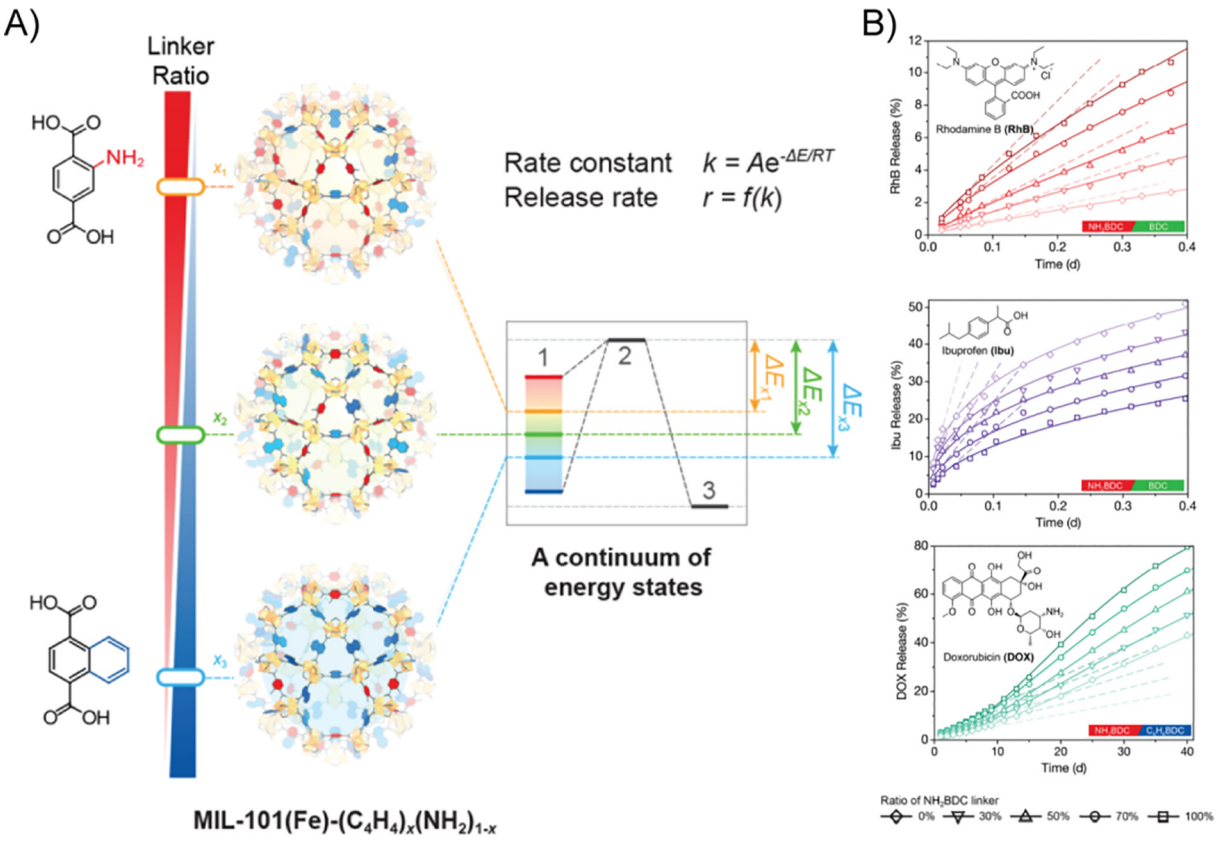

Fig. 54. A) MIL-101(Fe)-$(C_4H_4)_x(NH_2)_{1-x}$ ($0 < x < 1$) MTV-MOFs with continuous energy states from which guest release kinetics can be dialed-in over a wide range. B) Experimental (scatter dots) and fitted (curved lines) release kinetics of organic molecules from MTV MIL-101(Fe)-$(C_4H_4)_x(NH_2)_{1-x}$ samples as well as their initial release rates (dashed lines). Adapted from ref. [100] with permission from the American Chemical Society, Copyright 2017.

3.5. Biological applications

Although MOFs have been proposed as drug-delivery systems, contrast agents or in photothermal therapy [355–363], the number of MTV-MOFs is still very limited [89,100,216,226,253,364]. However, their intrinsic heterogenity and complexity situates them in an advantage position, respect others materials, making possible to present some unique features by tailoring host–guest interactions. An elegant example was reported by Dong *et al.*, [100] where they reported a family of mixed-linkers MIL-101(Fe) with a mixture of two and three functional groups (-H, $-NH_2$, $-C_4H_4$), affording MIL-101(Fe)-$(NH_2)_x$, MIL-101(Fe)-$(C_4H_4)_x$ and MIL-101(Fe)-$(C_4H_4)_x(NH_2)_{1-x}$ ($0 < x < 1$) (Fig. 54A), which enable to dialing-in the host–guest interactions with biological interesting molecules –ibuprofen (Ibu), rhodamine B (RhB) and doxorubicin(DOX)– and, even more interestingly, programm their release rate –mainly driven by diffusion [100]. For example, they observed that, in MIL-101(Fe)-$(NH_2)_x$, the release of RhB/DOX (Ibu) was slower (faster) with the increased amount of BDC linkers, meanwhile in MIL-101(Fe)-$(C_4H_4)_x$ it was observed the opposite trend (Fig. 54B). They found that stronger interactions between the functionalities of the MOF and guest molecules led to slower releases, while weaker ones will accelerate the process. This was also observed in MIL-101(Fe)-$(C_4H_4)_x(NH_2)_{1-x}$ system, where it was possible to tune their release rate up to 32-fold –*e. g.* the maximum release amount was shifted by 12 days for DOX. Interestingly, the authors applied a Weibull distribution function to quantify such interaction, which allowed to succesfully fit the release profile of studied drugs, and eventually predict the release of the guest molecules –opening the way for programmed linker ratio-based release kinetics. It is noteworthy that this special feature can be only achieved with such complex materials. In fact, physical mixtures of different single-component MOFs were not able to get the same results. The authors also investigated the co-release of two sets of probe molecules (RhB/Ibu and DOX/Ibu) in MIL-101(Fe)-$(C_4H_4)_x(NH_2)_{1-x}$, founding a consistent trend with what was observed for single-loaded experiments, which enabled them to set-up a controlled release strategy based on the dominant interaction between each guest molecule and the present functionalities in the precisely tailored mixed-component MOF.

Wang *et al.*, [253] taking advantage of a molecular vise strategy previously mentioned (Figs. 24 and 55A), reported an imaginative approach for the detection of biomarkers using MTV PCN-521 MOFs. They exploited the stronger coordinating character of biologically relevant molecules –cysteine, homocysteine and glutathione– to remove the metal ions residing in the vise metal-binding sites. In particular, they developed a test paper with the multicomponent metalated MOF that, in contact with the biomarkers, showed fluorescence, whose intensisty was directly related to the concentration of the corresponding biomarker (Fig. 55). Noteworthy, this system exhibited a very low detection limit –22.5 and 46.4 nM for *L*-cysteine and glutathione– and it was not interfered with the presence of urine –making it suitable for quick and direct test in physical examinations– and it could be recycled up to four times without depletion of its activity, which makes this test paper a suitable portable material for applications in real-world applications in areas where there is a lack of adequate medical instruments.

Mesoporous MOFs have been used as hosts to encapsulate active biomacromolecule species –proteins (enzyme) and DNA [355]. The heterogeneous nature of mixed-SBUs MOFs have been used to build up mesoporous cages in highly robust MOFs with a

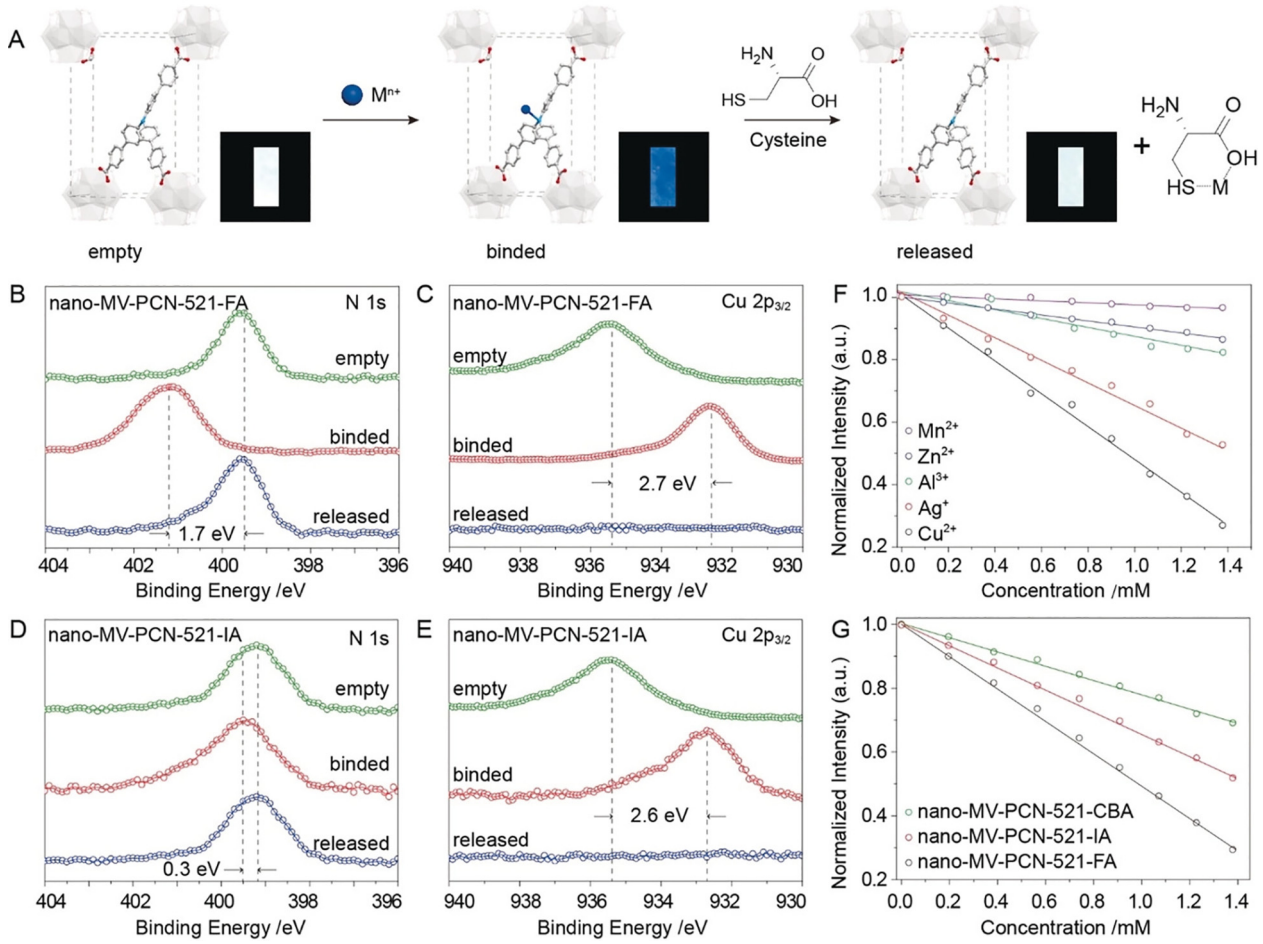

Fig. 55. A) Association/dissociation of metals in MV-PCN-521-FA. Fluorescence quenching and recovery displayed in test papers composed of nano-MV-PCN-521-FA N spectra (B) and Cu spectra (C) in XPS analysis of nano-MV-PCN-521-FA, quenched by Cu^{2+} and recovered by cysteine. N spectra (D) and Cu spectra (E) in XPS analysis of nano-MV-PCN-521-IA, quenched by Cu^{2+} and recovered by cysteine. Fluorescence intensity decrease in MV-PCN-521-FA (F) and MV-PCN-521-R (G) versus the concentration of M^{n+} and Cu^{2+}, respectively. Adapted from ref. [253] with permission from John Wiley & Sons, Copyright 2018.

large number of vertices and low connectivity. Among them, MOF-818 –featuring the smaller pores– showed both a remarkable water stability in a wide range of pH and still a considerable window-cage size to host relevant biomolecules, such as vitamin B12 and insulin with a size of 2.7 and 3.4 nm, respectively. In particular, MOF-818 was able to incorporate up to 4.4 and 2.8 nmol/mg of vitamin B12 and insulin, respectively. An emergent area of research in biological applications is the finding of antibacterial materials that could circumvent the severe problems in clinical therapy of antibiotic resistance strains. In particular, multidrug-resistant (MDR) pathogens are of particular concern, as conventional antibiotics agents are not capable to control efficiently the infection. MOFs community have started to explore solutions to this acuting problem. Mainly two different approaches have been followed with MOFs, either the pH-triggered controlled decomposition –releasing the constituting bactericidal cations– or the encapsulation of antimicrobial agents. Nevertheless, novel approaches are needed, and, at this respect, the special features of mixed-components MOFs offer unique opportunitites. Chen *et al* [226]. reported the use of a photosensitive mixed-metal ion MOF for photodynamic therapy (PDT) of wounds infected with MDR pathogens. The authors optimised the synthetic route of Zr_6-based PCN-224 MOF to obtain it in the form of uniform nanoparticles (NPs) and, in a second step, they post-synthetically partially substituted the zirconium metal ions at the SBUs with titanium ones, to yield PCN-224(Zr/Ti). They observed that the constituting ligand (TCPP) behave as an effective photosensitive (PS) entity in the network, and that the Ti ions boost the generation of reactive oxygen species (ROS), which enabled this heterogeneous MOF to perform *in-vivo* PDT under visible light, in contrast to what was observed for pristine PCN-224, where the light response was not so efficient in the visible region. Indeed, they found a nice efficiency for PCN-224(Zr/Ti) in the elimination of both normal and MDR Gram-positive (*S. aureus* and *S. epidermidis*)/negative (*E. coli* and *A. baumannii*) bacterias. In a first step, they applied the plate counting approach, culturing the distinct bacterias on agar plates. After 10 min of visible light irradiation, they found a severe reduction for each pathogen, being the most eliminated both normal and MDR *A. baumannii*. After 24 h, optical density measurements at 600 nm evidenced this material efficiently inhibited the proliferation of all bacteria –control experiments with TCPP and PCN-224 showed their lower efficiency respect PCN-224(Zr/Ti), which supported the key role of Ti ions for the enhanced photocatalytic performance on ROS generation. In addition, the authors performed and extensive study on the biocompatibility of PCN-224(Zr/Ti), by its intravenous injection on rats. They reported no obvious infection or inflammation of the major organs after 14 days. Also, apart from other experiments such as testing the retention of vitality of human umbilical vein endothelial cells, they monitored the white and red blood cells and platelets and did not observed any abnormal value, which clearly supported the biocompatibility of PCN-224(Zr/Ti) NPs. In

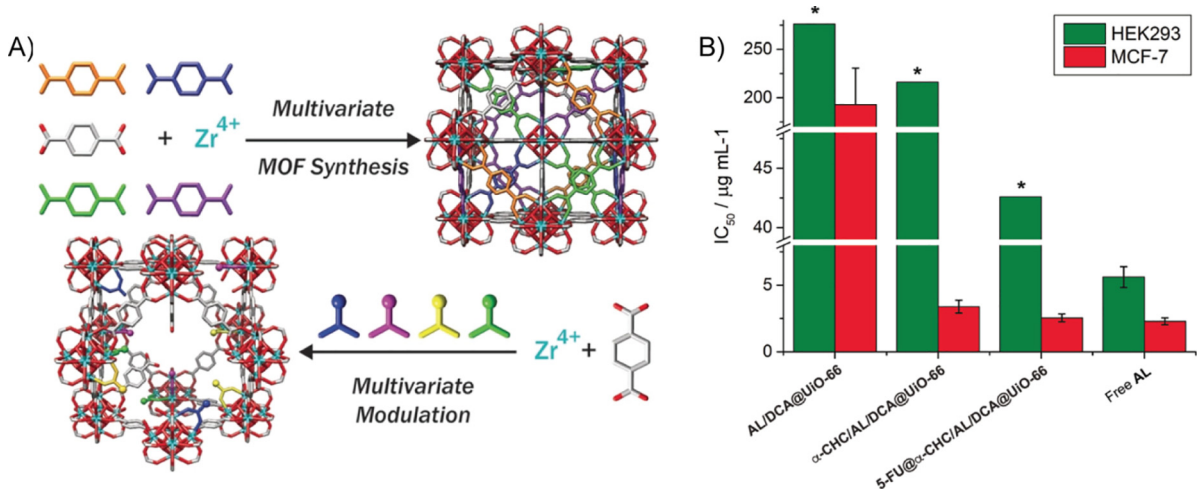

Fig. 56. A) Synthesis of UiO-66 as a MTV-MOF with multiple mixed linkers (top) or using multivariate modulation, to install multiple different modulators as defects within one MOF (bottom). B) Comparison of IC_{50} values, normalised to alendronate (**AL**), for various formulations against HEK293 and MCF-7 cells. Adapted from ref. [364] with permission from John Wiley & Sons, Copyright 2020.

a second part of the work, they structured this material on poly (lactic-co-glycolic acid) (PLGA), PCN-224(Zr/Ti)@PLGA, *via* electrospinning to obtain a dressing for the healing on rats of wounds infected by MDR pathogens. They reported these composite nanofibers significantly reduced the size of wound infected after seven days healing, and practically recovered after seven days more, which contrasted with the slower healing of control materials –PLGA and plain gauze. Also, they observed a lower level of inflammatory cytokines –critical parameter to estimate inflammatory diseases– on wounds treated with PCN-224(Zr/Ti)@PLGA respect controls. Finally, they showed this composite was also able to speed up the regeneration of the epithelial layer.

In an alternative manner, Abánades-Lázaro *et al.* [364] proposed a novel approach for the incorporation of up to three distinct anticancer drugs –α-cyano-4-hydroxycinnamic acid (α-CHHC), alendronate (AL) and dichloroacetate (DCA)– taking advantage of the defect sites at UiO-66, which will represent a significant advance in the use of MOFs in multimodal chemotherapeutic treatments [364]. The key point of this strategy resides on the use of drugs with carboxylate or phosphonate binding groups as modulators (Fig. 56A). Despite we have not considered the modulators in this review as mixed-component MOFs, with this example we have made an exemption, as they are the active components of the targeted application. As expected, the role of pK_a was dominant and determining the affinity of each modulator, and in the material α-CHHC/AL/DCA@UiO-66 their weight percentage was 2, 21.6 and 3.2%, respectively. Despite the high content of modulators, thanks to the great resilience and tolerance of Zr_6-MOFs to defects, the resulting material exhibited a good porosity, which allowed to postsyntethially incorporate a fourth anticancer drug –5-fluorouracil (5-FU). To prove the viability of these materials on cancer treatment, they were tested for anticancer selectivity against HEK293 kidney cells and MCF-7 by the MTS assay (Fig. 56B). They found that the materials with double drugs combinations, 5-FU/DCA@UiO-66 and α-CHHC/DCA@UiO-66, showed highly anticancer therapeutic activity and biocompatibility to HEK293 kidney cells, even at high doses. Despite the activity of AL@MOFs was reduced respect the free drug, triple and quadruple drug formulations showed increased selective cytotoxicity towards MCF-7 cells than free drugs, which evidenced the potential of mixed-component MOFs in the clinical anticancer treatment with a combination of drugs.

3.6. Environmental application: water remediation

Water pollution is one of the main environmental issues our society faces [365]. The continuous growth of world polutation together with the compelling consumerism of advances societies even make this problem more worrying for the sustainable development of future generations [366]. Common contaminants can be broadly divided into inorganic substances, heavy and radioactive metal ions, inorganic acids and oxyanions/cations; and organic pollutants which includes organic dyes, pharmaceutical and personal care products, herbicides and pesticides and industrial compounds/byproducts. Sources of contamination are scattered and diverse, but the vast majority can be connected to human activities such as agricultural and industrial practices [365]. Current technologies applied in decontamination protocols have not shown efficient for the removal of all contaminants to limits recommended by the World Health Organization (WHO), feature multistep sequences –which shown the risk of generation of secondary pollutants– and suffer from high-operating costs –which avoid to implement them worldwide, as it would be required, to face efficiently this global problem. Within this context, MOFs have strongly burst into water remediation as very promising materials seleccion [30,31,31–33]. Initially, they were scarcely applied in the field, mainly due to water-stability issues of first MOFs generations, a stigma it has take quite a lot of work and efforts to be redempted [367]. More recently, this problem has been overcome and a great amount of studies, based on adsorption and/or advanced oxidation processes (photocatalytic degradation), which evidenced their potential to be incorporated in decontamination protocols that would outperform existing technologies, have been reported [30,31,31–33]. Nevertheless, a great amount of work remains to be done within water remediation field, where the intrinsic heterogeneity and complexity of mixed-component MOFs makes them appealing candidates to outperform existing technologies and find solutions to the worrying contamination of aquatic ecosystems [293].

The intrinsic heterogeneous nature of multicomponent MOFs has been also exploited for environmental aplications. Yuan *et al.* showed the nice performance of PCN-134 (Fig. 12) in the capture and photocatalytic reduction of dichromate (Fig. 57) [162]. In this study, the authors took advantage of the tolerance of multicomponent PCN-134 to missing auxiliary-linkers, and the generated $-OH_2$

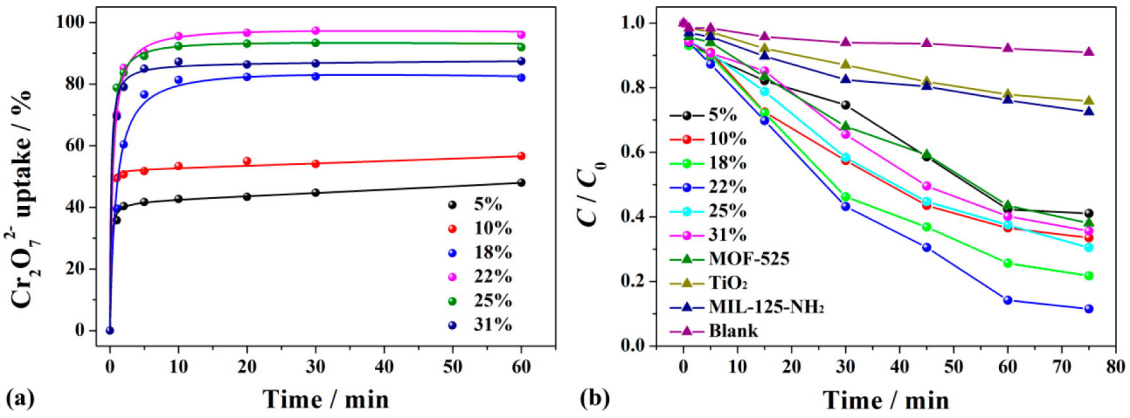

Fig. 57. (a) $Cr_2O_7^{2-}$ adsorption capacities and (b) photocatalytic activities for the reduction of $Cr_2O_7^{2-}$ under visible light irradiation of PCN-134 system with different TCPP molar ratios. Reproduced from ref. [162] with permission from the American Chemical Society, Copyright 2016.

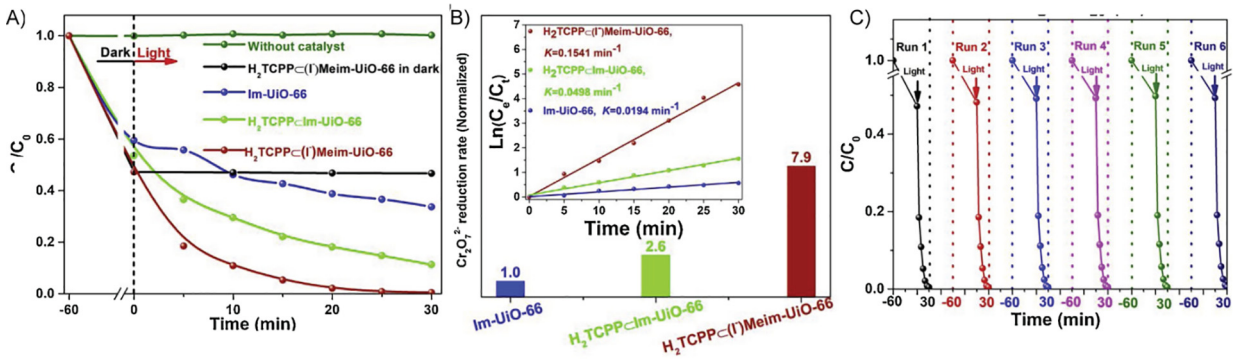

Fig. 58. A) The photoreduction of $Cr_2O_7^{2-}$ over Im-UiO-66, H_2TCPP ⊂ Im-UiO-66, and H_2TCPP⊂(I-)Meim-UiO-66B) Photoreduction rate of $Cr_2O_7^{2-}$ over Im-UiO-66, H_2-TCPP ⊂ Im-UiO-66, and H_2TCPP⊂(I-)Meim-UiO-66, the inset picture shows the photoreduction kinetics of corresponding catalysts. C) Reusability of H_2TCPP⊂(I-)Meim-UiO-66 for the photoreduction of $Cr_2O_7^{2-}$ under visible light. Adapted from ref. [159] with permission from Elsevier, Copyright 2019.

and –OH groups at the Zr_6-SBUs were used as anchoring points of $Cr_2O_7^{2-}$ species. The best performing material was PCN-134–22% TCPP, which was able to reduce the concentration of dichromate by 85 and 95% after 2 and 10 min, respectively. This material exhibited a balance between porosity and stability, which contrast with materials with lower contents of TCPP linker that exhibited a considerably lower $Cr_2O_7^{2-}$ adsorption. Noticeably, the adsorption capacity of PCN-134–22%TCPP was maintained even when competing anions $-F^-$, Cl^-, Br^-, NO_3^- and SO_4^{2-}– in double excess were used. In this work, they also investigate the photoreduction of chromium(VI) to chromium(III) of the adsorbed $Cr_2O_7^{2-}$ entities. They found PCN-134–22%TCPP showed the best photocatalytic activity, being comparable to TiO_2 and surpassing other photoactive MOFs such as MIL-125-NH_2 and MOF-525. This was attributed to the positive effect of missing linkers and the presence of photosensible TCPP linkers close to the anchored $Cr_2O_7^{2-}$ entities at the Zr_6 SBUs, which facilitates the electron transfer from TCPP to the substrates with the concominant reduction from Cr(VI) to Cr(III). Indeed, based on the extensive characterization of this process, the authors could propose a plausible mechanism for the photoreduction process. The TCPP linkers were excited and inject electrons into Zr_6-SBUs, leading to $TCPP^+$, and then, anchored dichromates were reduced into Cr(III) and the $TCPP^+$ reduced back to TCPP by ethanol.

Wang *et al.* [159] reported a multicomponent system constructed with TCPP and 2-(imidazol-1-yl)terephthalate (Im-BDC) that was in a post-synthetic step methylated with CH_3I to render H_2TCPP⊂(I^-)MeIm-UiO-66, which showed a very nice efficiency for the photoreduction of $Cr_2O_7^{2-}$ under visible light [159]. The efficiency of this material relied on the combination of the photosensitive nature of TCPP –enlarging the absorption range from 425 to 750 nm, respect the single-component Im-UiO-66– together with the ability of cationic methylimidazol and Zr_6-SBUs to incorporate dichromate moieties within MOF channels –by ion-exchange of I^- anions or electrostatic interactions with protonated pyrrole and anchored to defects of SBUs, respectively. Indeed, the authors attributed the better performance of H_2TCPP⊂(I^-)MeIm-UiO-66, respect other reported and related MOFs, for the photoreduction of Cr(VI) to Cr(III) to the improved adsorption of $Cr_2O_7^{2-}$ (Fig. 58A, B). This material exhibited a total conversion to Cr(III) after 30 min, as it was corroborated by X-ray photoelectron spectroscopy (XPS) data, and nearly eight times higher phototoactivity than pristine Im-UiO-66 [159]. Besides, reusability experiments showed the nice structural robustness of this system (Fig. 58C), while retaining its performance. In order to gain insight on the photocatalytic mechanism of this multicomponent MOF, the authors conducted an extensive steady-state photoluminescence, electrochemical impedance spectroscopy and transient photocurrent measurements study, combined with solid UV–Vis spectroscopy, electron spin resonance, XPS and theoretical calculations. From it, they proposed a photoreduction mechanism, which was based in a first step by the adsorption of $Cr_2O_7^{2-}$ entities through the protonated porphyrin, Zr_6-SBUs defects and imidazolium functionalities. Then, under visible light irradiation the excited electrons on TCPP linkers can be easily transfered directly to the adsorbed $Cr_2O_7^{2-}$ anions or in an indirect manner through the Zr_6-SBUs or the methylated imidazole decorating the channels,

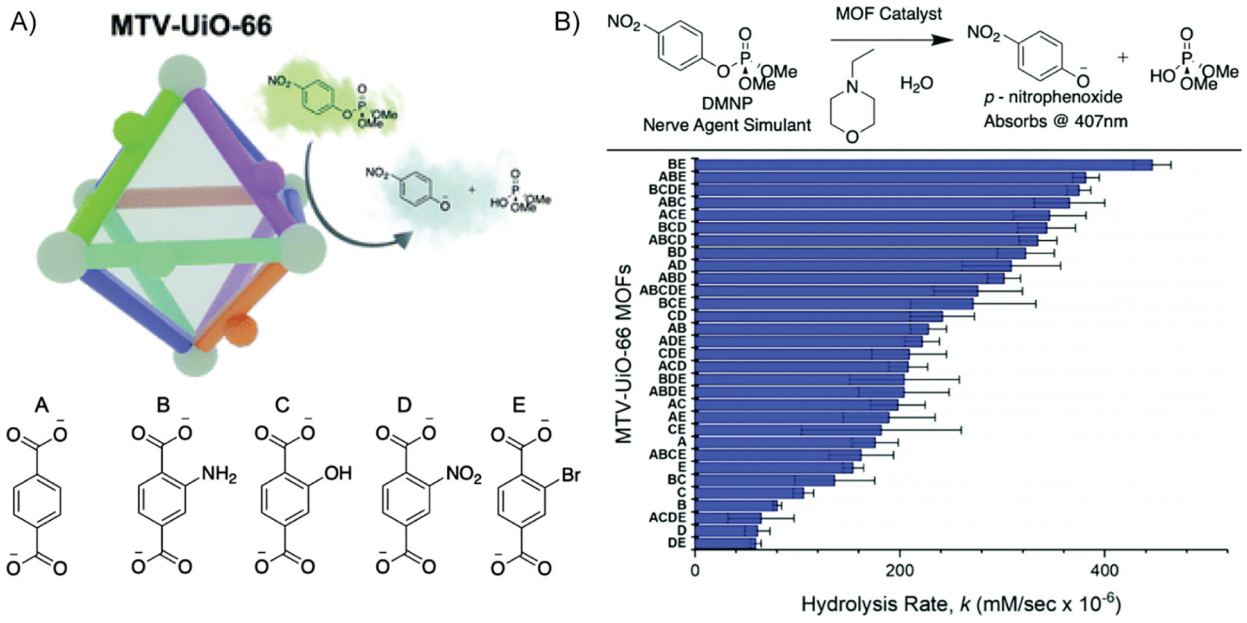

Fig. 59. A) Schematic representation of MTV-UiO-66 and ligands used for in the corresponding mixed ligand synthesis. B) Scheme of DMNP assay conditions. Bottom: Rate of catalytic degradation of DMNP by all MTV-UiO-66 MOFs. Adapted from ref. [104] with permission from the Royal Society of Chemistry, Copyright 2019.

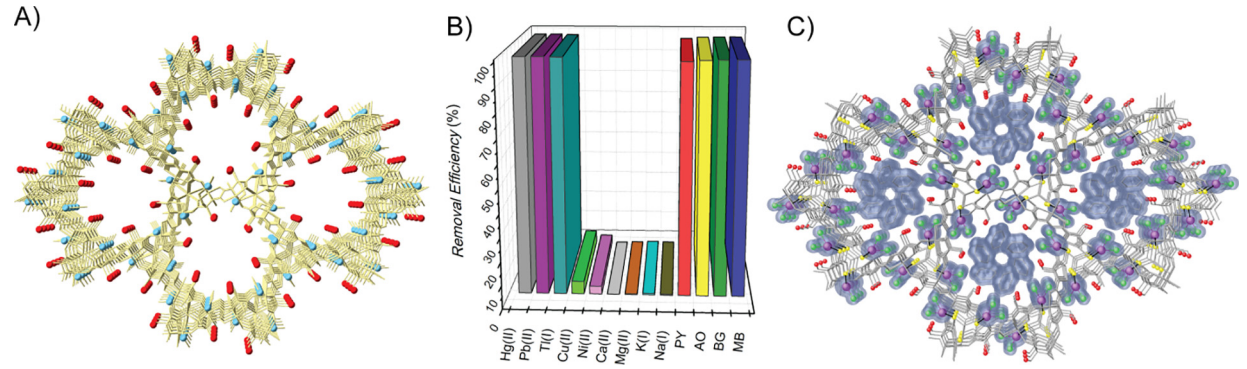

Fig. 60. A) Crystal structure of the MTV–MOF $\{Ca^{II}Cu^{II}_6[(S,S)\text{-methox}]_{1.43-1.46}(S,S)\text{-serimox}]_{1.57-1.54}(OH)_2(H_2O)\}\cdot 30H_2O$ (**2**) emphasising the *L*-serine (–CH2OH) and *L*-methionine (–CH2CH2SCH3) residues. B) Maximum recovery (after 6 h) of both inorganic and organic contaminants by MTV-MOF **2**. C) Single pore of the host–guest adsorbate showing $HgCl_2$ and methylene blue (MB) guest molecules held in the hexagonal nanopores of **2**. Adapted from ref. [370] with permission from the American Chemical Society, Copyright 2019.

being reduced to Cr(III) cations, while the I^- acted as sacrificial agents (hole scavengers) leading to I_2.

Kalaj *et al.* [96] reported the catalytic degradation of the chemical warfare agent (CWA) [228,368,369] simulant dimethyl 4-nitrophenylphosphate (DMNP) in an extense family of MTV-UiO-66 (Fig. 59A). They found the mixed-linkers MOFs showed superior DMNP degradation (at pH = 8) than physical mixtures of single component MOFs. The authors suggested that the presence of different functional groups within the same pore could play a synergistic role, which increase the activity against DMNP degradation (Fig. 59B). For example, the NH_2,Br-MTV-MOF exhibited three times more activity than the respective individual MOFs. Despite they could not found clear relationships between the chemical nature of the functionalities and their degradation activity, they observed that the amino functionality plays a main role on it [30,33]. Extensive characterisation and defect quantification clearly revealed there was no correlation between the increased activity in MTV-MOFs and the number of defects. This further supported the key catalytic degradation role played by different functionalities within the same pores and nicely illustrated the potential of such heterogenous and complex systems in solving existing real-world problems.

MTV-MOFs have been used by some of us, in a recent work, for the simultaneous capture of inorganic –heavy metals such as Hg^{2+}, Pb^{2+} and Tl^+– and organic –dyes such as Pyronin Y, Auramine O, Brilliant green and Methtylene blue– contaminants from water [370]. In particular, we reported two isoestructural MTV-MOFs, $\{Ca^{II}Cu^{II}_6[(S,S)\text{-methox}]_{1.43-1.46}(S,S)\text{-serimox}]_{1.57-1.54}(OH)_2(H_2O)\}\cdot 30H_2O$ (Fig. 60A) and $\{Ba^{II}Cu^{II}_6[(S,S)\text{-methox}]_{1.41-1.45}(S,S)\text{-serimox}]_{1.59-1.55}(OH)_2(H_2O)\}\cdot 31H_2O$, with functional channels decorated with $–CH_2–CH_2SCH_3$ and $–CH_2OH$ arms derived from the amino acids *L*-methionine and *L*-serine, respectively, and studied the removal performance of the $CaCu_6$ MTV-MOF for inorganic and organic contaminants. In a first step, it was investigated the separate adsorption of each type of contaminant. We reported the efficient adsorption of each type of organic dye separately and later on together. It was shown that the MTV-MOF improved its performance –in terms of kinetics and amount removed– respect the related single-component MOF with only serine-derived linkers, $\{Ca^{II}Cu^{II}_6[(S,S)\text{-serimox}]_3(OH)_2(H_2O)\}\cdot 39H_2O$ [371] previously reported, which

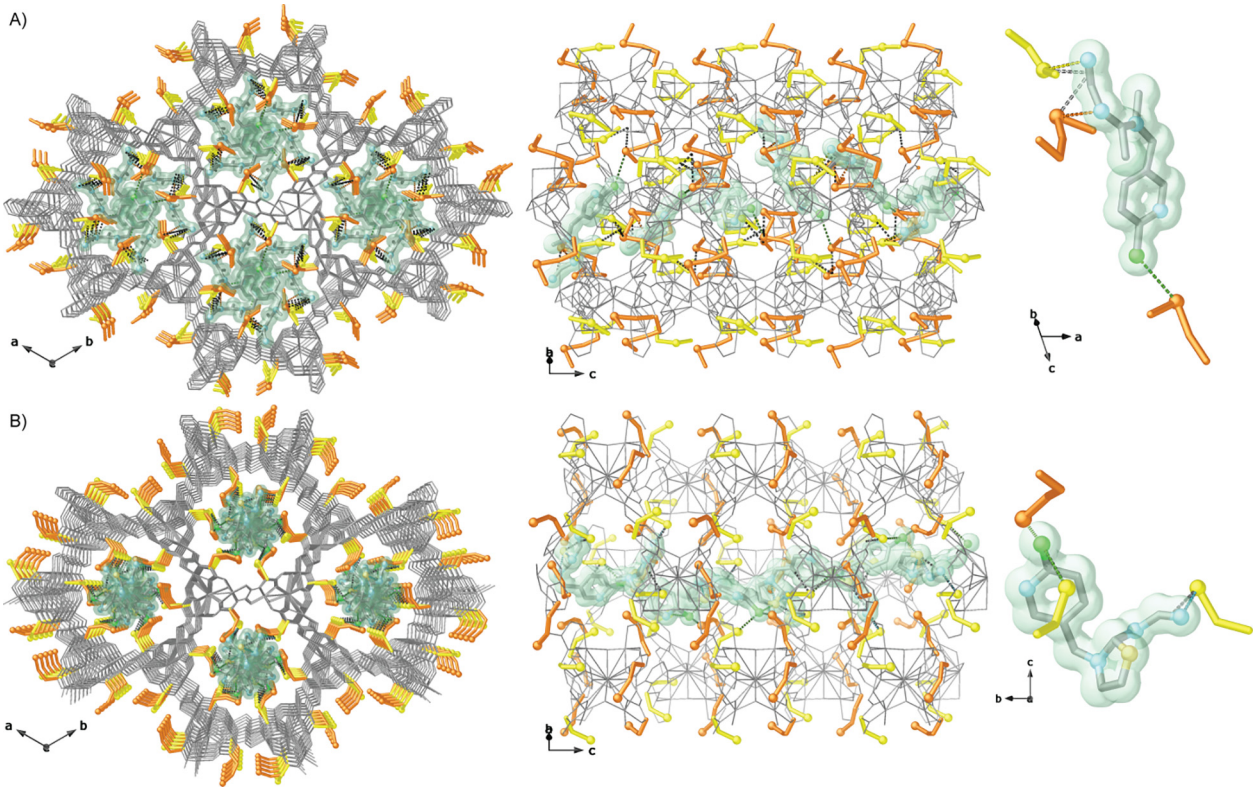

Fig. 61. Perspective views of the porous structure of the MTV-MOF $\{Sr^{II}Cu^{II}_6[(S,S)\text{-methox}]_{1.5}[(S,S)\text{-Mecysmox}]_{1.50}(OH)_2(H_2O)\}.36H_2O$ after capturing of acetamiprid (A) and thiacloprid (B). Metals and organic ligands are depicted as gray sticks, whereas the amino acid residues are represented with the following color code: $-CH_2CH_2SCH_3$: orange; $-CH_2SCH_3$: yellow. Guest molecules are represented as green solid surfaces. Reproduced from ref. [373] with permission from the American Chemical Society, Copyright 2021.

implied that the thioether groups participated in a cooperative manner with hydroxyl reidues in the capture of organic dyes. Remarkably, the removal of mixtures of organic contaminants was more efficient than in separate solutions. Also, we could observed an improved removal efficiency of heavy metals, respect the related isostructural material $\{Ca^{II}Cu^{II}_6[(S,S)\text{-methox}]_3(OH)_2(H_2O)\}\cdot 16H_2O$ [372] containing double amount of methionine residues. Then, we studied the capture properties of the presented MTV-MOF with a mixture of inorganic and organic contaminants. It could be observed that it was able to remove simultanuosly both types of contaminants of different nature (Fig. 60B). In fact, it could be revealed a slighlty improvement with respect to separate capture experiments, which implied a synergetic behaviour of both types of functionals groups decorating the channels in the capture process. The reusability and robustness of this material was demonstrated, after extraction of adsorbed contaminants by its consecutive suspension in 2-mercaptoethanol and ethanol, in a second cycle of adsorption with retention of removal performance and stability at ambient conditions for weeks. To probe the key role of the multivariate nature of this material, it was performed a reference experiment with physical mixtures of single component MOFs, and it could be observed a 15 and 20% worst removal of inorganic and organic contaminants, respectively. This role could be also evidenced by the unique visualization by SCXRD of both types of contaminants –methylene blue and $HgCl_2$– within MTV-MOF channels, which revealed the interactions between mercury(II) chloride and the thioether residues of methionione and the hydrogen-bonds between the methylene blue and the hydroxyl groups from serine, as well as the interactions within the confined space of MTV-MOF pores between both types of contaminants (Fig. 60C).

The great potential of MTV-MOFs in water remediation has been further confirmed, in a very recent publication, by some of us [373]. In this work, we explored the efficiency of a novel MTV-MOF towards neonicotinoid insecticides removal. The MTV-MOF, with formula $\{Sr^{II}Cu^{II}_6[(S,S)\text{-methox}]_{1.5}[(S,S)\text{-Mecysmox}]_{1.50}(OH)_2(H_2O)\} \cdot 36H_2O$ (where methox = bis[(*S*)-methionine]oxalyl diamide and Mecysmox = bis[*S*-methylcysteine]oxalyl diamide), features narrow functional channels decorated with both $-CH_2SCH_3$ and $-CH_2CH_2SCH_3$ thioalkyl chains (Fig. 61) and exhibits outstanding removal efficiencies, being capable to capture 100% of acetamiprid and thiacloprid in a single capture step under dynamic solid-phase extraction conditions. Moreover, the crystal structures of the resulting host–guest adsorbates, with both acetamiprid and thiacloprid, could be resolved (Fig. 61), allowing to visualize the synergistic host–guest interaction, between the two types os sulfur-containing thio-ether groups from the MTV-MOF and the functional groups from the guest contaminants, which help to understand the great capture properties of this material.

4. Perspectives: Potential unique applications of mixed component MOFs

Previous section has been entirely dedicated to current applications of mixed-component MOFs. Indeed, they find application in a wide variety of important fields due to their intrinsinsic key features, such as heterogeneity and complexity within order. Nevertheless, the explored applications with mixed-component MOFs are just the tip of the iceberg. Despite the high numbers of reported materials with interesting and exciting aplications, sometimes surpassing traditional MOFs and even currently used materials in real-world applications, this area of research in MOFs chemistry is just in its infancy. Indeed, even though the great advances reported here, it would be highly desirable to move subtantially forward, especially in mixed-ligands and metals systems, in increasing the hetereogenity of these materials in a controlled manner. This will require substancial efforts from synthetic groups, but the pay-off

will be considerable, and it will take us a step closer to the complexity observed in biological systems, which chemist always wish to emulate. In this context, it would be quite interesting to explore with enthusiam the combination of mixed-component and dynamism [374–382]. Really interesting results have been found on single component MOFs, and we humbly believe it would be a quite exciting chemical experience to combine different dynamic systems within the cavities of one mixed-component MOF, which could operate, in parallel or in tandem, for the efficient implementation of the desired tasks. So far, seminal work has been produced, focused on showing the viability of the concept [381]. However, this area is waiting to be explored and it would open new avenues of research. Hopefully, mixed-component MOFs could be the tool to transfer the fascinanting properties observed in molecular dynamic systems in homogenous phase to solid supports, which would bridge and match properties at the molecular level with real-world applications.

Even more importantly, it would be very helpful, if not a necessity, the development or search of physical characterization techniques that enable to obtain structural information, with atomic precision, of the distribution, organization and interactions of the different functional groups and/or metallic species constituting the mixed-component MOF. Considerable efforts have been performed within MOF community to seek them and some positive advances have been performed, as stated in this manuscript. However, this is currently the weakest point of this area of research and somehow hampers the exponential growth these materials are hailed to do. Thus, it would be highly desirable to find a friendly-used technique, compatible with the sometimes special stability (handling) conditions MOFs need and that could be easily available on synthetic labs to speed up the development of this area of research.

An important vertex of growth, for mixed-component MOFs, will come from the input from different scientific communities, *i.e.* materials scientist, physicists and biologist. This will fully unleash the potential of these unique materials. We strongly believe the heterogenity of these materials improve considerably their potential to be used in areas that in the present moment are just not considered. This, is most likely related to the fact that chemists are used to look always at the same traditional applications. However, an increasing attraction of interest of researchers from others fields will boost, undoubtedly, the range of applications that these materials will show in the near future. Some interesting examples of mixed-component MOFs have been published for laser writing and as supercapacitor, which evidenced the interest of this cross-fertilization between different fields [383–385]. Related to this point, we consider that two main areas of research could benefit from the intrinsic properties of mixed-component MOFs. They are (bio)enzymatic catalysis and the synthesis of heterometallic subnanometric clusters and nanoparticles. Hereunder, we will comment some of the unique properties it could be revealed if these two areas are explored.

4.1. (Bio)enzymatic catalysis

Enzymes are the biomolecules in charge to perform most of the key chemical reactions in life [386]. The efficiency, elegancy and simpleness with what they do these highly complex processes have been an endless source of inspiration for researchers working in the field of (bio)enzymatic catalysis, whose ultimate target is to implement systems with the same sophistication degree and functionality than enzymes. In this context, different materials have been proposed as artificial enzymes with the aim to unveil/understand, and eventually mimick, the reactivity, selectivity and ability to boost reactions of natural enzymes [387]. However, despite the considerable advances, great number of factors of main relevance for the catalytic activity of enzimes, are still shyly explored [388–391]. On this basis, it seems mandatory to keep performing basic research in order to achieve a better comprehension of the key processes in enzymes, and their effects in enzymatic catalysis. This knowledge will situate us in an advantaged position to develop materials able to mimick the catalytic efficiency of natural enzymes.

In the present context, single component MOFs have been explored as enzymes mimicks [355,356,392–400]. These works could be mainly grouped within three approaches: (*i*) MOFs with metalloporphyrins linkers, (*ii*) post-synthetic incorporation in MOFs of metallic complexes and organic compounds able to form hydrogen bonds and (*iii*) biocomposites of MOFs and natural enzymes [355,356,392–401]. These systems could be considered as a basic first-generation enzyme mimicks, because their heterogenity, diversity, flexibility and complexity –from a structural and chemical nature point-of-view– is quite limited. More recently, mixed-component MOFs have started being investigated in this field due to their potential to build up coordination environments that resemble the active centers of enzymes [132,210,252,255]. However, we think that some intrinsic features of mixed-component MOFs are barely exploited. For example, the channels of each MTV-MOF represent a unique and singular environment, which offers unprecedented opportunities. The size, shape and functionality of MTV-MOF pores will have a severe influence on the coordination environment of the encapsulated or *in-situ* synthesized enzyme mimick within MOFs channels, as well as on controlling the dynamic processes and their solvatation sphere, which in turn will have a great influence in the bioenzymatic catalytic activity. The intrinsic flexibility of MTV-MOFs constitutents will allow to investigate the influence of the dynamism of identical chemical environments on the bioenzimatic activity. Indeed, it is here worthy to highlight that this flexibility can be triggered by different external chemical and physical stimuli, which may represent an unprecedented opportunity in the area of *artificial* enzymes. The MOF channels will have a two-fold role on the bioenzimatic activity: (*i*) conferring enhanced stability to natural/artificial enzymes and (*ii*) controlling the size and chemical nature of the substrates that are going to access to the active center, which will have a severe impact on the regio- and stereoselectivity of the reaction. These are just some ideas based on our brainstorming meetings, and, undoubtedly, the presented concepts are much more limited by our more or less develop ability to think out of the box and dream on potential ways mixed-component MOFs could set the path than by the unforeseen possibilities for us that these materials possess.

4.2. Synthesis of heterometallic subnanometric clusters and nanoparticles

The development of metallic clusters of controlled size and composition have been an intensive field of research during the last decades, as consequence of the fascinanting properties metallic nanoparticles (NPs) [402] exhibited as well as of the promising ones of subnanometric metal clusters (subNMCs) [23,257–259,261,262]. Dealing with NPs, their remarkable applications have situated them in a privilegiated position and have attracted the interest of researchers from different research fields, from materials scientist –to investigate their high-scale synthesis– to biologist –looking for novel constrast agents– going through physicists –aiming to understand their fundamental physical properties–, to mention some of them [402,403]. Nevertheless, despite the advances of the field, some fundamental research is still needed to increase the control on the size, morphology and stability of NPs [404,405]. SubNMCs represent an intermediate scale of metallic materials that, until recently, were somehow bypassed as consequence of the overwhelming interest on NPs and isolated

atoms. However, the exciting properties of some of the few reported systems and the predicted ones, as consequence to belong to the realm of nano, have attracted the interest of numerous research groups [406]. Until few years ago, the preparation of such systems –particularly in high scale–, precise characterisation –structure with atomic resolution– and stability –under working conditions– have been their Achiles heel. In this context, some of us, reported for the first time the use of MOFs as outstanding platforms for the controlled synthesis and precise characterization of structural and functional stable Pd_4 subNMCs, which outperformed the state-of-the-art metal catalyst in carbene-mediated reactions in batch and in flow (>20 cycles) [257]. This represented the spark to initiate a research line in our group and other interesting catalytic materials, such as Pt_2 subNMCs [258], have been obtained. Our strategy to build these subNMCs have two approaches depending on the formal charge of the network and the functional groups decorating the network. Meanwhile neutral MOFs controlled the number and position of the incorporated metal ions with the functional groups decorating the channels, anionic MOFs controlled the number of post-synthetically incorporated metal ions by maintaining the electroneutrality of the network and electrostatic interactions with the network. These results suggest that it is not so trivial to think on applying the same strategy for obtaining heterobimetallic ones. Thus, here we propose to use heterogeneity of mixed-component MOFs, in particular of MTV-MOFs, to rationalize the synthesis of heterobimetallic NPs and subNMCs, by taking advantage of the presence of different functionalities in one compound and the different coordination affinities of distinct metal ions to control the number, distribution and stabilization of metal ions incorporated within MTV-MOFs before and after the reduction step. Here crystallography will play a pivotal role, and the selected MTV-MOFs will have to show a high degree of crystallinity and structural robustness to resist post-synthetic processes –metal incorporation and reduction. Heterogeneity within order will allow the direct visualization of the metal incorporation and its spatial distribution, which in turn will be of main importance to be able to eventually establish NPs/subNMCs metallic distribution and functionality relationships.

5. Conclusion

Previous reviews on technological applications of MOFs are mostly focused on describing multivariate [407,408], multicomponent [409], mixed-metals [6,42,188,410,411] and mixed ligands and metals MOFs [45], separately, or a combination of some of these types of mixed-component MOFs, for some specific applications [37,39,44]. Other bibliographic works include a cursory inspection of mixed-component MOFs within more general MOF reviews. Finally, the first specific reviews on mixed-component MOFs only focused on their description, but not in their applications [7,8,38,217,412,413]. Overall, as far as we know, this is the very first review focused exclusively on the applications (current/potential) performances of mixed-component MOFs as the central core of the work.

In these pages, we have first attempted to provide a comprehensive introduction and classification of all the different types of mixed-component MOFs that we have included in this review, mentioning also some exciting examples such as defects or hierarchical systems. This strategy was followed aiming at attracting the necessary interest of new researchers, especially from other fields. Then, we have focused on describing how the intrinsic features of mixed-component MOFs: heterogeneity and compositional and structural complexity, have been exploited in different areas of applications. To this end, we have tried to select some of the most representative and/or recent examples in each section of applications, with the aim to render a wide picture of the state-of-the-art.

After a short introduction to present the contents of this manuscript, we have presented relevant or characteristic examples of four types of mixed-components MOFs: (*i*) multivariate-MOFs, (*ii*) multicomponent MOFs, (*iii*) mixed-metals MOFs and (*iv*) mixed-ligand and -metals MOFs. Through these families, we have tried to highlight the unique advantages of these systems, while giving a critical vision of the different aspects that need to be improved in each particular subclass and, in general, as a novel class of compositional, structural and functional evoluted MOFs. We are confident that in the near future novel examples of each type of mixed component-MOFs will be reported, and as it has occurred with previous challenges that MOFs have faced, the remarked limitations will be solved.

Other questions to be solved will be both, the diversification of MOFs used as platforms to obtain mixed-component MOFs –most of them are representative carboxylate-based networks, *e.g.* MOFs, MOF-5, MOF-74, MIL-53 and 101, or ZIFs ones– and the expansion of the range of applications of mixed-components MOFs. Indeed, it would be highly interesting to expand the current investigations in mixed-component MOFs to other families of MOFs, even if it is not easy to fulfil all the needed requirements, such as tolerance to variance, high crystallinity and structural robustness. Moreover, as it can be observed in Fig. 3, most of the currently reported applications for mixed-component MOFs are gas adsorption/separation and heterogeneous catalysis. This is not surprising as, at the dawn of traditional MOFs, it occurred in a similar manner. However, it is evident the need to increase the number of reported examples for the other described appplications in this review and, as we have mentioned in the perspective section, explore new ones.

Mixed-component MOFs are far from being fully developed. Thus, more efforts from MOF community will be needed to expand the current boundaries of such special materials. Nevertheless, this is not incompatible with the transferability of knowledge from lab scale to real-world applications of some of the already reported examples, which outperform state of the art materials in diverse applications. This, even if challenging, will be easier than for single-component MOFs, as we could take advantage of the acquired knowledge and cross smoothier this bridge. In this connection, we have included a perspective section with very realistic proposals of plausible steps that could be conducted on shily explored areas of research, where we consider the intrinsic features of mixed-component MOFs will make a severe impact on their exponential development.

To conclude, it is worth mentioning the reminiscent character of some of the reported mixed-component MOFs with biological systems. Even we still can not compare with the degree of sophistication on composition and control on spatial distribution that living beings present, the reported highly complex systems have set the foundations to start dreaming on this way. Freely quoting Nobel Laureate Prof. Ben Feringa "we took inspiration from birds to build airplanes, even when at this moment we are not able to synthesize a single cell of a bird". In this context, the mixed-component MOFs developed aiming to evoque nature, apart from being exciting artificial systems from a conceptual and synthetic viewpoint, have the potential to exhibit unprecedented features as consequence of the synergetic interactions between distinct components, which will situate us in a new advantageous position to push the frontiers of knowledge in a very wide range of applications.

Declaration of Competing Interest

The authors declare that they have no known competing financial interests or personal relationships that could have appeared to influence the work reported in this paper.

Acknowledgements

This work was supported by the Ministero dell'Istruzione, dell'Università e della Ricerca (Italy), the Natural Science Foundation of Ningxia Province (China) (2020AAC02005) and the MINECO (Spain) (Projects PID2019–104778GB–I00, CTQ 2017–86735–P, RTC–2017–6331–5, Severo Ochoa program SEV–2016–0683 and Excellence Unit "Maria de Maeztu" CEX2019–000919–M). D.A. acknowledges the financial support of the Fondazione CARIPLO / "Economia Circolare: ricerca per un futuro sostenibile" 2019, Project code: 2019–2090, MOCA. Thanks are also extended to the "2019 Post–doctoral Junior Leader–Retaining Fellowship, la Caixa Foundation (ID100010434 and fellowship code LCF/BQ/PR19/11700011)", the "Ramon y Cajal Programme" and "Subvenciones concedidas a la excelencia científica de juniors investigadores, SEJI/2020/034" (J. F.–S.). E.P. acknowledges the financial support of the European Research Council under the European Union's Horizon 2020 research and innovation programme / ERC Grant Agreement No 814804, MOF–reactors.

References

[1] J.R. Long, O.M. Yaghi, The pervasive chemistry of metal-organic frameworks, Chem. Soc. Rev. 38 (2009) 1213–1214, https://doi.org/10.1039/b903811f.
[2] O.K. Farha, J.T. Hupp, Rational design, synthesis, purification, and activation of metal–organic framework materials, Acc. Chem. Res. 43 (8) (2010) 1166–1175, https://doi.org/10.1021/ar1000617.
[3] G. Maurin, C. Serre, A. Cooper, G. Férey, The new age of MOFs and of their porous-related solids, Chem. Soc. Rev. 46 (11) (2017) 3104–3107, https://doi.org/10.1039/C7CS90049J.
[4] Y. Cui, B. Li, H. He, W. Zhou, B. Chen, G. Qian, Metal-organic frameworks as platforms for functional materials, Acc. Chem. Res. 49 (3) (2016) 483–493, https://doi.org/10.1021/acs.accounts.5b00530.
[5] H. Furukawa, K.E. Cordova, M. O'Keeffe, O.M. Yaghi, The chemistry and applications of metal-organic frameworks, Science 341 (2013) 974, https://doi.org/10.1126/science.1230444.
[6] M.J. Kalmutzki, N. Hanikel, O.M. Yaghi, Secondary building units as the turning point in the development of the reticular chemistry of MOFs, Sci. Adv. 4 (10) (2018) eaat9180, https://doi.org/10.1126/sciadv.aat9180.
[7] Z. Ji, H. Wang, S. Canossa, S. Wuttke, O.M. Yaghi, Pore chemistry of metal-organic frameworks, Adv. Funct. Mater. 30 (41) (2020) 2000238, https://doi.org/10.1002/adfm.202000238.
[8] M. Li, D. Li, M. O'Keeffe, O.M. Yaghi, Topological analysis of metal-organic frameworks with polytopic linkers and/or multiple building units and the minimal transitivity principle, Chem. Rev. 114 (2) (2014) 1343–1370, https://doi.org/10.1021/cr400392k.
[9] H.-C. Zhou, J.R. Long, O.M. Yaghi, Introduction to metal-organic frameworks, Chem. Rev. 112 (2) (2012) 673–674, https://doi.org/10.1021/cr300014x.
[10] N. Stock, S. Biswas, Synthesis of metal-organic frameworks (MOFs): routes to various MOF topologies, morphologies, and composites, Chem. Rev. 112 (2) (2012) 933–969, https://doi.org/10.1021/cr200304e.
[11] A.D. Burrows, The Chemistry of Metal–Organic Frameworks. Synthesis, Characterization, and Applications, 2 Volumes. Edited by Stefan Kaskel., Angew. Chem. Int. Ed. 56 (2017) 1449–1449. doi:10.1002/anie.201611669.
[12] S.M. Cohen, Postsynthetic methods for the functionalization of metal-organic frameworks, Chem. Rev. 112 (2) (2012) 970–1000, https://doi.org/10.1021/cr200179u.
[13] C.K. Brozek, M. Dincă, Cation exchange at the secondary building units of metal-organic frameworks, Chem. Soc. Rev. 43 (16) (2014) 5456–5467, https://doi.org/10.1039/C4CS00002A.
[14] J.D. Evans, C.J. Sumby, C.J. Doonan, Post-synthetic metalation of metal–organic frameworks, Chem. Soc. Rev. 43 (16) (2014) 5933–5951, https://doi.org/10.1039/C4CS00076E.
[15] S.M. Cohen, The postsynthetic renaissance in porous solids, J. Am. Chem. Soc. 139 (8) (2017) 2855–2863, https://doi.org/10.1021/jacs.6b11259.
[16] M. Kalaj, S.M. Cohen, Postsynthetic modification: an enabling technology for the advancement of metal-organic frameworks, ACS Cent. Sci. 6 (7) (2020) 1046–1057, https://doi.org/10.1021/acscentsci.0c00690.
[17] T. Grancha, J. Ferrando-Soria, H.-C. Zhou, J. Gascon, B. Seoane, J. Pasán, O. Fabelo, M. Julve, E. Pardo, Postsynthetic improvement of the physical properties in a metal-organic framework through a single crystal to single crystal transmetallation, Angew. Chem. Int. Ed. 54 (22) (2015) 6521–6525, https://doi.org/10.1002/anie.201501691.
[18] H. Li, K. Wang, Y. Sun, C.T. Lollar, J. Li, H.-C. Zhou, Recent advances in gas storage and separation using metal–organic frameworks, Mater. Today. 21 (2) (2018) 108–121, https://doi.org/10.1016/j.mattod.2017.07.006.
[19] B. Li, H.-M. Wen, W. Zhou, B. Chen, Porous metal-organic frameworks for gas storage and separation: what, how, and why?, J Phys. Chem. Lett. 5 (20) (2014) 3468–3479, https://doi.org/10.1021/jz501586e.
[20] D. Yang, B.C. Gates, Catalysis by metal organic frameworks: perspective and suggestions for future research, ACS Catal. 9 (3) (2019) 1779–1798, https://doi.org/10.1021/acscatal.8b04515.
[21] D. Farrusseng, S. Aguado, C. Pinel, Metal-organic frameworks: opportunities for catalysis, Angew. Chem. Int. Ed. 48 (41) (2009) 7502–7513, https://doi.org/10.1002/anie.v48:41l0.1002/anie.200806063.
[22] A. Dhakshinamoorthy, Z. Li, H. Garcia, Catalysis and photocatalysis by metal organic frameworks, Chem. Soc. Rev. 47 (22) (2018) 8134–8172, https://doi.org/10.1039/C8CS00256H.
[23] M. Viciano-Chumillas, M. Mon, J. Ferrando-Soria, A. Corma, A. Leyva-Pérez, D. Armentano, E. Pardo, Metal-organic frameworks as chemical nanoreactors: synthesis and stabilization of catalytically active metal species in confined spaces, Acc. Chem. Res. 53 (2) (2020) 520–531, https://doi.org/10.1021/acs.accounts.9b00609.
[24] R.J. Young, M.T. Huxley, E. Pardo, N.R. Champness, C.J. Sumby, C.J. Doonan, Isolating reactive metal-based species in metal-organic frameworks – viable strategies and opportunities, Chem. Sci. 11 (16) (2020) 4031–4050, https://doi.org/10.1039/D0SC00485E.
[25] J. Gascon A. Corma F. Kapteijn F.X. Llabrés i Xamena, Metal organic framework catalysis: Quo vadis? ACS Catal. 4 2014 361 378 10.1021/cs400959k.
[26] J. Lee, O.K. Farha, J. Roberts, K.A. Scheidt, S.T. Nguyen, J.T. Hupp, Metal–organic framework materials as catalysts, Chem. Soc. Rev. 38 (5) (2009) 1450, https://doi.org/10.1039/b807080f.
[27] Z. Hu, B.J. Deibert, J. Li, Luminescent metal–organic frameworks for chemical sensing and explosive detection, Chem. Soc. Rev. 43 (16) (2014) 5815–5840, https://doi.org/10.1039/C4CS00010B.
[28] M.C. So, G.P. Wiederrecht, J.E. Mondloch, J.T. Hupp, O.K. Farha, Metal–organic framework materials for light-harvesting and energy transfer, Chem. Commun. 51 (17) (2015) 3501–3510, https://doi.org/10.1039/C4CC09596K.
[29] P. Horcajada, R. Gref, T. Baati, P.K. Allan, G. Maurin, P. Couvreur, G. Férey, R.E. Morris, C. Serre, Metal-organic frameworks in biomedicine, Chem. Rev. 112 (2) (2012) 1232–1268, https://doi.org/10.1021/cr200256v.
[30] S. Rojas, P. Horcajada, Metal-organic frameworks for the removal of emerging organic contaminants in Water, Chem. Rev. 120 (16) (2020) 8378–8415, https://doi.org/10.1021/acs.chemrev.9b00797.
[31] J. Li, X. Wang, G. Zhao, C. Chen, Z. Chai, A. Alsaedi, T. Hayat, X. Wang, Metal–organic framework-based materials: superior adsorbents for the capture of toxic and radioactive metal ions, Chem. Soc. Rev. 47 (7) (2018) 2322–2356, https://doi.org/10.1039/C7CS00543A.
[32] P.A. Kobielska, A.J. Howarth, O.K. Farha, S. Nayak, Metal–organic frameworks for heavy metal removal from water, Coord. Chem. Rev. 358 (2018) 92–107, https://doi.org/10.1016/j.ccr.2017.12.010.
[33] M. Mon, R. Bruno, J. Ferrando-Soria, D. Armentano, E. Pardo, Metal–organic framework technologies for water remediation: towards a sustainable ecosystem, J. Mater. Chem. A. 6 (12) (2018) 4912–4947, https://doi.org/10.1039/C8TA00264A.
[34] A.J. Rieth, S. Yang, E.N. Wang, M. Dincă, Record atmospheric fresh water capture and heat transfer with a material operating at the water uptake reversibility limit, ACS Cent. Sci. 3 (6) (2017) 668–672, https://doi.org/10.1021/acscentsci.7b00186.
[35] H. Kim, S. Yang, S.R. Rao, S. Narayanan, E.A. Kapustin, H. Furukawa, A.S. Umans, O.M. Yaghi, E.N. Wang, Water harvesting from air with metal-organic frameworks powered by natural sunlight, Science 356 (6336) (2017) 430–434, https://doi.org/10.1126/science:aam8743.
[36] H. Furukawa, F. Gándara, Y.-B. Zhang, J. Jiang, W.L. Queen, M.R. Hudson, O.M. Yaghi, Water adsorption in porous metal-organic frameworks and related materials, J. Am. Chem. Soc. 136 (11) (2014) 4369–4381, https://doi.org/10.1021/ja500330a.
[37] H. Furukawa, U. Müller, O.M. Yaghi, "Heterogeneity within order" in metal-organic frameworks, Angew. Chem. Int. Ed. 54 (11) (2015) 3417–3430, https://doi.org/10.1002/anie.201410252.
[38] L. Feng, K.-Y. Wang, G.S. Day, H.-C. Zhou, The chemistry of multi-component and hierarchical framework compounds, Chem. Soc. Rev. 48 (18) (2019) 4823–4853, https://doi.org/10.1039/C9CS00250B.
[39] A.D. Burrows, Mixed-component metal–organic frameworks (MC-MOFs): enhancing functionality through solid solution formation and surface modifications, CrystEngComm 13 (11) (2011) 3623, https://doi.org/10.1039/c0ce00568a.
[40] W. Kleist, F. Jutz, M. Maciejewski, A. Baiker, Mixed-linker metal-organic frameworks as catalysts for the synthesis of propylene carbonate from propylene oxide and CO_2, Eur. J. Inorg. Chem. 2009 (24) (2009) 3552–3561, https://doi.org/10.1002/ejic.200900509.
[41] K. Koh, A. Wong-Foy, A. Matzger, A crystalline mesoporous coordination copolymer with high microporosity, Angew. Chem. Int. Ed. 47 (4) (2008) 677–680, https://doi.org/10.1002/anie.200705020.
[42] M.Y. Masoomi, A. Morsali, A. Dhakshinamoorthy, H. Garcia, Mixed-metal MOFs: unique opportunities in metal-organic framework (MOF) functionality

and design, Angew. Chem. Int. Ed. 58 (43) (2019) 15188–15205, https://doi.org/10.1002/anie.201902229.
[43] H. Deng, C.J. Doonan, H. Furukawa, R.B. Ferreira, J. Towne, C.B. Knobler, B. Wang, O.M. Yaghi, Multiple functional groups of varying ratios in metal-organic frameworks, Science 327 (5967) (2010) 846–850, https://doi.org/10.1126/science:1181761.
[44] J. Jiao, W. Gong, X. Wu, S. Yang, Y. Cui, Multivariate crystalline porous materials: synthesis, property and potential application, Coord. Chem. Rev. 385 (2019) 174–190, https://doi.org/10.1016/j.ccr.2019.01.016.
[45] Q. Pang, B. Tu, Q. Li, Metal–organic frameworks with multicomponents in order, Coord. Chem. Rev. 388 (2019) 107–125, https://doi.org/10.1016/j.ccr.2019.02.022.
[46] C.-X. Chen, Z. Wei, J.-J. Jiang, Y.-Z. Fan, S.-P. Zheng, C.-C. Cao, Y.-H. Li, D. Fenske, C.-Y. Su, Precise modulation of the breathing behavior and pore surface in Zr-MOFs by reversible post-synthetic variable-spacer installation to fine-tune the expansion magnitude and sorption properties, Angew. Chem. Int. Ed. 55 (34) (2016) 9932–9936, https://doi.org/10.1002/anie.201604023.
[47] C.-X. Chen, Z.-W. Wei, J.-J. Jiang, S.-P. Zheng, H.-P. Wang, Q.-F. Qiu, C.-C. Cao, D. Fenske, C.-Y. Su, Dynamic spacer installation for multirole metal-organic frameworks: a new direction toward multifunctional MOFs achieving ultrahigh methane storage working capacity, J. Am. Chem. Soc. 139 (17) (2017) 6034–6037, https://doi.org/10.1021/jacs.7b01320.
[48] E.A. Kapustin, S. Lee, A.S. Alshammari, O.M. Yaghi, Molecular retrofitting adapts a metal-organic framework to extreme pressure, ACS Cent. Sci. 3 (6) (2017) 662–667, https://doi.org/10.1021/acscentsci.7b00169.
[49] X. Zhang, B.L. Frey, Y.-S. Chen, J. Zhang, Topology-guided stepwise insertion of three secondary linkers in zirconium metal-organic frameworks, J. Am. Chem. Soc. 140 (24) (2018) 7710–7715, https://doi.org/10.1021/jacs.8b04277.
[50] T. Islamoglu, S. Goswami, Z. Li, A.J. Howarth, O.K. Farha, J.T. Hupp, Postsynthetic tuning of metal-organic frameworks for targeted applications, Acc. Chem. Res. 50 (4) (2017) 805–813, https://doi.org/10.1021/acs.accounts.6b00577.
[51] C.K. Brozek, A.F. Cozzolino, S.J. Teat, Y.-S. Chen, M. Dincă, Quantification of site-specific cation exchange in metal-organic frameworks using multi-wavelength anomalous X-ray dispersion, Chem. Mater. 25 (15) (2013) 2998–3002, https://doi.org/10.1021/cm400858d.
[52] A. Krajnc, T. Kos, N. Zabukovec Logar, G. Mali, A simple NMR-based method for studying the spatial distribution of linkers within mixed-linker metal-organic frameworks, Angew. Chem. Int. Ed. 54 (36) (2015) 10535–10538, https://doi.org/10.1002/anie.201504426.
[53] Y. Zhao, N. Kornienko, Z. Liu, C. Zhu, S. Asahina, T.-R. Kuo, W. Bao, C. Xie, A. Hexemer, O. Terasaki, P. Yang, O.M. Yaghi, Mesoscopic constructs of ordered and oriented metal-organic frameworks on plasmonic silver nanocrystals, J. Am. Chem. Soc. 137 (6) (2015) 2199–2202, https://doi.org/10.1021/ja512951e.
[54] Q. Liu, H. Cong, H. Deng, Deciphering the spatial arrangement of metals and correlation to reactivity in multivariate metal-organic frameworks, J. Am. Chem. Soc. 138 (42) (2016) 13822–13825, https://doi.org/10.1021/jacs.6b08724.
[55] K.C. Jayachandrababu, R.J. Verploegh, J. Leisen, R.C. Nieuwendaal, D.S. Sholl, S. Nair, Structure elucidation of mixed-linker zeolitic imidazolate frameworks by solid-state 1 H CRAMPS NMR spectroscopy and computational modeling, J. Am. Chem. Soc. 138 (23) (2016) 7325–7336, https://doi.org/10.1021/jacs.6b02754.
[56] C. Castillo-Blas, V.A. de la Peña-O'Shea, I. Puente-Orench, J.R. de Paz, R. Sáez-Puche, E. Gutiérrez-Puebla, F. Gándara, Á. Monge, Addressed realization of multication complex arrangements in metal-organic frameworks, Sci. Adv. 3 (7) (2017), https://doi.org/10.1126/sciadv.1700773.
[57] U. Fluch, V. Paneta, D. Primetzhofer, S. Ott, Uniform distribution of post-synthetic linker exchange in metal–organic frameworks revealed by Rutherford backscattering spectrometry, Chem. Commun. 53 (48) (2017) 6516–6519, https://doi.org/10.1039/C7CC02631E.
[58] W. Schrimpf, J. Jiang, Z. Ji, P. Hirschle, D.C. Lamb, O.M. Yaghi, S. Wuttke, Chemical diversity in a metal–organic framework revealed by fluorescence lifetime imaging, Nat. Commun. 9 (2018) 1647, https://doi.org/10.1038/s41467-018-04050-w.
[59] T.-Y. Luo, C. Liu, X.Y. Gan, P.F. Muldoon, N.A. Diemler, J.E. Millstone, N.L. Rosi, Multivariate stratified metal-organic frameworks: diversification using domain building blocks, J. Am. Chem. Soc. 141 (5) (2019) 2161–2168, https://doi.org/10.1021/jacs.8b13502.
[60] N.M. Padial, B. Lerma-Berlanga, N. Almora-Barrios, J. Castells-Gil, I. da Silva, M. de la Mata, S.I. Molina, J. Hernández-Saz, A.E. Platero-Prats, S. Tatay, C. Martí-Gastaldo, Heterometallic titanium-organic frameworks by metal-induced dynamic topological transformations, J. Am. Chem. Soc. 142 (14) (2020) 6638–6648, https://doi.org/10.1021/jacs.0c00117.
[61] R.-W. Huang, Y.-S. Wei, X.-Y. Dong, X.-H. Wu, C.-X. Du, S.-Q. Zang, T.C.W. Mak, Hypersensitive dual-function luminescence switching of a silver-chalcogenolate cluster-based metal–organic framework, Nat. Chem. 9 (7) (2017) 689–697, https://doi.org/10.1038/nchem.2718.
[62] A. Burgun, C.J. Coghlan, D.M. Huang, W. Chen, S. Horike, S. Kitagawa, J.F. Alvino, G.F. Metha, C.J. Sumby, C.J. Doonan, Mapping-out catalytic processes in a metal-organic framework with single-crystal X-ray crystallography, Angew. Chem. Int. Ed. 56 (29) (2017) 8412–8416, https://doi.org/10.1002/anie.v56.2910.1002/anie.201611254.
[63] K. Rissanen, Crystallography of encapsulated molecules, Chem. Soc. Rev. 46 (9) (2017) 2638–2648, https://doi.org/10.1039/C7CS00090A.
[64] W.M. Bloch, N.R. Champness, C.J. Doonan, X-ray crystallography in open-framework materials, Angew. Chem. Int. Ed. 54 (44) (2015) 12860–12867, https://doi.org/10.1002/anie.201501545.
[65] F. Gándara, T.D. Bennett, Crystallography of metal–organic frameworks, IUCrJ. 1 (2014) 563–570, https://doi.org/10.1107/S2052252514020351.
[66] S. Furukawa, K. Hirai, Y. Takashima, K. Nakagawa, M. Kondo, T. Tsuruoka, O. Sakata, S. Kitagawa, A block PCP crystal: anisotropic hybridization of porous coordination polymers by face-selective epitaxial growth, Chem. Commun. (34) (2009) 5097, https://doi.org/10.1039/b909993j.
[67] A.M. Katzenmeyer, J. Canivet, G. Holland, D. Farrusseng, A. Centrone, Assessing chemical heterogeneity at the nanoscale in mixed-ligand metal-organic frameworks with the PTIR technique, Angew. Chem. Int. Ed. 53 (11) (2014) 2852–2856, https://doi.org/10.1002/anie.201309295.
[68] J.A. Boissonnault, A.G. Wong-Foy, A.J. Matzger, Core-shell structures arise naturally during ligand exchange in metal-organic frameworks, J. Am. Chem. Soc. 139 (42) (2017) 14841–14844, https://doi.org/10.1021/jacs.7b08349.
[69] K.C. Jayachandrababu, D.S. Sholl, S. Nair, Structural and mechanistic differences in mixed-linker zeolitic imidazolate framework synthesis by solvent assisted linker exchange and de novo routes, J. Am. Chem. Soc. 139 (16) (2017) 5906–5915, https://doi.org/10.1021/jacs.7b01660.
[70] Z. Ji, T. Li, O.M. Yaghi, Sequencing of metals in multivariate metal-organic frameworks, Science 369 (6504) (2020) 674–680, https://doi.org/10.1126/science:aaz4304.
[71] X. Kong, H. Deng, F. Yan, J. Kim, J.A. Swisher, B. Smit, O.M. Yaghi, J.A. Reimer, Mapping of functional groups in metal-organic frameworks, Science 341 (6148) (2013) 882–885, https://doi.org/10.1126/science:1238339.
[72] R. Kitaura, K. Fujimoto, S. Noro, M. Kondo, S. Kitagawa, A pillared-layer coordination polymer network displaying hysteretic sorption: [Cu2(pzdc)2(dpyg)]n (pzdc= Pyrazine-2,3-dicarboxylate; dpyg=1,2-Di(4-pyridyl)glycol), Angew. Chem. Int. Ed. 41 (2002) 133–135, https://doi.org/10.1002/1521-3773(20020104)41:1<133::AID-ANIE133>3.0.CO;2-R.
[73] B.J. Burnett, P.M. Barron, C. Hu, W. Choe, Stepwise synthesis of metal-organic frameworks: replacement of structural organic linkers, J. Am. Chem. Soc. 133 (26) (2011) 9984–9987, https://doi.org/10.1021/ja201911v.
[74] D. Han, F.-L. Jiang, M.-Y. Wu, L. Chen, Q.-H. Chen, M.-C. Hong, A non-interpenetrated porous metal–organic framework with high gas-uptake capacity, Chem. Commun. 47 (35) (2011) 9861, https://doi.org/10.1039/c1cc12858b.
[75] B.J. Burnett, W. Choe, Stepwise pillar insertion into metal–organic frameworks: a sequential self-assembly approach, CrystEngComm 14 (19) (2012) 6129, https://doi.org/10.1039/c2ce25545f.
[76] J. Park, D. Feng, S. Yuan, H. Zhou, Photochromic metal-organic frameworks: reversible control of singlet oxygen generation, Angew. Chem. Int. Ed. 54 (2) (2015) 430–435, https://doi.org/10.1002/anie.201408862.
[77] W. Xi, Y. Liu, Q. Xia, Z. Li, Y. Cui, Direct and post-synthesis incorporation of chiral metallosalen catalysts into metal-organic frameworks for asymmetric organic transformations, Chem. Eur. J. 21 (36) (2015) 12581–12585, https://doi.org/10.1002/chem.201501486.
[78] X. Zhao, X. Bu, Q.-G. Zhai, H. Tran, P. Feng, Pore space partition by symmetry-matching regulated ligand insertion and dramatic tuning on carbon dioxide uptake, J. Am. Chem. Soc. 137 (4) (2015) 1396–1399, https://doi.org/10.1021/ja512137t.
[79] Q.-G. Zhai, X. Bu, C. Mao, X. Zhao, L. Daemen, Y. Cheng, A.J. Ramirez-Cuesta, P. Feng, An ultra-tunable platform for molecular engineering of high-performance crystalline porous materials, Nat. Commun. 7 (2016) 13645, https://doi.org/10.1038/ncomms13645.
[80] Z. Li, Y. Liu, Q. Xia, Y. Cui, Chiral binary metal–organic frameworks for asymmetric sequential reactions, Chem. Commun. 53 (91) (2017) 12313–12316, https://doi.org/10.1039/C7CC06979K.
[81] Y. Gu, J. Zheng, K. Otake, M. Shivanna, S. Sakaki, H. Yoshino, M. Ohba, S. Kawaguchi, Y. Wang, F. Li, S. Kitagawa, Host-guest interaction modulation in porous coordination polymers for inverse selective CO_2/C_2H_2 separation, Angew. Chem. Int. Ed. 60 (21) (2021) 11688–11694, https://doi.org/10.1002/anie.v60.2110.1002/anie.202016673.
[82] S. Furukawa, K. Hirai, K. Nakagawa, Y. Takashima, R. Matsuda, T. Tsuruoka, M. Kondo, R. Haruki, D. Tanaka, H. Sakamoto, S. Shimomura, O. Sakata, S. Kitagawa, Heterogeneously hybridized porous coordination polymer crystals: fabrication of heterometallic core-shell single crystals with an in-plane rotational epitaxial relationship, Angew. Chem. Int. Ed. 48 (10) (2009) 1766–1770, https://doi.org/10.1002/anie.v48:1010.1002/anie.200804836.
[83] K. Koh, A.G. Wong-Foy, A.J. Matzger, MOF@MOF: microporous core–shell architectures, Chem. Commun. (41) (2009) 6162, https://doi.org/10.1039/b904526k.
[84] K. Hirai, S. Furukawa, M. Kondo, H. Uehara, O. Sakata, S. Kitagawa, Sequential functionalization of porous coordination polymer crystals, Angew. Chem. Int. Ed. 50 (35) (2011) 8057–8061, https://doi.org/10.1002/anie.v50.3510.1002/anie.201101924.
[85] R. Banerjee, A. Phan, B. Wang, C. Knobler, H. Furukawa, M. O'Keeffe, O.M. Yaghi, High-throughput synthesis of zeolitic imidazolate frameworks and application to CO 2 capture, Science 319 (5865) (2008) 939–943, https://doi.org/10.1126/science:1152516.
[86] R. Banerjee, H. Furukawa, D. Britt, C. Knobler, M. O'Keeffe, O.M. Yaghi, Control of pore size and functionality in isoreticular zeolitic imidazolate frameworks and their carbon dioxide selective capture properties, J. Am. Chem. Soc. 131 (11) (2009) 3875–3877, https://doi.org/10.1021/ja809459e.

[87] A. Burrows, C. Frost, M. Mahon, C. Richardson, Post-synthetic modification of tagged metal-organic frameworks, Angew. Chem. Int. Ed. 47 (44) (2008) 8482–8486, https://doi.org/10.1002/anie.200802908.
[88] S.J. Garibay, Z. Wang, K.K. Tanabe, S.M. Cohen, Postsynthetic modification: a versatile approach toward multifunctional metal-organic frameworks, Inorg. Chem. 48 (15) (2009) 7341–7349, https://doi.org/10.1021/ic900796n.
[89] K.M.L. Taylor-Pashow, J. Della Rocca, Z. Xie, S. Tran, W. Lin, Postsynthetic modifications of iron-carboxylate nanoscale metal−organic frameworks for imaging and drug delivery, J. Am. Chem. Soc. 131 (40) (2009) 14261–14263, https://doi.org/10.1021/ja906198y.
[90] W.J. Newsome, S. Ayad, J. Cordova, E.W. Reinheimer, A.D. Campiglia, J.K. Harper, K. Hanson, F.J. Uribe-Romo, Solid state multicolor emission in substitutional solid solutions of metal-organic frameworks, J. Am. Chem. Soc. 141 (28) (2019) 11298–11303, https://doi.org/10.1021/jacs.9b05191.
[91] J. Yu, Y. Cui, C.-D. Wu, Y. Yang, B. Chen, G. Qian, Two-photon responsive metal-organic framework, J. Am. Chem. Soc. 137 (12) (2015) 4026–4029, https://doi.org/10.1021/ja512552g.
[92] M. Lin Foo, S. Horike, T. Fukushima, Y. Hijikata, Y. Kubota, M. Takata, S. Kitagawa, Ligand-based solid solution approach to stabilisation of sulphonic acid groups in porous coordination polymer $Zr_6O_4(OH)_4(BDC)_6$ (UiO-66), Dalton Trans. 41 (45) (2012) 13791, https://doi.org/10.1039/c2dt31195j.
[93] K.M. Choi, K. Na, G.A. Somorjai, O.M. Yaghi, Chemical environment control and enhanced catalytic performance of platinum nanoparticles embedded in nanocrystalline metal-organic frameworks, J. Am. Chem. Soc. 137 (24) (2015) 7810–7816, https://doi.org/10.1021/jacs.5b03540.
[94] Z. Hu, A. Gami, Y. Wang, D. Zhao, A triphasic modulated hydrothermal approach for the synthesis of multivariate metal-organic frameworks with hydrophobic moieties for highly efficient moisture-resistant CO_2 capture, Adv. Sustain. Syst. 1 (11) (2017) 1700092, https://doi.org/10.1002/adsu.v1.1110.1002/adsu.201700092.
[95] J. Liang, Y.-Q. Xie, Q. Wu, X.-Y. Wang, T.-T. Liu, H.-F. Li, Y.-B. Huang, R. Cao, Zinc porphyrin/imidazolium integrated multivariate zirconium metal-organic frameworks for transformation of CO_2 into cyclic carbonates, Inorg. Chem. 57 (5) (2018) 2584–2593, https://doi.org/10.1021/acs.inorgchem.7b02983.
[96] M. Kalaj, J.M. Palomba, K.C. Bentz, S.M. Cohen, Multiple functional groups in UiO-66 improve chemical warfare agent simulant degradation, Chem. Commun. 55 (37) (2019) 5367–5370, https://doi.org/10.1039/C9CC02252J.
[97] A.D. Burrows, L.C. Fisher, C. Richardson, S.P. Rigby, Selective incorporation of functional dicarboxylates into zinc metal–organic frameworks, Chem. Commun. 47 (12) (2011) 3380, https://doi.org/10.1039/c1cc10143a.
[98] Y.-B. Zhang, H. Furukawa, N. Ko, W. Nie, H.J. Park, S. Okajima, K.E. Cordova, H. Deng, J. Kim, O.M. Yaghi, Introduction of functionality, selection of topology, and enhancement of gas adsorption in multivariate metal-organic framework-177, J. Am. Chem. Soc. 137 (7) (2015) 2641–2650, https://doi.org/10.1021/ja512311a.
[99] H.K. Chae, D.Y. Siberio-Pérez, J. Kim, Y. Go, M. Eddaoudi, A.J. Matzger, M. O'Keeffe, O.M. Yaghi, A route to high surface area, porosity and inclusion of large molecules in crystals, Nature 427 (6974) (2004) 523–527, https://doi.org/10.1038/nature02311.
[100] Z. Dong, Y. Sun, J. Chu, X. Zhang, H. Deng, Multivariate metal-organic frameworks for dialing-in the binding and programming the release of drug molecules, J. Am. Chem. Soc. 139 (40) (2017) 14209–14216, https://doi.org/10.1021/jacs.7b07392.
[101] T. Lescouet, E. Kockrick, G. Bergeret, M. Pera-Titus, S. Aguado, D. Farrusseng, Homogeneity of flexible metal–organic frameworks containing mixed linkers, J. Mater. Chem. 22 (20) (2012) 10287, https://doi.org/10.1039/c2jm15966j.
[102] S. Marx, W. Kleist, J. Huang, M. Maciejewski, A. Baiker, Tuning functional sites and thermal stability of mixed-linker MOFs based on MIL-53(Al), Dalton Trans. 39 (16) (2010) 3795, https://doi.org/10.1039/c002483j.
[103] F. Saraci, V. Quezada-Novoa, P.R. Donnarumma, A.J. Howarth, Rare-earth metal–organic frameworks: from structure to applications, Chem. Soc. Rev. 49 (22) (2020) 7949–7977, https://doi.org/10.1039/D0CS00292E.
[104] Y. Wang, L. Feng, W. Fan, K.-Y. Wang, X. Wang, X. Wang, K. Zhang, X. Zhang, F. Dai, D. Sun, H.-C. Zhou, Topology exploration in highly connected rare-earth metal-organic frameworks via continuous hindrance control, J. Am. Chem. Soc. 141 (17) (2019) 6967–6975, https://doi.org/10.1021/jacs.9b00122.
[105] G. Férey, C. Mellot-Draznieks, C. Serre, F. Millange, J. Dutour, S. Surblé, I. Margiolaki, A chromium terephthalate-based solid with unusually large pore volumes and surface area, Science 309 (5743) (2005) 2040–2042, https://doi.org/10.1126/science:1116275.
[106] C. Serre, C. Mellot-Draznieks, S. Surble, N. Audebrand, Y. Filinchuk, G. Ferey, Role of solvent-host interactions that lead to very large swelling of hybrid frameworks, Science 315 (5820) (2007) 1828–1831, https://doi.org/10.1126/science:1137975.
[107] C. Serre, F. Millange, C. Thouvenot, M. Noguès, G. Marsolier, D. Louër, G. Férey, Very large breathing effect in the first nanoporous chromium(III)-based solids: MIL-53 or Cr(III)(OH) x [O(2)C-C(6)H(4)-CO(2)] x [HO(2)C-C(6)H(4)-CO(2)H](x) x H(2)O(y), J. Am. Chem. Soc. 124 (2002) 13519–13526, https://doi.org/10.1021/ja0276974.
[108] J. Ma, L.D. Tran, A.J. Matzger, Toward topology prediction in Zr-based microporous coordination polymers: the role of linker geometry and flexibility, Cryst. Growth Des. 16 (7) (2016) 4148–4153, https://doi.org/10.1021/acs.cgd.6b00698.
[109] J. Pang, S. Yuan, J. Qin, C. Liu, C. Lollar, M. Wu, D. Yuan, H.-C. Zhou, M. Hong, Control the structure of Zr-tetracarboxylate frameworks through steric tuning, J. Am. Chem. Soc. 139 (46) (2017) 16939–16945, https://doi.org/10.1021/jacs.7b09973.
[110] J.H. Cavka, S. Jakobsen, U. Olsbye, N. Guillou, C. Lamberti, S. Bordiga, K.P. Lillerud, A new zirconium inorganic building brick forming metal organic frameworks with exceptional stability, J. Am. Chem. Soc. 130 (42) (2008) 13850–13851, https://doi.org/10.1021/ja8057953.
[111] L. Valenzano, B. Civalleri, S. Chavan, S. Bordiga, M.H. Nilsen, S. Jakobsen, K.P. Lillerud, C. Lamberti, Disclosing the complex structure of UiO-66 metal organic framework: a synergic combination of experiment and theory, Chem. Mater. 23 (7) (2011) 1700–1718, https://doi.org/10.1021/cm1022882.
[112] A. Kirchon, L. Feng, H.F. Drake, E.A. Joseph, H.-C. Zhou, From fundamentals to applications: a toolbox for robust and multifunctional MOF materials, Chem. Soc. Rev. 47 (23) (2018) 8611–8638, https://doi.org/10.1039/C8CS00688A.
[113] Z. Chen, S.L. Hanna, L.R. Redfern, D. Alezi, T. Islamoglu, O.K. Farha, Reticular chemistry in the rational synthesis of functional zirconium cluster-based MOFs, Coord. Chem. Rev. 386 (2019) 32–49, https://doi.org/10.1016/j.ccr.2019.01.017.
[114] R.J. Drout, L. Robison, Z. Chen, T. Islamoglu, O.K. Farha, Zirconium metal-organic frameworks for organic pollutant adsorption, Trends Chem. 1 (3) (2019) 304–317, https://doi.org/10.1016/j.trechm.2019.03.010.
[115] S. Wang, H. Reinsch, N. Heymans, M. Wahiduzzaman, C. Martineau-Corcos, G. De Weireld, G. Maurin, C. Serre, Toward a rational design of titanium metal-organic frameworks, Matter. 2 (2) (2020) 440–450, https://doi.org/10.1016/j.matt.2019.11.002.
[116] B. Bueken, F. Vermoortele, D.E.P. Vanpoucke, H. Reinsch, C.-C. Tsou, P. Valvekens, T. De Baerdemaeker, R. Ameloot, C.E.A. Kirschhock, V. Van Speybroeck, J.M. Mayer, D. De Vos, A flexible photoactive titanium metal-organic framework based on a $[Ti^{IV}_3(\mu_3\text{-}O)(O)_2(COO)_6]$ cluster, Angew. Chem. Int. Ed. 54 (47) (2015) 13912–13917, https://doi.org/10.1002/anie.201505512.
[117] J. Gao, J. Miao, P.-Z. Li, W.Y. Teng, L. Yang, Y. Zhao, B. Liu, Q. Zhang, A p-type Ti (IV)-based metal–organic framework with visible-light photo-response, Chem. Commun. 50 (2014) 3786–3788, https://doi.org/10.1039/C3CC49440C.
[118] M. Dan-Hardi, C. Serre, T. Frot, L. Rozes, G. Maurin, C. Sanchez, G. Férey, A new photoactive crystalline highly porous titanium(IV) dicarboxylate, J. Am. Chem. Soc. 131 (31) (2009) 10857–10859, https://doi.org/10.1021/ja903726m.
[119] J. Castells-Gil, N.M. Padial, N. Almora-Barrios, J. Albero, A.R. Ruiz-Salvador, J. González-Platas, H. García, C. Martí-Gastaldo, Chemical engineering of photoactivity in heterometallic titanium-organic frameworks by metal doping, Angew. Chem. Int. Ed. 57 (28) (2018) 8453–8457, https://doi.org/10.1002/anie.v57.2810.1002/anie.201802089.
[120] S. Wang, M. Cabrero-Antonino, S. Navalón, C. Cao, A. Tissot, I. Dovgaliuk, J. Marrot, C. Martineau-Corcos, L. Yu, H. Wang, W. Shepard, H. García, C. Serre, A robust titanium isophthalate metal-organic framework for visible-light photocatalytic CO_2 methanation, Chem. 6 (12) (2020) 3409–3427, https://doi.org/10.1016/j.chempr.2020.10.017.
[121] H. Reinsch, S. Waitschat, N. Stock, Mixed-linker MOFs with CAU-10 structure: synthesis and gas sorption characteristics, Dalton Trans. 42 (14) (2013) 4840, https://doi.org/10.1039/c3dt32355b.
[122] M. Kim, J.F. Cahill, Y. Su, K.A. Prather, S.M. Cohen, Postsynthetic ligand exchange as a route to functionalization of 'inert' metal–organic frameworks, Chem. Sci. 3 (1) (2012) 126–130, https://doi.org/10.1039/C1SC00394A.
[123] M. Kim, J.F. Cahill, H. Fei, K.A. Prather, S.M. Cohen, Postsynthetic ligand and cation exchange in robust metal-organic frameworks, J. Am. Chem. Soc. 134 (43) (2012) 18082–18088, https://doi.org/10.1021/ja3079219.
[124] O. Karagiaridi, M.B. Lalonde, W. Bury, A.A. Sarjeant, O.K. Farha, J.T. Hupp, Opening ZIF-8: a catalytically active zeolitic imidazolate framework of sodalite topology with unsubstituted linkers, J. Am. Chem. Soc. 134 (45) (2012) 18790–18796, https://doi.org/10.1021/ja308786r.
[125] K. Eum, K.C. Jayachandrababu, F. Rashidi, K. Zhang, J. Leisen, S. Graham, R.P. Lively, R.R. Chance, D.S. Sholl, C.W. Jones, S. Nair, Highly tunable molecular sieving and adsorption properties of mixed-linker zeolitic imidazolate frameworks, J. Am. Chem. Soc. 137 (12) (2015) 4191–4197, https://doi.org/10.1021/jacs.5b00803.
[126] J.A. Thompson, C.R. Blad, N.A. Brunelli, M.E. Lydon, R.P. Lively, C.W. Jones, S. Nair, Hybrid zeolitic imidazolate frameworks: controlling framework porosity and functionality by mixed-linker synthesis, Chem. Mater. 24 (10) (2012) 1930–1936, https://doi.org/10.1021/cm3006953.
[127] M.A. Gotthardt, R. Schoch, T.S. Brunner, M. Bauer, W. Kleist, Design of highly porous single-site catalysts through two-step postsynthetic modification of mixed-linker MIL-53(Al), Chemluschem 80 (1) (2015) 188–195, https://doi.org/10.1002/cplu.201402123.
[128] M.A. Gotthardt, S. Grosjean, T.S. Brunner, J. Kotzel, A.M. Gänzler, S. Wolf, S. Bräse, W. Kleist, Synthesis and post-synthetic modification of amine-, alkyne-, azide- and nitro-functionalized metal–organic frameworks based on DUT-5, Dalton Trans. 44 (38) (2015) 16802–16809, https://doi.org/10.1039/C5DT02276B.
[129] C. Liu, T. Li, N.L. Rosi, Strain-promoted "click" modification of a mesoporous metal-organic framework, J. Am. Chem. Soc. 134 (46) (2012) 18886–18888, https://doi.org/10.1021/ja307713q.
[130] J. An, O.K. Farha, J.T. Hupp, E. Pohl, J.I. Yeh, N.L. Rosi, Metal-adeninate vertices for the construction of an exceptionally porous metal-organic framework, Nat. Commun. 3 (2012) 604, https://doi.org/10.1038/ncomms1618.

[131] C. Liu, T.-Y. Luo, E.S. Feura, C. Zhang, N.L. Rosi, Orthogonal ternary functionalization of a mesoporous metal-organic framework via sequential postsynthetic ligand exchange, J. Am. Chem. Soc. 137 (33) (2015) 10508–10511, https://doi.org/10.1021/jacs.5b06780.
[132] A.M. Fracaroli, P. Siman, D.A. Nagib, M. Suzuki, H. Furukawa, F.D. Toste, O.M. Yaghi, Seven post-synthetic covalent reactions in tandem leading to enzyme-like complexity within metal-organic framework crystals, J. Am. Chem. Soc. 138 (27) (2016) 8352–8355, https://doi.org/10.1021/jacs.6b04204.
[133] L. Feng, K.-Y. Wang, X.-L. Lv, J.A. Powell, T.-H. Yan, J. Willman, H.-C. Zhou, Imprinted apportionment of functional groups in multivariate metal-organic frameworks, J. Am. Chem. Soc. 141 (37) (2019) 14524–14529, https://doi.org/10.1021/jacs.9b06917.
[134] J. Li, Y. Wang, Y. Yu, Q. Li, Functionality proportion and corresponding stability study of multivariate metal-organic frameworks, Chinese Chem. Lett. 29 (6) (2018) 837–841, https://doi.org/10.1016/j.cclet.2017.12.026.
[135] C.J. Doonan, W. Morris, H. Furukawa, O.M. Yaghi, Isoreticular metalation of metal–organic frameworks, J. Am. Chem. Soc. 131 (27) (2009) 9492–9493, https://doi.org/10.1021/ja903251e.
[136] D.N. Bunck, W.R. Dichtel, Mixed linker strategies for organic framework functionalization, Chem. Eur. J. 19 (3) (2013) 818–827, https://doi.org/10.1002/chem.201203145.
[137] P.V. Dau, S.M. Cohen, A. Bifunctional, Site-isolated metal-organic framework-based tandem catalyst, Inorg. Chem. 54 (2015) 3134–3138, https://doi.org/10.1021/ic502316v.
[138] K. Koh, A.G. Wong-Foy, A.J. Matzger, A porous coordination copolymer with over 5000 m^2/g BET surface area, J. Am. Chem. Soc. 131 (12) (2009) 4184–4185, https://doi.org/10.1021/ja809985t.
[139] K. Koh, A.G. Wong-Foy, A.J. Matzger, Coordination copolymerization mediated by $Zn_4O(CO_2R)$ 6 metal clusters: a balancing act between statistics and geometry, J. Am. Chem. Soc. 132 (42) (2010) 15005–15010, https://doi.org/10.1021/ja1065009.
[140] K. Koh, J.D. Van Oosterhout, S. Roy, A.G. Wong-Foy, A.J. Matzger, Exceptional surface area from coordination copolymers derived from two linear linkers of differing lengths, Chem. Sci. 3 (8) (2012) 2429, https://doi.org/10.1039/c2sc20407j.
[141] N. Klein, I. Senkovska, K. Gedrich, U. Stoeck, A. Henschel, U. Mueller, S. Kaskel, A mesoporous metal-organic framework, Angew. Chem. Int. Ed. 48 (2009) 9954–9957, https://doi.org/10.1002/anie.200904599.
[142] R. Grünker, V. Bon, P. Müller, U. Stoeck, S. Krause, U. Mueller, I. Senkovska, S. Kaskel, A new metal–organic framework with ultra-high surface area, Chem. Commun. 50 (26) (2014) 3450, https://doi.org/10.1039/c4cc00113c.
[143] I.M. Hönicke, I. Senkovska, V. Bon, I.A. Baburin, N. Bönisch, S. Raschke, J.D. Evans, S. Kaskel, Balancing mechanical stability and ultrahigh porosity in crystalline framework materials, Angew. Chem. Int. Ed. 57 (42) (2018) 13780–13783, https://doi.org/10.1002/anie.v57.4210.1002/anie.201808240.
[144] B. Li, H.-M. Wen, W. Zhou, J.Q. Xu, B. Chen, Porous metal-organic frameworks: promising materials for methane storage, Chem. 1 (4) (2016) 557–580, https://doi.org/10.1016/j.chempr.2016.09.009.
[145] L. Liu, K. Konstas, M.R. Hill, S.G. Telfer, Programmed pore architectures in modular quaternary metal-organic frameworks, J. Am. Chem. Soc. 135 (47) (2013) 17731–17734, https://doi.org/10.1021/ja4100244.
[146] S.J. Lee, C. Doussot, A. Baux, L. Liu, G.B. Jameson, C. Richardson, J.J. Pak, F. Trousselet, F.-X. Coudert, S.G. Telfer, Multicomponent metal-organic frameworks as defect-tolerant materials, Chem. Mater. 28 (1) (2016) 368–375, https://doi.org/10.1021/acs.chemmater.5b04306.
[147] S.J. Lee, C. Doussot, S.G. Telfer, Architectural diversity in multicomponent metal-organic frameworks constructed from similar building blocks, Cryst. Growth Des. 17 (6) (2017) 3185–3191, https://doi.org/10.1021/acs.cgd.7b00153.
[148] T.-Y. Zhou, B. Auer, S.J. Lee, S.G. Telfer, Catalysts confined in programmed framework pores enable new transformations and tune reaction efficiency and selectivity, J. Am. Chem. Soc. 141 (4) (2019) 1577–1582, https://doi.org/10.1021/jacs.8b11221.
[149] A. Dutta, A.G. Wong-Foy, A.J. Matzger, Coordination copolymerization of three carboxylate linkers into a pillared layer framework, Chem. Sci. 5 (10) (2014) 3729, https://doi.org/10.1039/C3SC53549E.
[150] L. Liu, S.G. Telfer, Systematic ligand modulation enhances the moisture stability and gas sorption characteristics of quaternary metal-organic frameworks, J. Am. Chem. Soc. 137 (11) (2015) 3901–3909, https://doi.org/10.1021/jacs.5b00365.
[151] L. Liu, T.-Y. Zhou, S.G. Telfer, Modulating the performance of an asymmetric organocatalyst by tuning its spatial environment in a metal-organic framework, J. Am. Chem. Soc. 139 (39) (2017) 13936–13943, https://doi.org/10.1021/jacs.7b07921.
[152] C.-C. Liang, Z.-L. Shi, C.-T. He, J. Tan, H.-D. Zhou, H.-L. Zhou, Y. Lee, Y.-B. Zhang, Engineering of pore geometry for ultrahigh capacity methane storage in mesoporous metal-organic frameworks, J. Am. Chem. Soc. 139 (38) (2017) 13300–13303, https://doi.org/10.1021/jacs.7b08347.
[153] L.K. Macreadie, R. Babarao, C.J. Setter, S.J. Lee, O.T. Qazvini, A.J. Seeber, J. Tsanaktsidis, S.G. Telfer, S.R. Batten, M.R. Hill, Enhancing multicomponent metal-organic frameworks for low pressure liquid organic hydrogen carrier separations, Angew. Chem. Int. Ed. 59 (15) (2020) 6090–6098, https://doi.org/10.1002/anie.v59.1510.1002/anie.201916159.
[154] J. Cornelio, T.-Y. Zhou, A. Alkaş, S.G. Telfer, Systematic tuning of the luminescence output of multicomponent metal-organic frameworks, J. Am. Chem. Soc. 140 (45) (2018) 15470–15476, https://doi.org/10.1021/jacs.8b09887.
[155] T. Li, M.T. Kozlowski, E.A. Doud, M.N. Blakely, N.L. Rosi, Stepwise ligand exchange for the preparation of a family of mesoporous MOFs, J. Am. Chem. Soc. 135 (32) (2013) 11688–11691, https://doi.org/10.1021/ja403810k.
[156] C. Liu, C. Zeng, T.-Y. Luo, A.D. Merg, R. Jin, N.L. Rosi, Establishing porosity gradients within metal-organic frameworks using partial postsynthetic ligand exchange, J. Am. Chem. Soc. 138 (37) (2016) 12045–12048, https://doi.org/10.1021/jacs.6b07445.
[157] B. Gui, Y. Meng, Y. Xie, J. Tian, G. Yu, W. Zeng, G. Zhang, S. Gong, C. Yang, D. Zhang, C. Wang, Tuning the photoinduced electron transfer in a Zr-MOF: toward solid-state fluorescent molecular switch and turn-on sensor, Adv. Mater. 30 (34) (2018) 1802329, https://doi.org/10.1002/adma.v30.3410.1002/adma.201802329.
[158] T.-T. Liu, J. Liang, R. Xu, Y.-B. Huang, R. Cao, Salen-Co(III) insertion in multivariate cationic metal–organic frameworks for the enhanced cycloaddition reaction of carbon dioxide, Chem. Commun. 55 (2019) 4063–4066, https://doi.org/10.1039/C8CC10268F.
[159] X.-S. Wang, C.-H. Chen, F. Ichihara, M. Oshikiri, J. Liang, L. Li, Y. Li, H. Song, S. Wang, T. Zhang, Y.-B. Huang, R. Cao, J. Ye, Integration of adsorption and photosensitivity capabilities into a cationic multivariate metal-organic framework for enhanced visible-light photoreduction reaction, Appl. Catal. B Environ. 253 (2019) 323–330, https://doi.org/10.1016/j.apcatb.2019.04.074.
[160] C. Wang, Z. Xie, K.E. deKrafft, W. Lin, Doping metal-organic frameworks for water oxidation, carbon dioxide reduction, and organic photocatalysis, J. Am. Chem. Soc. 133 (34) (2011) 13445–13454, https://doi.org/10.1021/ja203564w.
[161] K. Manna, T. Zhang, F.X. Greene, W. Lin, Bipyridine- and phenanthroline-based metal-organic frameworks for highly efficient and tandem catalytic organic transformations via directed C-H activation, J. Am. Chem. Soc. 137 (7) (2015) 2665–2673, https://doi.org/10.1021/ja512478y.
[162] S. Yuan, J.-S. Qin, L. Zou, Y.-P. Chen, X. Wang, Q. Zhang, H.-C. Zhou, Thermodynamically guided synthesis of mixed-linker Zr-MOFs with enhanced tunability, J. Am. Chem. Soc. 138 (20) (2016) 6636–6642, https://doi.org/10.1021/jacs.6b03263.
[163] D. Feng, K. Wang, Z. Wei, Y.-P. Chen, C.M. Simon, R.K. Arvapally, R.L. Martin, M. Bosch, T.-F. Liu, S. Fordham, D. Yuan, M.A. Omary, M. Haranczyk, B. Smit, H.-C. Zhou, Kinetically tuned dimensional augmentation as a versatile synthetic route towards robust metal–organic frameworks, Nat. Commun. 5 (2014) 5723, https://doi.org/10.1038/ncomms6723.
[164] H. Chevreau, T. Devic, F. Salles, G. Maurin, N. Stock, C. Serre, Mixed-linker hybrid superpolyhedra for the production of a series of large-pore iron(III) carboxylate metal-organic frameworks, Angew. Chem. Int. Ed. 52 (19) (2013) 5056–5060, https://doi.org/10.1002/anie.201300057.
[165] S.-T. Zheng, J.J. Bu, T. Wu, C. Chou, P. Feng, X. Bu, Porous indium-organic frameworks and systematization of structural building blocks, Angew. Chem. Int. Ed. 50 (38) (2011) 8858–8862, https://doi.org/10.1002/anie.v50.3810.1002/anie.201101957.
[166] S. Yuan, W. Lu, Y.-P. Chen, Q. Zhang, T.-F. Liu, D. Feng, X. Wang, J. Qin, H.-C. Zhou, Sequential linker installation: precise placement of functional groups in multivariate metal-organic frameworks, J. Am. Chem. Soc. 137 (9) (2015) 3177–3180, https://doi.org/10.1021/ja512762r.
[167] S. Yuan, Y.-P. Chen, J.-S. Qin, W. Lu, L. Zou, Q. Zhang, X. Wang, X. Sun, H.-C. Zhou, Linker installation: engineering pore environment with precisely placed functionalities in zirconium MOFs, J. Am. Chem. Soc. 138 (28) (2016) 8912–8919, https://doi.org/10.1021/jacs.6b04501.
[168] J. Pang, S. Yuan, J. Qin, M. Wu, C.T. Lollar, J. Li, N. Huang, B. Li, P. Zhang, H.-C. Zhou, Enhancing pore-environment complexity using a trapezoidal linker: toward stepwise assembly of multivariate quinary metal-organic frameworks, J. Am. Chem. Soc. 140 (39) (2018) 12328–12332, https://doi.org/10.1021/jacs.8b07411.
[169] P. Deria, J.E. Mondloch, E. Tylianakis, P. Ghosh, W. Bury, R.Q. Snurr, J.T. Hupp, O.K. Farha, Perfluoroalkane functionalization of NU-1000 via solvent-assisted ligand incorporation: synthesis and CO_2 adsorption studies, J. Am. Chem. Soc. 135 (45) (2013) 16801–16804, https://doi.org/10.1021/ja408959g.
[170] P. Deria, W. Bury, J.T. Hupp, O.K. Farha, Versatile functionalization of the NU-1000 platform by solvent-assisted ligand incorporation, Chem. Commun. 50 (16) (2014) 1965, https://doi.org/10.1039/c3cc48562e.
[171] P. Deria, Y.G. Chung, R.Q. Snurr, J.T. Hupp, O.K. Farha, Water stabilization of Zr 6 -based metal–organic frameworks via solvent-assisted ligand incorporation, Chem. Sci. 6 (9) (2015) 5172–5176, https://doi.org/10.1039/C5SC01784J.
[172] J. Liu, Z. Li, X. Zhang, K.-ichi. Otake, L. Zhang, A.W. Peters, M.J. Young, N.M. Bedford, S.P. Letourneau, D.J. Mandia, J.W. Elam, O.K. Farha, J.T. Hupp, Introducing nonstructural ligands to zirconia-like metal-organic framework nodes to tune the activity of node-supported nickel catalysts for ethylene hydrogenation, ACS Catal. 9 (4) (2019) 3198–3207, https://doi.org/10.1021/acscatal.8b04828.
[173] S. Goswami, H. Noh, L.R. Redfern, K. Otake, C.-W. Kung, Y. Cui, K.W. Chapman, O.K. Farha, J.T. Hupp, Pore-templated growth of catalytically active gold nanoparticles within a metal-organic framework, Chem. Mater. 31 (5) (2019) 1485–1490, https://doi.org/10.1021/acs.chemmater.8b04983.
[174] V. Guillerm, D. Maspoch, Geometry mismatch and reticular chemistry: strategies to assemble metal-organic frameworks with non-default

topologies, J. Am. Chem. Soc. 141 (42) (2019) 16517–16538, https://doi.org/10.1021/jacs.9b08754.
[175] T.T.M. Nguyen, H.M. Le, Y. Kawazoe, H.L. Nguyen, Reticular control of interpenetration in a complex metal–organic framework, Mater. Chem. Front. 2 (11) (2018) 2063–2069, https://doi.org/10.1039/C8QM00368H.
[176] H.L. Nguyen, T.T. Vu, D.-K. Nguyen, C.A. Trickett, T.L.H. Doan, C.S. Diercks, V.Q. Nguyen, K.E. Cordova, A complex metal-organic framework catalyst for microwave-assisted radical polymerization, Commun. Chem. 1 (2018) 70, https://doi.org/10.1038/s42004-018-0071-6.
[177] H. Kim, D. Kim, D. Moon, Y.N. Choi, S.B. Baek, M.S. Lah, Symmetry-guided syntheses of mixed-linker Zr metal–organic frameworks with precise linker locations, Chem. Sci. 10 (22) (2019) 5801–5806, https://doi.org/10.1039/C9SC01301F.
[178] V. Guillerm, T. Grancha, I. Imaz, J. Juanhuix, D. Maspoch, Zigzag ligands for transversal design in reticular chemistry: unveiling new structural opportunities for metal-organic frameworks, J. Am. Chem. Soc. 140 (32) (2018) 10153–10157, https://doi.org/10.1021/jacs.8b07050.
[179] S.J. Rettig, V. Sánchez, A. Storr, R.C. Thompson, J. Trotter, Polybis(4-azabenzimidazolato)-iron(II) and -cobalt(II). 3-D single diamond-like framework materials which exhibit spin canting and ferromagnetic ordering at low temperatures, J. Chem. Soc. Dalton Trans. (2000) 3931–3937, https://doi.org/10.1039/b002574g.
[180] Y. Liu, V.C. Kravtsov, R. Larsen, M. Eddaoudi, Molecular building blocks approach to the assembly of zeolite-like metal–organic frameworks (ZMOFs) with extra-large cavities, Chem. Commun. (14) (2006) 1488, https://doi.org/10.1039/b600188m.
[181] J.-P. Zhang, X.-M. Chen, Crystal engineering of binary metal imidazolate and triazolate frameworks, Chem. Commun. (16) (2006) 1689, https://doi.org/10.1039/b516367f.
[182] H. Hayashi, A.P. Côté, H. Furukawa, M. O'Keeffe, O.M. Yaghi, Zeolite A imidazolate frameworks, Nat. Mater. 6 (7) (2007) 501–506, https://doi.org/10.1038/nmat1927.
[183] Y.-Q. Tian, Y.-M. Zhao, Z.-X. Chen, G.-N. Zhang, L.-H. Weng, D.-Y. Zhao, Design and generation of extended zeolitic metal-organic frameworks (ZMOFs): synthesis and crystal structures of Zinc(II) imidazolate polymers with zeolitic topologies, Chem. Eur. J. 13 (15) (2007) 4146–4154, https://doi.org/10.1002/chem.200700181.
[184] N.T.T. Nguyen, H. Furukawa, F. Gándara, H.T. Nguyen, K.E. Cordova, O.M. Yaghi, Selective capture of carbon dioxide under humid conditions by hydrophobic chabazite-type zeolitic imidazolate frameworks, Angew. Chem. Int. Ed. 53 (40) (2014) 10645–10648, https://doi.org/10.1002/anie.201403980.
[185] J. Yang, Y.-B. Zhang, Q. Liu, C.A. Trickett, E. Gutiérrez-Puebla, M.Á. Monge, H. Cong, A. Aldossary, H. Deng, O.M. Yaghi, Principles of designing extra-large pore openings and cages in zeolitic imidazolate frameworks, J. Am. Chem. Soc. 139 (18) (2017) 6448–6455, https://doi.org/10.1021/jacs.7b02272.
[186] T. Wu, X. Bu, J. Zhang, P. Feng, New zeolitic imidazolate frameworks: from unprecedented assembly of cubic clusters to ordered cooperative organization of complementary ligands, Chem. Mater. 20 (24) (2008) 7377–7382, https://doi.org/10.1021/cm802400f.
[187] S. Abednatanzi, P. Gohari Derakhshandeh, H. Depauw, F.-X. Coudert, H. Vrielinck, P. Van Der Voort, K. Leus, Mixed-metal metal–organic frameworks, Chem. Soc. Rev. 48 (9) (2019) 2535–2565, https://doi.org/10.1039/C8CS00337H.
[188] C. Castillo-Blas, F. Gándara, Metal-organic frameworks incorporating multiple metal elements, Isr. J. Chem. 58 (9-10) (2018) 1036–1043, https://doi.org/10.1002/ijch.201800085.
[189] L. Chen, H.-F. Wang, C. Li, Q. Xu, Bimetallic metal–organic frameworks and their derivatives, Chem. Sci. 11 (21) (2020) 5369–5403, https://doi.org/10.1039/D0SC01432J.
[190] P.C.R. Soares-Santos, L. Cunha-Silva, F.A.A. Paz, R.A.Sá. Ferreira, J. Rocha, T. Trindade, Luís.D. Carlos, H.I.S. Nogueira, Photoluminescent 3D lanthanide–organic frameworks with 2,5-pyridinedicarboxylic and 1,4-phenylenediacetic acids, Cryst. Growth Des. 8 (7) (2008) 2505–2516, https://doi.org/10.1021/cg800153a.
[191] D.T. de Lill, A. de Bettencourt-Dias, C.L. Cahill, Exploring lanthanide luminescence in metal-organic frameworks: synthesis, structure, and guest-sensitized luminescence of a mixed europium/terbium-adipate framework and a terbium-adipate framework, Inorg. Chem. 46 (2007) 3960–3965, https://doi.org/10.1021/ic062019u.
[192] K.A. White, D.A. Chengelis, K.A. Gogick, J. Stehman, N.L. Rosi, S. Petoud, Near-infrared luminescent lanthanide MOF barcodes, J. Am. Chem. Soc. 131 (50) (2009) 18069–18071, https://doi.org/10.1021/ja907885m.
[193] C. Serre, F. Millange, C. Thouvenot, N. Gardant, F. Pellé, G. Férey, Synthesis, characterisation and luminescent properties of a new three-dimensional lanthanide trimesate: M((C_6H_3)–$(CO_2)_3$) (M = Y, Ln) or MIL-78, J. Mater. Chem. 14 (10) (2004) 1540–1543, https://doi.org/10.1039/B312425H.
[194] B. Iqbal, M. Saleem, S.N. Arshad, J. Rashid, N. Hussain, M. Zaheer, One-pot synthesis of heterobimetallic metal-organic frameworks (MOFs) for multifunctional catalysis, Chem. Eur. J. 25 (44) (2019) 10490–10498, https://doi.org/10.1002/chem.201901939.
[195] X. Song, M. Oh, M.S. Lah, Hybrid bimetallic metal-organic frameworks: modulation of the framework stability and ultralarge CO_2 uptake capacity, Inorg. Chem. 52 (19) (2013) 10869–10876, https://doi.org/10.1021/ic400844v.
[196] G. Kaur, R.K. Rai, D. Tyagi, X. Yao, P.-Z. Li, X.-C. Yang, Y. Zhao, Q. Xu, S.K. Singh, Room-temperature synthesis of bimetallic Co–Zn based zeolitic imidazolate frameworks in water for enhanced CO_2 and H_2 uptakes, J. Mater. Chem. A. 4 (39) (2016) 14932–14938, https://doi.org/10.1039/C6TA04342A.
[197] L.M. Aguirre-Díaz, F. Gándara, M. Iglesias, N. Snejko, E. Gutiérrez-Puebla, M.Á. Monge, Tunable catalytic activity of solid solution metal-organic frameworks in one-pot multicomponent reactions, J. Am. Chem. Soc. 137 (19) (2015) 6132–6135, https://doi.org/10.1021/jacs.5b02313.
[198] L.J. Wang, H. Deng, H. Furukawa, F. Gándara, K.E. Cordova, D. Peri, O.M. Yaghi, Synthesis and characterization of metal-organic framework-74 containing 2, 4, 6, 8, and 10 different metals, Inorg. Chem. 53 (12) (2014) 5881–5883, https://doi.org/10.1021/ic500434a.
[199] D. Kim, A. Coskun, Template-directed approach towards the realization of ordered heterogeneity in bimetallic metal-organic frameworks, Angew. Chem. Int. Ed. 56 (18) (2017) 5071–5076, https://doi.org/10.1002/anie.201702501.
[200] G. Ayoub, B. Karadeniz, A.J. Howarth, O.K. Farha, I. Đilović, L.S. Germann, R.E. Dinnebier, K. Užarević, T. Friščić, Rational synthesis of mixed-metal microporous metal-organic frameworks with controlled composition using mechanochemistry, Chem. Mater. 31 (15) (2019) 5494–5501, https://doi.org/10.1021/acs.chemmater.9b01068.
[201] J.D. Howe, C.R. Morelock, Y. Jiao, K.W. Chapman, K.S. Walton, D.S. Sholl, Understanding structure, metal distribution, and water adsorption in mixed-metal MOF-74, J. Phys. Chem. C. 121 (1) (2017) 627–635, https://doi.org/10.1021/acs.jpcc.6b1171910.1021/acs.jpcc.6b11719.s001.
[202] J.A. Botas, G. Calleja, M. Sánchez-Sánchez, M.G. Orcajo, Cobalt doping of the MOF-5 framework and its effect on gas-adsorption properties, Langmuir 26 (8) (2010) 5300–5303, https://doi.org/10.1021/la100423a.
[203] F. Trousselet, A. Archereau, A. Boutin, F.-X. Coudert, Heterometallic metal-organic frameworks of MOF-5 and UiO-66 families: insight from computational chemistry, J. Phys. Chem. C. 120 (43) (2016) 24885–24894, https://doi.org/10.1021/acs.jpcc.6b08594.
[204] M.A. Gotthardt, R. Schoch, S. Wolf, M. Bauer, W. Kleist, Synthesis and characterization of bimetallic metal–organic framework Cu–Ru-BTC with HKUST-1 structure, Dalton Trans. 44 (5) (2015) 2052–2056, https://doi.org/10.1039/C4DT02491E.
[205] M. Lammert, C. Glißmann, N. Stock, Tuning the stability of bimetallic Ce(IV)/Zr(IV)-based MOFs with UiO-66 and MOF-808 structures, Dalton Trans. 46 (2017) 2425–2429, https://doi.org/10.1039/C7DT00259A.
[206] F. Nouar, T. Devic, H. Chevreau, N. Guillou, E. Gibson, G. Clet, M. Daturi, A. Vimont, J.M. Grenèche, M.I. Breeze, R.I. Walton, P.L. Llewellyn, C. Serre, Tuning the breathing behaviour of MIL-53 by cation mixing, Chem. Commun. 48 (82) (2012) 10237, https://doi.org/10.1039/c2cc35348b.
[207] L. Mitchell, P. Williamson, B. Ehrlichová, A.E. Anderson, V.R. Seymour, S.E. Ashbrook, N. Acerbi, L.M. Daniels, R.I. Walton, M.L. Clarke, P.A. Wright, Mixed-metal MIL-100(Sc, M) (M=Al, Cr, Fe) for Lewis acid catalysis and tandem C-C bond formation and alcohol oxidation, Chem. Eur. J. 20 (51) (2014) 17185–17197, https://doi.org/10.1002/chem.201404377.
[208] I. Nevjestić, H. Depauw, K. Leus, V. Kalendra, I. Caretti, G. Jeschke, S. Van Doorslaer, F. Callens, P. Van Der Voort, H. Vrielinck, Multi-frequency (S, X, Q and W-band) EPR and ENDOR study of vanadium(IV) incorporation in the aluminium metal-organic framework MIL-53, ChemPhysChem 16 (14) (2015) 2968–2973, https://doi.org/10.1002/cphc.201500522.
[209] H. Depauw, I. Nevjestić, J. De Winne, G. Wang, K. Haustraete, K. Leus, A. Verberckmoes, C. Detavernier, F. Callens, E. De Canck, H. Vrielinck, P. Van Der Voort, Microwave induced "egg yolk" structure in Cr/V-MIL-53, Chem. Commun. 53 (60) (2017) 8478–8481, https://doi.org/10.1039/C7CC04651K.
[210] D.Y. Osadchii, A.I. Olivos-Suarez, Á. Szécsényi, G. Li, M.A. Nasalevich, I.A. Dugulan, P.S. Crespo, E.J.M. Hensen, S.L. Veber, M.V. Fedin, G. Sankar, E.A. Pidko, J. Gascon, Isolated Fe sites in metal organic frameworks catalyze the direct conversion of methane to methanol, ACS Catal. 8 (6) (2018) 5542–5548, https://doi.org/10.1021/acscatal.8b00505.
[211] H. Depauw, I. Nevjestić, G. Wang, K. Leus, F. Callens, E. De Canck, K. De Buysser, H. Vrielinck, P. Van Der Voort, Discovery of a novel, large pore phase in a bimetallic Al/V metal–organic framework, J. Mater. Chem. A. 5 (47) (2017) 24580–24584, https://doi.org/10.1039/C7TA08103K.
[212] M. Mon, J. Ferrando-Soria, M. Verdaguer, C. Train, C. Paillard, B. Dkhil, C. Versace, R. Bruno, D. Armentano, E. Pardo, Postsynthetic approach for the rational design of chiral ferroelectric metal-organic frameworks, J. Am. Chem. Soc. 139 (24) (2017) 8098–8101, https://doi.org/10.1021/jacs.7b03633.
[213] M. Dincă, J.R. Long, High-enthalpy hydrogen adsorption in cation-exchanged variants of the microporous metal–organic framework $Mn_3[(Mn_4Cl)_3(BTT)_8(CH_3OH)_{10}]_2$, J. Am. Chem. Soc. 129 (36) (2007) 11172–11176, https://doi.org/10.1021/ja072871f.
[214] S. Das, H. Kim, K. Kim, Metathesis in single crystal: complete and reversible exchange of metal ions constituting the frameworks of metal–organic frameworks, J. Am. Chem. Soc. 131 (11) (2009) 3814–3815, https://doi.org/10.1021/ja808995d.
[215] T.K. Prasad, D.H. Hong, M.P. Suh, High gas sorption and metal-ion exchange of microporous metal-organic frameworks with incorporated imide groups, Chem. Eur. J. 16 (47) (2010) 14043–14050, https://doi.org/10.1002/chem.201002135.
[216] C.K. Brozek, M. Dincă, Ti^{3+}-, $^{V2+/3}$+-, $C^{r2+/3}$+-, M^{n2}+-, and F^{e2}+-substituted MOF-5 and redox reactivity in Cr- and Fe-MOF-5, J. Am. Chem. Soc. 135 (34) (2013) 12886–12891, https://doi.org/10.1021/ja4064475.

[217] C.K. Brozek, M. Dincă, Cation exchange at the secondary building units of metal–organic frameworks, Chem. Soc. Rev. 43 (16) (2014) 5456–5467, https://doi.org/10.1039/C4CS00002A.
[218] X. Song, S. Jeong, D. Kim, M.S. Lah, Transmetalations in two metal–organic frameworks with different framework flexibilities: Kinetics and core–shell heterostructure, CrystEngComm 14 (18) (2012) 5753, https://doi.org/10.1039/c2ce26115d.
[219] D.F. Sava Gallis, M.V. Parkes, J.A. Greathouse, X. Zhang, T.M. Nenoff, Enhanced O2 selectivity versus N_2 by partial metal substitution in Cu-BTC, Chem. Mater. 27 (6) (2015) 2018–2025, https://doi.org/10.1021/cm5042293.
[220] J. Yang, B. Du, N. Yuan, X. Jia, J. Li, Vapor-assisted preparation of Mn/Fe/Co/Zn–Cu bimetallic metal–organic frameworks based on octahedron micron crystals (PCN-6′), New J. Chem. 43 (17) (2019) 6452–6456, https://doi.org/10.1039/C8NJ04724C.
[221] J.I. Feldblyum, M. Liu, D.W. Gidley, A.J. Matzger, Reconciling the discrepancies between crystallographic porosity and guest access as exemplified by Zn-HKUST-1, J. Am. Chem. Soc. 133 (45) (2011) 18257–18263, https://doi.org/10.1021/ja2055935.
[222] S. Hong, M. Oh, M. Park, J.W. Yoon, J.-S. Chang, M.S. Lah, Large H2 storage capacity of a new polyhedron-based metal–organic framework with high thermal and hygroscopic stability, Chem. Commun. (36) (2009) 5397, https://doi.org/10.1039/b909250a.
[223] M.S. Denny, L.R. Parent, J.P. Patterson, S.K. Meena, H. Pham, P. Abellan, Q.M. Ramasse, F. Paesani, N.C. Gianneschi, S.M. Cohen, Transmission electron microscopy reveals deposition of metal oxide coatings onto metal-organic frameworks, J. Am. Chem. Soc. 140 (4) (2018) 1348–1357, https://doi.org/10.1021/jacs.7b10453.
[224] J.G. Santaclara, A.I. Olivos-Suarez, A. Gonzalez-Nelson, D. Osadchii, M.A. Nasalevich, M.A. van der Veen, F. Kapteijn, A.M. Sheveleva, S.L. Veber, M.V. Fedin, A.T. Murray, C.H. Hendon, A. Walsh, J. Gascon, Revisiting the incorporation of Ti(IV) in UiO-type metal-organic frameworks: metal exchange versus grafting and their implications on photocatalysis, Chem. Mater. 29 (21) (2017) 8963–8967, https://doi.org/10.1021/acs.chemmater.7b03320.
[225] J. Tu, X. Zeng, F. Xu, X. Wu, Y. Tian, X. Hou, Z. Long, Microwave-induced fast incorporation of titanium into UiO-66 metal–organic frameworks for enhanced photocatalytic properties, Chem. Commun. 53 (23) (2017) 3361–3364, https://doi.org/10.1039/C7CC00076F.
[226] M. Chen, Z. Long, R. Dong, L. Wang, J. Zhang, S. Li, X. Zhao, X. Hou, H. Shao, X. Jiang, Titanium incorporation into Zr-porphyrinic metal-organic frameworks with enhanced antibacterial activity against multidrug-resistant pathogens, Small 16 (7) (2020) 1906240, https://doi.org/10.1002/smll.201906240.
[227] H. Choi, A.W. Peters, H. Noh, L.C. Gallington, A.E. Platero-Prats, M.R. DeStefano, M. Rimoldi, S. Goswami, K.W. Chapman, O.K. Farha, J.T. Hupp, Vapor-phase fabrication and condensed-phase application of a MOF-node-supported iron thiolate photocatalyst for nitrate conversion to ammonium, ACS Appl. Energy Mater. 2 (12) (2019) 8695–8700, https://doi.org/10.1021/acsaem.9b01664.
[228] J. Castells-Gil, N.M. Padial, N. Almora-Barrios, R. Gil-San-Millán, M. Romero-Ángel, V. Torres, I. da Silva, B.C.J. Vieira, J.C. Waerenborgh, J. Jagiello, J.A.R. Navarro, S. Tatay, C. Martí-Gastaldo, Heterometallic titanium-organic frameworks as dual-metal catalysts for synergistic non-buffered hydrolysis of nerve agent simulants, Chem. 6 (11) (2020) 3118–3131, https://doi.org/10.1016/j.chempr.2020.09.002.
[229] H.G.T. Nguyen, N.M. Schweitzer, C.-Y. Chang, T.L. Drake, M.C. So, P.C. Stair, O. K. Farha, J.T. Hupp, S.T. Nguyen, Vanadium-node-functionalized UiO-66: a thermally stable MOF-supported catalyst for the gas-phase oxidative dehydrogenation of cyclohexene, ACS Catal. 4 (8) (2014) 2496–2500, https://doi.org/10.1021/cs5001448.
[230] S. Yuan, Y. Chen, J. Qin, W. Lu, X. Wang, Q. Zhang, M. Bosch, T. Liu, X. Lian, H. Zhou, Cooperative cluster metalation and ligand migration in zirconium metal-organic frameworks, Angew. Chem. Int. Ed. 54 (49) (2015) 14696–14700, https://doi.org/10.1002/anie.201505625.
[231] K. Manna, P. Ji, F.X. Greene, W. Lin, Metal-organic framework nodes support single-site magnesium-alkyl catalysts for hydroboration and hydroamination reactions, J. Am. Chem. Soc. 138 (24) (2016) 7488–7491, https://doi.org/10.1021/jacs.6b03689.
[232] K. Manna, P. Ji, Z. Lin, F.X. Greene, A. Urban, N.C. Thacker, W. Lin, Chemoselective single-site Earth-abundant metal catalysts at metal–organic framework nodes, Nat. Commun. 7 (2016) 12610, https://doi.org/10.1038/ncomms12610.
[233] P. Ji, K. Manna, Z. Lin, X. Feng, A. Urban, Y. Song, W. Lin, Single-site cobalt catalysts at new $Zr_{12}(\mu_3\text{-}O)_8(\mu_3\text{-}OH)_8(\mu_2\text{-}OH)_6$ metal-organic framework nodes for highly active hydrogenation of nitroarenes, nitriles, and isocyanides, J. Am. Chem. Soc. 139 (20) (2017) 7004–7011, https://doi.org/10.1021/jacs.7b02394.
[234] P.J. Larson, J.L. Cheney, A.D. French, D.M. Klein, B.J. Wylie, A.F. Cozzolino, Anchored aluminum catalyzed meerwein–ponndorf–verley reduction at the metal nodes of robust MOFs, Inorg. Chem. 57 (12) (2018) 6825–6832, https://doi.org/10.1021/acs.inorgchem.8b00119.
[235] A.M. Abdel-Mageed, B. Rungtaweevoranit, M. Parlinska-Wojtan, X. Pei, O.M. Yaghi, R.J. Behm, Highly active and stable single-atom Cu catalysts supported by a metal-organic framework, J. Am. Chem. Soc. 141 (13) (2019) 5201–5210, https://doi.org/10.1021/jacs.8b11386.
[236] X. Feng, P. Ji, Z. Li, T. Drake, P. Oliveres, E.Y. Chen, Y. Song, C. Wang, W. Lin, Aluminum hydroxide secondary building units in a metal-organic framework support earth-abundant metal catalysts for broad-scope organic transformations, ACS Catal. 9 (4) (2019) 3327–3337, https://doi.org/10.1021/acscatal.9b00259.
[237] I.S. Kim, J. Borycz, A.E. Platero-Prats, S. Tussupbayev, T.C. Wang, O.K. Farha, J. T. Hupp, L. Gagliardi, K.W. Chapman, C.J. Cramer, A.B.F. Martinson, Targeted single-site MOF node modification: trivalent metal loading via atomic layer deposition, Chem. Mater. 27 (13) (2015) 4772–4778, https://doi.org/10.1021/acs.chemmater.5b01560.
[238] L.C. Gallington, I.S. Kim, W.-G. Liu, A.A. Yakovenko, A.E. Platero-Prats, Z. Li, T. C. Wang, J.T. Hupp, O.K. Farha, D.G. Truhlar, A.B.F. Martinson, K.W. Chapman, Regioselective atomic layer deposition in metal-organic frameworks directed by dispersion interactions, J. Am. Chem. Soc. 138 (41) (2016) 13513–13516, https://doi.org/10.1021/jacs.6b08711.
[239] M. Rimoldi, V. Bernales, J. Borycz, A. Vjunov, L.C. Gallington, A.E. Platero-Prats, I.S. Kim, J.L. Fulton, A.B.F. Martinson, J.A. Lercher, K.W. Chapman, C.J. Cramer, L. Gagliardi, J.T. Hupp, O.K. Farha, Atomic layer deposition in a metal-organic framework: synthesis, characterization, and performance of a solid Acid, Chem. Mater. 29 (3) (2017) 1058–1068, https://doi.org/10.1021/acs.chemmater.6b03880.s001.
[240] R.A. Hackler, R. Pandharkar, M.S. Ferrandon, I.S. Kim, N.A. Vermeulen, L.C. Gallington, K.W. Chapman, O.K. Farha, C.J. Cramer, J. Sauer, L. Gagliardi, A.B.F. Martinson, M. Delferro, Isomerization and selective hydrogenation of propyne: screening of metal-organic frameworks modified by atomic layer deposition, J. Am. Chem. Soc. 142 (48) (2020) 20380–20389, https://doi.org/10.1021/jacs.0c08641.
[241] Z. Thiam, E. Abou-Hamad, B. Dereli, L. Liu, A.-H. Emwas, R. Ahmad, H. Jiang, A. A. Isah, P.B. Ndiaye, M. Taoufik, Y. Han, L. Cavallo, J.-M. Basset, M. Eddaoudi, Extension of surface organometallic chemistry to metal-organic frameworks: development of a well-defined single site $[(\equiv Zr\text{–}O\text{–})W(=O)(CH_2tBu)_3]$ olefin metathesis catalyst, J. Am. Chem. Soc. 142 (39) (2020) 16690–16703, https://doi.org/10.1021/jacs.0c06925.
[242] W.M. Bloch, A. Burgun, C.J. Coghlan, R. Lee, M.L. Coote, C.J. Doonan, C.J. Sumby, Capturing snapshots of post-synthetic metallation chemistry in metal–organic frameworks, Nat. Chem. 6 (10) (2014) 906–912, https://doi.org/10.1038/nchem.2045.
[243] K. Manna, T. Zhang, W. Lin, Postsynthetic metalation of bipyridyl-containing metal-organic frameworks for highly efficient catalytic organic transformations, J. Am. Chem. Soc. 136 (18) (2014) 6566–6569, https://doi.org/10.1021/ja5018267.
[244] S.G. Dunning, J.E. Reynolds, K.M. Walsh, D.J. Kristek, V.M. Lynch, P. Kunal, S.M. Humphrey, Direct, one-pot syntheses of MOFs decorated with low-valent metal-phosphine complexes, Organometallics 38 (18) (2019) 3406–3411, https://doi.org/10.1021/acs.organomet.9b00319.
[245] J. He, N.W. Waggoner, S.G. Dunning, A. Steiner, V.M. Lynch, S.M. Humphrey, A PCP pincer ligand for coordination polymers with versatile chemical reactivity: selective activation of CO 2 gas over CO gas in the solid state, Angew. Chem. Int. Ed. 55 (40) (2016) 12351–12355, https://doi.org/10.1002/anie.v55.4010.1002/anie.201604730.
[246] T. Drake, P. Ji, W. Lin, Site isolation in metal-organic frameworks enables novel transition metal catalysis, Acc. Chem. Res. 51 (9) (2018) 2129–2138, https://doi.org/10.1021/acs.accounts.8b00297.
[247] J.S. Lee, E.A. Kapustin, X. Pei, S. Llopis, O.M. Yaghi, F.D. Toste, Architectural stabilization of a Gold(III) catalyst in metal-organic frameworks, Chem. 6 (1) (2020) 142–152, https://doi.org/10.1016/j.chempr.2019.10.022.
[248] H. Wang, Z. Shi, J. Yang, T. Sun, B. Rungtaweevoranit, H. Lyu, Y. Zhang, O.M. Yaghi, Docking of Cu^{I} and Ag^{I} in metal-organic frameworks for adsorption and separation of xenon, Angew. Chem. Int. Ed. 60 (7) (2021) 3417–3421, https://doi.org/10.1002/anie.202015262.
[249] M.I. Gonzalez, E.D. Bloch, J.A. Mason, S.J. Teat, J.R. Long, Single-crystal-to-single-crystal metalation of a metal-organic framework: a route toward structurally well-defined catalysts, Inorg. Chem. 54 (6) (2015) 2995–3005, https://doi.org/10.1021/acs.inorgchem.5b00096.
[250] H. Fei, S.M. Cohen, A robust, catalytic metal–organic framework with open 2,2′-bipyridine sites, Chem. Commun. 50 (37) (2014) 4810–4812, https://doi.org/10.1039/C4CC01607F.
[251] X. Feng, Y. Song, Z. Li, M. Kaufmann, Y. Pi, J.S. Chen, Z. Xu, Z. Li, C. Wang, W. Lin, Metal-organic framework stabilizes a low-coordinate iridium complex for catalytic methane borylation, J. Am. Chem. Soc. 141 (28) (2019) 11196–11203, https://doi.org/10.1021/jacs.9b04285.
[252] J. Baek, B. Rungtaweevoranit, X. Pei, M. Park, S.C. Fakra, Y.-S. Liu, R. Matheu, S. A. Alshmimri, S. Alshehri, C.A. Trickett, G.A. Somorjai, O.M. Yaghi, Bioinspired metal-organic framework catalysts for selective methane oxidation to methanol, J. Am. Chem. Soc. 140 (51) (2018) 18208–18216, https://doi.org/10.1021/jacs.8b11525.
[253] Y. Wang, Q. Liu, Q. Zhang, B. Peng, H. Deng, Molecular vise approach to create metal-binding sites in MOFs and detection of biomarkers, Angew. Chem. Int. Ed. 57 (24) (2018) 7120–7125, https://doi.org/10.1002/anie.201803201.
[254] H. Fei, S.M. Cohen, Metalation of a thiocatechol-functionalized Zr(IV)-based metal-organic framework for selective C-H functionalization, J. Am. Chem. Soc. 137 (6) (2015) 2191–2194, https://doi.org/10.1021/ja5126885.
[255] Y. Quan, Y. Song, W. Shi, Z. Xu, J.S. Chen, X. Jiang, C. Wang, W. Lin, Metal-organic framework with dual active sites in engineered mesopores for bioinspired synergistic catalysis, J. Am. Chem. Soc. 142 (19) (2020) 8602–8607, https://doi.org/10.1021/jacs.0c02966.
[256] M.I. Gonzalez, A.B. Turkiewicz, L.E. Darago, J. Oktawiec, K. Bustillo, F. Grandjean, G.J. Long, J.R. Long, Confinement of atomically defined metal

halide sheets in a metal–organic framework, Nature 577 (7788) (2020) 64–68, https://doi.org/10.1038/s41586-019-1776-0.
[257] F.R. Fortea-Pérez, M. Mon, J. Ferrando-Soria, M. Boronat, A. Leyva-Pérez, A. Corma, J.M. Herrera, D. Osadchii, J. Gascon, D. Armentano, E. Pardo, The MOF-driven synthesis of supported palladium clusters with catalytic activity for carbene-mediated chemistry, Nat. Mater. 16 (7) (2017) 760–766, https://doi.org/10.1038/nmat4910.
[258] M. Mon, M.A. Rivero-Crespo, J. Ferrando-Soria, A. Vidal-Moya, M. Boronat, A. Leyva-Pérez, A. Corma, J.C. Hernández-Garrido, M. López-Haro, J.J. Calvino, G. Ragazzon, A. Credi, D. Armentano, E. Pardo, Synthesis of densely packaged, ultrasmall Pt_2^0 clusters within a thioether-functionalized MOF: catalytic activity in industrial reactions at low temperature, Angew. Chem. Int. Ed. 57 (21) (2018) 6186–6191, https://doi.org/10.1002/anie.201801957.
[259] M.A. Rivero-Crespo, M. Mon, J. Ferrando-Soria, C.W. Lopes, M. Boronat, A. Leyva-Pérez, A. Corma, J.C. Hernández-Garrido, M. López-Haro, J.J. Calvino, E. V. Ramos-Fernandez, D. Armentano, E. Pardo, Confined Pt_1^{1+} water clusters in a MOF catalyze the low-temperature water-gas shift reaction with both CO_2 oxygen atoms coming from water, Angew. Chem. Int. Ed. 57 (52) (2018) 17094–17099, https://doi.org/10.1002/anie.201810251.
[260] E. V. Ramos-Fernández, J.C. Serrano-Ruiz, A. Sepúlveda-Escribano, J. Narciso, J. Ferrando-Soria, E. Pardo, CHAPTER 9. Metal Organic Frameworks: From Material Chemistry to Catalytic Applications, in: Heterog. Catal. Energy Appl., Royal Society of Chemistry, 2020: pp. 235–303. doi:10.1039/9781788019576-00235.
[261] C. Bilanin, E. Tiburcio, J. Ferrando-Soria, D. Armentano, A. Leyva-Pérez, E. Pardo, Crystallographic visualization of a double water molecule addition on a Pt_1-MOF during the low-temperature water-gas shift reaction, ChemCatChem 13 (4) (2021) 1195–1200, https://doi.org/10.1002/cctc.202001492.
[262] E. Tiburcio, R. Greco, M. Mon, J. Ballesteros-Soberanas, J. Ferrando-Soria, M. López-Haro, J.C. Hernández-Garrido, J. Oliver-Meseguer, C. Marini, M. Boronat, D. Armentano, A. Leyva-Pérez, E. Pardo, Soluble/MOF-supported palladium single atoms catalyze the ligand-, additive-, and solvent-free aerobic oxidation of benzyl alcohols to benzoic acids, J. Am. Chem. Soc. 143 (6) (2021) 2581–2592, https://doi.org/10.1021/jacs.0c12367.
[263] V. Guillerm, H. Xu, J. Albalad, I. Imaz, D. Maspoch, Postsynthetic selective ligand cleavage by solid-gas phase ozonolysis fuses micropores into mesopores in metal-organic frameworks, J. Am. Chem. Soc. 140 (44) (2018) 15022–15030, https://doi.org/10.1021/jacs.8b09682.
[264] A.G. Wong-Foy, O. Lebel, A.J. Matzger, Porous crystal derived from a tricarboxylate linker with two distinct binding motifs, J. Am. Chem. Soc. 129 (51) (2007) 15740–15741, https://doi.org/10.1021/ja0753952.
[265] X. Zhao, X. Wang, S. Wang, J. Dou, P. Cui, Z. Chen, D. Sun, X. Wang, D. Sun, Novel metal-organic framework based on cubic and trisoctahedral supermolecular building blocks: topological analysis and photoluminescent property, Cryst. Growth Des. 12 (6) (2012) 2736–2739, https://doi.org/10.1021/cg3002866.
[266] F. Nouar, J.F. Eubank, T. Bousquet, L. Wojtas, M.J. Zaworotko, M. Eddaoudi, Supermolecular building blocks (SBBs) for the design and synthesis of highly porous metal-organic frameworks, J. Am. Chem. Soc. 130 (6) (2008) 1833–1835, https://doi.org/10.1021/ja710123s.
[267] Z. Wang, V.C. Kravtsov, M.J. Zaworotko, Ternary nets formed by self-assembly of triangles, squares, and tetrahedra, Angew. Chem. Int. Ed. 44 (19) (2005) 2877–2880, https://doi.org/10.1002/anie.200500156.
[268] S.-T. Zheng, T. Wu, F. Zuo, C. Chou, P. Feng, X. Bu, Mimicking zeolite to its core: porous sodalite cages as hangers for pendant trimeric $M_3(OH)$ clusters (M = Mg, Mn Co, Ni, Cd), J. Am. Chem. Soc. 134 (4) (2012) 1934–1937, https://doi.org/10.1021/ja209800x.
[269] S.-T. Zheng, J.T. Bu, Y. Li, T. Wu, F. Zuo, P. Feng, X. Bu, Pore space partition and charge separation in cage-within-cage indium−organic frameworks with high CO_2 uptake, J. Am. Chem. Soc. 132 (48) (2010) 17062–17064, https://doi.org/10.1021/ja106903p.
[270] F. Bu, Q. Lin, Q. Zhai, L. Wang, T. Wu, S. Zheng, X. Bu, P. Feng, Two zeolite-type frameworks in one metal-organic framework with Zn 24 @Zn 104 cube-in-sodalite architecture, Angew. Chem. Int. Ed. 51 (34) (2012) 8538–8541, https://doi.org/10.1002/anie.201203425.
[271] S.-T. Zheng, T. Wu, B. Irfanoglu, F. Zuo, P. Feng, X. Bu, Multicomponent self-assembly of a nested Co24@Co48 metal-organic polyhedral framework, Angew. Chem. Int. Ed. 50 (35) (2011) 8034–8037, https://doi.org/10.1002/anie.201103155.
[272] S.-T. Zheng, C. Mao, T. Wu, S. Lee, P. Feng, X. Bu, Generalized synthesis of zeolite-type metal-organic frameworks encapsulating immobilized transition-metal clusters, J. Am. Chem. Soc. 134 (29) (2012) 11936–11939, https://doi.org/10.1021/ja305181y.
[273] B. Tu, Q. Pang, E. Ning, W. Yan, Y. Qi, D. Wu, Q. Li, Heterogeneity within a mesoporous metal-organic framework with three distinct metal-containing building units, J. Am. Chem. Soc. 137 (42) (2015) 13456–13459, https://doi.org/10.1021/jacs.5b07687.
[274] Q. Liu, Y. Song, Y. Ma, Y. Zhou, H. Cong, C. Wang, J. Wu, G. Hu, M. O'Keeffe, H. Deng, Mesoporous cages in chemically robust MOFs created by a large number of vertices with reduced connectivity, J. Am. Chem. Soc. 141 (1) (2019) 488–496, https://doi.org/10.1021/jacs.8b11230.
[275] D. Fujita, Y. Ueda, S. Sato, N. Mizuno, T. Kumasaka, M. Fujita, Self-assembly of tetravalent Goldberg polyhedra from 144 small components, Nature 540 (7634) (2016) 563–566, https://doi.org/10.1038/nature20771.
[276] P. Li, Q. Chen, T.C. Wang, N.A. Vermeulen, B.L. Mehdi, A. Dohnalkova, N.D. Browning, D. Shen, R. Anderson, D.A. Gómez-Gualdrón, F.M. Cetin, J. Jagiello, A.M. Asiri, J.F. Stoddart, O.K. Farha, Hierarchically engineered mesoporous metal-organic frameworks toward cell-free immobilized enzyme systems, Chem. 4 (5) (2018) 1022–1034, https://doi.org/10.1016/j.chempr.2018.03.001.
[277] A. Schoedel, L. Wojtas, S.P. Kelley, R.D. Rogers, M. Eddaoudi, M.J. Zaworotko, Network diversity through decoration of trigonal-prismatic nodes: two-step crystal engineering of cationic metal-organic materials, Angew. Chem. Int. Ed. 50 (48) (2011) 11421–11424, https://doi.org/10.1002/anie.201104688.
[278] M.-C. Dul, E. Pardo, R. Lescouëzec, Y. Journaux, J. Ferrando-Soria, R. Ruiz-García, J. Cano, M. Julve, F. Lloret, D. Cangussu, C.L.M. Pereira, H.O. Stumpf, J. Pasán, C. Ruiz-Pérez, Supramolecular coordination chemistry of aromatic polyoxalamide ligands: a metallosupramolecular approach toward functional magnetic materials, Coord. Chem. Rev. 254 (19-20) (2010) 2281–2296, https://doi.org/10.1016/j.ccr.2010.03.003.
[279] T. Grancha, J. Ferrando-Soria, M. Castellano, M. Julve, J. Pasán, D. Armentano, E. Pardo, Oxamato-based coordination polymers: recent advances in multifunctional magnetic materials, Chem. Commun. 50 (57) (2014) 7569–7585, https://doi.org/10.1039/C4CC01734J.
[280] C. Tan, X. Han, Z. Li, Y. Liu, Y. Cui, Controlled exchange of achiral linkers with chiral linkers in Zr-based UiO-68 metal-organic framework, J. Am. Chem. Soc. 140 (47) (2018) 16229–16236, https://doi.org/10.1021/jacs.8b09606.
[281] Q. Xia, Z. Li, C. Tan, Y. Liu, W. Gong, Y. Cui, Multivariate metal-organic frameworks as multifunctional heterogeneous asymmetric catalysts for sequential reactions, J. Am. Chem. Soc. 139 (24) (2017) 8259–8266, https://doi.org/10.1021/jacs.7b03113.
[282] X. Zhao, X. Bu, E.T. Nguyen, Q.-G. Zhai, C. Mao, P. Feng, Multivariable modular design of pore space partition, J. Am. Chem. Soc. 138 (46) (2016) 15102–15105, https://doi.org/10.1021/jacs.6b0790110.1021/jacs.6b07901.s00110.1021/jacs.6b07901.s002.
[283] S.-T. Zheng, X. Zhao, S. Lau, A. Fuhr, P. Feng, X. Bu, Entrapment of metal clusters in metal-organic framework channels by extended hooks anchored at open metal sites, J. Am. Chem. Soc. 135 (28) (2013) 10270–10273, https://doi.org/10.1021/ja4044642.
[284] J.-Q. Shen, P.-Q. Liao, D.-D. Zhou, C.-T. He, J.-X. Wu, W.-X. Zhang, J.-P. Zhang, X.-M. Chen, Modular and stepwise synthesis of a hybrid metal-organic framework for efficient electrocatalytic oxygen evolution, J. Am. Chem. Soc. 139 (5) (2017) 1778–1781, https://doi.org/10.1021/jacs.6b12353.
[285] A. Schoedel, W. Boyette, L. Wojtas, M. Eddaoudi, M.J. Zaworotko, A family of porous lonsdaleite-e networks obtained through pillaring of decorated kagomé lattice sheets, J. Am. Chem. Soc. 135 (38) (2013) 14016–14019, https://doi.org/10.1021/ja406030p.
[286] A. Schoedel, A.J. Cairns, Y. Belmabkhout, L. Wojtas, M. Mohamed, Z. Zhang, D. M. Proserpio, M. Eddaoudi, M.J. Zaworotko, The asc trinodal platform: two-step assembly of triangular, tetrahedral, and trigonal-prismatic molecular building blocks, Angew. Chem. Int. Ed. 52 (10) (2013) 2902–2905, https://doi.org/10.1002/anie.201206042.
[287] Y.-S. Wei, M. Zhang, P.-Q. Liao, R.-B. Lin, T.-Y. Li, G. Shao, J.-P. Zhang, X.-M. Chen, Coordination templated [2+2+2] cyclotrimerization in a porous coordination framework, Nat. Commun. 6 (2015) 8348, https://doi.org/10.1038/ncomms9348.
[288] Q.-G. Zhai, X. Bu, X. Zhao, D.-S. Li, P. Feng, Pore space partition in metal-organic frameworks, Acc. Chem. Res. 50 (2) (2017) 407–417, https://doi.org/10.1021/acs.accounts.6b00526.
[289] B. Tu, Q. Pang, H. Xu, X. Li, Y. Wang, Z. Ma, L. Weng, Q. Li, Reversible redox activity in multicomponent metal-organic frameworks constructed from trinuclear copper pyrazolate building blocks, J. Am. Chem. Soc. 139 (23) (2017) 7998–8007, https://doi.org/10.1021/jacs.7b03578.
[290] D.M. D'Alessandro, Exploiting redox activity in metal–organic frameworks: concepts, trends and perspectives, Chem. Commun. 52 (58) (2016) 8957–8971, https://doi.org/10.1039/C6CC00805D.
[291] B. Tu, L. Diestel, Z. Shi, W.R.L.N. Bandara, Y. Chen, W. Lin, Y. Zhang, S.G. Telfer, Q. Li, Harnessing bottom-up self-assembly to position five distinct components in an ordered porous framework, Angew. Chem. Int. Ed. 58 (16) (2019) 5348–5353, https://doi.org/10.1002/anie.201900863.
[292] H. Fei, J.F. Cahill, K.A. Prather, S.M. Cohen, Tandem postsynthetic metal ion and ligand exchange in zeolitic imidazolate frameworks, Inorg. Chem. 52 (7) (2013) 4011–4016, https://doi.org/10.1021/ic400048g.
[293] B. Tu, Q. Pang, D. Wu, Y. Song, L. Weng, Q. Li, Ordered vacancies and their chemistry in metal-organic frameworks, J. Am. Chem. Soc. 136 (41) (2014) 14465–14471, https://doi.org/10.1021/ja5063423.
[294] Y. Xiao, Y. Chu, S. Li, Y. Su, J. Tang, J. Xu, F. Deng, Primary adsorption sites of light alkanes in multivariate uio-66 at room temperature as revealed by solid-state NMR, J. Phys. Chem. C. 124 (6) (2020) 3738–3746, https://doi.org/10.1021/acs.jpcc.0c00184.
[295] H. Jiang, J. Jia, A. Shkurenko, Z. Chen, K. Adil, Y. Belmabkhout, L.J. Weselinski, A.H. Assen, D.-X. Xue, M. O'Keeffe, M. Eddaoudi, Enriching the reticular chemistry repertoire: merged nets approach for the rational design of intricate mixed-linker metal-organic framework platforms, J. Am. Chem. Soc. 140 (28) (2018) 8858–8867, https://doi.org/10.1021/jacs.8b04745.
[296] H. Furukawa, N. Ko, Y.B. Go, N. Aratani, S.B. Choi, E. Choi, A.Ö. Yazaydin, R.Q. Snurr, M. O'Keeffe, J. Kim, O.M. Yaghi, Ultrahigh porosity in metal-organic frameworks, Science 329 (5990) (2010) 424–428, https://doi.org/10.1126/science:1192160.

[297] J.-R. Li, R.J. Kuppler, H.-C. Zhou, Selective gas adsorption and separation in metal–organic frameworks, Chem. Soc. Rev. 38 (5) (2009) 1477, https://doi.org/10.1039/b802426j.
[298] J.-R. Li, J. Sculley, H.-C. Zhou, Metal-organic frameworks for separations, Chem. Rev. 112 (2) (2012) 869–932, https://doi.org/10.1021/cr200190s.
[299] R.-B. Lin, S. Xiang, H. Xing, W. Zhou, B. Chen, Exploration of porous metal–organic frameworks for gas separation and purification, Coord. Chem. Rev. 378 (2019) 87–103, https://doi.org/10.1016/j.ccr.2017.09.027.
[300] Y. He, R. Krishna, B. Chen, Metal–organic frameworks with potential for energy-efficient adsorptive separation of light hydrocarbons, Energy Environ. Sci. 5 (10) (2012) 9107, https://doi.org/10.1039/c2ee22858k.
[301] Z.R. Herm, E.D. Bloch, J.R. Long, Hydrocarbon separations in metal-organic frameworks, Chem. Mater. 26 (1) (2014) 323–338, https://doi.org/10.1021/cm402897c.
[302] Z. Bao, G. Chang, H. Xing, R. Krishna, Q. Ren, B. Chen, Potential of microporous metal–organic frameworks for separation of hydrocarbon mixtures, Energy Environ. Sci. 9 (12) (2016) 3612–3641, https://doi.org/10.1039/C6EE01886F.
[303] L. Yu, S. Xiong, Y. Lin, L. Li, J. Peng, W. Liu, X. Huang, H. Wang, J. Li, Tuning the channel size and structure flexibility of metal-organic frameworks for the selective adsorption of noble gases, Inorg. Chem. 58 (22) (2019) 15025–15028, https://doi.org/10.1021/acs.inorgchem.9b02449.
[304] M.T. Kapelewski, J. Oktawiec, T. Runčevski, M.I. Gonzalez, J.R. Long, Separation of xenon and krypton in the metal-organic frameworks M_2(m-dobdc) (M=Co, Ni), Isr. J. Chem. 58 (9-10) (2018) 1138–1143, https://doi.org/10.1002/ijch.201800117.
[305] D. Denysenko, M. Grzywa, M. Tonigold, B. Streppel, I. Krkljus, M. Hirscher, E. Mugnaioli, U. Kolb, J. Hanss, D. Volkmer, Elucidating gating effects for hydrogen sorption in MFU-4-type triazolate-based metal-organic frameworks featuring different pore sizes, Chem. Eur. J. 17 (6) (2011) 1837–1848, https://doi.org/10.1002/chem.201001872.
[306] L. Li, Y. Yang, M.H. Mohamed, S. Zhang, G. Veser, N.L. Rosi, J.K. Johnson, Fundamental insights into the reactivity and utilization of open metal sites in Cu(I)-MFU-4 l, Organometallics 38 (18) (2019) 3453–3459, https://doi.org/10.1021/acs.organomet.9b00351.
[307] M.H. Mohamed, Y. Yang, L. Li, S. Zhang, J.P. Ruffley, A.G. Jarvi, S. Saxena, G. Veser, J.K. Johnson, N.L. Rosi, Designing open metal sites in metal-organic frameworks for paraffin/olefin separations, J. Am. Chem. Soc. 141 (33) (2019) 13003–13007, https://doi.org/10.1021/jacs.9b06582.
[308] D. Denysenko, M. Grzywa, J. Jelic, K. Reuter, D. Volkmer, Scorpionate-type coordination in MFU-4 l metal-organic frameworks: small-molecule binding and activation upon the thermally activated formation of open metal sites, Angew. Chem. Int. Ed. 53 (23) (2014) 5832–5836, https://doi.org/10.1002/anie.201310004.
[309] A.M. Wright, C. Sun, M. Dincă, Thermal cycling of a MOF-based NO disproportionation catalyst, J. Am. Chem. Soc. 143 (2) (2021) 681–686, https://doi.org/10.1021/jacs.0c12134.
[310] E.S. Sanz-Pérez, C.R. Murdock, S.A. Didas, C.W. Jones, Direct capture of CO 2 from ambient air, Chem. Rev. 116 (19) (2016) 11840–11876, https://doi.org/10.1021/acs.chemrev.6b00173.
[311] Y. Lin, C. Kong, Q. Zhang, L. Chen, Metal-organic frameworks for carbon dioxide capture and methane storage, Adv. Energy Mater. 7 (4) (2017) 1601296, https://doi.org/10.1002/aenm.201601296.
[312] C.A. Trickett, A. Helal, B.A. Al-Maythalony, Z.H. Yamani, K.E. Cordova, O.M. Yaghi, The chemistry of metal–organic frameworks for CO_2 capture, regeneration and conversion, Nat. Rev. Mater. 2 (2017) 17045, https://doi.org/10.1038/natrevmats.2017.45.
[313] J. Yu, L.-H. Xie, J.-R. Li, Y. Ma, J.M. Seminario, P.B. Balbuena, CO 2 capture and separations using MOFs: computational and experimental studies, Chem. Rev. 117 (14) (2017) 9674–9754, https://doi.org/10.1021/acs.chemrev.6b00626.
[314] O. Shekhah, Y. Belmabkhout, Z. Chen, V. Guillerm, A. Cairns, K. Adil, M. Eddaoudi, Made-to-order metal-organic frameworks for trace carbon dioxide removal and air capture, Nat. Commun. 5 (2014) 4228, https://doi.org/10.1038/ncomms5228.
[315] S. Nandi, S. Collins, D. Chakraborty, D. Banerjee, P.K. Thallapally, T.K. Woo, R. Vaidhyanathan, Ultralow parasitic energy for postcombustion CO_2 capture realized in a nickel isonicotinate metal-organic framework with excellent moisture stability, J. Am. Chem. Soc. 139 (5) (2017) 1734–1737, https://doi.org/10.1021/jacs.6b10455.
[316] K. Chen, D.G. Madden, T. Pham, K.A. Forrest, A. Kumar, Q. Yang, W. Xue, B. Space, J.J. Perry, J. Zhang, X. Chen, M.J. Zaworotko, Tuning pore size in square-lattice coordination networks for size-selective sieving of CO_2, Angew. Chem. Int. Ed. 55 (35) (2016) 10268–10272, https://doi.org/10.1002/anie.201603934.
[317] P. Nugent, Y. Belmabkhout, S.D. Burd, A.J. Cairns, R. Luebke, K. Forrest, T. Pham, S. Ma, B. Space, L. Wojtas, M. Eddaoudi, M.J. Zaworotko, Porous materials with optimal adsorption thermodynamics and kinetics for CO_2 separation, Nature 495 (7439) (2013) 80–84, https://doi.org/10.1038/nature11893.
[318] T.M. McDonald, J.A. Mason, X. Kong, E.D. Bloch, D. Gygi, A. Dani, V. Crocellà, F. Giordanino, S.O. Odoh, W.S. Drisdell, B. Vlaisavljevich, A.L. Dzubak, R. Poloni, S.K. Schnell, N. Planas, K. Lee, T. Pascal, L.F. Wan, D. Prendergast, J.B. Neaton, B. Smit, J.B. Kortright, L. Gagliardi, S. Bordiga, J.A. Reimer, J.R. Long, Cooperative insertion of CO_2 in diamine-appended metal-organic frameworks, Nature 519 (7543) (2015) 303–308, https://doi.org/10.1038/nature14327.
[319] A.M. Fracaroli, H. Furukawa, M. Suzuki, M. Dodd, S. Okajima, F. Gándara, J.A. Reimer, O.M. Yaghi, Metal-organic frameworks with precisely designed interior for carbon dioxide capture in the presence of water, J. Am. Chem. Soc. 136 (25) (2014) 8863–8866, https://doi.org/10.1021/ja503296c.
[320] Z. Hu, K. Zhang, M. Zhang, Z. Guo, J. Jiang, D. Zhao, A combinatorial approach towards water-stable metal-organic frameworks for highly efficient carbon dioxide separation, ChemSusChem 7 (10) (2014) 2791–2795, https://doi.org/10.1002/cssc.201402378.
[321] P.-Q. Liao, X.-W. Chen, S.-Y. Liu, X.-Y. Li, Y.-T. Xu, M. Tang, Z. Rui, H. Ji, J.-P. Zhang, X.-M. Chen, Putting an ultrahigh concentration of amine groups into a metal–organic framework for CO_2 capture at low pressures, Chem. Sci. 7 (10) (2016) 6528–6533, https://doi.org/10.1039/C6SC00836D.
[322] A. Corma, H. García, F.X. Llabrés i Xamena, Engineering metal organic frameworks for heterogeneous catalysis, Chem. Rev. 110 (2010) 4606–4655. doi:10.1021/cr9003924.
[323] J. Juan-Alcañiz, J. Gascon, F. Kapteijn, Metal–organic frameworks as scaffolds for the encapsulation of active species: state of the art and future perspectives, J. Mater. Chem. 22 (20) (2012) 10102, https://doi.org/10.1039/c2jm15563j.
[324] P. Valvekens, F. Vermoortele, D. De Vos, Metal–organic frameworks as catalysts: the role of metal active sites, Catal. Sci. Technol. 3 (6) (2013) 1435, https://doi.org/10.1039/c3cy20813c.
[325] W. Kleist, M. Maciejewski, A. Baiker, MOF-5 based mixed-linker metal–organic frameworks: Synthesis, thermal stability and catalytic application, Thermochim. Acta. 499 (1-2) (2010) 71–78, https://doi.org/10.1016/j.tca.2009.11.004.
[326] L. Zhang, S. Yuan, L. Feng, B. Guo, J. Qin, B. Xu, C. Lollar, D. Sun, H. Zhou, Pore-environment engineering with multiple metal sites in rare-earth porphyrinic metal-organic frameworks, Angew. Chem. Int. Ed. 57 (18) (2018) 5095–5099, https://doi.org/10.1002/anie.201802661.
[327] S. Yuan, J.-S. Qin, J. Li, L. Huang, L. Feng, Y. Fang, C. Lollar, J. Pang, L. Zhang, D. Sun, A. Alsalme, T. Cagin, H.-C. Zhou, Retrosynthesis of multi-component metal–organic frameworks, Nat. Commun. 9 (2018) 808, https://doi.org/10.1038/s41467-018-03102-5.
[328] M. Dincă, F.P. Gabbaï, J.R. Long, Organometallic chemistry within metal-organic frameworks, Organometallics 38 (18) (2019) 3389–3391, https://doi.org/10.1021/acs.organomet.9b00539.
[329] Y. Zhang, B. Gui, R. Chen, G. Hu, Y. Meng, D. Yuan, M. Zeller, C. Wang, Engineering a zirconium MOF through tandem ‘‘click” reactions: a general strategy for quantitative loading of bifunctional groups on the pore surface, Inorg. Chem. 57 (4) (2018) 2288–2295, https://doi.org/10.1021/acs.inorgchem.7b03123.
[330] T. Zhang, Y.-Q. Hu, T. Han, Y.-Q. Zhai, Y.-Z. Zheng, Redox-active cobalt(II/III) metal-organic framework for selective oxidation of cyclohexene, ACS Appl. Mater. Interfaces. 10 (18) (2018) 15786–15792, https://doi.org/10.1021/acsami.7b19323.
[331] R.H. Palmer, C.-W. Kung, J. Liu, O.K. Farha, J.T. Hupp, Nickel–carbon–zirconium material derived from nickel-oxide clusters installed in a metal-organic framework scaffold by atomic layer deposition, Langmuir 34 (47) (2018) 14143–14150, https://doi.org/10.1021/acs.langmuir.8b02166.
[332] X. Feng, Y. Pi, Y. Song, C. Brzezinski, Z. Xu, Z. Li, W. Lin, Metal-organic frameworks significantly enhance photocatalytic hydrogen evolution and CO_2 reduction with earth-abundant copper photosensitizers, J. Am. Chem. Soc. 142 (2) (2020) 690–695, https://doi.org/10.1021/jacs.9b12229.
[333] S. Yuan, P. Zhang, L. Zhang, A.T. Garcia-Esparza, D. Sokaras, J.-S. Qin, L. Feng, G. S. Day, W. Chen, H.F. Drake, P. Elumalai, S.T. Madrahimov, D. Sun, H.-C. Zhou, Exposed equatorial positions of metal centers via sequential ligand elimination and installation in MOFs, J. Am. Chem. Soc. 140 (34) (2018) 10814–10819, https://doi.org/10.1021/jacs.8b04886.
[334] Y. Pi, X. Feng, Y. Song, Z. Xu, Z. Li, W. Lin, Metal-organic frameworks integrate Cu photosensitizers and secondary building unit-supported fe catalysts for photocatalytic hydrogen evolution, J. Am. Chem. Soc. 142 (23) (2020) 10302–10307, https://doi.org/10.1021/jacs.0c03906.
[335] M.D. Allendorf, C.A. Bauer, R.K. Bhakta, R.J.T. Houk, Luminescent metal–organic frameworks, Chem. Soc. Rev. 38 (5) (2009) 1330, https://doi.org/10.1039/b802352m.
[336] R. Haldar, L. Heinke, C. Wöll, Advanced photoresponsive materials using the metal-organic framework approach, Adv. Mater. 32 (20) (2020) 1905227, https://doi.org/10.1002/adma.201905227.
[337] S. Xing, C. Janiak, Design and properties of multiple-emitter luminescent metal–organic frameworks, Chem. Commun. 56 (82) (2020) 12290–12306, https://doi.org/10.1039/D0CC04733C.
[338] J.-Q. Liu, Z.-D. Luo, Y. Pan, A. Kumar Singh, M. Trivedi, A. Kumar, Recent developments in luminescent coordination polymers: designing strategies, sensing application and theoretical evidences, Coord. Chem. Rev. 406 (2020) 213145, https://doi.org/10.1016/j.ccr.2019.213145.
[339] P.-P. Cui, X.-D. Zhang, P. Wang, Y. Zhao, M. Azam, S.I. Al-Resayes, W.-Y. Sun, Zinc(II) and Copper(II) hybrid frameworks via metal-ion metathesis with enhanced gas uptake and photoluminescence properties, Inorg. Chem. 56 (22) (2017) 14157–14163, https://doi.org/10.1021/acs.inorgchem.7b02235.
[340] W. Chen, J.-Y. Wang, C. Chen, Q. Yue, H.-M. Yuan, J.-S. Chen, S.-N. Wang, Photoluminescent metal–organic polymer constructed from trimetallic clusters and mixed carboxylates, Inorg. Chem. 42 (4) (2003) 944–946, https://doi.org/10.1021/ic025871j.

[341] W.J. Newsome, A. Chakraborty, R.T. Ly, G.S. Pour, D.C. Fairchild, A.J. Morris, F.J. Uribe-Romo, J-dimer emission in interwoven metal–organic frameworks, Chem. Sci. 11 (17) (2020) 4391–4396, https://doi.org/10.1039/D0SC00876A.
[342] W.P. Lustig, Z. Shen, S.J. Teat, N. Javed, E. Velasco, D.M. O'Carroll, J. Li, Rational design of a high-efficiency, multivariate metal–organic framework phosphor for white LED bulbs, Chem. Sci. 11 (7) (2020) 1814–1824, https://doi.org/10.1039/C9SC05721H.
[343] Y.-N. Zeng, H.-Q. Zheng, J.-F. Gu, G.-J. Cao, W.-E. Zhuang, J.-D. Lin, R. Cao, Z.-J. Lin, Dual-emissive metal-organic framework as a fluorescent "switch" for ratiometric sensing of hypochlorite and ascorbic acid, Inorg. Chem. 58 (19) (2019) 13360–13369, https://doi.org/10.1021/acs.inorgchem.9b02251.
[344] A.A. Talin, A. Centrone, A.C. Ford, M.E. Foster, V. Stavila, P. Haney, R.A. Kinney, V. Szalai, F. El Gabaly, H.P. Yoon, F. Léonard, M.D. Allendorf, Tunable electrical conductivity in metal-organic framework thin-film devices, Science 343 (6166) (2014) 66–69, https://doi.org/10.1126/science:1246738.
[345] Y. Ye, L. Gong, S. Xiang, Z. Zhang, B. Chen, Metal-organic frameworks as a versatile platform for proton conductors, Adv. Mater. 32 (21) (2020) 1907090, https://doi.org/10.1002/adma.201907090.
[346] D.-W. Lim, H. Kitagawa, Proton transport in metal-organic frameworks, Chem. Rev. 120 (16) (2020) 8416–8467, https://doi.org/10.1021/acs.chemrev.9b00842.
[347] F. Yang, G. Xu, Y. Dou, B. Wang, H. Zhang, H. Wu, W. Zhou, J.-R. Li, B. Chen, A flexible metal–organic framework with a high density of sulfonic acid sites for proton conduction, Nat. Energy. 2 (11) (2017) 877–883, https://doi.org/10.1038/s41560-017-0018-7.
[348] W.J. Phang, H. Jo, W.R. Lee, J.H. Song, K. Yoo, B. Kim, C.S. Hong, Superprotonic conductivity of a UiO-66 framework functionalized with sulfonic acid groups by facile postsynthetic oxidation, Angew. Chem. Int. Ed. 54 (17) (2015) 5142–5146, https://doi.org/10.1002/anie.201411703.
[349] S. Mukhopadhyay, J. Debgupta, C. Singh, R. Sarkar, O. Basu, S.K. Das, Designing UiO-66-based superprotonic conductor with the highest metal-organic framework based proton conductivity, ACS Appl. Mater. Interfaces. 11 (14) (2019) 13423–13432, https://doi.org/10.1021/acsami.9b01121.
[350] S. Devautour-Vinot, E.S. Sanil, A. Geneste, V. Ortiz, P.G. Yot, J. Chang, G. Maurin, Guest-assisted proton conduction in the sulfonic mesoporous MIL-101 MOF, Chem. Asian J. 14 (20) (2019) 3561–3565, https://doi.org/10.1002/asia.v14.2010.1002/asia.201900608.
[351] S. Nandi, S. Wang, M. Wahiduzzaman, V. Yadav, K. Taksande, G. Maurin, C. Serre, S. Devautour-Vinot, Multivariate sulfonic-based titanium metal-organic frameworks as super-protonic conductors, ACS Appl. Mater. Interfaces. 13 (17) (2021) 20194–20200, https://doi.org/10.1021/acsami.1c03644.
[352] T. Grancha, J. Ferrando-Soria, J. Cano, P. Amorós, B. Seoane, J. Gascon, M. Bazaga-García, E.R. Losilla, A. Cabeza, D. Armentano, E. Pardo, Insights into the dynamics of grotthuss mechanism in a proton-conducting chiral bio MOF, Chem. Mater. 28 (13) (2016) 4608–4615, https://doi.org/10.1021/acs.chemmater.6b01286.
[353] R. Moi, A. Ghorai, S. Banerjee, K. Biradha, Amino- and sulfonate-functionalized metal-organic framework for fabrication of proton exchange membranes with improved proton conductivity, Cryst. Growth Des. 20 (8) (2020) 5557–5563, https://doi.org/10.1021/acs.cgd.0c00732.
[354] G.S. Mohammad-Pour, K.O. Hatfield, D.C. Fairchild, K. Hernandez-Burgos, J. Rodríguez-López, F.J. Uribe-Romo, A solid-solution approach for redox active metal-organic frameworks with tunable redox conductivity, J. Am. Chem. Soc. 141 (51) (2019) 19978–19982, https://doi.org/10.1021/jacs.9b10639.
[355] Y. Chen, S. Ma, Biomimetic catalysis of metal–organic frameworks, Dalton Trans. 45 (24) (2016) 9744–9753, https://doi.org/10.1039/C6DT00325G.
[356] C. Doonan, R. Riccò, K. Liang, D. Bradshaw, P. Falcaro, Metal-organic frameworks at the biointerface: synthetic strategies and applications, Acc. Chem. Res. 50 (6) (2017) 1423–1432, https://doi.org/10.1021/acs.accounts.7b00090.
[357] G. Lan, K. Ni, W. Lin, Nanoscale metal–organic frameworks for phototherapy of cancer, Coord. Chem. Rev. 379 (2019) 65–81, https://doi.org/10.1016/j.ccr.2017.09.007.
[358] I. Abánades Lázaro, R.S. Forgan, Application of zirconium MOFs in drug delivery and biomedicine, Coord. Chem. Rev. 380 (2019) 230–259, https://doi.org/10.1016/j.ccr.2018.09.009.
[359] K. Ni, T. Luo, G.T. Nash, W. Lin, Nanoscale metal-organic frameworks for cancer immunotherapy, Acc. Chem. Res. 53 (9) (2020) 1739–1748, https://doi.org/10.1021/acs.accounts.0c00313.
[360] J. Yang, Y. Yang, Metal-organic frameworks for biomedical applications, Small. 16 (10) (2020) 1906846, https://doi.org/10.1002/smll.v16.1010.1002/smll.201906846.
[361] X. Jiang, C. He, W. Lin, Supramolecular metal-based nanoparticles for drug delivery and cancer therapy, Curr. Opin. Chem. Biol. 61 (2021) 143–153, https://doi.org/10.1016/j.cbpa.2021.01.005.
[362] H.D. Lawson, S.P. Walton, C. Chan, Metal-organic frameworks for drug delivery: a design perspective, ACS Appl. Mater. Interfaces. 13 (6) (2021) 7004–7020, https://doi.org/10.1021/acsami.1c01089.
[363] Y. Song, L. Wang, Z. Xie, Metal-organic frameworks for photodynamic therapy: emerging synergistic cancer therapy, Biotechnol. J. 16 (2) (2021) 1900382, https://doi.org/10.1002/biot.201900382.
[364] I. Abánades Lázaro, C.J.R. Wells, R.S. Forgan, Multivariate Modulation of the Zr MOF UiO-66 for Defect-Controlled Combination Anticancer Drug Delivery, Angew. Chem. Int. Ed. 59 (13) (2020) 5211–5217, https://doi.org/10.1002/anie.v59.1310.1002/anie.201915848.
[365] L. Giusti, A review of waste management practices and their impact on human health, Waste Manag. 29 (8) (2009) 2227–2239, https://doi.org/10.1016/j.wasman.2009.03.028.
[366] United Nations, Transforming our world: the 2030 Agenda for Sustainable Development, (2015). https://sustainabledevelopment.un.org/post2015/transformingourworld.
[367] C. Wang, X. Liu, N. Keser Demir, J.P. Chen, K. Li, Applications of water stable metal–organic frameworks, Chem. Soc. Rev. 45 (18) (2016) 5107–5134, https://doi.org/10.1039/C6CS00362A.
[368] N.S. Bobbitt, M.L. Mendonca, A.J. Howarth, T. Islamoglu, J.T. Hupp, O.K. Farha, R.Q. Snurr, Metal-organic frameworks for the removal of toxic industrial chemicals and chemical warfare agents, Chem. Soc. Rev. 46 (11) (2017) 3357–3385, https://doi.org/10.1039/C7CS00108H.
[369] E. Barea, C. Montoro, J.A.R. Navarro, Toxic gas removal metal-organic frameworks for the capture and degradation of toxic gases and vapours, Chem. Soc. Rev. 43 (2014) 5419–5430, https://doi.org/10.1039/C3CS60475F.
[370] M. Mon, R. Bruno, E. Tiburcio, M. Viciano-Chumillas, L.H.G. Kalinke, J. Ferrando-Soria, D. Armentano, E. Pardo, Multivariate metal-organic frameworks for the simultaneous capture of organic and inorganic contaminants from water, J. Am. Chem. Soc. 141 (34) (2019) 13601–13609, https://doi.org/10.1021/jacs.9b06250.
[371] M. Mon, R. Bruno, E. Tiburcio, P.-E. Casteran, J. Ferrando-Soria, D. Armentano, E. Pardo, Efficient capture of organic dyes and crystallographic snapshots by a highly crystalline amino-acid-derived metal-organic framework, Chem. Eur. J. 24 (67) (2018) 17712–17718, https://doi.org/10.1002/chem.201803547.
[372] M. Mon, F. Lloret, J. Ferrando-Soria, C. Martí-Gastaldo, D. Armentano, E. Pardo, Selective and efficient removal of mercury from aqueous media with the highly flexible arms of a BioMOF, Angew. Chem. Int. Ed. 55 (37) (2016) 11167–11172, https://doi.org/10.1002/anie.201606015.
[373] C. Negro, H. Martínez Pérez-Cejuela, E.F. Simó-Alfonso, J.M. Herrero-Martínez, R. Bruno, D. Armentano, J. Ferrando-Soria, E. Pardo, Highly efficient removal of neonicotinoid insecticides by thioether-based (multivariate) metal-organic frameworks, ACS Appl. Mater. Interfaces. 13 (24) (2021) 28424–28432, https://doi.org/10.1021/acsami.1c08833.
[374] V.N. Vukotic, K.J. Harris, K. Zhu, R.W. Schurko, S.J. Loeb, Metal–organic frameworks with dynamic interlocked components, Nat. Chem. 4 (6) (2012) 456–460, https://doi.org/10.1038/nchem.1354.
[375] V.N. Vukotic, S.J. Loeb, Coordination polymers containing rotaxane linkers, Chem. Soc. Rev. 41 (18) (2012) 5896, https://doi.org/10.1039/c2cs35141b.
[376] K. Zhu, C.A. O'Keefe, V.N. Vukotic, R.W. Schurko, S.J. Loeb, A molecular shuttle that operates inside a metal–organic framework, Nat. Chem. 7 (6) (2015) 514–519, https://doi.org/10.1038/nchem.2258.
[377] A.-H. Sue, R.V. Mannige, H. Deng, D. Cao, C. Wang, F. Gándara, J.F. Stoddart, S. Whitelam, O.M. Yaghi, Heterogeneity of functional groups in a metal–organic framework displays magic number ratios, Proc. Natl. Acad. Sci. 112 (18) (2015) 5591–5596, https://doi.org/10.1073/pnas.1416417112.
[378] P.R. McGonigal, P. Deria, I. Hod, P.Z. Moghadam, A.-J. Avestro, N.E. Horwitz, I. C. Gibbs-Hall, A.K. Blackburn, D. Chen, Y.Y. Botros, M.R. Wasielewski, R.Q. Snurr, J.T. Hupp, O.K. Farha, J.F. Stoddart, Electrochemically addressable trisradical rotaxanes organized within a metal–organic framework, Proc. Natl. Acad. Sci. 112 (36) (2015) 11161–11168, https://doi.org/10.1073/pnas.1514485112.
[379] Q. Chen, J. Sun, P. Li, I. Hod, P.Z. Moghadam, Z.S. Kean, R.Q. Snurr, J.T. Hupp, O. K. Farha, J.F. Stoddart, A redox-active bistable molecular switch mounted inside a metal-organic framework, J. Am. Chem. Soc. 138 (43) (2016) 14242–14245, https://doi.org/10.1021/jacs.6b09880.
[380] B.H. Wilson, S.J. Loeb, Integrating the mechanical bond into metal-organic frameworks, Chem. 6 (7) (2020) 1604–1612, https://doi.org/10.1016/j.chempr.2020.06.016.
[381] B.H. Wilson, C.S. Vojvodin, G. Gholami, L.M. Abdulla, C.A. O'Keefe, R.W. Schurko, S.J. Loeb, Precise spatial arrangement and interaction between two different mobile components in a metal-organic framework, Chem. 7 (1) (2021) 202–211, https://doi.org/10.1016/j.chempr.2020.11.009.
[382] A.J. Stirk, B.H. Wilson, C.A. O'Keefe, H. Amarne, K. Zhu, R.W. Schurko, S.J. Loeb, Applying reticular synthesis to the design of Cu-based MOFs with mechanically interlocked linkers, Nano Res. 14 (2) (2021) 417–422, https://doi.org/10.1007/s12274-020-3123-z.
[383] R. Ma, H. Jiang, C. Wang, C. Zhao, H. Deng, Multivariate MOFs for laser writing of alloy nanoparticle patterns, Chem. Commun. 56 (18) (2020) 2715–2718, https://doi.org/10.1039/C9CC09144K.
[384] C. Young, J. Kim, Y.V. Kaneti, Y. Yamauchi, One-step synthetic strategy of hybrid materials from bimetallic metal-organic frameworks for supercapacitor applications, ACS Appl. Energy Mater. 1 (5) (2018) 2007–2015, https://doi.org/10.1021/acsaem.8b00103.
[385] Y. Jiao, J. Pei, D. Chen, C. Yan, Y. Hu, Q. Zhang, G. Chen, Mixed-metallic MOF based electrode materials for high performance hybrid supercapacitors, J. Mater. Chem. A. 5 (3) (2017) 1094–1102, https://doi.org/10.1039/C6TA09805C.
[386] V.L. Schramm, Introduction: principles of enzymatic catalysis, Chem. Rev. 106 (2006) 3029–3030, https://doi.org/10.1021/cr050246s.
[387] Y. Okamoto, T.R. Ward, Supramolecular Enzyme Mimics, in: Compr. Supramol. Chem. II, Elsevier, 2017: pp. 459–510. doi:10.1016/B978-0-12-409547-2.12551-X.
[388] P.K. Agarwal, A biophysical perspective on enzyme catalysis, Biochemistry 58 (6) (2019) 438–449, https://doi.org/10.1021/acs.biochem.8b01004.

[389] Z.D. Nagel, J.P. Klinman, A 21st century revisionist's view at a turning point in enzymology, Nat. Chem. Biol. 5 (8) (2009) 543–550, https://doi.org/10.1038/nchembio.204.
[390] K.A. Reynolds, R.N. McLaughlin, R. Ranganathan, Hot spots for allosteric regulation on protein surfaces, Cell 147 (7) (2011) 1564–1575, https://doi.org/10.1016/j.cell.2011.10.049.
[391] Z.D. Nagel, S. Cun, J.P. Klinman, Identification of a long-range protein network that modulates active site dynamics in extremophilic alcohol dehydrogenases, J. Biol. Chem. 288 (20) (2013) 14087–14097, https://doi.org/10.1074/jbc.M113.453951.
[392] M. Zhang, Z.-Y. Gu, M. Bosch, Z. Perry, H.-C. Zhou, Biomimicry in metal–organic materials, Coord. Chem. Rev. 293–294 (2015) 327–356, https://doi.org/10.1016/j.ccr.2014.05.031.
[393] K. Chen, C.-D. Wu, Designed fabrication of biomimetic metal–organic frameworks for catalytic applications, Coord. Chem. Rev. 378 (2019) 445–465, https://doi.org/10.1016/j.ccr.2018.01.016.
[394] S.M. Cohen, Z. Zhang, J.A. Boissonnault, Toward "metalloMOFzymes": metal-organic frameworks with single-site metal catalysts for small-molecule transformations, Inorg. Chem. 55 (15) (2016) 7281–7290, https://doi.org/10.1021/acs.inorgchem.6b00828.
[395] I. Nath, J. Chakraborty, F. Verpoort, Metal organic frameworks mimicking natural enzymes: a structural and functional analogy, Chem. Soc. Rev. 45 (15) (2016) 4127–4170, https://doi.org/10.1039/C6CS00047A.
[396] E. Gkaniatsou, C. Sicard, R. Ricoux, J.-P. Mahy, N. Steunou, C. Serre, Metal–organic frameworks: a novel host platform for enzymatic catalysis and detection, Mater. Horizons. 4 (1) (2017) 55–63, https://doi.org/10.1039/C6MH00312E.
[397] X. Lian, Y. Fang, E. Joseph, Q. Wang, J. Li, S. Banerjee, C. Lollar, X. Wang, H.-C. Zhou, Enzyme–MOF (metal–organic framework) composites, Chem. Soc. Rev. 46 (11) (2017) 3386–3401, https://doi.org/10.1039/C7CS00058H.
[398] J.-S. Qin, S. Yuan, C. Lollar, J. Pang, A. Alsalme, H.-C. Zhou, Stable metal–organic frameworks as a host platform for catalysis and biomimetics, Chem. Commun. 54 (34) (2018) 4231–4249, https://doi.org/10.1039/C7CC09173G.
[399] Q. Qiu, H. Chen, Y. Wang, Y. Ying, Recent advances in the rational synthesis and sensing applications of metal-organic framework biocomposites, Coord. Chem. Rev. 387 (2019) 60–78, https://doi.org/10.1016/j.ccr.2019.02.009.
[400] S. Dutta, J. Kim, P. Hsieh, Y. Hsu, Y.V. Kaneti, F. Shieh, Y. Yamauchi, K.C.-W. Wu, Nanoarchitectonics of biofunctionalized metal-organic frameworks with biological macromolecules and living cells, Small Methods. 3 (11) (2019) 1900213, https://doi.org/10.1002/smtd.201900213.
[401] M. Mon, R. Bruno, S. Sanz-Navarro, C. Negro, J. Ferrando-Soria, L. Bartella, L. Di Donna, M. Prejanò, T. Marino, A. Leyva-Pérez, D. Armentano, E. Pardo, Hydrolase–like catalysis and structural resolution of natural products by a metal–organic framework, Nat. Commun. 11 (2020) 3080, https://doi.org/10.1038/s41467-020-16699-3.
[402] L. Liu, A. Corma, Metal catalysts for heterogeneous catalysis: from single atoms to nanoclusters and nanoparticles, Chem. Rev. 118 (10) (2018) 4981–5079, https://doi.org/10.1021/acs.chemrev.7b00776.
[403] J. Perezjuste, I. Pastorizasantos, L. Lizmarzan, P. Mulvaney, Gold nanorods: synthesis, characterization and applications, Coord. Chem. Rev. 249 (17-18) (2005) 1870–1901, https://doi.org/10.1016/j.ccr.2005.01.030.
[404] M. Grzelczak, J. Pérez-Juste, P. Mulvaney, L.M. Liz-Marzán, Shape control in gold nanoparticle synthesis, Chem. Soc. Rev. 37 (9) (2008) 1783, https://doi.org/10.1039/b711490g.
[405] L. Xu, W. Ma, L. Wang, C. Xu, H. Kuang, N.A. Kotov, Nanoparticle assemblies: dimensional transformation of nanomaterials and scalability, Chem. Soc. Rev. 42 (7) (2013) 3114, https://doi.org/10.1039/c3cs35460a.
[406] B. Ni, X. Wang, Chemistry and properties at a sub-nanometer scale, Chem. Sci. 7 (7) (2016) 3978–3991, https://doi.org/10.1039/C6SC00432F.
[407] T.M. Osborn Popp, O.M. Yaghi, Sequence-dependent materials, Acc. Chem. Res. 50 (3) (2017) 532–534, https://doi.org/10.1021/acs.accounts.6b00529.
[408] A. Helal, Z.H. Yamani, K.E. Cordova, O.M. Yaghi, Multivariate metal-organic frameworks, Natl. Sci. Rev. 4 (2017) 296–298, https://doi.org/10.1093/nsr/nwx013.
[409] J.-S. Qin, S. Yuan, Q. Wang, A. Alsalme, H.-C. Zhou, Mixed-linker strategy for the construction of multifunctional metal–organic frameworks, J. Mater. Chem. A. 5 (9) (2017) 4280–4291, https://doi.org/10.1039/C6TA10281F.
[410] R. Rajak, R. Kumar, S.N. Ansari, M. Saraf, S.M. Mobin, Recent highlights and future prospects on mixed-metal MOFs as emerging supercapacitor candidates, Dalton Trans. 49 (34) (2020) 11792–11818, https://doi.org/10.1039/D0DT01676D.
[411] Z.H. Syed, F. Sha, X. Zhang, D.M. Kaphan, M. Delferro, O.K. Farha, Metal-organic framework nodes as a supporting platform for tailoring the activity of metal catalysts, ACS Catal. 10 (19) (2020) 11556–11566, https://doi.org/10.1021/acscatal.0c03056.
[412] W. Xu, B. Tu, Q. Liu, Y. Shu, C.-C. Liang, C.S. Diercks, O.M. Yaghi, Y.-B. Zhang, H. Deng, Q. Li, Anisotropic reticular chemistry, Nat. Rev. Mater. 5 (10) (2020) 764–779, https://doi.org/10.1038/s41578-020-0225-x.
[413] M.L. Foo, R. Matsuda, S. Kitagawa, Functional hybrid porous coordination polymers, Chem. Mater. 26 (1) (2014) 310–322, https://doi.org/10.1021/cm402136z.